



Formation of Optimised Particles for Formulation and Processing

A thesis presented for the degree of
Doctor of Philosophy
in the Faculty of Science
of the University of Strathclyde

by

Francesca Perciballi

Strathclyde Institute of Pharmacy and Biomedical Sciences
December, 2017

Declaration of Author's Rights

This thesis is the result of the author's original research. It has been composed by the author and has not been previously submitted for examination which has led to the award of a degree.

The copyright of this thesis belongs to the author under the terms of the United Kingdom Copyright Acts as qualified by University of Strathclyde Regulation 3.50. Due acknowledgement must always be made of the use of any material contained in or derived from, this thesis.

Signed:

Date:

Acknowledgements

I would like to thank my supervisor Professor Alastair Florence for the opportunity to work with him and his team in the Future Manufacturing Research Hub in Continuous Manufacturing and Advanced Crystallization (CMAC) within the University of Strathclyde and allow me to become an independent researcher.

Special thanks to Dr Cameron Brown, Dr Huaiyu Yang, Dr Thomas McGlone, Dr Andrea Johnston, Dr John Robertson, Dr Nazer Rajoub, Dr Keddon Powell, Dr Humera Siddique, Mr Vishal Raval, Dr Naomi Briggs, Dr Anna Jawor-Baczynska, Prof Fausto Gironi, Mrs Anne Goudie, Dr John Mack and Dr Eduardo Lopez Montero.

I would also like to express my gratitude towards the Engineering and Physical Sciences Research Council (EPSRC) for their financial support and to GlaxoSmithKline (GSK), in particular to Mr Julien Douillet and Dr Jorge Calderon De Anda, for the opportunity to perform an industrial placement during the PhD study, their valuable input and support.

Finally, I would like to thank my family and Flavio for the support, love and encouragement.

Abstract

Pharmaceutical crystals frequently exhibit unfavourable bulk solid properties leading to low downstream processing efficiency and additional unit operations to enhance processing characteristics. Novel particle engineering techniques such as spherical crystallization or spherical agglomeration can be used in order to obtain spherical agglomerates with enhanced properties.

Spherical agglomerates are produced through cooling crystallization in ethanol-water mixture under specific process conditions involving liquid-liquid phase separation; hence ternary phase diagrams were determined experimentally. The liquid-liquid phase region was found to increase with increasing temperature, whilst absent at 20°C. Ibuprofen agglomerates crystallised in the presence of liquid-liquid phase separation showed an increased flowability and higher yield compared to the standard cooling crystallization process.

Spherical agglomerates of lovastatin were prepared by suspension of crystals in water and agglomeration through the action of another solvent called bridging liquid. All the solvents except alkenes led to the formation of spherical agglomerates as long as a sufficient amount is added. The influence of amount of bridging liquid and agitation rate on the properties of lovastatin spherical agglomerates obtained from methyl isobutyl ketone are investigated. With increasing amount of bridging liquid the particle size increased and the shape became irregular.

In a separate chapter, a combined cooling antisolvent seeded crystallization process was monitored using process analytical technologies to investigate the agglomeration under different process conditions. A novel in-house image analysis algorithm coded in MATLAB was used to analyse images of agglomerates recorded by ParticleView V19 probe through descriptors. Images showed that seeds were already aggregated before addition to the reactor indicating an insufficient dispersion. Experiments using the same seed loading led to products with slightly variable particle size distribution but different degree of breakage ranging from moderate to significant breakage. Stronger crystals with larger size were produced when a temperature cycle was applied. Overall this work showed that agglomeration processes can lead to product with enhanced properties, and advanced the scientific understanding of the

agglomeration mechanisms through implementation of process analytical technologies hence facilitating the scale-up and selection of control strategies.

Contents

Declaration of Author's Rights	ii
Acknowledgements	iii
Abstract	iv
List of Figures	ix
List of Tables.....	xvi
List of Abbreviations.....	xvii
Notations	xix
Chapter 1. Introduction.....	22
1.1 Pharmaceutical drugs	23
1.2 Continuous pharmaceutical processes.....	26
1.3 Crystallization	31
1.3.1 Solubility and supersaturation	31
1.3.2 Nucleation.....	36
1.3.3 Crystal growth.....	42
1.3.4 Agglomeration	46
1.4 Attributes of pharmaceuticals.....	60
Chapter 2. Aims and Objectives	63
2.1 Aims	64
2.2 Objectives	65
Chapter 3. Materials and Methods.....	66
3.1 Materials.....	67
3.2 Methods.....	67
3.2.1 X-Ray Powder Diffraction.....	67
3.2.2 Spectroscopy.....	68
3.2.3 Imaging.....	68
3.2.4 Particle sizing.....	69
3.2.5 Flow property.....	70
3.2.6 Thermal analysis	71

Chapter 4. Ternary Phase Diagrams of Ibuprofen in Ethanol-Water Solutions for Understanding Crystallization and Agglomeration.....	72
4.1 Introduction	73
4.2 Ibuprofen	74
4.3 Experimental	78
4.3.1 Determination of solubility	78
4.3.2 Determination of ternary phase diagrams	79
4.3.3 Cooling crystallization experiments	79
4.3.4 Solid characterisation.....	80
4.4 Results and discussion.....	81
4.4.1 Solubility.....	81
4.4.2 Ternary phase diagrams	83
4.4.3 Cooling crystallization.....	88
4.4.4 Solid characterisation.....	92
4.5 Summary	95
Chapter 5. Agglomeration Study of a Pharmaceutical Active Ingredient	97
5.1 Introduction	98
5.1.1 Aims and objectives.....	99
5.2 Experimental	100
5.2.1 Setup and procedures	100
5.2.2 Image analysis.....	103
5.3 Results and discussion.....	106
5.3.1 Image analysis of GSK106	106
5.3.2 In situ monitoring of growth of GSK106.....	119
5.3.3 Filtration and drying	122
5.3.4 Comparison between probes and threshold	128
5.4 Summary	130
Chapter 6. Spherical Agglomeration in Suspension of Lovastatin.....	132
6.1 Introduction	133

6.2	Experimental	136
6.2.1	Materials	136
6.2.2	Methods	139
6.3	Result and discussion	145
6.3.1	Selection of bridging liquid using small scale experiments	145
6.3.2	Classification of agglomeration and non-agglomeration promoting solvents through molecular descriptors using PCA	148
6.3.3	Spherical agglomeration under fixed agitation rate	152
6.3.4	Spherical agglomeration under stepped shear approach	157
6.3.5	Conceptual design of continuous spherical agglomeration	169
6.4	Summary	173
Chapter 7.	Conclusions and Future Work.....	176
7.1	Conclusions	177
7.2	Future work	180
7.2.1	Ternary phase diagram of ibuprofen in ethanol/water solutions for understanding crystallization and agglomeration	180
7.2.2	Agglomeration study of an active pharmaceutical pngredient	181
7.2.3	Spherical agglomeration in suspension of lovastatin.....	182
References	184
Appendices	199
Appendix 1	Supporting information related to chapter 5.....	200
Appendix 2	Supporting information related to chapter 6.....	202
Pubblications	204

List of Figures

Figure 1.1 Solid forms. Adapted from Byn <i>et al.</i> ³	24
Figure 1.2 FDA approved solid state classification system. Adapted from Aitipamula <i>et al.</i> ⁶	25
Figure 1.3 Simplified quality control diagram using QbT. Adapted from Yu <i>et al.</i> ¹¹	27
Figure 1.4 Diagram illustrating solubility curve, metastable zone width and supersolubility curve. Creation of supersaturation in crystallization processes from solution: cooling crystallization (temperature change), evaporation (solute concentration change), antisolvent crystallization (solvent composition change). Adapted from Mullin ²⁸	33
Figure 1.5 Illustration of a typical cooling crystallization process. On cooling, the system moves from T^* to T_{nuc} , where nucleation occurs resulting in the formation of stable crystal nuclei, before following the trajectory of crystal growth. Adapted from Mullin ²⁸	34
Figure 1.6 Mechanisms of nucleation. Adapted from Myerson <i>et al.</i> ²⁷	36
Figure 1.7 Free energy change during nucleation. Adapted from Myerson <i>et al.</i> ²⁷ ..	38
Table 1.1. Primary nucleation expressions. From Myerson <i>et al.</i> ²⁷	39
Figure 1.8 The classical and two-step nucleation model. Adapted from Galkin <i>et al.</i> ⁴⁸	40
Figure 1.9 Diagram illustrating MSZWs of primary and secondary nucleation. Adapted from Ulrich <i>et al.</i> ⁵⁹	41
Figure 1.10 Crystal-solution interface for growth. Adapted from Myerson <i>et al.</i> ²⁷ ..	43
Table 1.2 Growth expressions from Randolph <i>et al.</i> ⁶¹ , Garside <i>et al.</i> ⁶² and Burton <i>et al.</i> ⁶³	44
Figure 1.11 Schematic of adsorption layer theory. Adapted from Mullin ²⁸	45
Figure 1.12 Single crystal (left) and agglomerates (right) of paracetamol. ⁷²	46
Figure 1.13 Schematic of agglomeration. A: two particles brought together by hydrodynamics on a microscopic length scale; B: aggregation, particles held together by short range molecular forces; C: agglomeration, formation of crystalline bridges between particles. Adapted from Beckmann <i>et al.</i> ⁷⁰	48
Table 1.3: Agglomeration kernel and efficiency expressions from Hounslow <i>et al.</i> ⁷⁶ , Thompson <i>et al.</i> ⁸¹ and Zauner <i>et al.</i> ⁸²	52

Figure 1.14 Agglomeration mechanisms of spherical crystallization techniques. Emulsion solvent diffusion (top), emulsion based spherical crystallization (center) and spherical agglomeration or agglomeration in suspension (bottom). Adapted from Peña <i>et al.</i> ⁸⁷ and Kawashima <i>et al.</i> ⁸⁸	55
Figure 1.15 Attributes from crystallization processes. Adapted from Variankaval <i>et al.</i> ⁵	60
Table 1.4 Particle attributes controlled during crystallization. Adapted from Variankaval <i>et al.</i> ⁵ and Cronin <i>et al.</i> ¹¹⁵	61
Figure 4.1 Ibuprofen structure. Figure showing molecular structure of ibuprofen, systematic name (R,S)-2-(4-(2-methylpropyl)phenyl)propanoic acid.	74
Figure 4.2 Ibuprofen packing arrangement: form I (left) and form II (right), CCDC references IBPRAC and IBPRAC04, respectively.	76
Figure 4.3 Scanning electron micrograph of ibuprofen Form I.	76
Figure 4.4 IR spectra for the ibuprofen solution, pure ethanol and pure water.	80
Figure 4.5 Solubility (g solute/g solvent) of ibuprofen in binary solvent mixtures as wt % of ethanol (on a solute free-basis) from 20°C to 55°C. Standard deviation bars are based on 3 replicates; for solubility curves of ibuprofen in pure water and 10% ethanol, the error bars are smaller than the symbol size.	81
Figure 4.6 Ternary phase diagrams of ibuprofen, ethanol and water from 20°C to 55°C expressed in mass fraction.	83
Figure 4.6 continued.....	84
Figure 4.6 continued.....	85
Figure 4.6 continued.....	86
Figure 4.7 Regions of the ternary phase diagram of ibuprofen in ethanol-water mixtures: 1) undersaturated liquid phase, 2) liquid-liquid phase separation, 3) liquid-liquid phase separation with solid and 4) liquid-solid phase.	87
Figure 4.8 FBRM total counts/s with temperature profile, IR peak height and PVM images of exp.1, starting at 45°C in region 1 and ending in liquid-solid region 5 (Figure 4.6).....	90
Figure 4.9 FBRM total counts/s with temperature profile, IR peak height for ibuprofen crystallization experiment 2. Graph showing crystallization from liquid-	

liquid phase separation starting at 45°C in region 2 and ending in liquid-solid region 4 (Figure 4.6).....	91
Figure 4.10 Graph showing nucleation from liquid-liquid phase separation at 45°C in liquid-liquid-solid region 3 and ending in liquid-solid region 4 (Figure 4.6).....	92
Figure 4.11 Ibuprofen habits (10X magnification): a) marketed ibuprofen, b) ibuprofen crystallized from exp.1 and c) ibuprofen agglomerates from exp.2 (liquid-liquid phase separation).....	93
Table 4.3 Results of the analysis of the product obtained from exp.1 (standard crystallization) and exp.2 (crystallization through the liquid-liquid phase separation).	93
Table 4.4 Properties of ibuprofen samples in the range 0-1000 µm.	94
Figure 4.12 X-Ray powder diffraction pattern of ibuprofen: raw material (black), recrystallised from exp.1 (red) and recrystallised from exp.2 (blue).....	94
Figure 4.13 DSC curves of ibuprofen: raw material (blue), recrystallized from exp.1 (green) and recrystallized from exp.2 (red).....	95
Figure 5.1 Schematic of reactor used for the experiments.....	100
Table 5.1 Table illustrating experimental conditions for growth experiments.	101
Figure 5.2 Schematic overview of imaging analysis procedure using PVM Analysis Toolbox.	104
Table 5.2 Shape and size descriptors extracted from Borchert and co-workers ¹⁷⁵ after binarization.....	106
Figure 5.3 Variation of particle number, circularity and circle equivalent diameter (CED, µm) for experiments a) N1, b) N2, c) N3, d) N4, e) N5, f) N6. PVM images are shown at 0 min (seed crystals), 10 min and 30 min after the addition of seeds.	107
Figure 5.4 Population densities analysed during 5 minutes after addition of seeds in the vessel from left to right: size, shape and grey-scale for experiment N1, N2, N3 and N4.	111
Figure 5.4 continued.....	112
Figure 5.5 PVM images of seed crystals for experiment N1, N2, N3 and N4.....	114
Figure 5.7 PVM images of seed crystals for experiment N5 and N6.	116
Figure 5.8 Mean of CED and particle number of experiments N1, N2, N3, N4, N5 and N6.	118

Figure 5.9 FBRM CLDs overlay collected at different stages during growth of agglomerated particles, from seeding to the end of the process for experiment N1.	119
Figure 5.10 FBRM CLDs overlay along with mean square weight at end of the process (before temperature cycle is applied to experiment N5 and N6).	121
Figure 5.11 PVM images of agglomerates captured at 90 minutes after seeding for experiment N3, N5, N6 and at 72 minutes for experiment N4.	122
Figure 5.12 Microscopic images of agglomerates for experiment N5 and N6 at the end of the process.	123
Figure 5.13 SEM and microscope image of experiment N1 and N6 after temperature-cycle.	123
Figure 5.14 Result of the particle size analysis for GSK106 crystals obtained from the Malvern 2000 instrument.	124
Figure 5.15 Microscope images of crystals end of process, after 10 and 1 hr after agitation at 90 rpm.	126
Figure 5.16 Decrease of dv_{50} during agitation at 90 rpm and loss on drying.	127
Figure 5.17 Comparison between descriptors obtained with a single threshold value or multi-segment thresholds for N1.	129
Figure 6.1 Proposed mechanism of agglomeration in suspension for two immiscible liquids: conditioning (a), wetting of seeds (b), coalescence (c) and consolidation (d). Adapted from reference 13.	134
Figure 6.2 Molecular structure of lovastatin (left) and crystal habit (right).	136
Figure 6.3 Lovastatin packing arrangement. CCDC reference CEKBEZ	137
Table 6.1 Properties of solvents used as bridging liquid. From Murov ²⁰⁵ and Van Oss ²⁰⁶ Thati <i>et al.</i> ²⁰⁷	138
Figure 6.4 Setup for batch experiments comprising syringe pump and PAT.	141
Table 6.2 Experimental conditions of batch fixed shear approach experiments.	143
Table 6.3 Portion of bridging liquid (ml) delivered at each stage.	144
Figure 6.5 Stirring rate effect on screening experiments: a) 400 rpm, b) 700 rpm and c) 1000 rpm. MIBK used as bridging liquid.	145
Figure 6.6 The evolution of lovastatin particles agglomeration during screening experiments in the Crystalline. Images were taken from the vial containing from 0 to 160 μ l BL (MIBK), 4 mL DL and 0.2 g particles stirred at 20°C and 1000 rpm at (a)	

0 mins showing suspended particles, (b) 120 μ l of BL added, small flocs, (c) 140 μ l of BL added, larger agglomerates becoming apparent and (d) 160 μ l of BL added, where the curvature of a large agglomerate can be seen as the dark region nearly occluding the image.	146
Figure 6.7 Pictures of crystalline vials from seed suspension to nearly paste behaviour.....	147
Figure 6.8 Non agglomerating behaviour from seed suspension to dissolution of seeds.	147
Figure 6.9 Encrustation on the stirrer (left) during screening of bridging liquid.....	148
Figure 6.10 PCA Score Plot based on MOE descriptors for the solvents tested for classification of agglomerating and non-agglomerating behaviour.	149
Figure 6.11 Volume of bridging liquid determined from screening experiments. For the sake of clarity, the green bar represents the bridging liquid range where spherical agglomerates could be produced, whereas incomplete agglomeration or irregular agglomerates with paste-like behaviour are observed for volumes below the minimum amount (blue bar) or above the maximum amount (sum of blue and green bar) respectively.....	151
Figure 6.12 X-Ray powder diffraction pattern of lovastatin: starting material (blue) and agglomerates produced from MIBK (red).....	152
Table 6.4 Counts/s and SWMCL after 15 mins of suspension of lovastatin in water and at the end of the experiments using MIBK as bridging liquid.	153
Figure 6.13 In situ FBRM counts/s and square weighted mean chord length for experiment carried at 700 rpm and 0.7 BLR.....	154
Figure 6.14 Product obtained from batch agglomeration in suspension experiments at 20°C using MIBK as bridging liquid. A1 and A2 from agitation of 550 rpm with low (BLR of 0.6) and high (BLR of 0.8) amount respectively; A3 from agitation of 700 rpm with BLR of 0.7; A4 and A5 from agitation of 850 rpm with low and high amount respectively.	155
Table 6.5 Properties of lovastatin samples in the range 0-1000 μ m. BD = bulk density, TD = tapped density, CI = Carr's Index and HR = Hausner Ratio. Data are reported in the format mean \pm std dev based on 5 replicates.	157

Figure 6.16 Paste on the tubing delivering bridging liquid and PVM probe (left) and paste on the FBRM probe (right).	158
Figure 6.17 FBRM counts/s and SWMCL of the agglomeration experiment using one addition of bridging liquid at 550 rpm.	159
Figure 6.18 PVM images from experiment using one addition of bridging liquid. From top left to bottom right: a) slurry before addition; b) agglomerates at the end of addition at 550 rpm; c) agglomerates when agitated at 700 rpm; d) agglomerates at end of process at 850 rpm.	161
Figure 6.19 Image of lovastatin agglomerates (left) and microscope image of agglomerates (right) obtained from experiment using single stage addition of bridging liquid after drying.	161
Figure 6.20 FBRM counts/s and SWMCL of the agglomeration experiment using two additions of bridging liquid at 550 rpm and 700 rpm.	162
Figure 6.21 PVM images from experiment using two additions of bridging liquid. From top left to bottom right: a) slurry at the end of first addition at 550 rpm; b) agglomerates during the second addition; c) agglomerates at the end of second addition at 700 rpm; d) agglomerates at the end of process at 850 rpm.	163
Figure 6.22 Image of lovastatin agglomerates (left) and microscope image of agglomerates (right) obtained from experiment using two stage addition of bridging liquid after drying.....	164
Figure 6.23 FBRM counts/s and SWMCL of the agglomeration experiment using three addition of bridging liquid at 550 rpm and 700 rpm.....	164
Figure 6.24 PVM images from experiment using three additions of bridging liquid. From top left to bottom right: a) slurry before addition; b) agglomerates at the end of first addition at 550 rpm; c) agglomerates at the end of second addition at 700 rpm; d) agglomerates at end of process at 850 rpm.....	165
Figure 6.25 Image of lovastatin agglomerates (left) and microscope image of agglomerates (right) obtained from experiment using three addition of bridging liquid after drying.....	166
Table 6.6 Properties of lovastatin samples obtained from stepped shear approach experiments. Data are reported in the format mean±std dev based on 4 replicates.	168

Figure 6.27 Automated spherical agglomeration platform implemented with the Perceptive Engineering control interface.....	170
Figure 6.28 Perceptive Engineering control interface for the multi vessel spherical agglomeration platform.....	171
Figure 6.29 SWMCL, agitation rate and pressure profile used to identify the relation between process variables and product attributes.....	172
Figure 6.30 Product obtained from the continous spherical agglomeration platform at 20°C using MIBK as bridging liquid.....	173

List of Tables

Table 1.1. Primary nucleation expressions. From Myerson <i>et al.</i> ²⁷	39
Table 1.2 Growth expressions from Randolph <i>et al.</i> ⁶¹ , Garside <i>et al.</i> ⁶² and Burton <i>et al.</i> ⁶³	44
Table 1.3 Agglomeration kernel and efficiency expressions from Hounslow <i>et al.</i> ⁷⁶ , Thompson <i>et al.</i> ⁸¹ and Zauner <i>et al.</i> ⁸²	52
Table 1.4 Particle attributes controlled during crystallization. Adapted from Variankaval <i>et al.</i> ⁵ and Cronin <i>et al.</i> ¹¹⁶	61
Table 4.1 Experimental conditions of cooling crystallization experiments.....	79
Table 4.2 Solubility of ibuprofen in binary solvent mixtures. Not reported for concentrations in the liquid-liquid phase region.	82
Table 4.3 Results of the analysis of the product obtained from exp.1 (standard crystallization) and exp.2 (crystallization through the liquid-liquid phase separation).	93
Table 4.4 Properties of ibuprofen samples in the range 0-1000 μm	97
Table 5.1 Table illustrating experimental conditions for growth experiments.	101
Table 5.2 Shape and size descriptors extracted from Borchert and co-workers ¹⁷⁵ after binarization.....	106
Table 6.1 Properties of solvents used as bridging liquid. From Murov ²⁰⁵ and Van Oss ²⁰⁶ Thati <i>et al.</i> ²⁰⁷	138
Table 6.2 Experimental conditions of batch fixed shear approach experiments.	143
Table 6.3 Portion of bridging liquid (ml) delivered at each stage.	144
Table 6.4 Counts/s and SWMCL after 15 mins of suspension of lovastatin in water and at the end of the experiments using MIBK as bridging liquid.	153
Table 6.5 Properties of lovastatin samples in the range 0-1000 μm . BD = bulk density, TD = tapped density, CI = Carr's Index and HR = Hausner Ratio. Data are reported in the format mean \pm std dev based on 5 replicates.	157
Table 6.6 Properties of lovastatin samples obtained from stepped shear approach experiments. Data are reported in the format mean \pm std dev based on 4 replicates.	168

List of Abbreviations

API	Active Pharmaceutical Ingredient
ATR-FTIR	Attenuated Total Reflectance Fourier Transformed Infrared
BCS	Biopharmaceuticals Classification System
BLR	Ratio of volume of bridging liquid in mL to gram of solid
BSR	Bridging Liquid to Solid ratio
CCDC	Cambridge Crystallographic Data Centre
CED	Circle Equivalent Diameter
CI	Carr's Index
CLD	Chord Length Distribution
CMAC	Continuous Manufacturing and Advanced Crystallization
CNT	Classical Nucleation Theory
CQA	Critical Quality Attributes
DMSO	Dimethyl sulfoxide
DSC	Differential Scanning Calorimetry
EMA	European Medicines Agency
Exp.	Experiment
QESD	Quasi Emulsion Solvent Diffusion
EPSRC	Engineering and Physical Sciences Research Council
FDA	Food and Drug Administration
FBRM	Focused Beam Reflectance Measurement
GMP	Good Manufacturing Practice
GSK	GlaxoSmithKline
HR	Hausner Ratio
ICH	International Council for Harmonisation of Technical Requirements for Pharmaceuticals for Human Use
IR	Infrared

LOD	Loss on Drying
MIBK	Methyl Isobutyl Ketone
MOE	Molecular Operating Environment
MPC	Model Predictive Control
MSMPR	Mixed Suspension Mixed Product Removal
MSZW	Metastable Zone Width
NMR	Nuclear Magnetic Resonance
NSAID	Nonsteroidal Anti-inflammatory-Drug
PAT	Process Analytical Technology
PCA	Principal Component Analysis
PSD	Particle Size Distribution
PVM	Particle Vision and Measurement
QbD	Quality by Design
QbT	Quality by Testing
RTD	Residence Time Distribution
SA	Spherical Agglomeration
SEM	Scanning Electron Microscopy
SWMCL	Square Weighted Mean Chord Length
UV	Ultra violet
XRPD	X-Ray Powder Diffraction

Notations

a	Actual solute activity	$[\text{mol L}^{-1}/\text{mol L}^{-1}]$
a^*	Equilibrium solute activity	$[\text{mol L}^{-1}/\text{mol L}^{-1}]$
A	Pre-exponential factor	$[\text{nuclei m}^{-3}\text{s}^{-1}]$
B	Secondary nucleation rate	$[\text{nuclei m}^{-3}\text{s}^{-1}]$
b	Exponent of nucleation	–
c	Actual solute concentration	$[\text{mol L}^{-1}]$
c^*	Equilibrium solute concentration	$[\text{mol L}^{-1}]$
c_i	Concentration at interface	$[\text{mol L}^{-1}]$
$d_{3,0}$	Mean particle size third and zeroth moment	$[\text{m}]$
d_{imp}	Impeller diameter	$[\text{m}]$
g	Exponent of crystal growth	–
G	Crystal growth rate	$[\text{m s}^{-1}]$
G_b	Bridge growth rate	$[\text{m s}^{-1}]$
J	Primary nucleation rate	$[\# \text{m}^{-3}\text{s}^{-1}]$
k	Boltzmann constant	$[1.38 \times 10^{-23} \text{J K}^{-1}]$
K	Kelvin	$[\text{K}]$
k_1, k_2	Constant in the agglomeration efficiency	–
K_{agg}	Agglomeration rate	$[\# \text{m}^{-3}\text{s}^{-1}]$
$k_{b \text{ het}}$	Heterogeneous nucleation rate constant	$[\# \text{s}^{-1}]$
k_b	Nucleation rate constant	$[\# \text{s}^{-1}]$
k_{bcf}	Burton, Cabrera and Frank growth rate parameter	–
k_d	Diffusion rate constant	$[\text{m}^2\text{s}^{-1}]$
K_{disr}	Disruption rate	$[\# \text{s}^{-1}]$
k_g	Growth rate factor	$[\text{m s}^{-1}]$
k_r	Rate constant	–
l_m	Geometric mean of two diameters	$[\text{m}]$
L_1, L_2	Crystal size	$[\text{m}]$
L^*	Initial contact length of two colliding particles	$[\text{m}]$
m	Mass deposited over time	
M	Mumtaz number	–

M_{50}	Dimensionless strength corresponding to an agglomeration efficiency of 0.5	–
N_1, N_2	Concentration of particle in suspension	[# m ⁻³]
p	Parameter in size-dependent growth equation Empirical parameter	–
q	Empirical constant	–
r	Radius of cluster Empirical parameter	[nm] –
r_{agg}	Agglomeration rate	[# m ⁻³ s ⁻¹]
r_c	Critical nuclei radius	[nm]
R	Gas constant	[8.314 J mol ⁻¹ K ⁻¹]
s	Empirical parameter	–
S	Supersaturation ratio	–
t	Time	[s]
t_{cem}	Cementation time	[s]
t_r	Contact time for creation of bridge	[s]
T^*	Solubility temperature	[K]
T_{nuc}	Nucleation temperature	[K]
α	Slope of the fit $\psi (M)$	–
β_{agg}	Agglomeration kernel	[m ³ s ⁻¹]
β_{coll}	Collision kernel or crystal collision rate	[m ³ s ⁻¹]
β_{disr}	Disruption kernel	[min m ⁻³]
γ	Interfacial tension Constant in size-dependent growth equation	[J m ⁻²] –
$\dot{\gamma}$	Shear rate	[s ⁻¹]
ε	Energy dissipation rate	[m ² s ⁻³]
θ	Contact angle	[radians]
η	Liquid dynamic viscosity	[kg m ⁻¹ s ⁻¹]
μ_2	Second moment of the crystal size distribution	[m ² m ⁻³]
μ_{solid}	Chemical potential of the solid phase	[kJ mol ⁻¹]
$\mu_{solution}$	Chemical potential of the solute in solution	[kJ mol ⁻¹]
$\Delta\mu$	Chemical potential change	[kJ mol ⁻¹]

v	Volume of the cluster	[m ³]
ρ	Density of solid	[g cm ⁻³]
σ	Relative supersaturation	–
σ^*	Yield stress	[Pa]
θ	Contact angle	[radians]
ψ	Aggregation efficiency	–
ΔE	Activation energy	[J mol ⁻¹]
ΔG	Free energy change	[kJ mol ⁻¹]
ΔG_{cr}	Critical energy change	[kJ mol ⁻¹]
ΔG_S	Surface free energy	[kJ mol ⁻¹]
ΔG_V	Volume free energy	[kJ mol ⁻¹]

Chapter 1. Introduction

1.1 Pharmaceutical drugs

Pharmaceutical drugs or drugs can be defined as chemical substances intended to be used as cures, treatments, prevention of disease and in medical diagnosis. Drugs are classified in different ways, such as mode of action, route of administration, biological system affected, or therapeutic effects, though a widely used classification system for pharmaceuticals is the Anatomical Therapeutic Classification (ATC) System. An important differentiation within drugs is between small-molecule drugs, which include most of pharmaceuticals and large molecules or biopharmaceuticals which include recombinant proteins, vaccines and blood products. The criterion used to distinguish the two groups is their molecular weight, where small molecules have a molecular weight below 900 daltons (500 daltons for orally administered drugs), whilst large molecules have higher molecular weights.¹

Drugs may be administered in many different dosage forms: creams, injectable solutions, inhalants, sprays, powders, capsules or tablets, depending on the required application and the characteristic of the active pharmaceutical ingredient (API). The transformation from the original drug molecule to the final marketed product that is involved in large scale production must combine technical feasibility with economic sustainability and so effective, robust manufacturing processes that deliver consistent product quality are essential. The majority of drugs are produced as dry solid dosage forms as this presents the most chemically stable form and can be readily processed at industrial scale, is convenient for transportation, packaging and storage and tablets can be easily carried and consumed.² Oral solid dosage forms account for 80 % of the marketed drug products and more than 95 % of the top-selling drug products.³

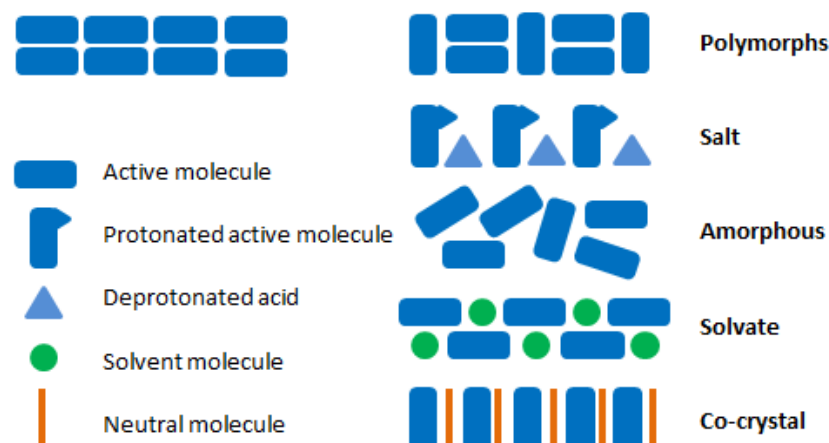


Figure 1.1 Solid forms. Adapted from Byn *et al.*³

Solid APIs can be classified into two categories: crystalline and amorphous. For definition, a crystalline material is a solid having long range order within the unit cell (the smallest group of ordered constituents of a crystal) repeated regularly, while an amorphous material is a solid which lacks such ordering. Crystalline materials are mainly classified into 4 main types: polymorphs, salts, solvates and co-crystals, depending on the components and the arrangement in the unit cell (Figure 1.1).

The delivery of a drug in a safe and economic way depends on the physicochemical properties of its solid state and at the same time, its efficacy depends on the interaction with the appropriate target in the human body at the molecular level. Solid form also dictates key physical properties including aqueous solubility and dissolution rate that can directly impact on oral bioavailability. For low-solubility compounds (dose solubility volume > 250 mL), the rate limiting step is the dissolution of the API in the gastrointestinal fluid and hence can dictate its bioavailability.⁴ More than 90 % of small molecular drugs demonstrate a low solubility in water, encouraging the investigation of different solid forms as potential routes to enhance bioavailability.⁵ The physical properties of the API, including crystal form, size and shape may also impact on wettability, flow, mixing and compaction properties that are of relevance to the ease of manufacture.

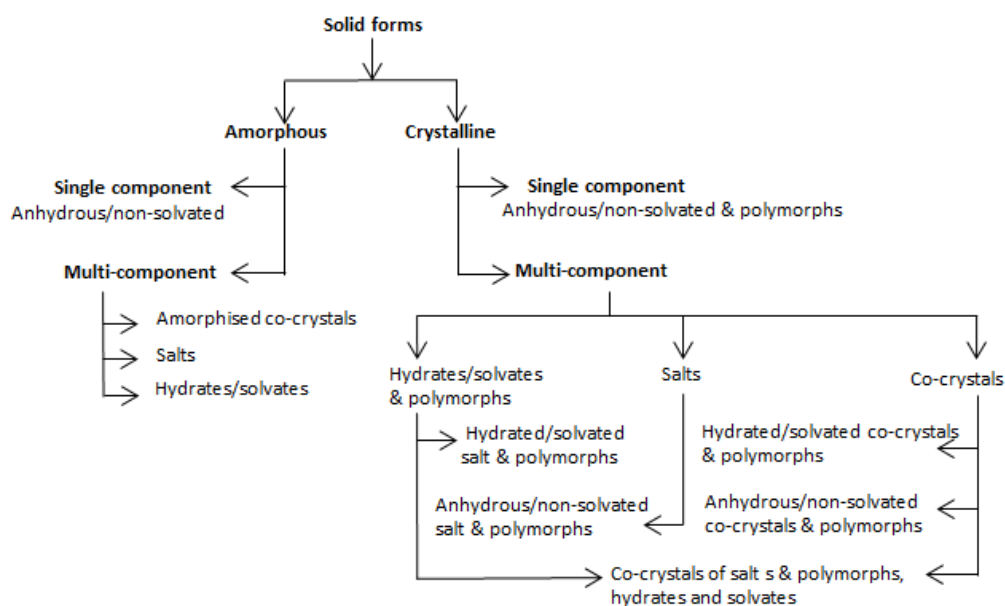


Figure 1.2 FDA approved solid state classification system. Adapted from Aitipamula *et al.*⁶

With the increasing number of publications and patents reporting novel solid state structure, the Food and Drug Administration (FDA) reviewed the solid form classification system to allow the correct classification of novel forms and grouping under multi-component systems for different forms.⁶ Figure 1.2 illustrates the proposed classification system for novel solid state structures of an API.

There are a wide range of techniques that can be used to assess novel solid state structures, such as spectroscopy: Infrared (IR), Raman and solid state Nuclear Magnetic Resonance (NMR) spectroscopy; X-ray Powder Diffraction (XRPD), and Differential Scanning Calorimetry (DSC). Generally new solid state structures are investigated and characterised during preclinical development with salt selection and polymorph screening studies to obtain all possible forms. However, since a change in the polymorphic forms can occur when energy is imposed to the material, such as exposure to elevated temperature or pressure during moving through the manufacturing process, further understanding of the transformations of solid forms and their relative physical stability is required. This informs selection of solid form that will be resistant to undergoing structural transitions under the conditions it will likely be exposed to during processing e.g. T, %RH and P.

A well-documented case of the impact of an unexpected polymorphic change in the pharmaceutical industry is the drug Ritonavir used for the treatment of HIV (trade name Norvir®).⁷ In 1998, several capsules failed the dissolution test and after examination of the content by microscopy and XRPD, a more stable polymorph with lower solubility was discovered. This new polymorph was also found in the bulk storage and formulation areas. Subsequently, the formulation was no longer suitable for the manufacturing process as it failed the dissolution release test. This reduced release of API would reduce the bioavailability of the product rendering it ineffective. As a consequence, the product was recalled from market two years after its release in 1998, which had a significant cost to the company and more importantly, a change of the treatment for the patients until the API was reformulated. In 2010, 60 million tablets of the blood pressure drug Avalide® were recalled from the market due to the appearance of another polymorph after the granulation step and 1.5 million tablets of the blood thinner Coumadin, were recalled from the market due to a higher dosage of active ingredient in the tablets.⁸ There have been significant developments in recent years aimed at enhancing the rigour of polymorph and solid form screening to identify all practically feasible forms. Once a solid form has been selected that has the required chemical and physical properties and stability the crystallization process must be developed to enable production of the API in a suitably pure state. Scale up of traditional batch crystallization processes has been extensively covered in the literature and can be demanding on time and materials contributing to the overall cost of developing new medicines.⁹⁻¹⁰

1.2 Continuous pharmaceutical processes

Continuous processes are well established in oil and gas, food, chemicals, polymers and plastics industries where a production rate of tons per hour is common. However to date, the pharmaceutical industry has mostly relied on batch processes since the quality is ensured in a way that a batch can be either accepted or rejected.¹¹ Production relies on a sequence of batch methods, carried out in accordance with the Quality System (QS) regulation and Good Manufacturing Practice (GMP). Quality

assurance and control requirements in the pharmaceutical industry are increasingly defined using critical quality attributes (CQAs). Processes must be developed that exploit knowledge of the critical material properties (CMPs) and critical process parameters (CPPs) that must be controlled in order to achieve the required CQAs that will assure patient benefit and safety. These approaches are embodied within the drive to adopt Quality by Design (QbD) in pharmaceutical manufacturing (ICH Q8 (R2)).

For example, under the current quality by testing (QbT) regulatory framework for generic drugs, product quality is ensured by testing the materials from the start to the end product using a fixed manufacturing process (Figure 1.3). All drug substances and excipients must meet the manufacturer's and FDA approved specifications or other standards dictated by US Pharmacopoeia Convention (USP) or European Pharmacopoeia (Eu.Ph) to be used in the manufacturing processes. In process and end product testing is then carried out with product quarantined until results confirm specification has been met. At this stage product can then be released for distribution to patients. Whilst this approach does assure patient quality it does lead to inefficiencies, with inventory held up at various stages of production at significant cost. QbD provides a framework that exploits improved fundamental understanding of structure, property, process and performance relationships to provide enhanced assurance and enables greater reliance on PAT and real time release testing (RTRT).

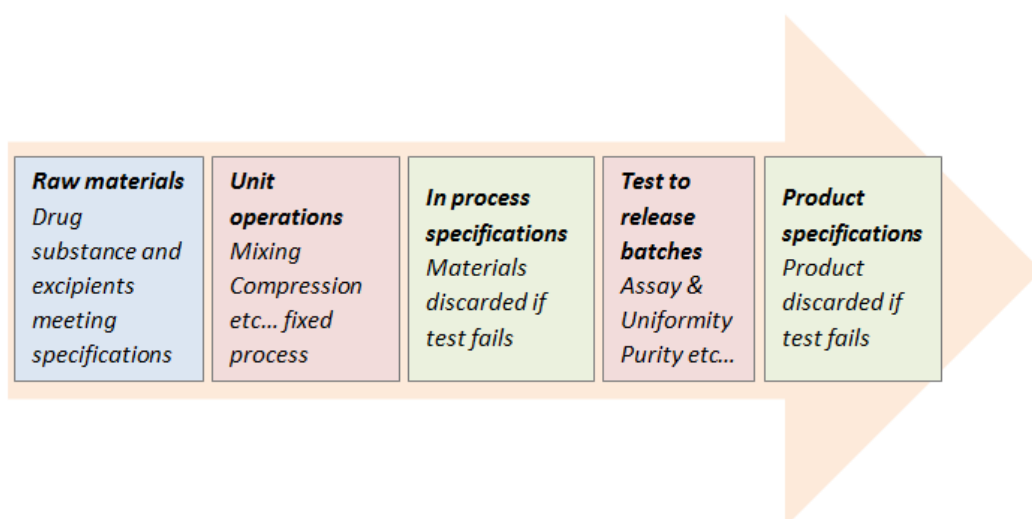


Figure 1.3 Simplified quality control diagram using QbT. Adapted from Yu *et al.*¹¹

Under QbT, any change to a drug substance manufacturing process previously approved may result in providing supplementary information to the regulatory body since the specifications contribute to meet the consistency of a manufacturing process. From a regulatory standpoint, the registration authorities are mostly interested in the product quality and whether the quality of a drug manufactured batch is similar to the quality of the batches used for the clinical trials.¹²⁻¹³ A limitation therefore of QbT lies in the fact that it is based on the inspection of final outcome, i.e. when failure has already happened leading to reworking or even waste of material. Therefore, over the last few years, the FDA has promoted the concept of QbD and the International Committee of Harmonization (ICH) have issued a number of guidelines that pertain to QbD, e.g. from ICH Q8 to Q11 to guide industry on how to prepare regulatory submissions. The focus of this concept is that quality is not tested into the product but rather it should be built into a product. Hence there is increased interest in developing ways to better design drug substance with patient needs considering also drug product and process design, with both knowledge of the risks during manufacturing the product and the best mitigation strategies of these risks.¹¹ Whilst improved batch processes will continue to have a role, there is increasing interest in exploiting the potential benefits of continuous operation for achieving these goals.

For example, the rules for scale-up of different equipment working in batch mode involved in the design of larger scale are not just based on geometrical similarity and it is required to have a better understanding of the effects of different scales. Moreover, the capital invested in equipment and space is extremely high.¹⁴ In contrast continuous processing tends to enable more straightforward scale-up, whether by increasing scale of equipment, increased duration of operation time or numbering up (or scale-out) approaches.

However, resistance to change arises from potential cost, lack of knowledge of the new technologies. Nevertheless in recent years, the potential to manufacture safer, more effective and high-quality products with a reduced cost and time have sparked renewed interest in continuous production within the pharmaceutical industry.¹⁵⁻¹⁶

For example, this increasing interest resulted in the establishment of major collaborative consortiums that include both industry and academia such as the

Novartis-MIT Centre for Continuous Manufacturing funded for \$65 million started in 2009, and the Centre for Innovative Manufacturing in Continuous Manufacturing and Crystallization (CMAC) with a funding portfolio of £150 million started in 2011.¹⁷ Continuous manufacturing is also seeing increased uptake with marketed products now using continuous technologies, in particular for drug product.¹⁸⁻¹⁹

The advantages reported when adopting continuous processing are²⁰:

- Provide better control and reproducibility of products resulting in more efficient production of quality products eliminating the batch to batch variability when working at steady state condition.
- Cost and time saving: the reduction of cost through decreasing labour and equipment costs.
- Reduce waste: the amount of waste is reduced as a result of the improved yield under better control of the process.
- Energy reduction: batch processes consume large amounts of energy and converting to continuous could cut around 95 % of the usage.
- Application of Process Analytical Technology (PAT) for control in real time of continuous processes with the integration of models and simulations to support the development and control of continuous processes.
- Decrease the environmental impact by providing smaller footprint with reduced infrastructures.
- Use of the numbering-up instead of scale-up working with micro-reactors in parallel without altering the scale thus running at high production rate or smaller quantity when required and avoiding high volume storage. This may reduce potential hazardous events and accumulation of hazardous reagents.
- Eliminate breaks between manufacturing steps and reducing human errors during the start-and-stop in batch operation.

Pharmaceutical manufacturing can be divided into two main stages, known as primary (drug substance) and secondary (drug product). These stages are often carried out in different geographical sites or even by different manufacturers. The primary stage involves the production of APIs that can be obtained by chemical synthesis, biological processing, work-up and crystallization/re-crystallization,

isolation and drying steps. Subsequent physical manipulation may also take place such as size reduction (e.g. micronisation) to achieve a required specification. The primary stage includes also the production of excipient(s); in general, these excipients are manufactured by main stream suppliers with the pharmaceutical specifications e.g. compliance with EP or USP standards.

Secondary processing involves the formulation of the API and excipient into the final product. The formulation can include powder blending, extrusion, granulation, compaction, drying, tableting and coating stages. The formulation can be followed by further physical manipulation such as drying, size reduction, size enlargement, filtration and sterilization. Finally the product is filled into the final packaging.¹¹

Crystallization is a key step in manufacturing as it is the major purification technique used in pharmaceutical industry. The design and control of a crystallization process is focused on obtaining yield, purity as well as targeted properties such as the right polymorphic form, morphology, crystal size and crystal size distribution (CSD) which will have a large impact on the secondary downstream processing. These properties need to be consistent through time, since a lack of product consistency can result in downtime, reworking of material to avoid poor drug quality. The adoption of continuous crystallization may lead to several advantages with respect to batch operation such as better impurity rejection, prevention of oiling out, control of CSD, decrease residence time distribution (RTD) and higher yield with recycle.¹⁴ However, it is worth noticing that a continuous process itself is more complex to design, requiring longer experimentation to develop because of the interplaying of parameters and it simply may not be suitable for all processes.

However, adoption of continuous processing requires capital investment for new facilities as well as conversion of the already established facilities and experienced workforce to operate continuous manufacturing plants.²¹ Another hurdle to overcome is the filing/submissions of continuous process documentation to the regulators including the FDA and European Medicines Agency (EMA) given the fact that the pharmaceutical industry is highly regulated and based on submitted documentation for batch manufacturing technologies. Consistency of product quality through implementation of process automation and wider adoption of real-time PAT for

monitoring and control of CQAs are several of the potential advantages to prove the benefits of continuous manufacturing.²²

1.3 Crystallization

Crystallization is a common separation and purification technique used in the chemical and pharmaceutical industries. Depending on the application, crystalline product may be produced from a solution or a melt. Crystallization from solution is the most commonly used in the pharmaceutical industry. During crystallization, crystals with a highly repeating structure are formed, leaving the impurities in solution. There are generally four different methods for inducing crystallization from solution such as cooling, anti-solvent, chemical reaction and evaporation. It is important to choose the most appropriate and efficient method according to the dependency of solubility on temperature. A combination of these methods can also be exploited in order to improve the performance of a crystallization process.²³⁻²⁶

Crystallization is more driven by kinetic aspects rather than thermodynamic, typically described by the rate at which the crystals nucleate and grow under the prevailing process conditions. Supersaturation, whether induced by evaporation, anti-solvent or reaction is the main driving force of crystallization.²⁷ Crystallization involves two main stages, firstly nucleation or the birth of nuclei and secondly growth or enlargement of these nuclei and these are covered in further detail below.

1.3.1 Solubility and supersaturation

The fundamental thermodynamic parameter of solution crystallization is the solubility, defined as the solution concentration in equilibrium with the crystalline solid at a specific temperature and pressure. These solutions are also called saturated solutions, in fact there is a maximum amount of solute that can be dissolved in a given amount of solvent for a fixed temperature and pressure. There are a variety of concentration units to express the composition of a solution; therefore the mass of solute per mass of solvent is often the best unit to use for quantitative applications. In thermodynamics, the equilibrium condition of a saturated solution can be expressed by the chemical potential ($\Delta\mu$). The chemical potential, μ of a molecule in

solution and in the solid phase are respectively μ_{solution} and μ_{solid} such that at equilibrium:

$$\Delta\mu = \mu_{\text{solution}} - \mu_{\text{solid}} \quad (1.1)$$

$$\Delta\mu = 0 \quad (1.2)$$

$$\mu_{\text{solution}} = \mu_{\text{solid}} \quad (1.3)$$

Under a given composition and fixed conditions of temperature and pressure, a solution is undersaturated ($\Delta\mu > 0$), where no crystallization occurs and dissolution is the thermodynamically favoured process. For $\Delta\mu < 0$, the solution is supersaturated, or else the concentration of solid is higher than the equilibrium solubility, hence nucleation and growth can take place to return the system to equilibrium. When $\Delta\mu = 0$, the solution is saturated and an equilibrium between solid and liquid exists and nucleation or growth cannot occur.²⁷ The chemical potential is defined by the reference state chemical potential (μ_0) and the activity (a):

$$\mu = \mu_0 + RT \ln a \quad (1.4)$$

where R = gas constant ($8.314 \text{ J mol}^{-1} \text{ K}^{-1}$), T = temperature (K), a = activity of the solute in the solution. The supersaturation can be expressed as:

$$S = \exp\left(\frac{\Delta\mu}{RT}\right) \quad (1.5)$$

Where $\Delta\mu$ is the difference in the chemical potential and S is the supersaturation. If a is the actual solute activity and a^* is the equilibrium solute activity, the S can be expressed as activity ratio:

$$\ln S = \frac{\Delta\mu}{RT} = \ln \frac{a}{a^*} \quad (1.6)$$

Assuming an ideal solution (activity coefficient of each component equal to one), supersaturation can be approximated by a concentration ratio:

$$S = \frac{c}{c^*} \quad (1.7)$$

Or as a relative supersaturation σ :

$$\sigma = S - 1 \quad (1.8)$$

Where c^* is the concentration at equilibrium at fixed temperature and pressure and c is the actual solution concentration.

A solution can become supersaturated by using different techniques such as cooling, evaporation of the solvent, addition of an anti-solvent to reduce the solubility of the solute in the solvent, chemical reaction leading to the formation of a less soluble product from soluble reactants, or by combination of two or more techniques.²⁷

The choice of a technique for supersaturation generation depends on several factors such as the steepness of the solubility curve with temperature, the volatility of the solvent or the heat sensitivity of the components. The solubility curve or saturated line indicates the concentration of saturated solution at given temperature.

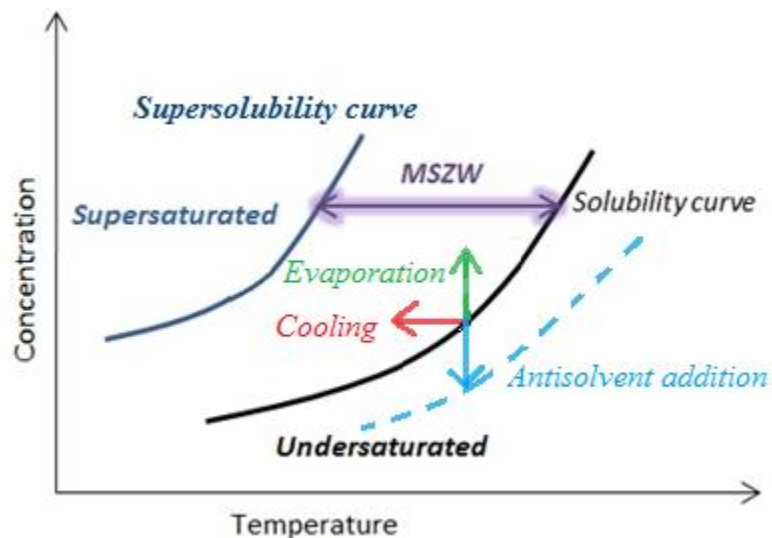


Figure 1.4 Diagram illustrating solubility curve, metastable zone width and supersolubility curve. Creation of supersaturation in crystallization processes from solution: cooling crystallization (temperature change), evaporation (solute concentration change), antisolvent crystallization (solvent composition change). Adapted from Mullin²⁸

The crystallization path induced by the three different methods can be described on the concentration-temperature diagram (Figure 1.4).²⁸ Cooling and anti-solvent crystallization are generally preferred for pharmaceutical crystallization over evaporation.

Nucleation is a kinetic process and solutions have a maximum level of supersaturation that can be reached before they become unstable or nucleate which depends on a wide range of process conditions including temperature, agitation, cooling rate and impurities. For a cooling crystallization, the metastable zone width (MSZW) can be defined as the temperature difference, ΔT between the temperature of the solubility point T^* to the temperature of nucleation T_{nuc} :

$$\Delta T = T^* - T_{nuc} \quad (1.9)$$

The metastable zone is a region between the stable zone (where the crystallization is not possible, even in presence of crystals, defined by the solubility curve) and the labile zone (where spontaneous nucleation can occur).

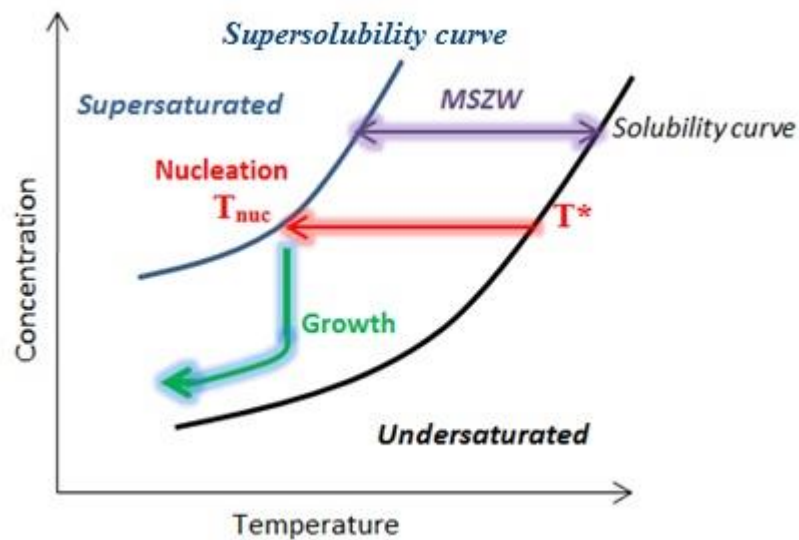


Figure 1.5 Illustration of a typical cooling crystallization process. On cooling, the system moves from T^* to T_{nuc} , where nucleation occurs resulting in the formation of stable crystal nuclei, before following the trajectory of crystal growth. Adapted from Mullin²⁸

The width of the metastable zone gives an indication of the tendency of the system to nucleate, e.g. a large metastable zone indicates systems which have less tendency to nucleate or slower rates of nucleation.

In Figure 1.5, a typical phase diagram for cooling crystallization is illustrated including trajectories for nucleation and crystal growth. For batch cooling crystallization, the MSZW is usually characterised by the polythermal method. Starting from a composition at saturation (the solubility temperature) and decreasing the temperature of the solution, the system moves through the solubility into a labile region where the solution is supersaturated. Nucleation occurs at the supersolubility curve (or metastable limit) resulting in the formation of stable crystal nuclei and subsequent crystals grow at a rate dictated by the supersaturation.²⁹

A certain amount of crystals must be present in order to be detected and thus the measured MSZW is sensitive to the detection technique used. The most common techniques for measurement of the MSZW include refractive index, in situ-imaging, turbidity, focused beam reflectance measurement (FBRM) and spectroscopy such as ATR-FTIR and UV-vis.³⁰⁻³³ Furthermore, measurements of the MSZW for different cooling rates can be employed to determine nucleation parameters such as order and the constant of nucleation hence providing information for crystallization control.³³⁻³⁶

The temperature dependent solubility curve is a thermodynamic property of the system and is thus fixed for a given solvent-solute system. The MSZW is a kinetic boundary and can change depending on process parameters including temperature profile, cooling rate, rate of supersaturation generation, solution history, presence of impurities, agitation and volume. For example, increasing agitation (intense mixing and high shear) and using slower cooling rates reduce the MSZW.^{34, 37-38}

Whilst spontaneous nucleation can only occur within the supersaturated region (often named labile region), supersaturated solutions that lie within the MSZW will support growth of crystals. Hence the addition of seed particles to act as initial growth surface is possible and is commonly used as the working space for crystallization processes. The seeding operation is carried out within the MSZW by addition of a small amount of crystals (with pre-determined properties) to the crystalliser with the aim of growing the particles to obtain a targeted population of product crystals with desired attributes. Strategies for seeding include avoiding the MSZW limits which

promote undesirable phenomena such as uncontrolled secondary nucleation or agglomeration, and also avoiding the solubility limit which would result in a low crystal growth rate and longer process times.

1.3.2 Nucleation

Crystallization is generally described as a two-step process which involves the creation of new crystals (nucleation) and the subsequent growth of these crystals to larger sizes.²⁷ Nucleation occurs in a supersaturated solution with the formation of new, small crystalline entities. In homogeneous solutions, free of all particulates, primary nucleation is the starting phenomena of phase transformation and this creates the initial crystal population. This population may act as sites for crystal growth or may lead to the formation of agglomerates when more crystals are attached together. Nucleation is generally divided into two main categories by the presence or absence of existing crystal nuclei (external entities) (Figure 1.6).

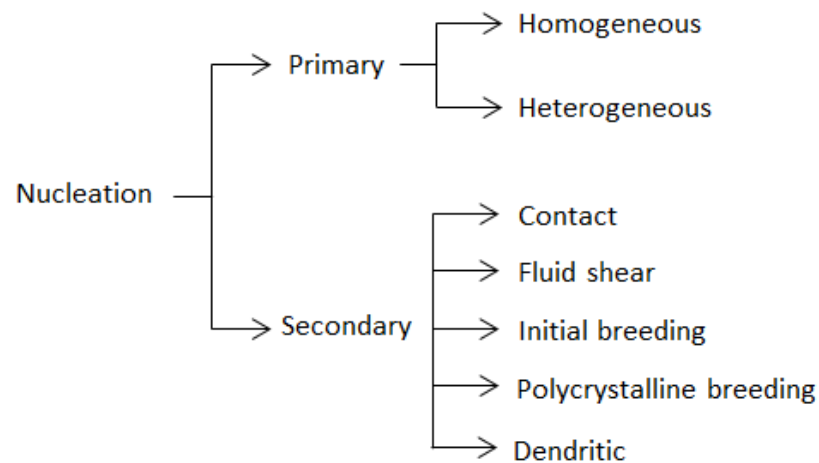


Figure 1.6 Mechanisms of nucleation. Adapted from Myerson *et al.*²⁷

1.3.2.1 Primary nucleation

When nucleation occurs without any particulates present this is referred to as homogeneous primary nucleation.²⁷

Homogeneous nucleation occurs in bulk solution free of particulates, whilst heterogeneous nucleation is induced by foreign particles which act as hetero-nuclei thus accelerating the nucleation process. Heterogeneous nucleation is the most

favoured phenomenon in systems due to the likelihood of finding foreign particles such as impurities and even bubbles which can act as nucleation sites and is widely regarded as the most practically relevant mechanism to describe industrial processes. The total free energy required for heterogeneous nucleation is lower due to the presence of these foreign entities and hence nuclei appear more readily and at lower supersaturation values with respect to homogeneous nucleation. In saturated solutions, the system is at equilibrium and nuclei form and re-dissolve in solution. For nucleation, the solution must be supersaturated and the unstable nuclei need to arrange themselves as stable ordered nuclei or clusters. In supersaturated solutions, the large number of solute molecules/clusters with limited molecular movement increases the likelihood of the formation of stable nuclei.

According to Classical Nucleation Theory (CNT), these clusters are spherical in shape with periodicity like a crystal and they are formed by a molecular addition mechanism described by an Arrhenius expression (equation 1.14). Furthermore, nucleation in supersaturated solution can be described similarly to the condensation of vapour to liquid.³⁹⁻⁴¹ The clusters change their size repeatedly by addition or depletion of a single molecule and only clusters above a critical size survive in solution. Assuming that clusters are spherical with radius r , the total excess free energy (ΔG) required for their formation is the sum of the volume excess free energy (ΔG_V) and the surface excess free energy (ΔG_S):

$$\Delta G = \Delta G_V + \Delta G_S \quad (1.10)$$

$$\Delta G = -\frac{4\pi r^3 \Delta\mu}{3v} + 4\pi r^2 \gamma \quad (1.11)$$

ΔG_S can be obtained from the surface area and the interfacial tension (γ), and the volume free energy (ΔG_V) is given by the volume of the cluster (v) and the difference in chemical potential ($\Delta\mu$).²⁷

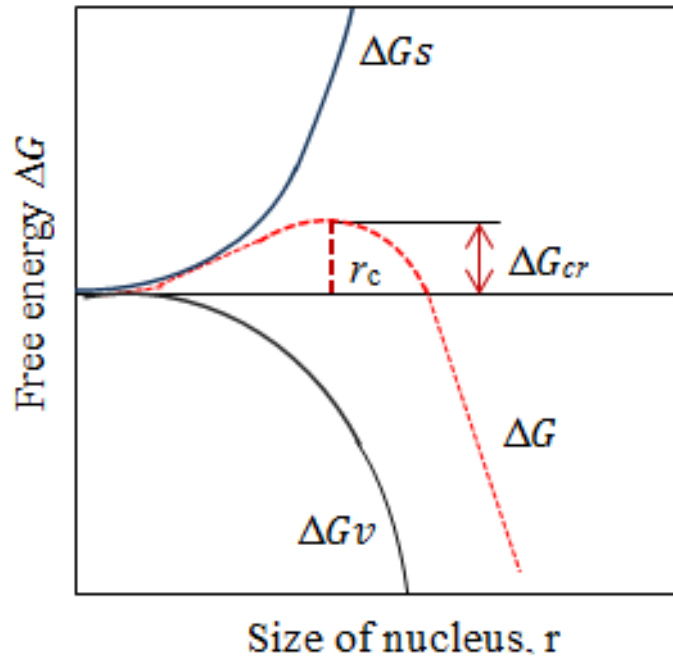


Figure 1.7 Free energy change during nucleation. Adapted from Myerson *et al.*²⁷

Clusters with size r_c are stable and energetically favourable for growth, whilst clusters smaller than the critical size will dissolve and fail to nucleate. For nucleation to occur, the maximum energy ΔG_{cr} required for the formation of a stable nucleus must be produced in the system (Figure 1.7).

However, the production of this energy is not uniform within the system and manifests as fluctuations of molecular velocities and supersaturations; hence nucleation is favoured only in the locations with equal or higher energy than ΔG_{cr} . The critical nucleus size can be obtained from equation 1.11 when the derivative of total free energy with respect to size is zero ($\frac{d\Delta G}{dr} = 0$):

$$r_c = \frac{-2\gamma v}{\Delta\mu} \quad (1.12)$$

The energy required for the formation of a stable nucleus ΔG_{cr} can be calculated by using equation 1.11 and 1.12, with the following expression:

$$\Delta G_{cr} = \frac{16\pi\gamma^3 v^2}{3\Delta\mu^2} = \frac{16\pi\gamma^3 v^2}{3(kT\ln S)^2} \quad (1.13)$$

Where S is the supersaturation, T is the temperature (K) and k is the Boltzmann constant (1.38×10^{-23} J/K). At higher supersaturation, the energy barrier decreases and the critical radius decreases. The rate of formation of nuclei or primary nucleation rate J can be simply expressed as an Arrhenius equation, which describes the number of nuclei formed per unit of time and volume:

$$J = A \exp\left(\frac{-\Delta G_{cr}}{kT}\right) \quad (1.14)$$

Where A is the pre-exponential factor, dependent on the rate of attachment between molecules and the critical nucleus.⁴¹

Table 1.1 shows some expressions of nucleation kinetics available in literature. As can be seen, the nucleation rate is mainly dependent on supersaturation, temperature and interfacial tension.^{27, 42-44}

Table 1.1. Primary nucleation expressions. From Myerson *et al.*²⁷

Nucleation	Equation	Reference
Homogeneous	$J = A \exp\left[\frac{-16\gamma^3 v^2}{3k^3 T^3 (\ln S)^2}\right]$	20
Heterogeneous	$J = k_{b \text{ het}} \exp\left[\frac{-16\gamma^3 v^2 f(\theta)}{3k^3 T^3 (\ln S)^2}\right]$	20

However, the postulated value of the pre-exponential factor is assumed to be in the range 10^{15} - 10^{25} $\text{m}^{-3}\text{s}^{-1}$ and often this assumption leads to over prediction of the nucleation rate with respect to the experimental value. In recent years, several studies suggest that nucleation can be described via a two-step model.⁴⁵⁻⁴⁷ According to this model, droplets of dense liquid are formed in supersaturated solutions (solute molecules form clusters) and these clusters restructure into compact and stable structures (Figure 1.8).⁴⁸ Considering that two steps are involved in this nucleation model, two energy barriers must be crossed before nucleation can begin.⁴⁹⁻⁵⁰

Experimental data to support the validity of this theory are available for proteins, colloidal particles and small organic molecules using dynamic and static light scattering, differential scanning calorimetry (DSC), and small angle X-ray scattering (SAXS).⁵¹⁻⁵⁴

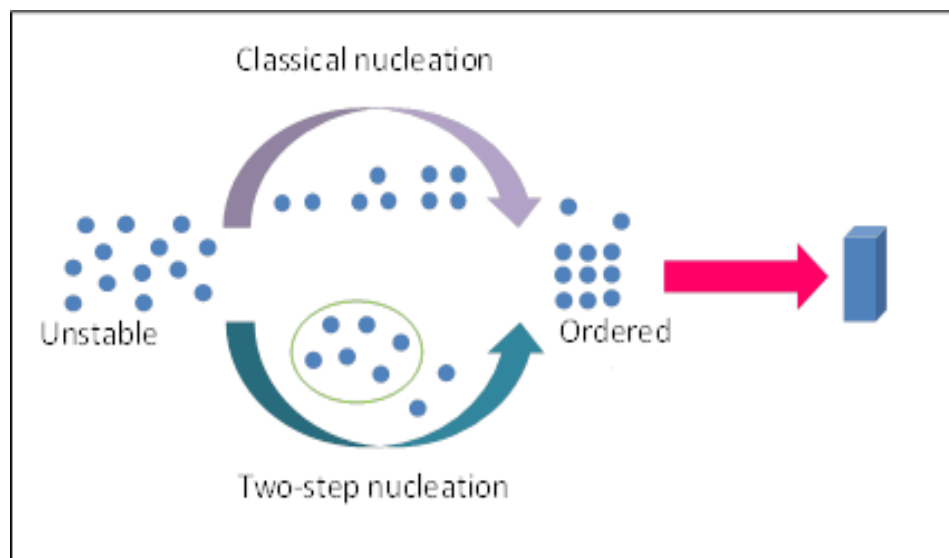


Figure 1.8 The classical and two-step nucleation model. Adapted from Galkin *et al.*⁴⁸

There is limited information about how the molecules restructure in dense liquid-like droplets, thus the mechanistic understanding of the second step is unclear. This second step is proposed as the rate limiting step, which confirms the observation that the time for nucleation is longer for more complex molecules since these exhibit more challenges in arranging themselves into appropriate lattice structures with dependencies on their conformational flexibility.⁴⁹

1.3.2.2 Secondary nucleation

Secondary nucleation is also an important nucleation phenomenon which considers crystal formation occurring in the presence of other crystals (parent crystals).

The most common secondary nucleation mechanism is contact nucleation (contact breeding). Contact nucleation is due to collisions between particles (crystal-crystal) or with the environment, such as crystal-crystallizer wall and crystal-impeller resulting in the production of smaller crystals.⁵⁵⁻⁵⁶

Secondary nuclei can also be removed from the parent crystal under fluid shear, generally known as surface breeding.⁵⁷ Small crystallites formed on the surface of seed crystals during processing or after re-suspension can be removed from the surface and act as secondary nuclei; this phenomenon is known as initial breeding.⁵⁸ Dendrite and polycrystalline aggregates formed from crystals at high levels of supersaturation can lead to the formation of fragments which act as nuclei; phenomena also known as dendritic and polycrystalline breeding respectively.²⁷

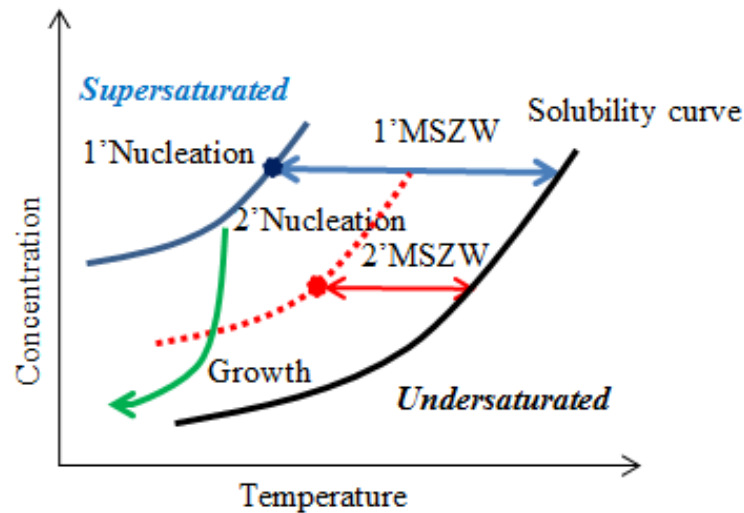


Figure 1.9 Diagram illustrating MSZWs of primary and secondary nucleation. Adapted from Ulrich *et al.*⁵⁹

Secondary nucleation occurs at lower levels of supersaturation with respect to primary nucleation hence the characteristic metastable zone width is nearer to the solubility curve, as shown in Figure 1.9.⁵⁹ Secondary nucleation can be an unfavourable process as it may contribute to a broad crystal size distribution. If a supersaturation level is not controlled, it can lead to broad particle size distributions (PSD) with the production of fines thus compromising downstream processing. However in some cases, secondary nucleation is desirable, especially when seed crystals with the same characteristics of the parent crystals are required, i.e. seeding processes.

Generally, seed crystals are intentionally left in reactors to promote nucleation of the desired form to drive reproducibility from a previous batch. It is worth mentioning that secondary nucleation, spanning a range of different mechanisms, is not

completely controllable since it can start from minor crevices in reactor walls where product from a previous crystallization may be entrapped. As previously discussed, nucleation is the first and most challenging step of a crystallization process, and several difficulties in terms of understanding, characterising and controlling currently exist. The challenge in characterising nucleation lies in the fact that nuclei with critical size cannot be readily detected by in-situ measurements and it can be detected only when crystals reach a detectable size for the instrument in use. In some cases, formation of thin crusts at the boundary of the liquid and the vessel known as fouling or encrustation can become a problem in characterising nucleation since fragments can act as secondary nuclei thus invalidating the detection of primary nucleation. The modelling and prediction of nucleation is often based on empirical expressions that do not account for the influence of operating conditions hence up until the last decade, industrial applications relied upon seeding to control the product outcome. With increasing availability of in-line PAT such as FBRM, coupled with control strategies such as Direct Nucleation Control (DNC), optimal operation can be achieved by varying process conditions until a desired, preselected response is obtained.⁶⁰

1.3.3 Crystal growth

Crystal growth is the second stage of crystallization following nucleation, in which nuclei grow into larger, faceted crystals. Crystal growth includes a series of steps by which an atom/molecule from solution is incorporated into the surface of a crystal, leading to an increase in size. Several theories have been postulated, including surface energy theory, diffusion theory and adsorption layer theory.

The first theory on crystal growth was presented by Gibbs in back in the 1800's and is known as the surface energy theory. Within this theory, the crystal grows in a supersaturated solution until it reaches an "equilibrium shape" which is associated with a minimum surface energy. The equilibrium shape is related to the free energy of the faces and each face grows at a rate proportional to its respective surface energy.

For diffusion theory, the deposition of atoms on a crystal face is considered as a diffusion process. According to this theory, a stagnant film of liquid exists near the

growing face through which solute molecules have to diffuse to reach the surface. The rate of crystal growth is proportional to the concentration difference between the solid surface and the bulk solution.²⁷ This theory describes growth as a two-step process. In the first step, solute molecules diffuse from the bulk solution to the crystal face (absorption onto the crystal surface) and then these molecules arrange themselves into the crystal lattice during the second step; both steps take place under different concentration gradients (Figure 1.10).

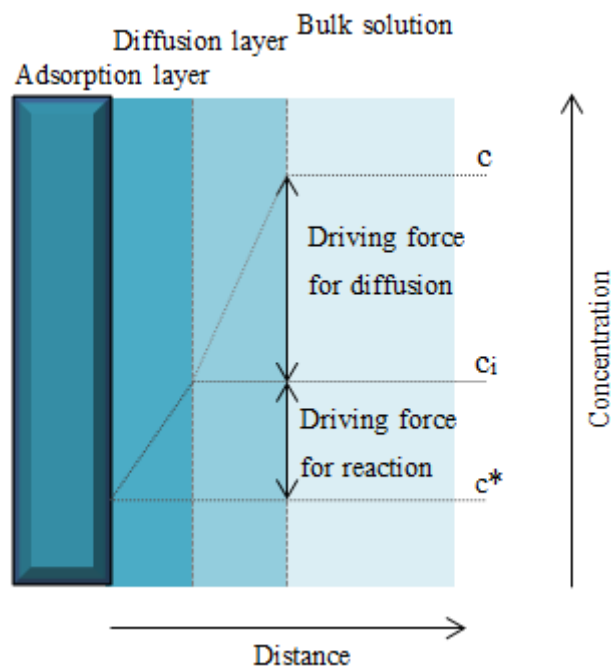


Figure 1.10 Crystal-solution interface for growth. Adapted from Myerson *et al.*²⁷

The diffusion and integration steps can be mathematically described using the following equation:

$$\frac{dm}{dt} = k_d A (c - c_i) \quad (1.15)$$

$$\frac{dm}{dt} = k_r A (c_i - c^*)^r \quad (1.16)$$

where c , c_i and c^* are the solute concentration in the bulk, the solute concentration in solution at the crystal-solution interface and the equilibrium concentration respectively, m is the mass of solid deposited on the surface over time t , A is the surface area of the crystal, k_d is the diffusion coefficient of mass transfer, k_r is a rate constant and r is the integration order, generally valued between 1 and 2.

For convenience, equations 1.15 and 1.16 are combined together to obtain the growth rate, eliminating the interfacial concentration which is difficult to obtain. This yields a growth rate expression using an overall concentration difference:

$$\frac{dm}{dt} = k_g A (c - c^*)^g \quad (1.17)$$

where k_g and g are the overall growth rate factor and growth exponent respectively. Considering the two steps involved, two cases can be discussed in terms of the controlling step. When $k_d < k_r$, the crystal growth rate is controlled by the diffusion of the molecules through the diffusion layer and this is called diffusion or mass transfer limitation. When $k_r < k_d$, the growth rate is controlled by the rate of solute integration at the crystal surface and this is known as surface integration controlled growth. Table 1.2 shows some of the common expressions available in the literature for growth. As can be seen, the growth rate is mainly dependent on supersaturation and temperature.⁶¹⁻⁶³

Table 1.2 Growth expressions from Randolph *et al.*⁶¹, Garside *et al.*⁶² and Burton *et al.*⁶³

Mechanism	Equation	Reference
Growth	$G = k_g e^{-(\Delta E/kT)} S^g$	54
Size-dependent Growth	$G = G^0 (1 + \gamma L)^p$	55
Burton-Cabrera-Frank	$G = \frac{k_g}{k_{bcf}} S^2 \tanh\left[\frac{k_{bcf}}{S}\right]$	56

Adsorption layer theory based on a model provided by Kossel, Stranski and Volmer (KSV theory) with consideration made around the crystal surface structure. According to this model, the crystal surface is made up of cubic units and each layer

has a monoatomic height and it is limited by steps (or edges). These steps contain kinks and the area between steps is called terrace where growth units, clusters or vacancies can be found (Figure 1.11).

For the structure of the surface discussed, growth units attached to the terrace forms via only one bond, whereas two and three bonds are available for units attached to steps and kinks respectively.²⁸

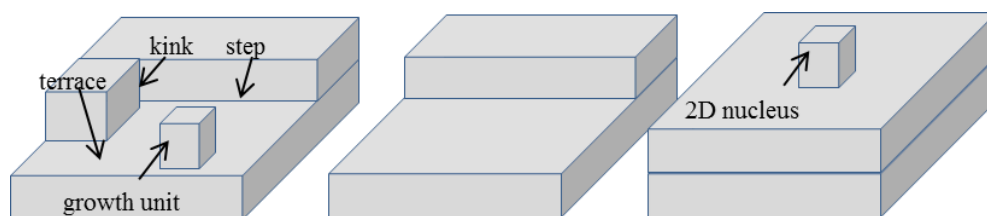


Figure 1.11 Schematic of adsorption layer theory. Adapted from Mullin²⁸

The kink site is the most favoured position and growth will proceed via attachment of units along the step until the face edge is reached, completing a whole plane. This mechanism of growth is known as layer growth or single nucleation growth and is represented in Figure 1.11. Thereafter, a new centre of crystallization or 2D nucleus must be attached to the surface before growth proceeds. If the nucleation rate is faster than the time required for the step to complete the surface, 2D nuclei may form all over the surface and on the top of other nuclei (forming many layers). This growth mechanism is commonly known as the birth and spread or multi-nucleation multilayer growth model.⁶⁴

Seeded crystallization such as controlled growth of seed crystals, is the most common method used in industrial application for moving towards a target product, eliminating primary nucleation from the crystallization process. Seeding approaches include model based methods and supersaturation control, which easily allow crystallisers to operate at low supersaturations within the metastable zone width, away from the metastable limit.⁶⁵ Provided the system remains supersaturated, crystals present will continue to grow, the rate of which is influenced by supersaturation, temperature, agitation, impurities and the occurrence of agglomeration.

Seeds are generally produced via milling, high shear mixing, grinding, and sieving. However, these processes influence significantly the properties and quality of the seed material such as introducing disorder, causing amorphization, inducing phase transformations and creating surface roughness, which subsequently will impact on crystal growth and the final product outcome.⁶⁶⁻⁶⁸ An accurate understanding of crystal growth processes and surface properties is extremely important for model prediction and process development. Reliable models facilitate the design of a process to achieve target crystal sizes or meet therapeutic effects, thus reducing problems for API manufacture and formulation.

1.3.4 Agglomeration

As discussed previously, nucleation and growth are the primary particle formation processes during crystallization. However under agitation, secondary processes such as particle breakage and agglomeration can occur, thus affecting particle attributes such as product form, shape and PSD.⁶⁹ Agglomeration is a particle size enlargement process by which small crystals adhere and grow together to form larger solid particles and the characteristics of an agglomerate depend on the mechanism of agglomeration and the process conditions.⁷⁰

Moreover, depending on the application, the internal structure of an agglomerate may have an open structure to allow rapid dissolution for pharmaceuticals or a more dense structure which allows slow release of its components which may be useful in specific applications.⁷¹ Agglomerated particles do not exist as discrete crystals and have an appearance comprising multiple crystals (Figure 1.12).

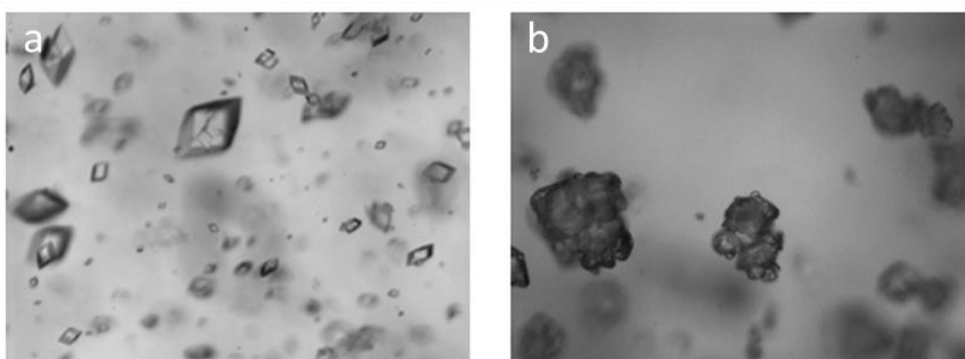


Figure 1.12 Single crystal (left) and agglomerates (right) of paracetamol.⁷²

For agglomeration to occur, two or more particles have to collide and through a cementation process a solid bridge is formed between particles. For solid bridge to be formed, supersaturation is required and the higher it is, the more likely the strength of the bridge.⁷⁰

Crystal agglomeration can be described as a three stage process (Figure 1.13):

- (i) Crystal collision: attractive forces must exceed repulsive forces otherwise disintegration will be predominant;
- (ii) Attractive forces hold the crystals together: formation of loosely bound aggregates which are weak and easy to disintegrate;
- (iii) Aggregates are strengthened into agglomerates by the formation of strong crystalline bridge.

It is evident that the likelihood of particles to undergo agglomeration strongly depends on the characteristics of the surface and the collision between particles. The main particle interactions are Van der Waals attractions, electrostatic forces and steric effects which each depend on surface charges, shape and size of the particles, solution composition, temperature and the particle separation distance.⁷⁰ Surface charge or zeta potential is usually used for the description of particles dispersed in aqueous solutions forming an electrical double layer with opposite charge (overall electroneutral), which in turn is influenced by a number of parameters such as pH, ionic strength or presence of additives; where a lower surface charge support agglomeration and a higher surface charge inhibits agglomeration by hindering the first contact.

Investigation of the degree of agglomeration of paracetamol in ternary mixtures of acetone-toluene-water and pure solvents such as ethylene glycol, isopropanol and acetic acid showed a lower degree of agglomeration in systems of more polar solvents.⁷³ In these systems, a high polarity coincided with hydrogen-bond donating and accepting capabilities and polar solvents interact strongly with both donating and accepting sites of the paracetamol surface thus hindering the adhesion between the surface and formation of crystalline bridges. In addition, for a high concentration of acetone in the ternary mixtures, the degree of agglomeration was higher and agglomerates were stronger than the other systems.

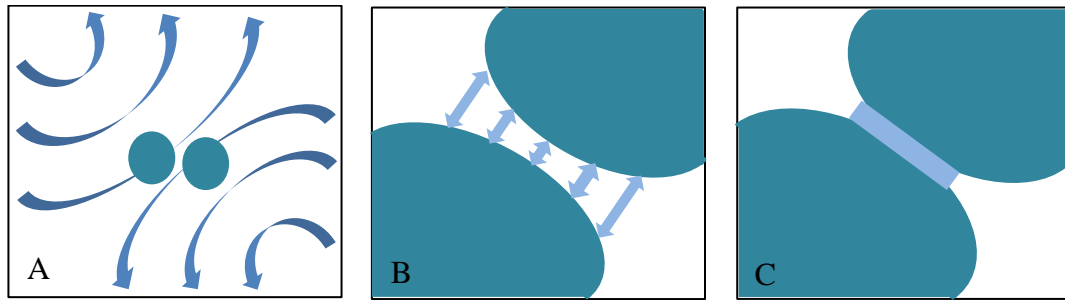


Figure 1.13 Schematic of agglomeration. A: two particles brought together by hydrodynamics on a microscopic length scale; B: aggregation, particles held together by short range molecular forces; C: agglomeration, formation of crystalline bridges between particles. Adapted from Beckmann *et al.*⁷⁰

Agglomeration is mainly classified into two types such as primary and secondary. Primary agglomeration refers to the formation of composite crystals from “mal-growth” of crystals which it is dependent on the internal arrangement and it occurs from single crystals. The composite crystals are formed by individual crystals arranged within a structure of parallel units and common examples are dendrites and twins. Primary agglomeration is postulated to be a consequence of impurity interaction or diffusion limitations at high growth rates but only a few reports are available on primary agglomeration kinetics.⁷¹

Secondary agglomeration is the most common type of agglomeration and it refers to the formation of aggregates or agglomerates in suspension due to the collision of more than one crystal induced by flow. Often confusion exists between the terms aggregate and agglomerate for particle description. To clarify, an aggregate is a group of particles which have undergone the first two stages of the above mechanism (Figure 1.13), whilst an agglomerate has undergone all three stages.⁷⁴

Furthermore, agglomerates are irreversibly formed in a supersaturated solution and can be disrupted only by crystal breakage, attrition and erosion, whereas an aggregate can be formed in a saturated or supersaturated solution and can be disrupted, redispersed and form secondary agglomerates.⁷⁵

In addition, aggregates and agglomerates show different strengths of interparticle bonds, for example by compression of the powder under a microscope slide; aggregates will undergo considerable breakage resulting in a larger number of fines,

whereas agglomerates will remain relatively unchanged. Coagulates and flocculates are other common terms used which refer to groups of two or more particles held together by weak cohesive forces.

The agglomeration rate r_{agg} can be expressed via a bimolecular reaction as:⁷⁶

$$r_{\text{agg}} = \beta_{\text{agg}} N_1 N_2 \quad (1.18)$$

Where β_{agg} is the agglomeration rate coefficient or kernel and relates the rate of aggregation events per unit volume of suspension to the number density N_1 and N_2 expressed as concentration of particles per unit volume. The kernel depends on the mechanism of agglomeration and particle size; smaller particles (less than 1 μm) collide and agglomerate due to Brownian motion resulting from fluctuation in solution, known as perikinetic agglomeration, whilst larger particles agglomerate due to collisions resulting from velocity gradients in the bulk solution, known as orthokinetic agglomeration, both assuming a ‘perfect’ well-mixed stirrer tank. In 1916, Smoluchowski presented an agglomeration kinetic expression for particle collision due to fluid shear (orthokinetic case).⁷⁷

Assuming collisions of perfect efficiencies (or where all collisions result in agglomeration), the collision rate of two spherical particles resulting from the collision in a laminar shear field with shear rate $\dot{\gamma}$ (orthokinetic agglomeration) can be expressed as:

$$r_{\text{coll}} = \frac{1}{6} \dot{\gamma} (L_1 + L_2)^3 N_1 N_2 \quad (1.19)$$

Where L_1 and L_2 are the particle size of the aggregating particles. Consequently, the Smoluchowski’s kernel due to fluid shear is expressed as:

$$\beta_{\text{agg}} = \beta_{\text{coll}} = \sqrt{\frac{8\pi\varepsilon}{15\nu} d_{3.0}^3} \quad (1.20)$$

Where β_{coll} is the collision kernel (or collision frequency) and describes the likelihood of two collided particles to generate a stable agglomerate and depend on

particle size and flow regime of the continuous phase, ε is the energy dissipation rate, ν is the liquid kinematic viscosity and $d_{3.0}$ is a mean particle size for a monodisperse system and is calculated from the third and the zeroth moments of the number density function. From the expression it can be noticed that the agglomeration rate increases with the volume of the particle and the velocity gradient; the larger the particle, the higher the probability to be involved in an agglomeration event. However, the aggregation efficiency is relatively low and decreases with increasing particle size thus imposing limitations on particle size and justifying the introduction of size terms in the Smoluchowski model. This is thought to be due to not all the collisions being successful in promoting agglomeration due to fluid shear.

A further extension of Smoluchowski model which accounts for an efficiency term can be introduced relating the two constants:⁷⁶

$$\psi = \beta_{\text{agg}} / \beta_{\text{coll}} \quad (1.21)$$

Where the efficiency of aggregation ψ depends on the strength of the neck formed between two colliding particles and to the hydrodynamic forces acting to pull the particles apart.⁷⁶

The most common expression used for modelling the agglomeration process with an efficiency extension is based on the so-called Mumtaz number M , where the number is a dimensionless measurement of the strength of the crystalline bridge between the aggregates.^{76, 78-79} A semi-empirical model for estimating ψ , considering the initial contact of two colliding particles along a line of length L^* , can be defined by the expression below, where M is:

$$\psi = \frac{(M/M_{50})^\alpha}{1 + (M/M_{50})^\alpha} \quad (1.22)$$

$$M = \frac{\sigma^* L^* G}{\mu d_{3.0}^2 \dot{\gamma}^2} \quad (1.23)$$

Where M_{50} is a fit parameter of the model used to represent the value of the Mumtaz number when ψ is equal to 0.5, which means that 50 % of the collisions lead to a single agglomerated particle; α is the slope of the fit for $\psi (M)$, σ^* is the yield stress and represents the fracture stress of the crystalline bridge.

Several expressions have been described in the literature for ψ , however the most common approach is to use the ratio of two characteristic times, namely, the cementation time t_{cem} or the time required to create a strong bridge between particles and the interaction time t_r or the contact time available to build such a bridge, expressed as the following equations.⁸⁰

$$\psi = \left(1 + k_1 \frac{t_{cem}}{t_r}\right)^{-1} \quad (1.24)$$

$$t_r = 0.1 \left(\frac{d_{imp}}{\varepsilon}\right)^{1/3} \quad (1.25)$$

$$t_{cem} = k_2 \frac{(\varepsilon\nu)^{1/2} l_m^2}{G_b} \quad (1.26)$$

Where k_1 and k_2 are constant, d_{imp} is the diameter of the impeller in the crystallizer G_b , is the bridge growth rate, l_m is the geometric mean of the two effective diameters, ν is the kinematic viscosity and ε is the energy dissipation rate.

Disruption and breakage of the newly formed aggregates may also occur due to fluid shear or collision, where the crystalline bridges are not completely cemented.

Disruption and breakage can be expressed similarly to the agglomeration rate mentioned above, to give an expression:

$$K_{disr}(L_1, L_2) = \beta_{disr}(L_1 + L_2)^3 \quad (1.27)$$

Where β_{disr} is the disruption kernel and the disruption rate is proportional to the particle volumes and increases with increasing particle size.⁷⁴ The disruption mechanism of turbulent crystal-shear forces is dominant over the agglomeration process. Furthermore, even for disruption, supersaturation can be taken into account and this gives rise to the expression:

$$K_{\text{disr}}(L_1, L_2, \varepsilon, S) = \beta_0 \varepsilon^r S^s f(L_1, L_2) \quad (1.28)$$

Where the disruption rate can be expressed with a power law function of the dissipation energy and supersaturation, where disruption increases with increasing power input and decreasing supersaturation.

Mechanisms of breakage can differ however and depending on the breakage event, can be described with three different functions: 1) particle splitting: where there are two daughter particles of the same size or similar; 2) attrition or abrasion: where two daughter particles are of different size; 3) multiple breakage or micro-attrition: where there are many daughter particles.

The overall agglomeration rate, considering the process of aggregation by collision and potential breakage can be expressed with a general empirical formulation:

$$K_{\text{agg}}(L_1, L_2, \varepsilon, S) = \beta_{\text{agg}} \varepsilon^p S^q f(L_1, L_2) \quad (1.29)$$

The rate of agglomeration can be expressed with a power law function of the energy dissipation and supersaturation, where agglomeration increases with decreasing power input and increasing supersaturation, while the size of crystals can be expressed into account with a different function.⁷¹ Many models and expressions have been published for the agglomeration kernel with factors which appear to affect agglomeration such as process parameters and particle properties like characteristic lengths. Common models used in the literature can be found in table 1.3.^{76, 81-82}

Table 1.3: Agglomeration kernel and efficiency expressions from Hounslow *et al.*⁷⁶, Thompson *et al.*⁸¹ and Zauner *et al.*⁸²

Model	Equation	Reference
Hounslow <i>et al.</i>	$K_{\text{agg}} = \psi \beta_{\text{coll}}$	69
Thompson <i>et al.</i>	$K_{\text{agg}} = \beta_{\text{agg}} \frac{(L_1^3 - L_2^3)^2}{L_1^3 + L_2^3}$	74
Zauner <i>et al.</i>	$K_{\text{agg}} = 5.431 * 10^{-17} \left(1 + 2.296 \varepsilon^{\frac{1}{2}} - 2.429 \varepsilon \right) S^{2.15}$	75

The parameters of the agglomeration kernels are deduced from experimental data of PSD and require the solution of population balance equations which are used to describe mathematically the PSD.⁷¹

The formation of agglomerates can be observed in any stage of solid-state processing, from particle generation to storage thus changing the resulting product performance. These agglomerates can be desirable or undesirable depending on downstream processing and application of the product. Traditionally, agglomeration is exploited by industry to achieve the desired product properties such as increased filterability of particles from the mother liquor, or reducing dust-release and avoiding segregation during handling and processing. Agglomerates can be more difficult to wash because mother liquor and impurities can be entrained inside the solid particles. Agglomeration can also improve the flowability and compaction properties of particles. However, this is only generally true for spherical agglomeration; irregularly shaped agglomerates have negative effects in these respects when compared to single crystals. Agglomeration is not limited to occurrence in agitated fluid crystallization; it can also be pursued in processes such as granulation where a liquid binder is used for agglomerating particles in rotating dishes, drums or pans.

1.3.4.1 Spherical crystallization

Pharmaceutical powders are usually granulated or agglomerated in a spherical shape since this promotes: a) production of agglomerates with free flowability and uniform packing abilities required for processing, b) enhancement of filtration, c) an increase in dissolution rates due to the internal structure of the agglomerates, d) direct tableting since the agglomerates can be easily combined with other components due their improved micromeritic properties, e) uniform coating of agglomerates may be possible.

Generally, the pharmaceutical industry relies on wet or dry granulation to produce spherical agglomerates. The choice to perform one or the other depends on the physical and chemical stability of the compound to be in contact with liquids.

However, it is advantageous if the granules/agglomerates can be produced after the precipitation of crystals during the crystallization step such is in spherical crystallization processes.

Spherical crystallization is a particle design technique that simultaneously combines the crystallization and agglomeration to transform crystals into compacted spherical forms in which agglomerates possess improved micromeritic properties such as flowability and compressibility due to the isotropic texture of the agglomerates, and in several cases improved dissolution rates and enhanced bioavailability attributed to the enhanced wettability of the particles or to the loose structure of the agglomerates along with fine primary particles.⁸³⁻⁸⁴ Agglomerates with improved properties may be suitable for direct compression and therefore allow reduction of equipment space and cost, lower labour costs, decreased energy consumption and processing time since only crystallization, filtration, drying, blending and tableting are required for the production of tablets.

1.3.4.1.1 Spherical crystallization methods

Spherical crystallization can be carried out via four methods:

- Spherical Agglomeration (SA)
- Emulsion solvent diffusion (ESD)
- Ammonia Diffusion System (ADS)
- Neutralization

In the first instance, agglomeration in suspension was developed as a particle size-enlargement method which consists of adding a small quantity of bridging liquid to a suspension of nano- or micro-particles to produce spherical agglomerates.⁸⁵ This method has been extensively used for the selective separation of coal from multi-component solid suspensions.⁸⁶

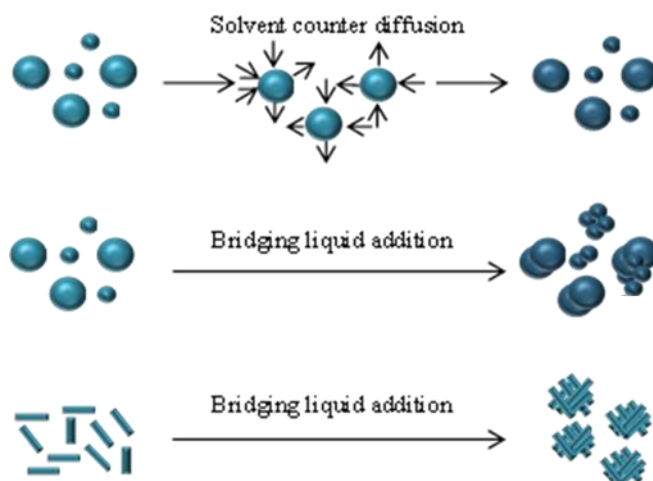


Figure 1.14 Agglomeration mechanisms of spherical crystallization techniques. Emulsion solvent diffusion (top), emulsion based spherical crystallization (center) and spherical agglomeration or agglomeration in suspension (bottom). Adapted from Peña *et al.*⁸⁷ and Kawashima *et al.*⁸⁸

Inorganic compounds such as graphite, silica, sand, glass and calcium carbonate were also studied as model compounds with the aim of investigating the mechanisms, kinetics and effects of process variables on spherical agglomerates.⁸⁸⁻⁹¹

In Figure 1.14, the most common spherical crystallization mechanisms for two and three solvent systems are illustrated. The difference between two and three solvent systems is actually the presence or absence of agglomeration. Generally, a mixture of miscible or partially miscible solvents is required for the application of spherical crystallization. Combinations of solvents which are suitable for spherical crystallization are usually selected by trial and error and a systematic selection based on solvent and solid properties is relatively limited in terms of general rules which can be used as starting point.⁹²

Two solvent systems are normally emulsion based spherical crystallization, where a “good solvent” readily dissolves the compound to be crystallised, and a “poor solvent” acts as an anti-solvent to create the required supersaturation. The “affinity” between the drug and the good solvent is stronger than that between the two solvents. Due to the increased interfacial tension, the drug solution is dispersed into the poor solvent creating emulsion droplets, even though the pure solvents are normally miscible. The poor solvent promotes crystallization inside the emulsion droplet due to the establishment of a counter diffusion of the good solvent and the poor solvent

into and out of the emulsion droplet.⁹³ Furthermore, oil in water (or water in oil) systems can undergo emulsion based spherical crystallization due to the immiscibility between the two solvents.

The ESD approach is considered to be simpler than SA, but challenges lie on the selection of the additive for the emulsification and for the diffusion of the poor solvent in the dispersed phase. On the other hand, SA has been more frequently used than other methods because it doesn't require the formation and stabilisation of an emulsion thus it is easier for operation and selection of the solvent system. Using ESD, the poorly compressible crystals of acebutolol hydrochloride were agglomerated via a two-solvent system showing improved compressibility for direct tableting with respect to the single crystals.⁹⁴

In order to design and control size, shape and internal structure of the agglomerates, the mechanism of particle formation and the kinetic model as a function of the droplet size were investigated using a ketoprofen-acetone-water system using Mowiol® 8-88 to improve the dispersion of the ketoprofen solution and it was reported that the shape and structure (internal and external) of the agglomerates were dependent on the solvent/anti-solvent ratio and the difference in temperature between the two solvents.⁹⁵

In addition, spherical crystallization in binary mixtures may occur via different mechanisms such as quasi-emulsion solvent diffusion (QESD) or spherical agglomeration (SA) depending on the ratio between good and poor solvents, which subsequently changes the composition of the system.⁹⁶ A ternary system requires a good solvent to dissolve the drug, a poor solvent for precipitation and a bridging liquid to promote the agglomeration of the precipitated drug. The good and poor solvents are completely miscible and the stronger "affinity" between these solvents than the affinity between drug and good solvent induces the precipitation of the drug. The bridging liquid must be immiscible with the poor solvent and acts as an inter-particle binder which preferentially wets the particles. Under agitation, collision between wet precipitated particles enhances adhesion with the formation of liquid bridges and facilitates the agglomeration. Formation of liquid bridges between particles was explained to be the result of interfacial tension and capillary forces exerted between two particles in contact.⁹⁶⁻⁹⁷

Salicylic acid was the first pharmaceutical compound to be agglomerated into a spherical shape by mixing an API-ethanol solution with a water-chloroform mixture. Factors such as agitation rate, temperature, bridging liquid content and residence time were recognised to be the most important parameters affecting the properties of the agglomerates produced. Other pharmaceutical compounds such as aminophylline and sodium theophylline monohydrate were also agglomerated using the same solvent system. In these works, the mean agglomerate size was shown to decrease with increasing agitation and decreasing bridging liquid content.^{83, 98-99}

In addition, the spherical crystallization process was defined for the first time as a process in which nucleation, growth and agglomeration occur simultaneously to create spherical agglomerates.

Modification of the spherical crystallization technique such as ammonia diffusion is reported for enoxacin; where an ammonia-water solution of enoxacin was added to an agitated mixture of acetone and dichloromethane. Diffusion of acetone inside droplets caused the precipitation of crystals and the ammonia-water droplets collected the crystals precipitated and transformed them into spherical agglomerates. In this study, the ammonia-water mixture played both the role of good solvent and bridging liquid, and the agglomeration behaviour was described in terms of a ternary phase diagram.¹⁰⁰ With this method, also norfloxacin and ampicillin tri-hydrate were agglomerated into a spherical shape.¹⁰¹⁻¹⁰²

The neutralization method has been used to transform fine crystals of tolbutamide into spherical agglomerates. The drug was dissolved in a sodium hydroxide solution and added to an aqueous solution of hydroxypropylmethylcellulose (HPMC). Neutralization of the sodium hydroxide solution was carried out with the addition of hydrochloric acid, which promoted crystallization, and ethyl ether was added dropwise to promote agglomeration of the crystals.¹⁰³

Monitoring techniques for spherical crystallization have not been widely implemented to date. Using in-situ image analysis, the agglomeration kinetic of salicylic acid was investigated via the use of a CCD camera positioned outside the vessel, therefore a non-invasive technique.¹⁰⁴

1.3.4.1.2 Influence of process parameters

Studies have been carried out to investigate the influence of process parameters on the resulting product.^{88, 105-108} Concerning the solvent composition, an optimum amount of bridging liquid to be added to the systems or a range of operations must be identified, since lower or higher than the optimum amounts can lead to a product not completely agglomerated with fine crystals, the formation of very large agglomerates or a paste (two liquid phase separations with a slurry on the top layer). In general, the average agglomerate size is influenced by the amount of bridging liquid and the size of the raw material. For lactose, the action of the bridging liquid depends on the particle size, for raw material of particle size below 100 μm , the average diameter of agglomerates increases with increasing amount of bridging liquid, and for particles above 260 μm , where the average diameter of agglomerates was independent of the amount of bridging liquid and showing that agglomeration was incomplete with a tendency to be more porous.¹⁰⁹

The second important parameter was identified as the hydrodynamic condition. The effect of agitation rate can affect the average diameter of agglomerates and also an optimum agitation rate must be identified, since increasing agitation can lead to more consolidated agglomerates, whilst exceeding the optimum agitation rate, disruptive forces can be predominant and for sufficient high stirring rate the final agglomerates tend to be less porous and stronger.¹¹⁰

The effect of temperature was investigated for the spherical agglomeration of salicylic acid from the water-ethanol-chloroform mixture. The temperature influences the amount of precipitated crystals available for agglomeration. At lower temperatures, the recovery of salicylic acid increases, while the average crystal size and solubility of bridging liquid in the system decreases. The agglomerates were bulky, less spherical and more porous with increasing temperature. The kinetics of nucleation, growth and agglomeration were found to follow a first order with respect to the increasing number of agglomerates.⁹⁷

More recently, the influence of operating parameters such as solvent systems and the amount of bridging liquid, feeding rate, residence time, agitation rate, temperature and concentration of solution on factors including the flowability, mechanical strength and elastic recovery were investigated. Prolonged time under agitation

produced stronger, compacted spherical agglomerates and an increase in the agglomerate size with increasing initial solute concentration. When lower initial solute concentration was investigated, more fines and more porous agglomerates were obtained. Other properties such as the feed rate of the solution into the anti-solvent was found important; an increase in the feed rate corresponded to a decrease of the agglomerate size, due to the different rate of supersaturation generation at low vs high feed rate. The agglomerate size and fracture stress were found to increase with decreasing temperature which is due to the increased supersaturation at lower temperatures, which in turn increases nucleation and inter-particle growth between colliding particles.^{2, 111}

1.3.4.1.3 Continuous spherical crystallization

The first continuous spherical agglomeration process in suspension of a drug was carried out with a mixed suspension, mixed product removal (MSMPR) crystallizer using one stage, feeding a sulfamethoxazole aqueous suspension and using a benzene solution with white beeswax as a binder. Similar to batch studies, the average size of agglomerates decreased with decreasing bridging liquid feeding rate, whilst increasing with decreasing agitation rate and feeding rate of the sulfamethoxazole aqueous suspension. In addition, a kinetic study of agglomeration was carried out using a population balance model (PBM) and the agglomeration rate was found to increase with particles of size above 200 μm , while the agglomeration rate was independent of particle sizes below this value.¹¹²

Presently, PAT were shown to be beneficial for monitoring the dynamics of spherical crystallization. Using FBRM, steady state operation and chord length distribution (CLD) were monitored and the influence of operating parameters on the product attributes of benzoic acid agglomerates produced via continuous spherical agglomeration was examined. A two-stage MSMPR was developed which enabled to decouple and control the nucleation and growth from the agglomeration mechanism.

⁸⁷ Another example of continuous operation was reported for the continuous emulsion solvent diffusion method of albuterolol sulfate using a single-stage MSMPR. Steady state operation in the crystallizer was monitored in-line using FBRM and achieved rapidly after 30 minutes with a yield of 95 %. The influence of

process parameters such as solvent/anti-solvent ratio, emulsifier concentration, residence time, and reactor scale on the properties of the agglomerates formed during the crystallization process was also examined. Scale-up issues related to the use of high anti-solvent/solvent ratios were solved by the integration of a recycle loop.¹¹³

1.4 Attributes of pharmaceuticals

Pharmaceutical manufacturing relies on crystallization processes to achieve high purity and to produce the desired final product. The operating conditions at which crystallization processes are carried out determine the attributes of products such as purity, polymorphic form, size and shape distribution.¹¹⁴ As crystallization from solution is the most applied method in the pharmaceutical industry, the principal bottleneck in the production of large-scale manufacturing is related to the control of the above mentioned attributes to achieve the target. These attributes determine the efficiency of downstream processes such as filtration, washing and drying, the handling of the final product in terms of flowability, storage conditions, dusting, segregation phenomena, compatibility and tableting, and the product effectiveness around bioavailability and shelf-life.

In order to maximise the manufacturing efficiency along with the product specifications, different objectives to achieve the abovementioned attributes need to be specified during the development of crystallization processes. In Figure 1.15, target outcomes expected from crystallization processes are listed in order of importance. Chemical purity is the most critical attribute of the product as this affects drug toxicity and dissolution and is a fundamental regulatory requirement in terms of patient safety.

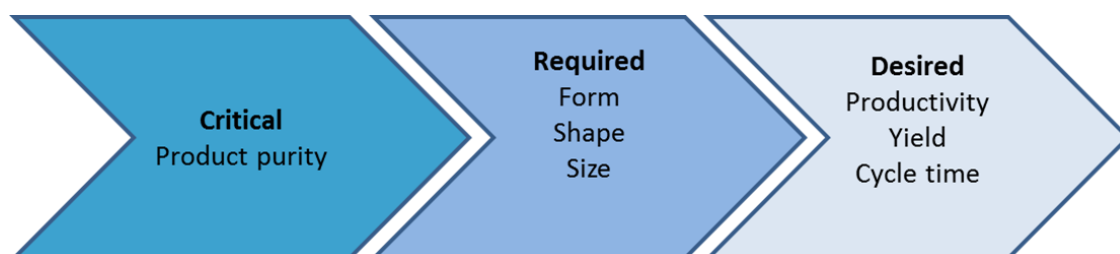


Figure 1.15 Attributes from crystallization processes. Adapted from Variankaval *et al.*⁵

Following on from this, the next required attributes are polymorphic form and specification for crystal size and morphology. The latter is not necessarily a specified requirement unless it affects the bioavailability and processability of the drug substance. If the therapeutic performance is affected by variation in polymorphic form and PSD, regulatory documentation is in place for manufacturing within specification to guarantee patient safety and drug efficiency.⁵

After establishment of specifications for the product attributes during the process design, other factors such as high yield (> 90 %), cycle time (< 24 h for crystallization, filtration and drying) and volume productivity (slurry concentration 10 ± 5 wt %) are considered to maximise the manufacturing efficiency. While these factors are not expected to impact on the patient directly, their consideration is of primary importance for cost-conscious operations providing significant incentives to seek manufacturing efficiency. However, these factors are not independent, and one may be achieved at the expense of another, hence a rational compromise in process development is generally pursued.⁵

The advent of novel control strategies offers the opportunity to increase crystal product quality, reduction or elimination of batch failures; hence consistency and uniformity of production can be ensured and delivered.

Table 1.4 Particle attributes controlled during crystallization. Adapted from Variankaval *et al.*⁵ and Cronin *et al.*¹¹⁵

Attribute	Effects
Polymorph	Melting temperature, solubility, bioavailability and physical properties
Particle size	Dissolution rate/profile, filtration and drying rate, bulk powder flow, compactibility and filterability
PSD	Dissolution rate/profile, filtration and drying rate, bulk powder flow, compactibility and filterability, processing consistency
Morphology	Mechanical strength, bulk powder flow, compactibility and filterability, processing properties
Surface	Bulk powder flow, agglomerate/aggregation formation, growth rate

Table 1.4 shows the product attributes resulting from crystallization processes and the effects on bulk properties.^{5, 115-116}

Many routes are available for tailoring attributes to result in more favourable characteristics, for example, manipulation of crystal morphology by changing the solvent of crystallization or addition of surfactants and tailor made additives may improve the handling of compounds which are difficult to filter, wash, dry or formulate.¹¹⁷⁻¹¹⁹ On the other hand, a change of solvent leads to a change in solubility of the compound which it can have a dramatic effect on crystal properties and yield; in addition the solvent may already be predetermined by the synthetic route upstream. In this respect, spherical crystallization is a valid alternative to the abovementioned crystallization procedures for the manipulation of the crystal morphology and should be routinely used if possible for its ability of optimising multiple attributes at once.¹²⁰

Chapter 2. Aims and Objectives

2.1 Aims

The overall aim of the present research is the investigation of spherical agglomeration processes as a route to optimise the flowability of pharmaceutical relevant compounds that are poorly soluble in water, difficult to handle in formulation and processing step.

In order to achieve this, understanding of agglomeration mechanisms and identification of relationship between processing conditions and particle attributes is essential.

The research therefore has targeted the development of a spherical crystallization process for ibuprofen, implementation of in-line PATs to investigate the particle agglomeration and the development of an agglomeration from suspension for lovastatin with understanding the role of specific process parameters.

The learning has application on the development and optimisation of continuous spherical agglomeration processes.

2.2 Objectives

Ibuprofen and lovastatin has been used as model compounds due to the poor flowability of its bulk powder that can be difficult to handle in downstream processing.

Due to previous literature on the agglomeration of ibuprofen in aqueous ethanol solution, the ethanol-water system was selected for the development of a spherical crystallization process of ibuprofen. This resulted in target objectives of determining the ternary phase diagrams at several temperatures to enable the understanding of the system and design the crystallization process to produce ibuprofen agglomerates. This includes the development of a method to distinguish regions of the phase diagram, implementation of process analytical technologies for process understanding by identifying conditions required for the formation of agglomerates. The flowability of the products was evaluated by Carr's index to demonstrate the improvement of the flow property. Main particle attributes such as particle size distribution was also evaluated using laser diffraction technique.

The technique of spherical agglomeration in suspension was investigated for lovastatin in order to modify its crystal habit and improve particle properties. This work includes developing a method for the selection of a solvent or bridging liquid to promote spherical agglomeration of lovastatin suspended in water and define the optimal volume of bridging liquid to deliver compacted spherical agglomerates.

This work is also focused on scale-up of the process and understanding of the influence of processing conditions on particle attributes at scale. Product attributes such as particle size and flowability are determined and the influence of bridging liquid amount and mixing is evaluated. The information obtained could enable the design of continuous spherical agglomeration process, hence give benefits for scale-up and allow the implementation of control strategies.

Chapter 3. Materials and Methods

3.1 Materials

Ibuprofen BP/Eur.Ph. (99.8%, CAS 15687-27-1) was purchased from *Shasun Pharmaceuticals Limited* (Felixstowe, United Kingdom). Ibuprofen was supplied as racemate (R,S)-2-(4-(2-methylpropyl)phenyl)propanoic acid. Lovastatin (99.4%, CAS 75330-75-5) was purchased from *Molekula Limited* (Newcastle Upon Tyne, United Kingdom). Deionised water was sourced on-site from a Thermo Fisher Scientific Barnstead RO water purification system and Milli-Q Integral. All solvents were purchased from Sigma Aldrich or Fisher Scientific ($\geq 99.8\%$ purity). GSK106 and other reagents used in this work were supplied on-site from GSK (Particle Sciences, Devices & Engineering, Stevenage site).

3.2 Methods

Crystalline materials were characterised (form, particle size, and morphology) using both inline and offline techniques. These include Focused Beam Reflectance Measurement (FBRM), Particle Vision Measurement (PVM), X-Ray Powder Diffraction (XRPD), Laser Diffraction, and Microscopy. Concentration of solute was monitored using inline React-IR probe. Methods related to GSK106 are provided in the specific chapter.

3.2.1 X-Ray Powder Diffraction

XRPD is the most common technique used for identification of polymorph materials.¹²¹ A compound can exhibit more than one polymorphic form, chemically identical to each other but with different arrangement in the crystal lattice, in turn resulting in distinct diffraction patterns thus XRPD is the most appropriate tool to distinguish between mixed phase and polymorphic pure API. Lowest boundary of detection for a polymorph in a binary mixture was reported as low as 0.5wt%.¹²² XRPD was performed on ~50 mg of dried sample placed in a 28 well plate, supported by kapton film (7.5 μm thickness). Data were collected on a Bruker AXS D8 Advance transmission diffractometer equipped with θ/θ geometry and primary monochromatic radiation (Cu $K\alpha_1\lambda= 1.54056\text{\AA}$), a Braun 1D position sensitive

detector (PSD) and an automated multi-position x-y sample stage. Data were collected in the 2θ range of $5-35^\circ$ with a 0.01° 2θ step size and 1 s step^{-1} count time.

3.2.2 Spectroscopy

Spectroscopy is an important technique used for qualitative and quantitative identification of chemicals entities and analysis can be performed using both off-line and online operation with bench top spectrometers and fibre probes respectively.¹²³

There are several advantages when inline probes are integrated in processes. Compared to off-line techniques, these probes offer the opportunity of monitoring and collection of real-time data, implementation of control strategies to deliver the target product and elimination of manual sampling.¹²⁴

On the contrary, some challenges are associated with the use of inline probes since these introduce local changes in the hydrodynamic environment and their position needs to be adjusted to capture information of the process and avoid creation of dead zone where the solid can accumulate.

Alternatives to on-line probes rely on non-invasive methods which avoid contact between probe and sample, and more details can be found elsewhere.¹²⁵ In this work, measurements of solution concentration were collected using a Mettler Toledo ReactIR 15 probe with MCT detector and connected via a flexible AgX fiber conduit to a ReactIR spectrometer. Spectra in the range of $650 - 2500 \text{ cm}^{-1}$ were acquired over 16 scans with 8 cm^{-1} resolution. Analysis of the spectra was performed using iC IR software version 4.3.35. Background measurements (air) and reference solvent spectra were acquired prior to sample collections.

3.2.3 Imaging

3.2.3.1 Microscopy

Optical images were acquired using a Leica model DMI6000M microscope equipped with a motorized stage and Leica DFC495 camera with $5\times$, $10\times$, $20\times$, $40\times$, $100\times$ magnification objective lenses. Images were analysed with the software supplied LAS v.4.8 software (Leica). Particles were also examined using Field Emission-Scanning Electron Microscope (FE-SEM) using a Hitachi SU6600 at The Advanced Materials Research Laboratory (AMRL)-University of Strathclyde.

3.2.3.2 Particle Vision Measurement (PVM)

PVM (Mettler Toledo®) provide real-time microscopic images of particles for immediate and comprehensive process understanding regarding crystal shape and size. This is a powerful tool for characterisation of transient and elusive mechanism that can be critical for product quality, i.e. occurrence of oiling out or monitoring polymorphic transformation if different morphologies are involved. PVM probe is equipped with high resolution CCD camera and internal illumination source to obtain high quality images regardless the concentration of suspension or in the presence of emulsions. The illumination system consists of six laser sources arranged circularly around the objective tube and the CCD camera can be adjusted to capture images through the probe micrometer (manual adjustment). Quantitative information, such as equivalent diameter, particle number, aspect ratio and convexity can be extracted from the collected images by using image analysis toolbox. Moreover, this information could be used for determining useful kinetic parameters since information on crystal shape and size can be extracted. The software supplied iC PVM was used to record both digital images with a field view of $1075 \mu\text{m} \times 825 \mu\text{m}$ and video sequences. In-situ images of slurry were acquired using a PVM version V819.

3.2.4 Particle sizing

3.2.4.1 Focused Beam Reflectance Measurement (FBRM)

FBRM probe (Mettler Toledo®) is commonly used for inline collection of particle counts and particle dimension or droplets using chord length measurement using the principle of laser back scattering. Chord length is simply defined as the straight line distance from one edge to another edge of a particle, which is therefore related its size and shape. A rotating optical lens at the probe tip deflects the laser beam creating a circular path, which scan the particle surface producing pulses of reflected light. These pulses are detected as thousands of individual chord lengths and represented as a chord length distribution (CLD). The value of a chord length is obtained multiplying of the reflection time required from a continuous signal to reflect back to the probe and the laser scan speed. The focal point of the FBRM laser

is adjusted inside the probe ($-20\mu\text{m}$) to provide excellent sensitivity to real-time change in count and dimensions of particle population.

Data were collected using FBRM probe G400 (Mettler Toledo) attached to a control computer. The software supplied with FBRM version 4.4.29 was used to record in real-time and analyse data post-process. Unless otherwise stated, an acquisition time of 15 seconds was used for data collection. CLD were exported to Office Excel or Origin as either un-weighted or square weighted number distributions for further analysis.

3.2.4.2 Laser diffraction

Laser diffraction measurements were obtained using a Mastersizer 3000 system (Malvern Instruments®) integrated with Aero S dry powder dispersion unit, able to measure particle size in the range 10 nm - 3.5 mm. Solid samples were placed on the tray and a dispersion pressure of 0.5 bar was used to characterise the PSD. Sample feed rate was controlled using a vibrating feeder which allows that a suitable sample concentration is available for the measurement and an efficient dispersion of the sample.

Samples were analysed five times and measurements were averaged to produce a single distribution. The following parameters were calculated and used for characterization of PSD: $d_v(10)$, the particle diameter corresponding to 10 % of volume distributions; $d_v(50)$, the particle diameter corresponding to 50 % of volume distributions; $d_v(90)$, the particle diameter corresponding to 90 % of volume distributions and $d(4,3)$ for the volume mean diameter; the span has been widely used to describe the width of the distribution, and this width was calculated from the difference between $d_v(90)$ and $d_v(10)$ divided by the $d_v(50)$.

3.2.5 Flow property

Optimum flowability of powders is a crucial requirement in the manufacturing process of solid dosage form. Therefore a section “Flowability” in the European Pharmacopoeia (Ph.Eur.) provides procedures to examine the ability of a powder to flow. Generally, the flowability is measured by the determination of the angle of repose, Carr’s index (CI) and Hausner Ratio (HR). In this work, CI was used to

characterise the flowability of powders. Bulk density (BD) and tapped density (TD) were determined with the graduated cylinder measurement method.

A 10 mL graduated cylinder was used for better accuracy of reading volumes (0.2 mL). The cylinder was filled with a certain mass of powder (Sartorius Quintix 124-1S) and the initial volume was recorded (bulk or unsettled apparent volume, V_0). Tapped density was carried out with an Autotap (Quantachrome®) until no change in the volume was noted (final tapped volume, V_f). The tapped volume was selected as the volume obtained after 1250 taps.

From the poured and tapped volume, the CI and HR were calculated as follow:

$\times 100$

$$\text{CI (\%)} = \frac{V_0 - V_f}{V_0} \times 100 \quad (2.1)$$

$$\text{HR} = \frac{V_0}{V_f} \quad (2.2)$$

Alternatively, these quantities may be calculated using the measured values for bulk and tapped densities, information can be found elsewhere.¹²⁶⁻¹²⁷

3.2.6 Thermal analysis

Melting points and enthalpy of fusion were measured using Differential Scanning calorimetry (DSC). An amount between 2-3 mg of each sample was accurately weighed into an aluminium pan with pierced lid. Samples were heated from 25-100°C (for ibuprofen) and 25-200°C (for lovastatin) at a heating rate of 10°C/min, under flowing helium purge gas at 40 ml/min. DSC measurement was collected using a DSC214 Polyma instrument (Netzsch®). Blank correction was carried out with an empty pan prior to sample analysis. Analysis was carried out with Netzsch Proteus Analysis Software v7.0.1 to give the melting peak temperatures.

Chapter 4. Ternary Phase Diagrams of
Ibuprofen in Ethanol-Water Solutions
for Understanding Crystallization and
Agglomeration

4.1 Introduction

The technique of crystallization from solution is used extensively as a method for the isolation and purification of APIs. More than 90% of pharmaceuticals contain a crystallization step during their production.⁵ This also provides an opportunity to control the performance of particles in key downstream formulation and product processing stages through the modification of particle attributes. An understanding of the crystallization process is vital to control nucleation, growth and the resulting final product attributes such as, particle size, shape and purity.

Therefore the solubility (liquid and liquid/solid phase boundary) is of fundamental importance and routinely determined to enable the understanding and control of crystallization processes. However, the complexity of the molecules to be crystallised (e.g. racemic mixtures or co-crystals) along with the use of solvent mixtures for productivity, often lead to the formation of multiple phases, e.g. liquid/liquid and liquid/liquid/solid.¹²⁸⁻¹²⁹ This can also appear as oiling out or liquid-liquid demixing. When liquid-liquid phase separation occurs, due to difference in local environments, a significant impact on the rate processes and product attributes can occur.¹³⁰ Liquid-liquid phase separation has been reported for solutions of macromolecules such as proteins^{48, 131-136} or polymers¹³⁷⁻¹³⁹. However, experimental studies recently confirmed the existence of liquid-liquid demixing for compounds with lower molecular weights.¹⁴⁰⁻¹⁴² Depending on the position in the solubility diagram, a liquid/liquid phase region can be considered to be either thermodynamically stable or metastable. An example of a stable case was reported for vanillin-water system at a temperature above 51°C¹⁴³, while a metastable case was observed for a derivative of methoxyacrylate from water-ethanol mixture.¹⁴⁴ A further case of crystallization from metastable liquid/liquid phase was proposed by Vessler *et al.*¹⁴⁵ for temperature-induced crystallization of a Sanofi Aventis API (basic formula: C₃₅H₄₁N₃O₂). In this case, liquid-liquid phase separation hindered both primary and secondary nucleation and when nucleation occurred, it was observed inside the droplets, leading to spherical agglomerates.

Previous work on solubility of ibuprofen in pure ethanol and water/ethanol solutions reported the detection of liquid/liquid phase separation between 20°C and 40°C.¹⁴⁶⁻¹⁴⁷ However, no ternary phase diagram has been determined to clarify the effect of

composition and temperature on the equilibrium composition of the system. In addition, crystallization under different conditions through liquid-liquid phase separation has not been extensively investigated and the understanding of the system behaviour can contribute to future industrial application.¹⁴⁸

In this current study, we have investigated the system ibuprofen-ethanol-water. In order to enable control of the crystallization process, ternary phase diagrams in the temperature range 20-55°C have been determined. Investigation of crystallization from liquid and liquid/liquid phases were carried out in a vessel monitored with FBRM, ATR-FTIR.

4.2 Ibuprofen

Ibuprofen is a commonly used analgesic and antipyretic belonging to the class of nonsteroidal anti-inflammatory drugs (NSAIDs) and included in the World's Health Organization List of Essential Medicine. In addition, like aspirin, paracetamol and codeine, ibuprofen is an over the counter drug thus it is sold directly to the consumer without prescription. Ibuprofen is effective at reducing fever, pain and inflammation, which makes it the ideal drug for treating diseases such as rheumatoid arthritis, osteoarthritis and painful menstrual period amongst other disease states.

Similar to other NSAIDs, Ibuprofen's mechanism of action is related to the inhibition of the production of prostaglandin within the body, which leads to inflammation reduction.

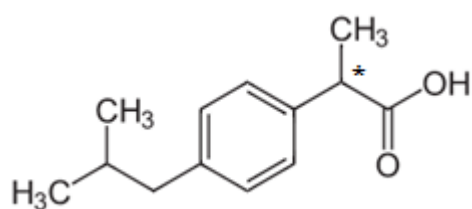


Figure 4.1 Ibuprofen structure. Figure showing molecular structure of ibuprofen, systematic name (R,S)-2-(4-(2-methylpropyl)phenyl)propanoic acid.

Ibuprofen is a colourless crystalline solid with the molecular formula C₁₃H₁₈O₂ and is shown in Figure 4.1. It has a molar mass of 206.29 g/mol, a density of 1.095 g/cm³, a melting point of 77°C and a boiling point of 157°C. Ibuprofen is a racemic mixture,

where the carbon atom between the methyl group and the carboxylic acid group is a chiral atom and therefore responsible for ibuprofen R and S optical isomers.

Ibuprofen is marketed as a racemic mixture which contains equal quantities of R(-)-ibuprofen and S(+)-ibuprofen, although only the S(+)-enantiomer has the desired pharmacological activity of inhibiting cyclooxygenase (COX), while the R(-)-enantiomer has no pharmacological effect and it is non-harmful as well. In addition, the human body is able to convert a substantial fraction of the dose of R(-)-ibuprofen (50%-60%) to S(+)-ibuprofen. Therefore, there is not enough interest from pharmaceutical industries to the synthesis of pure S(+)-ibuprofen.

Ibuprofen is a Biopharmaceutics Classification System (BCS) class II drug with low solubility in water because of its hydrophobic structure consisting mostly of hydrocarbon groups which are non-polar and not interacting with water while the carboxylic group contains electronegative atoms that make it polar and hydrogen bond with water. The issue around low solubility of ibuprofen in water has been solved by salt formation where ibuprofen and lysine react together to form ibuprofen lysinate. This salt has higher solubility in water because it is able to form more hydrogen bonds with water due to the increased number of polar groups such as amine and carboxylic groups in the molecule.

Ibuprofen was known to have only one polymorph, the stable form I and can be characterised with space group *P*21/*c* (monoclinic system), however recently a procedure has been reported for the crystallization of another form¹⁴⁹, form II.

Polymorphism of ibuprofen is shown as differences in the crystal packing arrangements of the molecule in Figure 4.2, as reported in the Cambridge Crystallographic Database Centre (CCDC).

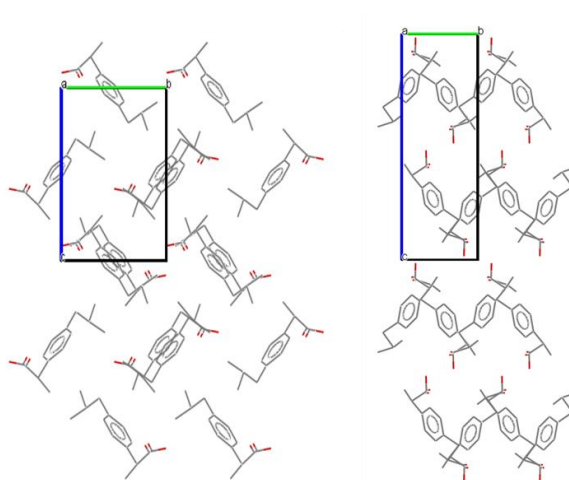


Figure 4.2 Ibuprofen packing arrangement: form I (left) and form II (right), CCDC references IBPRAC and IBPRAC04, respectively.

Form I normally has a plate or a needle-like morphology (Figure 4.3), and it is the only form observed at ambient temperature. For form II, no images are available in the literature. Ibuprofen bulk powder shows disadvantages affecting the manufacturing properties, for example the flowability is poor due to high cohesivity and adhesivity, the tableting behaviour is bad because the powder is prone to capping and sticks to tablet punches during compression. In addition, ibuprofen shows bad dissolution behaviour due to its hydrophobic structure.¹⁵⁰

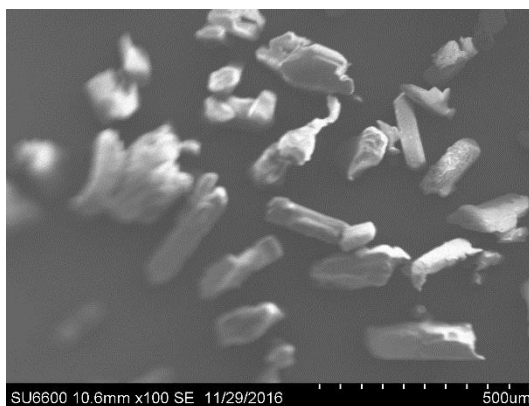


Figure 4.3 Scanning electron micrograph of ibuprofen Form I.

In this respect, ibuprofen is generally granulated before tableting; a step which is time and energy intensive and made use of solvents and heat.

During the past 40 years, several methods such as special crystallization technique, modification of the external crystal habit or preparation with excipients are described in the literature to overcome the issues concerning the poor properties of ibuprofen and to enhance its manufacturing.

Interest in the application of spherical crystallization to improve particle properties and downstream efficiency of ibuprofen was increased in the past years, with particular attention to the choice of excipient^{107, 151}, surfactant¹⁵² or binding agent¹⁵³ in addition to the usual solvent system for crystallization. Ibuprofen with improved flowability and compressibility was obtained using the technique called quasi-emulsion solvent diffusion which is a spherical crystallization technique. With this technique, the crystallization of droplet-like entities from solution of ethanol and water in the presence of acrylic polymer led to the production of controlled-release microspheres of ibuprofen. The observations suggested that final particle size could be tuned by manipulation of the concentration of the drug and polymer and the agitation rate in the vessel.¹⁵⁴

Spherical agglomerates of ibuprofen with improved properties were prepared by phase separation method from binary mixture of water with either ethanol, acetone, tetrahydrofuran without surfactant.¹⁴⁸ Crystal habit modification was obtained via a standard cooling crystallization in a mixture of 50% ethanol solution. Crystallization through phase separation led to precipitation of spherical agglomerates of ibuprofen with high flowability due to its spherical shape and compressibility due to the isotropy of the agglomerates texture compared to the marketed ibuprofen. In addition, dissolution was slightly improved due to the porous nature of the agglomerates.

Besides difference of the agglomerates produced, different crystal habits with different properties can also be obtained when ibuprofen is crystallised from different solvents.

A study described the difference in crystal habit of ibuprofen obtained from batch seeded cooling crystallization processes in several organic solvents.¹¹⁷ It was found that the habit of ibuprofen was dependent from the solvent used and in turn, the crystal habit influenced properties like bulk density, compressibility and flowability. Ibuprofen crystallised from methanol and ethanol showed polyhedral crystal habit

having the highest bulk density and the best flowability, with ethanol showing improved compressibility whilst ibuprofen crystallised from hexane showed needle-shape morphology having the worst properties compared to the other samples.

An extension of the previous work studied the modification of crystal habit of ibuprofen obtained from different crystallization methods such as antisolvent, cooling and evaporative crystallization and the effect on the flow properties of the samples.¹⁵⁵ It was found that different crystal habits like needle, plate and cubic with different flow properties were obtained which correspond to what was previously reported. In addition, it was observed that ibuprofen with improved flowability can be successfully produced from antisolvent crystallization process in acetonitrile water system. However no improvement of the dissolution rate was reported.

Although, many works have been focused to improve the properties of ibuprofen affecting the tableting process, several studies reported the production of ibuprofen with improved dissolution behaviour from antisolvent crystallization in the presence of surfactants¹⁵⁶ and by formation of inclusion complex with cyclodextrin¹⁵⁷ before the synthesis of the more soluble salt ibuprofen lysinate.

4.3 Experimental

4.3.1 Determination of solubility

The solubility of ibuprofen was determined gravimetrically between 20-55°C in pure ethanol, pure water and binary mixtures in the range of 10-90% by mass of ethanol (on solute-free basis).¹⁵⁸ For this work a Crystalline (Technobis Crystallization Systems) comprised of eight independent reactors equipped with cameras and turbidity detectors was used. 8 mL vials were prepared with pure ethanol, pure water or binary mixtures, along with excess solid ibuprofen. These vials were stirred with teflon-coated magnetic stirrers for 24 hours. The temperature of the vials was kept constant within $\pm 0.1^\circ\text{C}$. For sampling the solution, 1 mL was removed via preheated syringes to avoid crystallization. The syringe was then emptied through a filter (PTFE, 0.22 μm) to transfer the solution free of solids into pre-weighed glass vials. These vials were covered to prevent evaporation and weighed with their contents. The cover was then removed and the samples were dried in ventilated enclosures at

room temperature ($\sim 25\text{ }^{\circ}\text{C}$). The weight of the samples was recorded repeatedly during the drying process to establish the point at which the weight remained constant and the water and ethanol were completely evaporated. The weight of the final dry sample was used for calculation of the solubility and the values were expressed in gram of solute per grams of solvent. Each point consists of a minimum of 3 replicates.

4.3.2 Determination of ternary phase diagrams

The ternary phase boundaries of ibuprofen in ethanol and water at the temperatures of 20°C , 35°C , 45°C and 55°C were investigated. Eight glass vials of 8 mL containing a mixture of ibuprofen, ethanol and water with the desired proportions were prepared using an analytical balance (Sartorius Quintix 124-1S). These vials were then placed in the Crystalline and kept at constant temperature and stirred at 900 rpm for more than 2 hours until phase equilibrium was reached. Then, one of the components, either water or ethanol, was added dropwise into the solution. Vials were then reweighed to determine the added mass and allowed to equilibrate for 1 hour. Addition continued until a different phase appeared (e.g. clear solution changed to liquid/liquid).¹⁵⁹ A smaller amount of the other component was then added to the solution with the aim of returning back to the previous phase region. The phase boundaries were identified as being between two steps back and forth when a change of phase was detected. To validate the phase boundaries a number of starting proportions were carried out along the phase boundary. These experiments were followed with the help of the in situ cameras with a resolution of $5\text{-}11\text{ }\mu\text{m}/\text{pixel}$ and a depth of field of 2.5 mm.

4.3.3 Cooling crystallization experiments

Experiments were performed in a 100 mL Easymax 102 (Mettler Toledo) equipped with a 38 mm 45° pitch blade turbine impeller. Experimental conditions are given in Table 4.1. Both solutions were cooled from 45°C to 35°C at a rate of $0.1\text{ }^{\circ}\text{C}/\text{min}$ and agitated at a rate of 400 rpm. Throughout these experiments, data from FBRM (model G400), ATR-FTIR (ReactIR 15) and PVM (model V819) probes were recorded. FBRM and ATR-FTIR samples were logged once every 15 s and PVM images were recorded at a rate of 8 fps.

Table 4.1 Experimental conditions of cooling crystallization experiments.

Exp.	Ibuprofen (wt%)	Ethanol (wt%)	Water (wt%)
1	64.6	27	8.4
2	11.5	29.5	59

Water and ethanol spectra were compared to the experimental spectra and the peak at 1213 cm^{-1} was selected to follow the ibuprofen concentration (Figure 4.4).

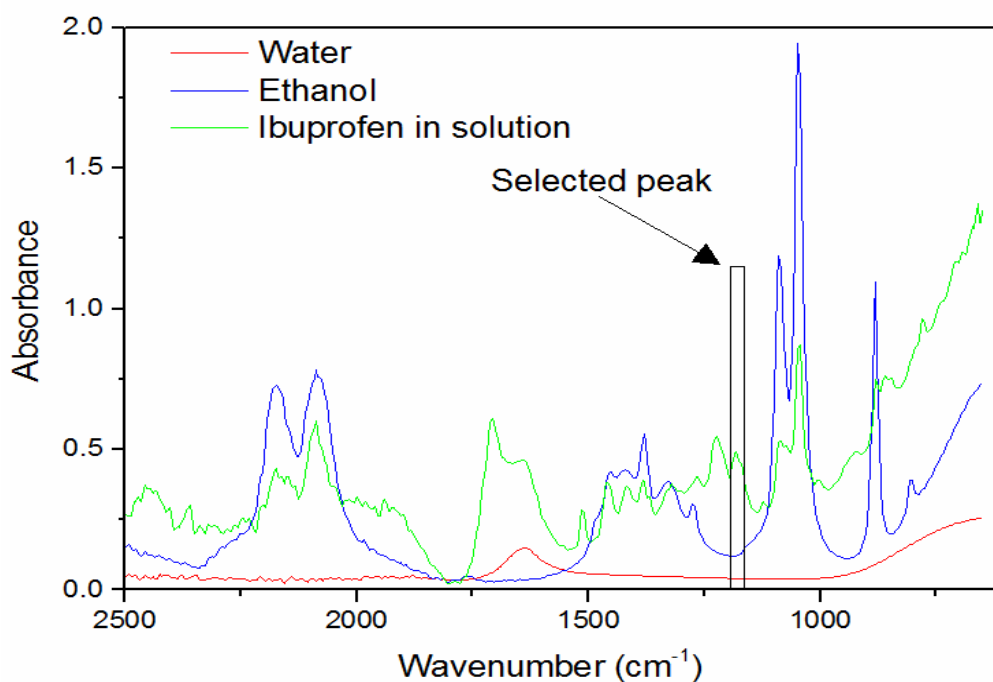


Figure 4.4 IR spectra for the ibuprofen solution, pure ethanol and pure water.

4.3.4 Solid characterisation

The suspension of each experiment was filtered using a Buchner filtration system under vacuum with Whatman filtering paper and dried in an oven overnight.

Products were characterized off-line via XRPD, laser diffraction, microscopy and DSC to assess the influence of liquid-liquid phase separation on the final product. Flow properties were also measured and compared with the raw ibuprofen in order to identify which product held improved properties.

The yield of the samples was calculated from ratio between the recrystallized mass and the mass of initial dissolved solid, expressed in term of percentage.

4.4 Results and discussion

4.4.1 Solubility

The solubility of ibuprofen in ethanol-water mixtures from 20°C to 55°C are shown in Figure 4.5 and Table 4.1. The results show a high solubility of ibuprofen in pure ethanol and a very low solubility in pure water. In both cases, the solubility obtained was proportional to the temperature and ethanol concentration. In pure water and mixtures up to 10 wt% ethanol the solubility of ibuprofen is below 0.001 g/g. The solubility of ibuprofen in pure water at 20°C was found to be 1.41×10^{-4} g/g.

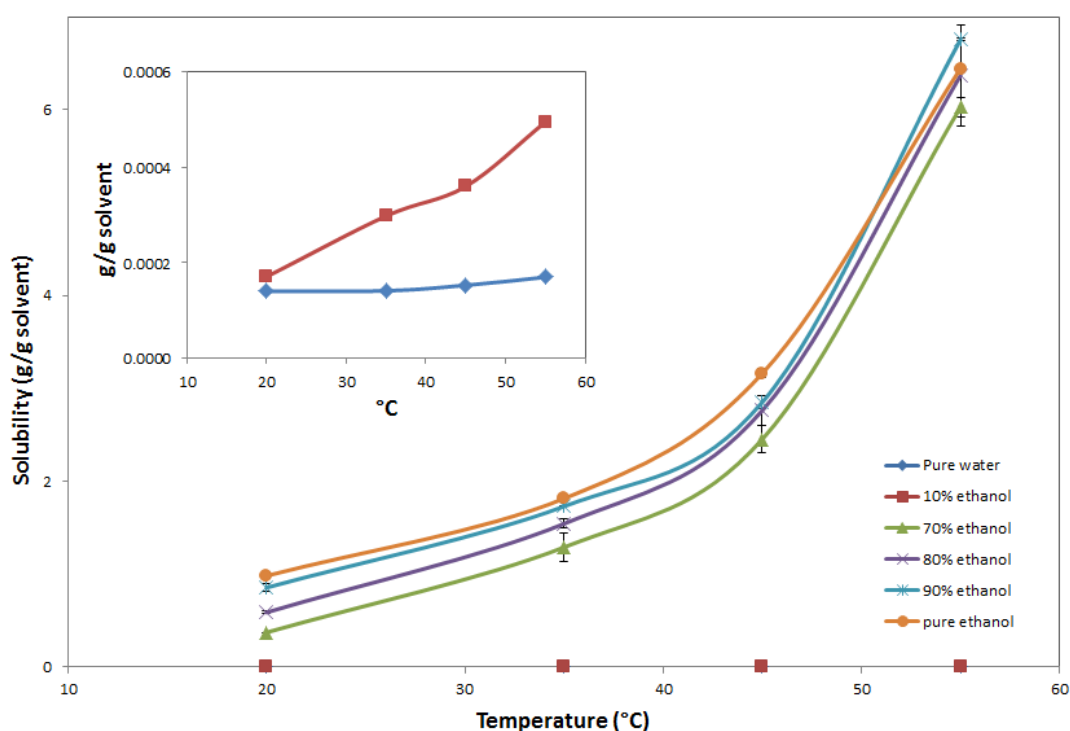


Figure 4.5 Solubility (g solute/g solvent) of ibuprofen in binary solvent mixtures as wt % of ethanol (on a solute free-basis) from 20°C to 55°C. Standard deviation bars are based on 3 replicates; for solubility curves of ibuprofen in pure water and 10% ethanol, the error bars are smaller than the symbol size.

Data from previous works^{146-147, 160} are in good agreement with the results presented in this study, i.e. 1.41×10^{-4} g/g of water and 1.43×10^{-4} g/g of water at 20°C for this study and Manrique et al.¹⁴⁷ respectively. At 55°C a synergistic peak is detected, for which the solubility increases slightly from 6.443 g/g in pure ethanol to 6.752 g/g in

mixture of 10 wt% of water. Liquid/liquid equilibrium was detected between 10 and 70 wt% of ethanol and liquid/liquid/solid equilibrium is obtained in the same range.

Table 4.2 Solubility of ibuprofen in binary solvent mixtures. Not reported for concentrations in the liquid-liquid phase region.

Ethanol wt. %	T = 20 °C		T = 35 °C		T = 45 °C		T = 55 °C	
	Solubility (g/g solvent)	Standard deviation	Solubility (g/g solvent)	Standard deviation	Solubility (g/g solvent)	Standard deviation	Solubility (g/g solvent)	Standard deviation
0	1.41x10 ⁻⁴	6.15x10 ⁻⁵	1.42x10 ⁻⁴	3.76x10 ⁻⁵	1.53x10 ⁻⁴	3.38x10 ⁻⁵	1.70x10 ⁻⁴	1.04x10 ⁻⁴
10	1.71x10 ⁻⁴	3.66 x10 ⁻⁵	2.98 x10 ⁻⁴	1.53x10 ⁻⁴	3.60x10 ⁻⁴	2.34x10 ⁻⁵	4.95x10 ⁻⁴	5.51 x10 ⁻⁵
20	4.21x10 ⁻⁴	4.30 x10 ⁻⁵	-----	-----	-----	-----	-----	-----
30	1.43x10 ⁻³	9.63 x10 ⁻⁵	-----	-----	-----	-----	-----	-----
40	0.0104	3.32 x10 ⁻⁵	-----	-----	-----	-----	-----	-----
50	0.0525	1.38 x10 ⁻³	-----	-----	-----	-----	-----	-----
60	0.1768	1.63 x10 ⁻³	-----	-----	-----	-----	-----	-----
70	0.3726	3.58 x10 ⁻³	1.2898	0.1550	2.4513	0.1470	6.0257	0.1091
80	0.5879	0.0150	1.5434	0.0525	2.7609	0.1630	6.3677	0.5410
90	0.8552	0.0412	1.7297	6.19x10 ⁻³	2.8586	0.0654	6.7542	0.0158
100	0.9823	0.0347	1.8145	0.0143	3.1602	0.0465	6.4430	0.0325

4.4.2 Ternary phase diagrams

Figure 4.6 shows the ternary phase diagrams of ibuprofen, ethanol and water at 20, 35, 45 and 55 °C. The points in the phase diagrams are obtained by experimental observations following the previously detailed methodology.

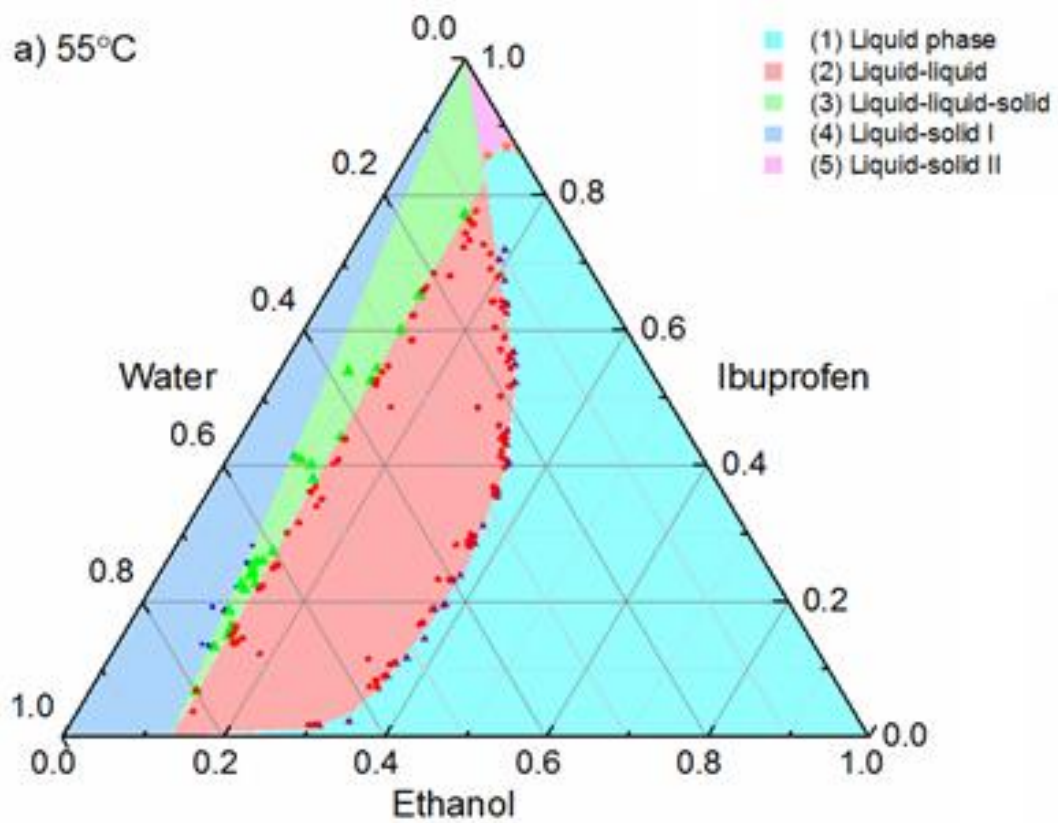


Figure 4.6 Ternary phase diagrams of ibuprofen, ethanol and water from 20°C to 55°C expressed in mass fraction.

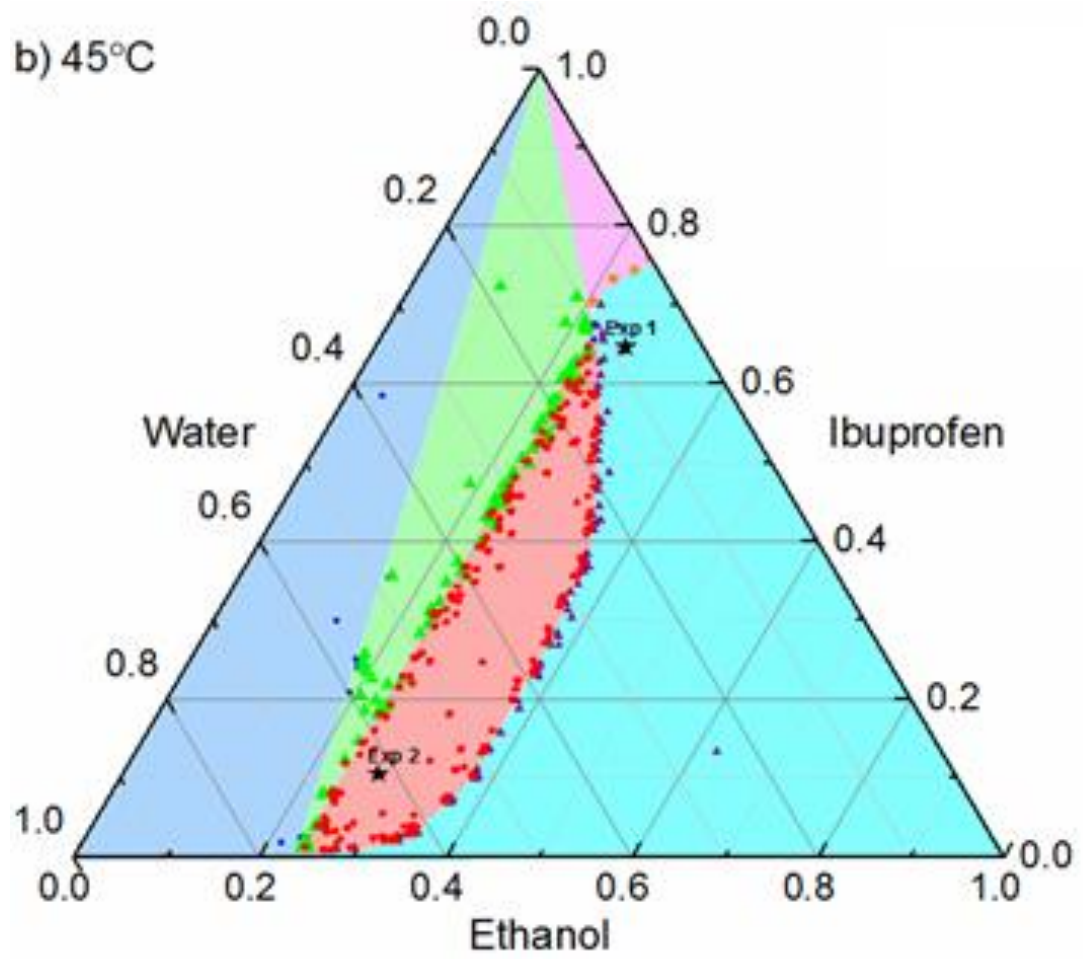


Figure 4.6 continued

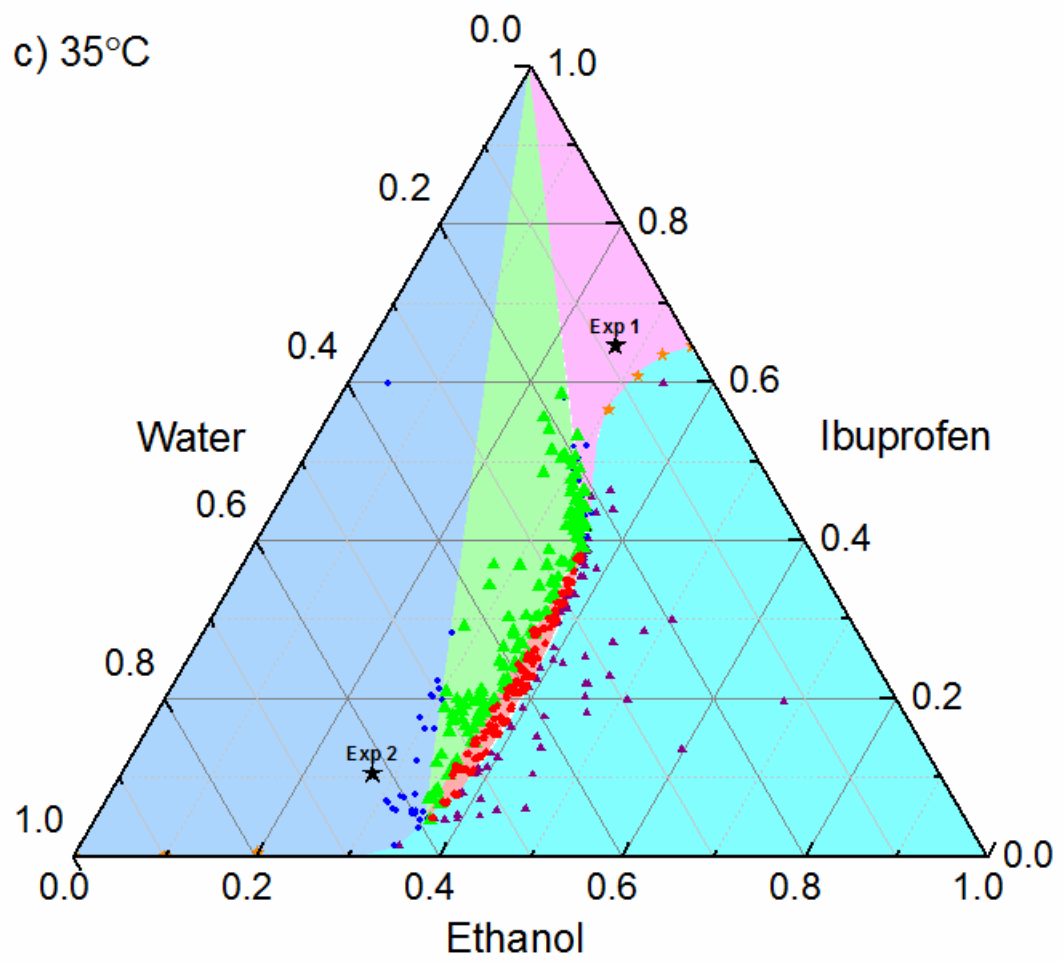


Figure 4.6 continued

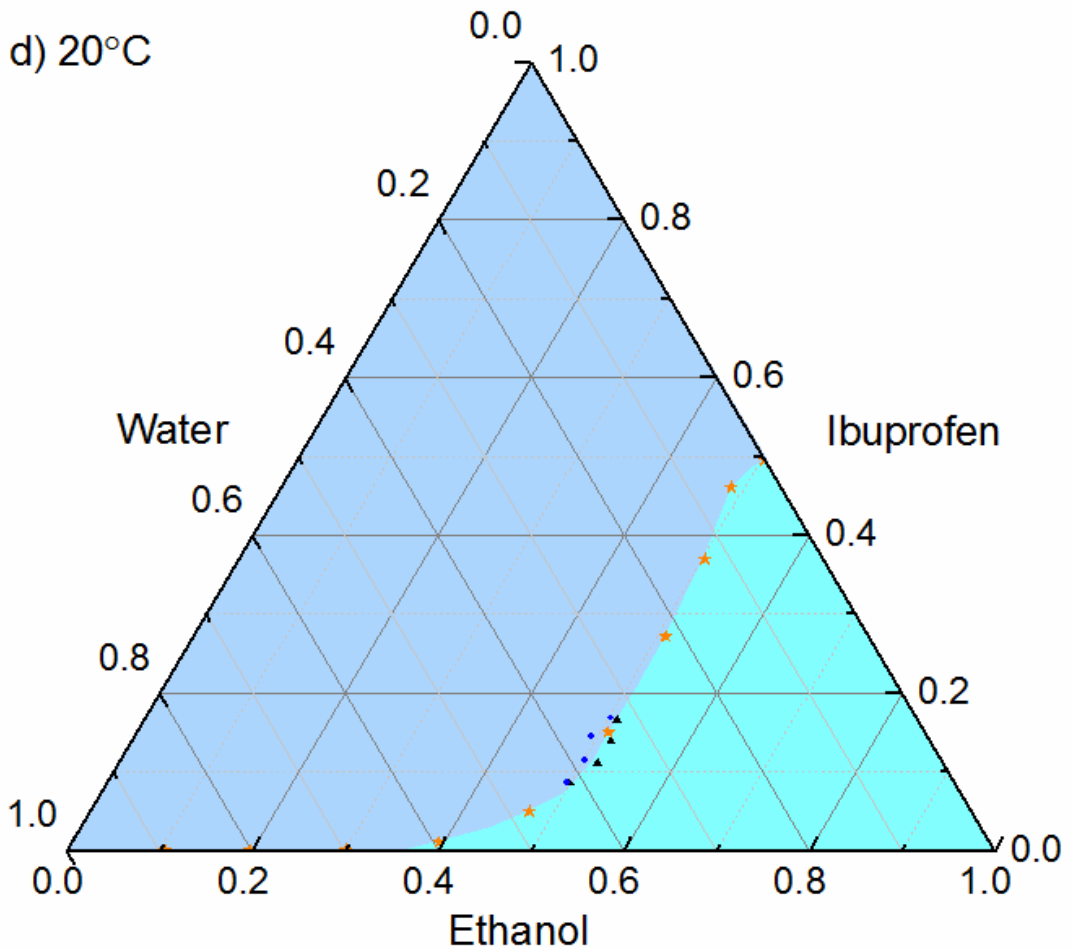


Figure 4.6 continued

From 35 to 55 °C, the diagrams are comprised of five different regions, shown in Figure 4.6 and Figure 4.7: (1) undersaturated liquid phase, (2) liquid-liquid phase separation, (3) liquid-liquid phase separation with solid and two (4) and (5) liquid-solid phases.

Region 1 covers mixtures with higher wt% of ethanol. In region 2 equilibrium is reached by separation of two liquid phases: a water rich solution with low ibuprofen content and an ethanol rich solution with high ibuprofen content. Region 3 is a three-phase region where the equilibrium is reached by two liquid phases saturated with ibuprofen. Excess ibuprofen above the saturation concentration exists as a separate solid phase. This solid phase can be present in either of the liquid phases. Regions 4 and 5 are representative of supersaturated solution of ibuprofen where solid

ibuprofen is in equilibrium with water rich solution (liquid-solid phase I) and ethanol rich solution (liquid-solid phase II), respectively.

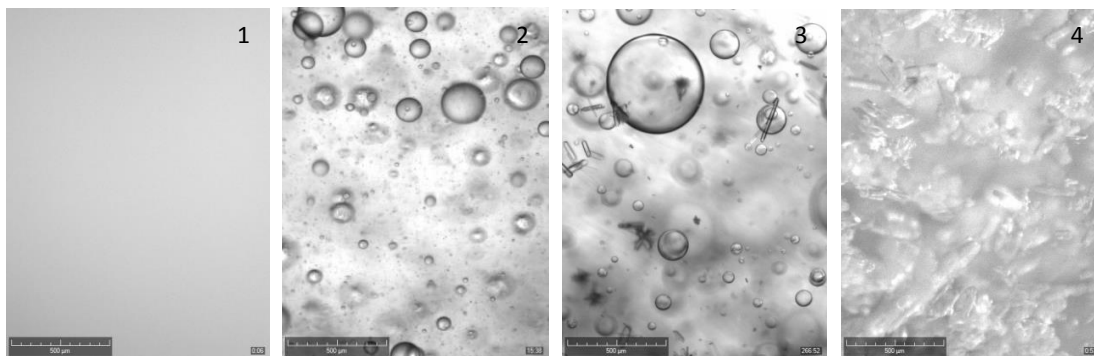


Figure 4.7 Regions of the ternary phase diagram of ibuprofen in ethanol-water mixtures: 1) undersaturated liquid phase, 2) liquid-liquid phase separation, 3) liquid-liquid phase separation with solid and 4) liquid-solid phase.

The size of the liquid-liquid region (2) and immiscible behaviour can be seen to decrease between 55 °C and 35 °C. The phase diagram shows an absence of liquid-liquid phase region at 20 °C, i.e. only the liquid and liquid-solid regions remain.

The liquid-solid solubility curve between the liquid-liquid phase separation region and liquid-liquid-solid region is a straight line.¹⁵⁹ In the liquid-solid regions, the solubility of ibuprofen increases with ethanol concentration. However the influence of the temperature in these regions is much more important for highest values of ethanol mass fraction on the right side of the phase diagram than for lower ones on the left side.

The liquid-liquid phase region increases with temperature and expand into the water-rich part of the diagram. At increasing temperature liquid-liquid phase separation gradually occurs at lower ethanol concentration and the miscibility between the phases tends to decrease with increasing temperature.

Along with region 2, the liquid-liquid-solid region (3) and the liquid-solid water-rich solution region (4) decrease in size with increasing temperature. Similar behaviour is noticed for region 5, which decreases in size, confined by the solubility curves of ibuprofen in ethanol-rich solution and the liquid-liquid-solid phase separation boundary. A reason is that the solubility of ibuprofen in ethanol-rich solution increases with temperature and lead to the decrease of size for region 5.

Consequently, region 1 (homogeneous solution) expands slightly with increasing temperature. From 20 to 55°C regardless of solute composition, there is no liquid–liquid phase separation when the ethanol concentration is above 70 wt% (on solute free basis). Similarly, there is no liquid–liquid phase separation at 35°C when the ethanol concentration is less than about 20%, at 45°C and 55°C when the ethanol concentration is less than about 10%.

When the temperature is decreased from 35 to 20°C, region 2 disappears first, and then region 3. Simultaneously, the liquid-solid regions (4 and 5) merge into one region.

However, the liquid-liquid phase separation into two immiscible liquid layers of ibuprofen in ethanol-water mixtures above 20°C has been previously reported though the phenomenon was not investigated further.^{148, 161} Here we explore the process of crystallization from different starting points and the knowledge of the phase diagrams can enable the control over particle attributes. The results also show that at 20°C the solubility of ibuprofen increase about 10 times, from 0.0014 g/g to 0.010 g/g, when the composition of solution is increasing from 30 to 40 wt% ethanol. As previously reported by Rashid et al¹⁴⁶ for ibuprofen-ethanol-water system and Yang et al¹⁶² for butylparaben-ethanol-water system, the hydrophobic nature of a molecule and its interaction with binary solvent systems has been shown to be responsible for the separation of solution into two immiscible layers. In case of no agitation, the ethanol-rich phase is found on top of the water-rich phase.¹⁴⁶

In contrast to other systems, which present an increase of the liquid–liquid miscibility with temperature, in this case the liquid–liquid phase separation increases with increasing temperature.¹⁴²

4.4.3 Cooling crystallization

Based on the ternary phase diagrams at 20°C, 35°C, 45°C and 55°C, two cooling crystallization experiments were developed to look at the effect on particle attributes. Points 1 and 2 in Figure 4.6 show the location used for the start and end of the cooling crystallization. Experiment 1 started region in the homogeneous liquid region and ended in the liquid-solid region as a standard solution crystallization. Experiments 2 studied the formation of solid from liquid–liquid phase region via

liquid-liquid-solid region into the liquid-solid region. During the experiments, the nucleation of crystals was confirmed from the latent heat of phase transformation associated with the crystallization event.

In the case of crystal nucleation through a homogeneous solution, a rapid increase of the FBRM total counts/s was readily detected, whereas through a liquid-liquid phase separation, the interpretation of FBRM is complicated by the presence and dynamics of dispersed liquid phase in addition to the birth of crystals. Specifically, when a liquid-liquid phase separated mixture undergoes a cooling process, the FBRM probe detects the number of droplets, then suddenly the counts/s decreases while the mixture approaches the nucleation temperature as can be easily assessed from trend of experiment 2 (Figure 4.9). The liquid-liquid phase separation is due to the presence of ibuprofen in the water/ethanol solution and the change of solute concentration for the continuous and dispersed phases leads to a reduction in number of droplets. In addition, nucleation through liquid-liquid phase separation is associated with a sharp peak in the IR response, which is not similar to the crystallization from homogeneous solution (Figure 4.8 and Figure 4.9) and PVM is deemed necessary for clarifying the crystallization processes.

Experiment 1. When the solution was heated to 45°C and kept at this temperature, the solute was fully dissolved and both the IR response and the FBRM counts/s were constant (Figure 4.8). The PVM confirmed the absence of particles (Figure 4.8).

Nucleation occurred when the system was kept for 1 hour and 20 minutes at the final temperature of 35°C. Finally, the crystals grew in the supersaturated solution, which also showed in the PVM image at 3 hours and 30 minutes in Figure 4.8. Fouling on the PVM probe was observed.

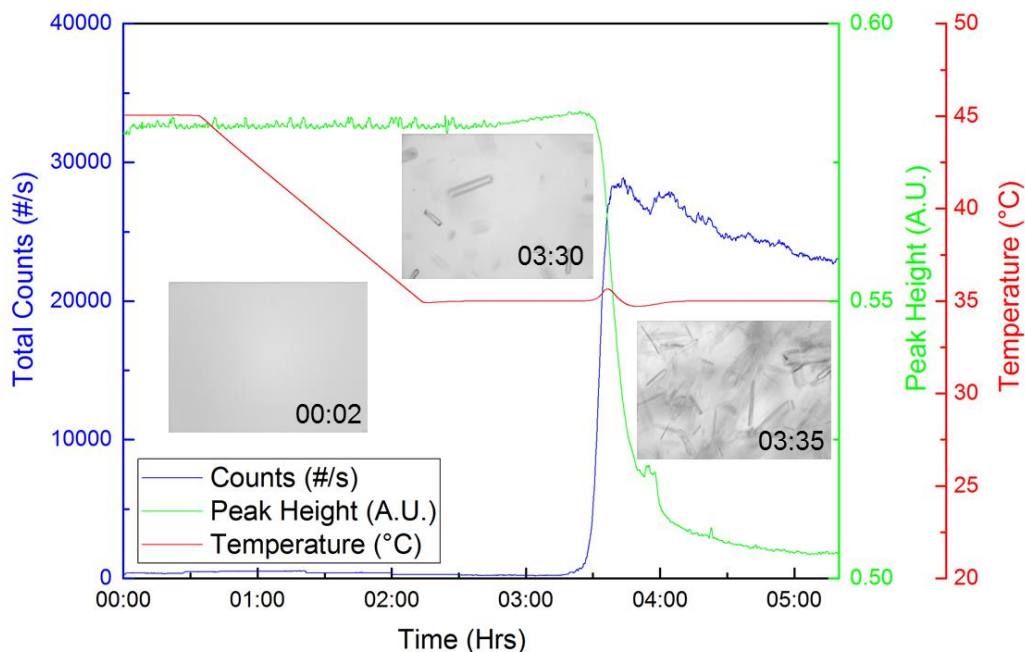


Figure 4.8 FBRM total counts/s with temperature profile, IR peak height and PVM images of exp.1, starting at 45°C in region 1 and ending in liquid-solid region 5 (Figure 4.6).

The PVM images confirmed that for crystallization outside the liquid-liquid phase separation region, the growth is the predominant mechanism and the crystals can grow as single entities.

Experiment 2. The experiment started in the liquid-liquid phase separation region, with a solution of a low ibuprofen (11.5 wt%) and high water (59 wt%) content. During the cooling from 45°C to 35°C, the mixture changed from region 2 (liquid-liquid phase) to region 3, where crystal nucleation occurred in the three-phase region at constant temperature of 35°C, then the process ended in region 4 (liquid-solid region). During the process, the FBRM and IR responses were recorded and the result is illustrated in Figure 4.9.

FBRM confirmed that the initial phase at 45°C was a liquid-liquid phase separation by counting a considerable number of droplets generated per second. As can be seen in the PVM image in Figure 4.10, droplets were captured (2 minutes after the experiment started). Crystal nucleation occurred when the system was kept for 47 minutes at constant temperature of 35°C. Both nucleation and the transition between the liquid-liquid-solid and liquid-solid phase is shown in Figure 4.10 for better

investigation of the events, as this occurred quickly over 2 minutes. When the nucleation of ibuprofen occurred, a sharp decrease of FBRM total counts/s and IR peak height was observed.

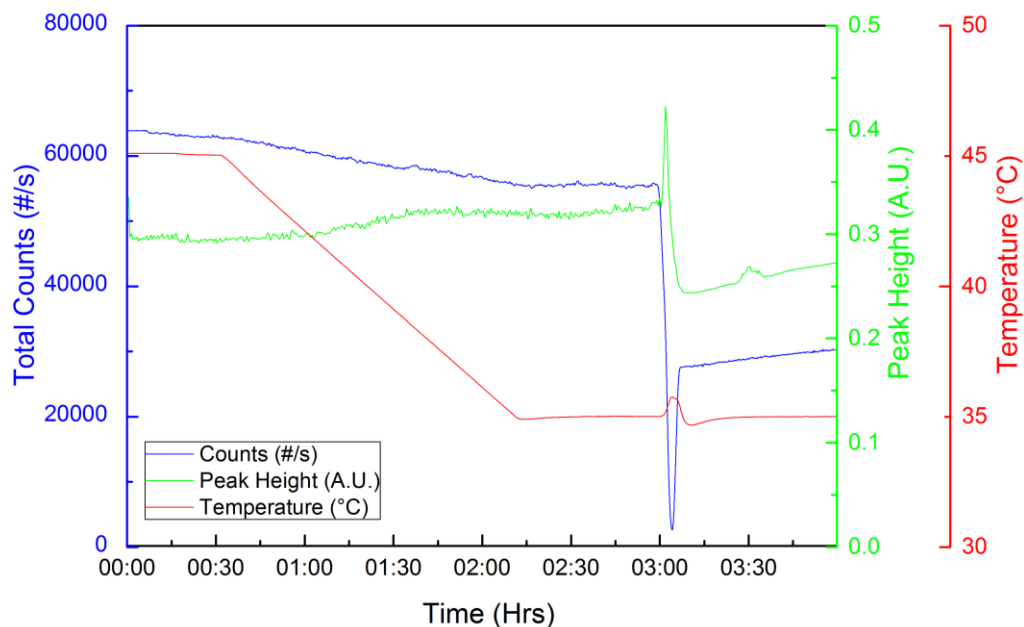


Figure 4.9 FBRM total counts/s with temperature profile, IR peak height for ibuprofen crystallization experiment 2. Graph showing crystallization from liquid-liquid phase separation starting at 45°C in region 2 and ending in liquid-solid region 4 (Figure 4.6).

During crystallization, the overall concentration of ibuprofen in the liquid-liquid phase decreased, leading to a redissolution of the droplets and an increase of the miscibility of the liquid phases.

Agglomerates of plate-like crystals were observed in the solution, as shown in the PVM image in Figure 4.10 (3 hours and 2 minutes).

Growth and agglomeration of crystal consumed the ibuprofen in solution quickly and the droplets gradually disappeared; the system moved from liquid-liquid-solid (region 3) to liquid-solid (region 4), as can be seen in the last PVM image in Figure 4.10 at 3 hours and 4 minutes.

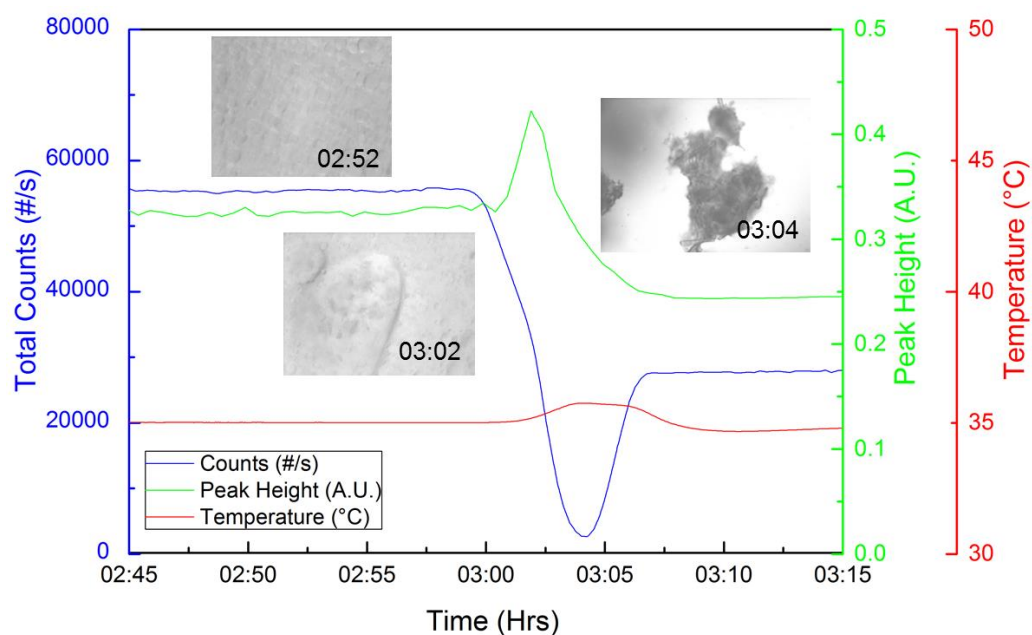


Figure 4.10 Graph showing nucleation from liquid-liquid phase separation at 45°C in liquid-liquid-solid region 3 and ending in liquid-solid region 4 (Figure 4.6).

From the observed measurements, the system undergoes several transformations: (a) liquid-liquid phase separation, (b) nucleation, growth and agglomeration in liquid-liquid-solid region and (c) growth and agglomeration in liquid-solid phase.

Agglomeration occurring during crystallization through the liquid-liquid phase separation has been reported for the system erythromycin ethylsuccinate-THF-water¹²⁴, butyl paraben-ethanol-water¹⁵⁸ and 4,4 dihydroxydiphenylsulfone (DHDPS)-water-acetone¹⁶³ in the presence of liquid-liquid phase separation.

However, further work is required in order to clarify the influence of liquid-liquid phase separation on the resulting product.

4.4.4 Solid characterisation

Raw material ibuprofen and final product crystals obtained with standard crystallization and through liquid-liquid phase separation are shown in Figure 4.11. The scale in each picture is 200 μm . As can be seen in Figure 4.11a-b, the product obtained from exp.1 (standard solution crystallization) was mostly formed of single crystals having similar morphology of the raw material, in contrast to the product from exp.2 which show recrystallized ibuprofen heavily agglomerated from the crystallization through liquid-liquid phase separation (Figure 4.11c).

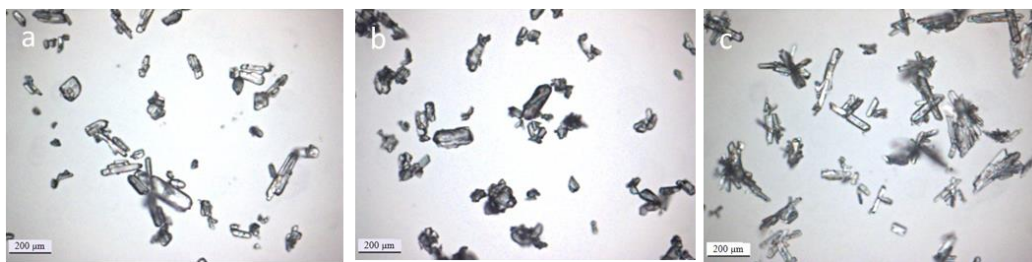


Figure 4.11 Ibuprofen habits (10X magnification): a) marketed ibuprofen, b) ibuprofen crystallized from exp.1 and c) ibuprofen agglomerates from exp.2 (liquid-liquid phase separation).

The particle size distributions of final crystals for each experiment are listed in Table 4.4. As can be seen, the d_{v50} of crystals from standard crystallization was two times bigger than the d_{v50} of agglomerates from crystallization through liquid-liquid phase separation. However these results appeared to be inconsistent with the particles collected from offline microscopy (Figure 4.11). A possible explanation should be related to the procedure of sizing in the dry unit; the small ball bearing and the applied pressure used to move the particles through the cell may cause breakage or deagglomeration of the agglomerates before the measurement. Considering this, a useful method to look for differences in the PSD would have been to compare the results from dry and the wet dispersion unit.

From Table 4.3, it can be noticed that a good yield was obtained only for exp.2- around 86% compared to the poor yield obtained for exp.1-around 31%. A reason for that is the much lower solubility at the end point for exp.2 compared to exp.1.

Table 4.3 Results of the analysis of the product obtained from exp.1 (standard crystallization) and exp.2 (crystallization through the liquid-liquid phase separation).

	Dv10	Dv50	Dv90	Span	Yield
Exp.1	54	135	277	1.6	30.7
Exp.2	19.5	68.2	177	2.3	86.1

In Table 4.4, bulk and tapped density along with Carr index and Husner ratio of the products obtained in the experiments are presented. Starting material is also presented for comparison. Product obtained from experiment 1 shows a Carr index of 18.7, which is indicative of a fairly flowing product compared to the product

obtained from experiment 2, which has a value of 8.8, thus indicating a free flowing behaviour.

Table 4.4 Properties of ibuprofen samples in the range 0-1000 μm .

Sample	BD (g/ml)	TD (g/ml)	CI (%)	HR
Raw material	0.358 ± 0.004	0.494 ± 0.013	27.42 ± 2.50	1.38 ± 0.05
Exp. 1	0.422 ± 0.002	0.519 ± 0.003	18.75 ± 0.00	1.23 ± 0.00
Exp. 2	0.313 ± 0.014	0.344 ± 0.028	8.77 ± 3.24	1.10 ± 0.04

The XRPD (Figure 4.12) and DSC (Figure 4.13) results of ibuprofen remained unchanged in each experiment, indicating no polymorph transformation under the condition employed for cooling crystallization experiments.

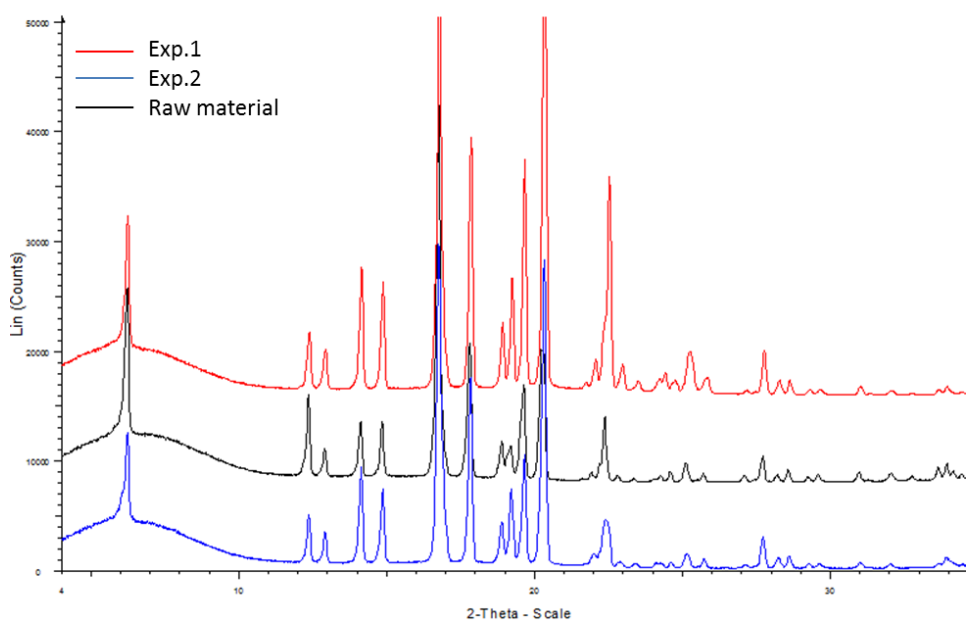


Figure 4.12 X-Ray powder diffraction pattern of ibuprofen: raw material (black), recrystallised from exp.1 (red) and recrystallised from exp.2 (blue).

The determined melting temperatures were found in the range of 76.9-77.3°C and were in good agreement with the values obtained from literature.¹⁶⁴

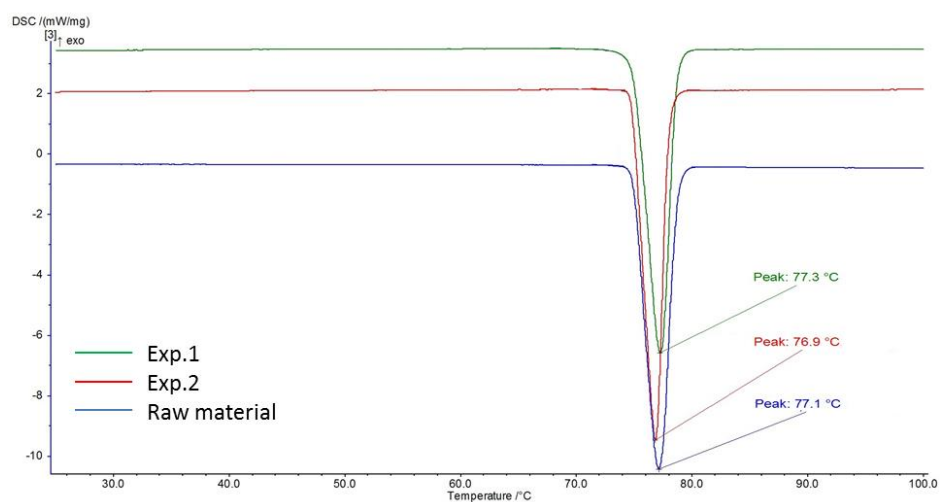


Figure 4.13 DSC curves of ibuprofen: raw material (blue), recrystallized from exp.1 (green) and recrystallized from exp.2 (red).

4.5 Summary

The overall aim of this work was to explore the ternary phase diagrams of ibuprofen-ethanol-water at 20°C, 35°C, 45°C and 55°C to enable a better process design of ibuprofen crystallization involving binary mixtures. The solubility of ibuprofen in pure water and with 10 wt% of ethanol is below 0.001 g/g, whereas in pure ethanol the solubility is definitely higher, reaching 6.44 g/g at 55°C. At 20°C, the solubility of ibuprofen in homogeneous water-ethanol solutions increases substantially when the ethanol concentration increases from 30 wt% to 40 wt%. Ibuprofen induces liquid-liquid phase separation in ethanol-water mixtures in the range of temperature 35-55°C. This phase separation is temperature dependent and solvent-composition dependent and occurred between 10 wt% and 70 wt% of ethanol concentration. The ternary phase diagrams were determined experimentally using microscope camera for identification of regions. Five different regions were identified for each ternary phase diagram at temperature above 35°C: a liquid phase region, two liquid-solid regions, a liquid-liquid phase region and a liquid-liquid-solid region. However at 20°C solely two regions were identified and the diagram presents simple solid-liquid equilibrium.¹⁴⁶⁻¹⁴⁷

Crystallization experiments with and without oiling-out were investigated with combination of FBRM, ATR-FTIR and PVM. These experiments showed that the

product attributes depends significantly from the composition of the starting solution. In the results of the present study, from a cooling crystallization process without traversing liquid-liquid phase separation region, long plate with negligible agglomeration and a narrower distribution were produced, whereas from process involving a liquid-liquid phase separated mixtures, the crystals were more agglomerated and with a wider distribution. Although it was believed that lower particle size was obtained due to attrition and breakage in the instrument used for sizing measurement. Crystallization through the liquid-liquid phase separation resulted in better yield compared to standard crystallization. In all the experiments, recrystallized ibuprofen contained only one polymorphic form and had similar melting temperature of the starting material.

In addition, when particles were agglomerated, the product flow properties were greatly improved from fairly flowing behaviour of the raw material to the free flowing behaviour of the agglomerated product. These agglomerates were produced using different operating conditions compared to the conditions reported in the literature, showing the importance of the ternary phase diagrams for the identification of the design space across which agglomerates with optimized properties can be produced.¹⁴⁸ Additionally, ternary phase diagrams can be used to identify the region where controlled seeded crystallization can be performed and phase separation can be prevented since the occurrence of liquid-liquid phase separation is normally undesired during crystallization processes because impurities are often more soluble in the solute-rich phase hence leading to impure crystals and unsatisfactory particle size.¹⁶⁵⁻¹⁶⁷

Chapter 5. Agglomeration Study of a Pharmaceutical Active Ingredient

This chapter describes work carried out at GSK, Stevenage, UK as part of an industrial placement during my PhD. The work is confidential, so will be an embargoed chapter and will not appear in the final, open version of this thesis.

5.1 Introduction

In industrial crystallization processes, the influence of process parameters on the attributes of solid product such as form, shape and particle size distribution is extensively studied to achieve the required understanding and control of a crystallization process. In most cases, the desired particle size distribution is dictated by the needs of downstream processing (washing, filtration, drying) or end product specifications.¹⁶⁸ The occurrence of agglomeration whether of seeds or of recrystallized particles can have the largest impact on a seeded crystallization and product quality, where the aim is to add seed crystals in order to provide growth surface to achieve controlled growth of crystals whilst avoiding unwanted primary nucleation to achieve a unimodal crystal size distribution and target product size.

However, the surface properties of seeds crystals may be altered during the seed generation process (i.e. dry or wet milling) and this can have a significant impact on crystal growth and consequently on final particle size distribution.¹⁶⁹ Moreover, if agglomeration occurs in the seeding vessel, the surface area available for growth will be reduced and it may result in broadening the particle size distribution (PSD) and entrapment of solvent between particles, impeding purification or drying. Therefore, agglomeration is often an unwanted process during seeded crystallization due to its negative impact on product properties and in some cases strategies to avoid its occurrence are also sought.

Both the detection and the degree of agglomeration have been studied indirectly through the measurement of initial and final particle size distribution¹⁷⁰ and directly through imaging methods¹⁷¹. Whilst these agglomerates can often be recognised by eye, it would be extremely wasteful to manually sort particles into agglomerates or single crystals. The use of microscopy based methods based on human assessments has been replaced in recent times with more automated techniques.¹⁷²⁻¹⁷⁴

Automated characterisation of particles between single crystal and agglomerate through image analysis can be carried out automatically, relying on a number of image descriptors linked to size, shape and colour of the particle imaged. This categorisation of particles can be achieved by thresholding, principal component analysis or machine learning.^{170, 172, 175}

After crystallization, particles are typically isolated using agitated filter driers, where filtration and drying are carried out in a single vessel. Industrial filtration is usually performed applying positive pressure of nitrogen to remove the excess of solvent, before the drying step is performed under vacuum to remove the remaining solvent.

Depending on the physical properties of solvent to be removed and for improving the efficiency of process design, a washing stage including multiple washes is often included with the aim of removing impurities whilst avoiding precipitating out any materials/impurities from the mother liquor. Furthermore, the washing solvent can be used to displace a high boiling point solvent used in the process which would lead to very long drying times and could compromise the stability of the compound if higher drying temperatures are required. In addition, (vigorous) stirring over a prolonged period of time can be required to break up agglomerates due to entrapment of mother liquor.¹⁷⁶⁻¹⁷⁸

The work described in this chapter has been carried out on a pharmaceutical active ingredient during an industrial placement at GSK (Stevenage, UK) which, for confidentiality reasons, cannot be named and will be referred to as GSK 106.

5.1.1 Aims and objectives

The goal of this project is the understanding of agglomeration process and the effect of process parameters on agglomeration and on the physical properties of the agglomerates. The aims and objectives can be divided into two main research areas.

The first study was to develop understanding of the agglomeration behaviour of GSK106 during seeded crystallization process using in-situ Process Analytical technology (PAT). In-situ analysis is always preferred over off-line approaches as this enables monitoring and control in real-time and avoid sample preparation stage which may change the nature of the material. Both FBRM and PVM were used for gathering information about the true state of particles during the process. Images

recorded by the PVM probe were analysed offline through an in-house image analysis algorithm coded in MATLAB 2015a to detect likelihood of agglomeration using descriptors.

The second study focused on the understanding of the effect of crystallization parameters on the washing efficiency of the cake post primary filtration, and the sensitivity to attrition in the drying step of the agglomerates. Agglomeration can have a negative effect on the drug substance particle properties, such as broadening the particle size distribution and reducing the efficiency of cake washing because mother liquor and impurities can become trapped in the particles hence compromising the quality of the drug product. Product properties such as particle size, shape, loss on drying and residual solvent were evaluated using the appropriate techniques.

5.2 Experimental

5.2.1 Setup and procedures

Setup. All seeded crystallization experiments were carried out in a temperature-controlled 1L jacketed dished bottom glass crystalliser with a 3 blade retreat-curve glass impeller (Figure 5.1). In order to monitor and collect meaningful data during the crystallization process, the crystalliser was equipped with: a temperature probe, an FBRM G400 probe and a PVM V19 probe. The reactor temperature was controlled by means of a chiller (Huber).

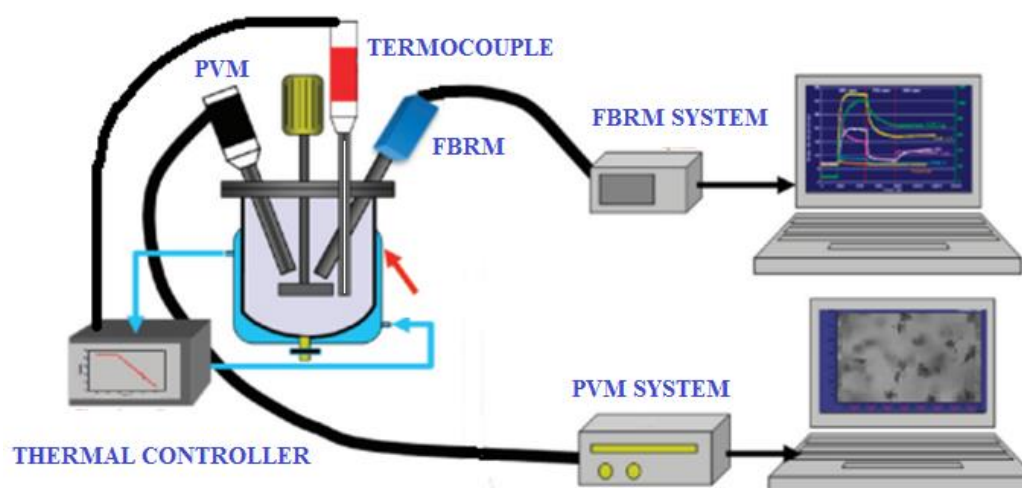


Figure 5.1 Schematic of reactor used for the experiments.

Experimental procedure. Growth and agglomeration behaviours of GSK106 was investigated by adding seed crystals of the compound whilst varying operating conditions such as agitation rate, composition of dispersant for seeds slurry, amount of seeds and antisolvent addition time (Table 5.1). The operating conditions investigated for the set of experiments were selected based on the three main mechanisms likely to impact agglomeration in the crystallization process: (1) seed load (% w/w) and their dispersion in the bulk upon diluent composition, (2) mixing, and (3) supersaturation caused by antisolvent addition rate. Seed particle size was specific and had to be fixed.

Table 5.1 Table illustrating experimental conditions for growth experiments.

Exp.	Seed prep. (v/v DMSO: water)	Seed mass (% w/w)	Agitation rate (rpm)	Antisolvent addition time (mins)
N1	6:1	0.5	260	120
N2	6:1	0.5	150	30
N3	4:1	0.5	150	15
N4	4:1	0.5	260	15
N5	4:1	0.1	150	30
N6	4:1	0.1	260	45

The upper and lower conditions used in the experiments were to deliver an industrially relevant, robust and scaleable process. Table 5.1 shows the experimental conditions which were used for the seeded experiments. For N5 and N6 an additional temperature cycle was added before the end of the experiments.

The crude reaction mixtures of GSK106, 11 wt % of GSK106 in a solution of DMSO:water (97.3:2.7 wt/wt), were prepared such as having the same composition and provided for these studies by GSK and for confidentiality reason will not be discussed in this report. Seeds crystals of GSK106 were previously prepared by dry milling. A constant seed size of 5 μm (d_{v50}) was used for all the experiments. The reaction mixture of GSK106 was charged into the vessel, heated to 45°C and an amount of 0.25 wt of water (0.25 gram per gram of the starting material) was added

over 5 minutes to adjust the solution composition. After the addition of water, the solution was stirred at 45°C for at least 30 minutes to ensure complete dissolution. Once equilibrated, the solution was cooled down to 20°C over an hour. The reactor was then kept at constant temperature and the mixture was stirred at the desired stirring rate. The seeds (0.005 wt) were suspended in DMSO:water mixtures (0.03 volumes per gram of starting material) in a vial and then the slurry was added to the reactor. A similar volume of mixture was then used to rinse the vial and added to the reactor to avoid losses of seeds. Two levels of DMSO:water ratio of 4:1 and 6:1 v/v were used for preparing the slurry suspension of seeds; a different period of time was used to disperse the seeds, i.e. seeds in mixture 4:1 were dispersed for 1 minute and in 6:1 v/v were dispersed for 2 minutes prior to charging into the reactor contents. Two levels of agitation rate were investigated at 260 rpm and 150 rpm and antisolvent addition time between 15-120 minutes was chosen. After an hour of aging at 20°C, a mixture of 58:42 w/w of DMSO:water (3.8 wt) was then added to promote growth of particles to the target size. After completion of the antisolvent addition, the slurry was then aged for an hour at 20°C.

Additionally, a temperature cycle was added to experiment N5 and N6: the reaction mixture was heated to 75°C and hold at this temperature for at least 90 minutes then cooled to 20°C over 4 hours to investigate the effect of dissolution induced by the heating on product properties such as shape and strength of particles before and after agitation in the filter-dryer. Moreover, it must be noticed that the amount of seeds used was 5 times lower than experiments from N1 to N4, to address if the lower concentration of solids in the slurry has dispersion homogeneity.

The sequences of images of the particles in suspension were captured using the PVM probe, with a rate of 1 image every 2 seconds. Every sequence of images was then converted in 8-bit grey-scale image using icPVM v7.0 software. The chord length distribution of particles was recorded using the FBRM probe, with a rate of 1 sample every 15 seconds. The trends were analysed using icFBRM v4.3 software.

Slurry samples were removed from the bulk, before filtration, to determine the starting particle size distribution of the product. The slurries were then filtered in a filtration drying unit of 1L volume (20 µm mesh filter) at 250 mbarg head pressure of nitrogen and the cake was allowed to deliquor (to trickle point). The cake was then

washed by charging a mixture of 4:1 v/v of DMSO:water (3 vol) and allowing to soak without agitation to remove impurities and avoid precipitating any product or impurities from the mother liquor. Then the cake was washed with water (4 times of 3.0 vol, followed by 2 times of 6.0 vol) under 250 mbarg positive pressure of nitrogen to remove the DMSO prior to drying because DMSO has a higher boiling point it would require a long drying to remove it from the solid. Finally, the cake was blowdown with flow-through nitrogen at 1 barg to achieve values of loss of drying (LOD) in the range of 10-15% w/w.

The wet cake was then agitated at 90 rpm and 20°C and samples were taken from the cake every 5, 10 and 60 minutes to assess attrition and investigate the effect of operating conditions on the mechanical strength of particles. Particle size distributions (PSDs) and the degree of attrition were assessed by measuring the PSD with laser diffraction technique using a Malvern Mastersizer® 2000. An Olympus® BX 51 optical microscope with magnification of 5x, 10x, 20x and 50x was used to characterise shape, size and breakage of crystals. Surface morphology of crystals was observed using a scanning electron microscopy performed using a Hitachi® SEM 1000 table top microscope at 15.00 kV. The water content was measured by Loss on Drying (LOD) technique using a Mettler Toledo® HR-83 moisture analyser at a temperature of 120°C using an aluminium pan and weighing ca. 1.0 g of sample. Residual content of DMSO in the final dried material, to comply with final specific requirement, was measured using proton nuclear magnetic resonance spectroscopy (¹H NMR 400 MHz) and for all the experiments the value was within the specification (less than 0.2%w/w DMSO relative to GSK106). The cake was then dried overnight at 65°C under vacuum (50 mbar) with agitation of 90 rpm.

5.2.2 Image analysis

For the quantitative analysis of the images, which were acquired with the PVM probe, a set of four image processing functions were assembled which accounts for the acquisition of images in backscattering operating mode (black particles over white background). These functions were developed in-house⁷² (unpublished work of Dr C. Brown, University of Strathclyde) and used successfully to study the agglomeration behaviour of paracetamol in 3-methyl-1-butanol¹⁶. Each function is

implemented in MATLAB R2015a and uses the Image Processing Toolbox and the Statistic and Machine Learning Toolbox add-ons to carry out a structured analysis of the images (Figure 5.2). The advantage of the use of computer software scripts is a faster method compared to the usual microscopy method, i.e. a computational time to analyse a set of 300 images in a minute. Moreover, the scripts use the images from the PVM probe, which is one of the most useful tools for real time understanding of processes like crystallization, liquid-liquid phase separation/oiling out and polymorphic transformation. With the PVMA Toolbox, 20 different descriptors accounting for size, shape and colour of particles can be generated and their mean value with standard deviation and mode extracted (Appendix 1).

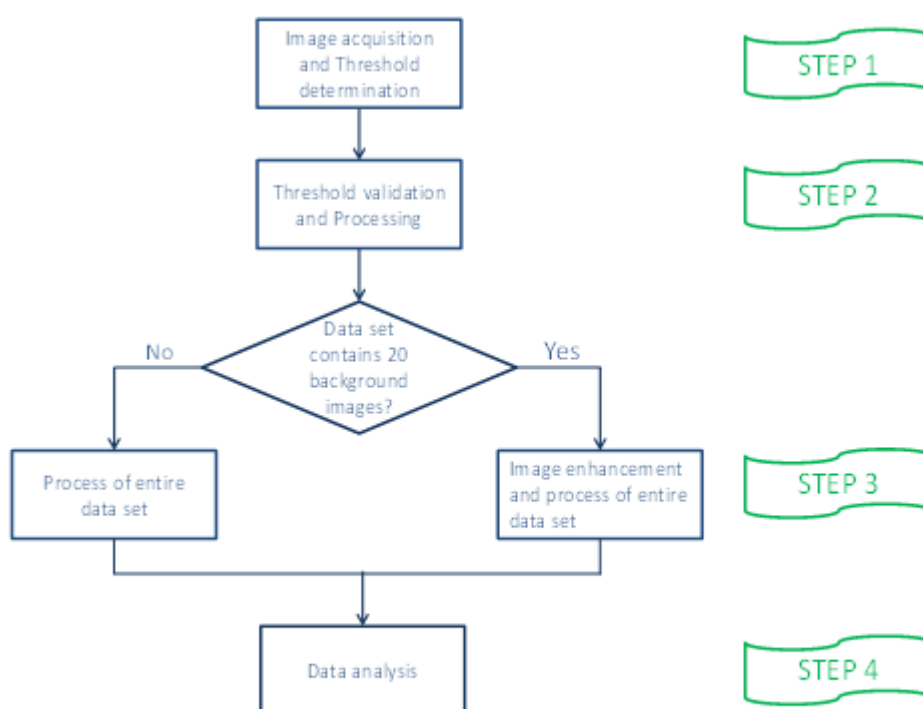


Figure 5.2 Schematic overview of imaging analysis procedure using PVM Analysis Toolbox.

STEP 1: Each PVM image is an 8-bit intensity image i.e. each pixel in the image can have a value from 0 (black) to 255 (white). When the threshold value is identified, its value will lie between these two values, consequently any pixels with a value greater than it will be converted to white (255) and any less than converted to black (0).

STEP 2: The threshold value determined in the first step is then tested over a set of images. In each image, pixels are converted to black or white using a threshold value of 100, then with a closing operation of 3x3 square structuring elements, smaller gaps are closed and holes are filled. The regions touching the border are removed.

STEP 3: An entire dataset of images can thus be analysed at a selected threshold. The function generates a *.mat file to be used for onward analysis the feature extraction and particle identification.








STEP 4: The function uses the file from step 3 to calculate descriptors like solidity, circularity and heterogeneity for each time step. The duration of each time step depends on the capture rate of the probe which, in turn, controls how many images are grouped together to produce the descriptor distribution. It is recommended to select a time step which will contain a minimum of 300-500 particles to produce a meaningful distribution.

Descriptors. Table 5.2 presents a few examples of shape and their descriptor values extracted from Borchert and co-workers (detailed information of these descriptors can be found in Appendix 1.¹⁷⁵

These are (1) circularity, defined as the ratio of the projected area to the area of the circle with the same perimeter, where a projected area is the area of pixels occupied by a particle, (2) convexity, defined as the ratio of the convex perimeter to the perimeter of the particle region, (3) solidity, here defined as the ratio of the pixel area to the convex area, and (4) circle equivalent diameter, defined as diameter of circle with the same projected area as the particle.

It can be seen that particles on the second and fourth row are mostly single plate-like crystals, which correspond to the morphology of the seed crystals. These crystals have higher values of the three shape measurements, i.e. solidity, circularity and convexity and a lower value of circle equivalent diameter.

Table 5.2 Shape and size descriptors extracted from Borchert and co-workers¹⁷⁵ after binarization.

Shape	CED (μm)	Solidity	Circularity	Convexity
	288	0.78	0.23	0.68
	266	0.79	0.30	0.79
	491	0.55	0.14	0.61
	65	0.96	0.65	0.90
	138	0.89	0.63	0.86
	325	0.89	0.44	0.77
	371	0.69	0.19	0.65

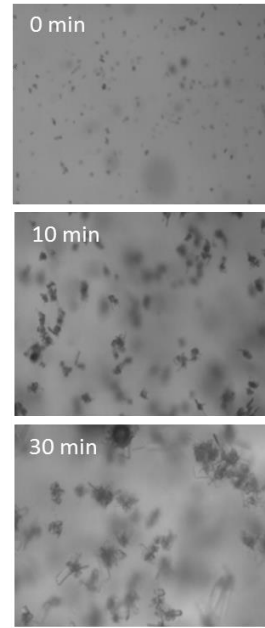
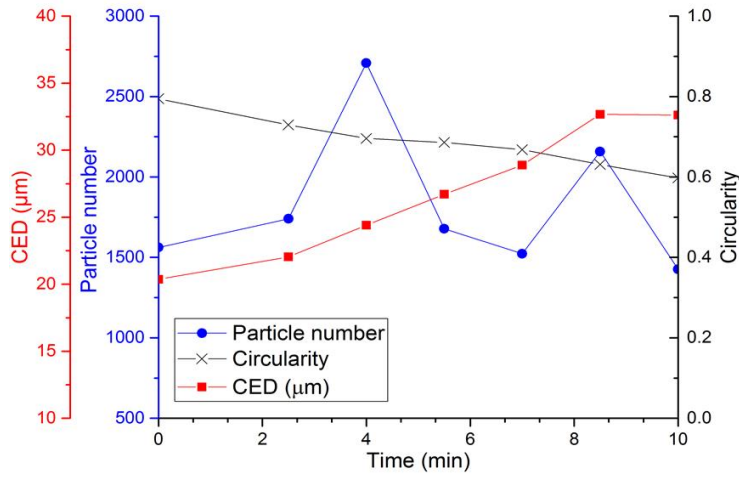
In addition, these descriptors were successfully used previously to characterise particles having different morphologies ranging from needle shaped¹⁷⁹ to rhombic shaped¹⁷¹ crystals indicating a high probability to positively characterise the particles obtained during this process.

5.3 Results and discussion

5.3.1 Image analysis of GSK106

Numerous possible descriptors for agglomeration detection and their description have been used in the literature but selecting the optimal method is critical. In this work, the selection of features was guided by several considerations. First, on a rapid look of PVM images, seed crystals appeared to undergo aggregation/agglomeration during slurry preparation, thus complicating a proper selection of the descriptors. Therefore, the dispersion homogeneity of seeds was analysed for the first 10 minutes of recorded images. In addition, this interval of time was limited to 10 minutes in order to avoid excessive overlapping particles located on the front of the window and behind that precludes identifying single particles reliably.

(a) N1



(b) N2

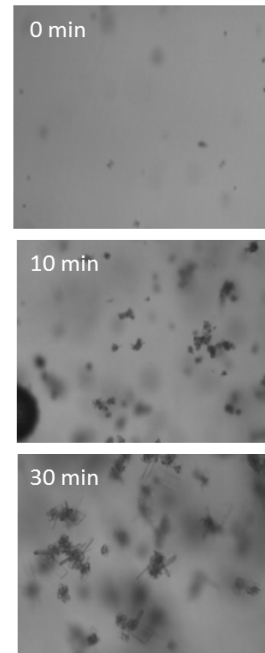
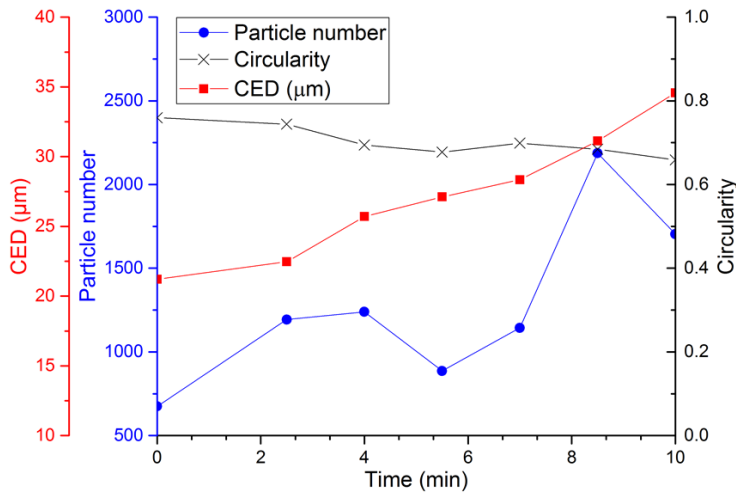
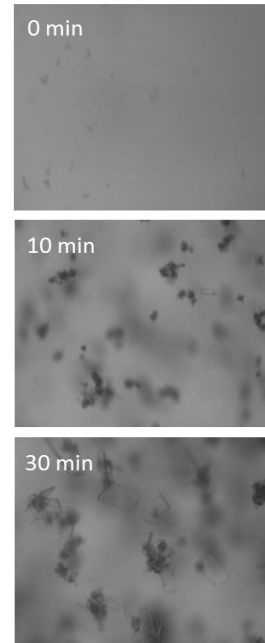
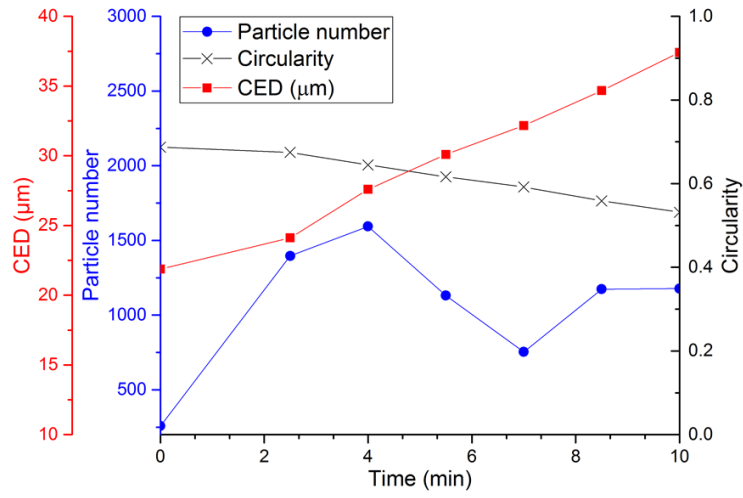


Figure 5.3 Variation of particle number, circularity and circle equivalent diameter (CED, μm) for experiments a) N1, b) N2, c) N3, d) N4, e) N5, f) N6. PVM images are shown at 0 min (seed crystals), 10 min and 30 min after the addition of seeds.

(c) N3



(d) N4

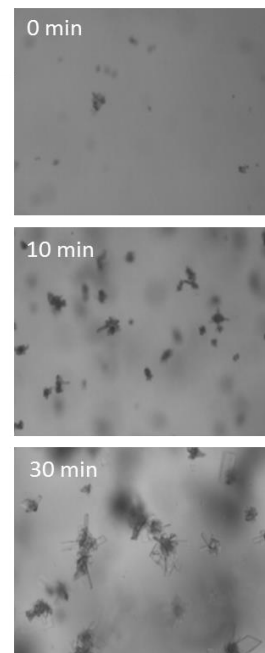
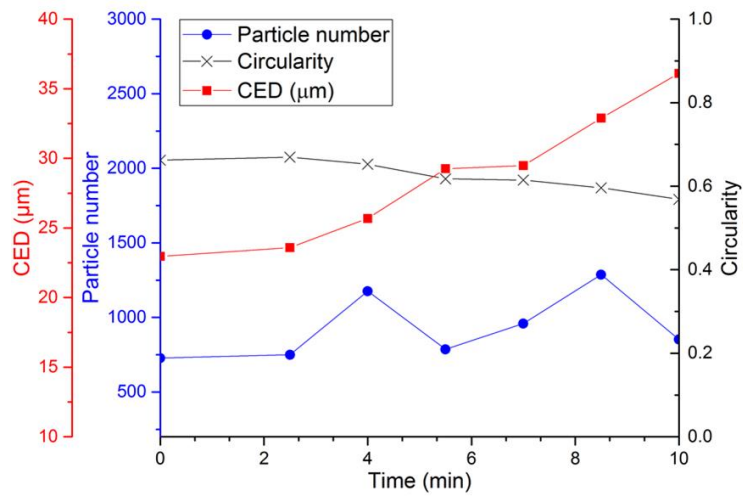
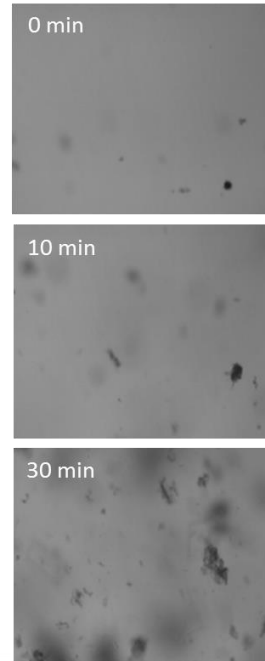
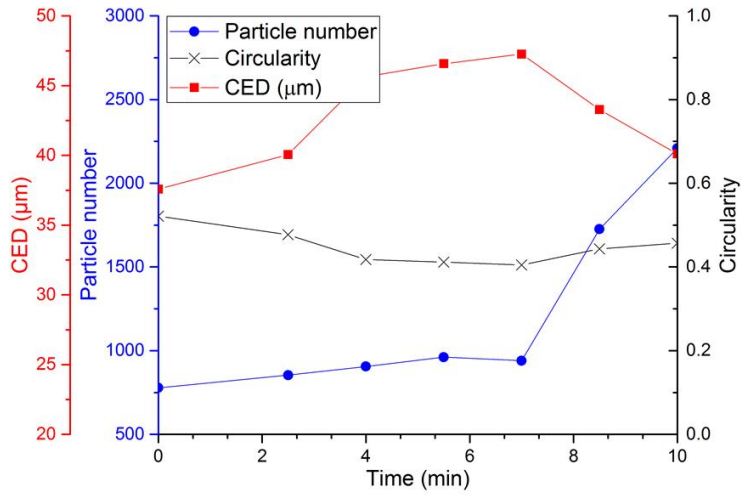


Figure 5.3 continued

(e) N5



(f) N6

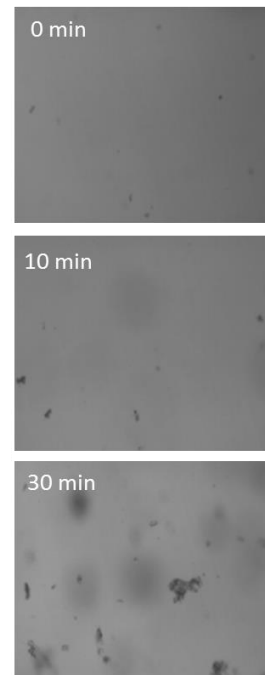
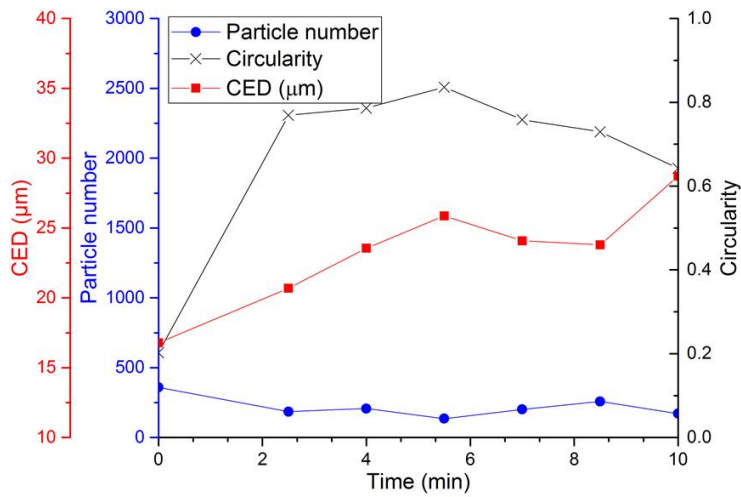


Figure 5.3 continued

Figure 5.3 shows the variation in the mode value of circularity, circle equivalent diameter based on projected area (CED, μm) along with number of particles

identified in each population. It should be noted, prior to starting any analysis that the number of particles for experiment N6 was lower than any other experiment thus suggesting that the distribution may not be representative for the population. It can be seen that from experiment N1 to N4, the PVM images show predominately agglomeration of seed crystals at time 0. However, this is in contrast with the high value of circularity (ca. 0.7) which suggests that the population is mostly formed of single crystals, based on the values suggested by Borchert and co-workers¹⁷⁵. This value of circularity does not seem to capture the system behaviour and a choice could be the refinement of the analysis evaluating the entire descriptor distribution. For experiment N5 and N6, the circularity is observed between 0.2 and 0.5, thus suggesting agglomeration of the seed crystals in the early stage based on the values suggested by Borchert and co-workers¹⁷⁵. Increase in size (CED) due to the enlargement of agglomerates already formed can be noticed for the particles from experiment N1 to N4, whilst the trend of experiment N5 seems to suggest a decrease in particle size between 5 and 10 minutes. However, this trend doesn't supply sufficient information if this reduction in particle size is due to additional breakage of agglomerates of seed crystals or prevention of agglomeration process. When compared with the PVM images (Figure 5.3), it was found that single plate-like crystals grew besides agglomerates for experiment N5 and N6, which highlight that a better dispersion of the seeds can be achieved by decreasing the seeds amount and highlight the weakly aggregation of seed crystals. However, the aggregation/agglomeration of seeds can't be totally eliminated.

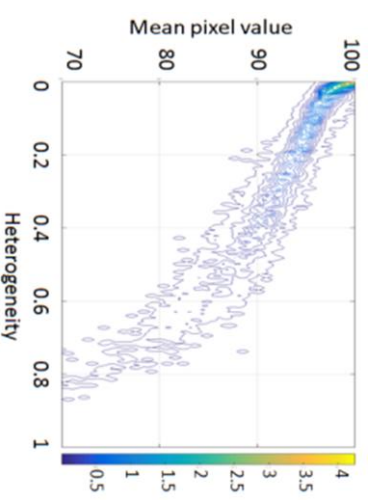
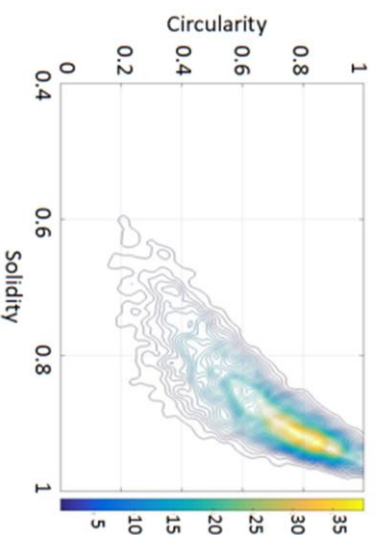
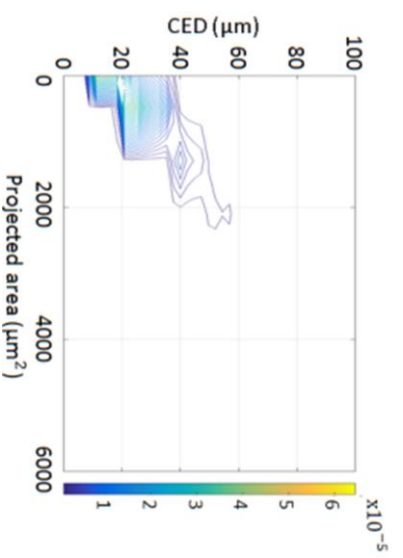
Influence of seed dispersion. In order to understand which operating conditions influenced the degree of agglomeration of the compound under investigation, the PVM datasets were analysed based on the method detailed by Borchert and co-workers¹⁷⁵, analysing the entire descriptor distribution. Six descriptors were chosen to get a deeper insight of the agglomeration process, namely CED, projected area, circularity and solidity, mean pixel value and heterogeneity. These descriptors represent the population of particles in size: CED vs projected area, shape: circularity vs solidity and greyscale: mean pixel value vs heterogeneity.

Size

Shape

Grayscale

N1



N2

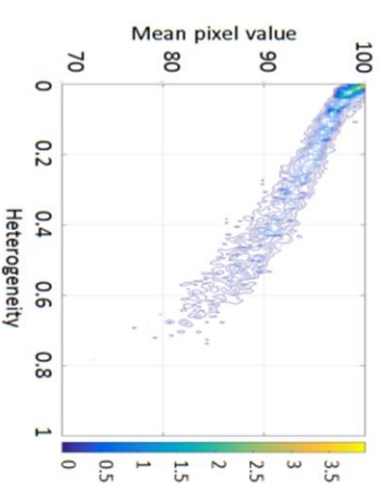
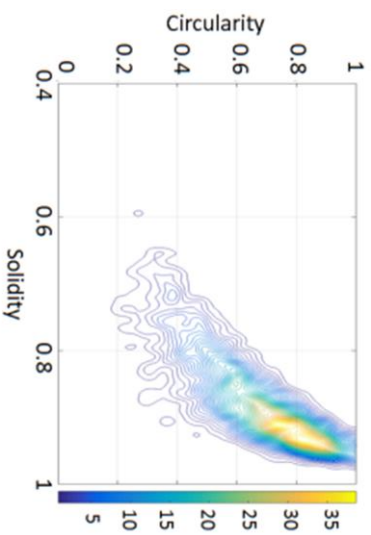
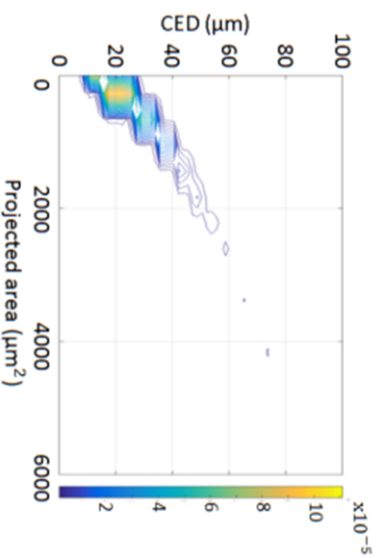


Figure 5.4 Population densities analysed during 5 minutes after addition of seeds in the vessel from left to right: size, shape and grey-scale for experiment N1, N2, N3 and N4.

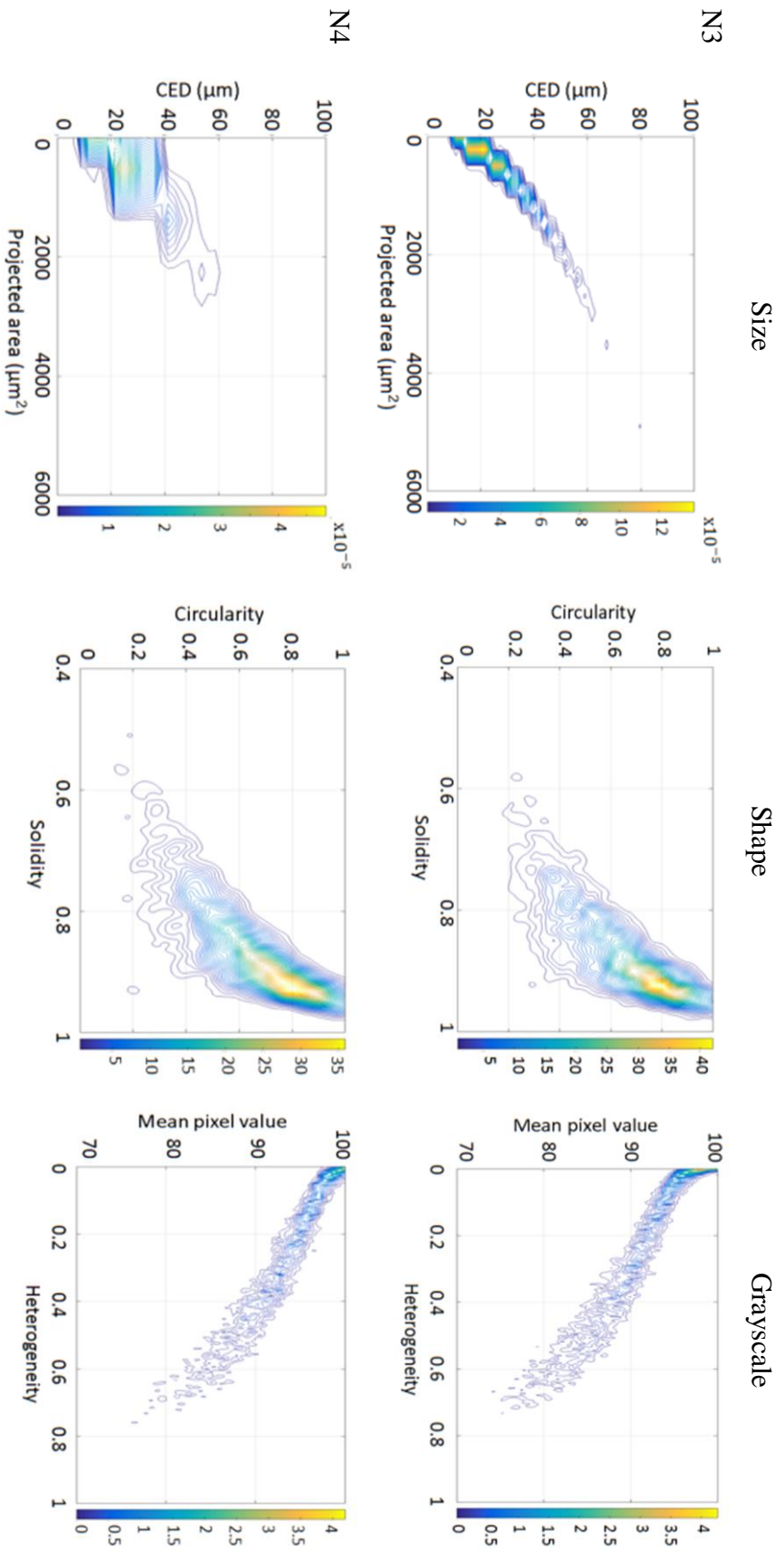


Figure 5.4 continued

Seed crystals of experiment from N1 to N4 were prepared by dispersing the same amount of seeds in the same total volume but having different solvent:antisolvent ratios (6:1 or 4:1 v/v) and length of the dispersion time, with the aim to study the influence of mixture composition and dispersing time on the dispersion ability of the seed crystals. Characterisation of the seed crystals, and their dispersion ability was carried out by analysing the first 5 minutes after addition in the crystalliser. Descriptor population maps representing the first 5 minutes of recorded PVM images for experiments N1, N2, N3 and N4 are reported in Figure 5.4.

Comparison of the populations shows slight differences between size and shape of crystals, with most change in the grey-scale map. Values of heterogeneity below 0.4 should suggest the presence of agglomerates in the process which is in good agreement with the values proposed of Alander *et al.*¹⁷¹ For experiments N1 and N4 (higher stirring rate), the area of the seed crystals is mostly below $1000 \mu\text{m}^2$ and the CED is in the region of 20 and 30 μm . Most of the seed crystals have circularity and solidity higher than 0.4 and 0.6 respectively. Therefore, the increase in particle population in medium solidity and low circularity observed would be consistent with the aggregation of seeds, thus indicating that the volume ratio of solvent:antisolvent used and the prolonged dispersion of seeds had little effect on break-up existing agglomerates. This is also confirmed by visual inspection of the PVM images (Figure 5.5) and the highest number of particles detected for N1.

The populations of experiments N2 and N3 show slight differences between size and shape of seed crystals, without changes in the grey-scale map. Although lower values of heterogeneity suggests the presence of agglomerates for both the populations. The area of the seed crystals is reaching values greater than a $1000 \mu\text{m}^2$ for experiment N3 and the CED up to 50 μm . Both projected area and CED are higher for experiment N2 and N3 compared to experiment N1 and N4. Most of the seeds have circularity above 0.4 and solidity above 0.7, thus confirming again the aggregation of seed crystals for both experiments. The degree of agglomeration of seed crystals seems to be higher for experiments N3 which have been carried out with shorter dispersion time and slower stirring rate. From an inspection of the first PVM images of the four experiments (Figure 5.5), the seed crystals of experiment N1, when using higher ratio solvent:antisolvent and higher stirring rate, seems to be better dispersed

compared to experiment N2, N3 and N4, also confirmed by the highest number of particles detected among the other experiments (Figure 5.3).

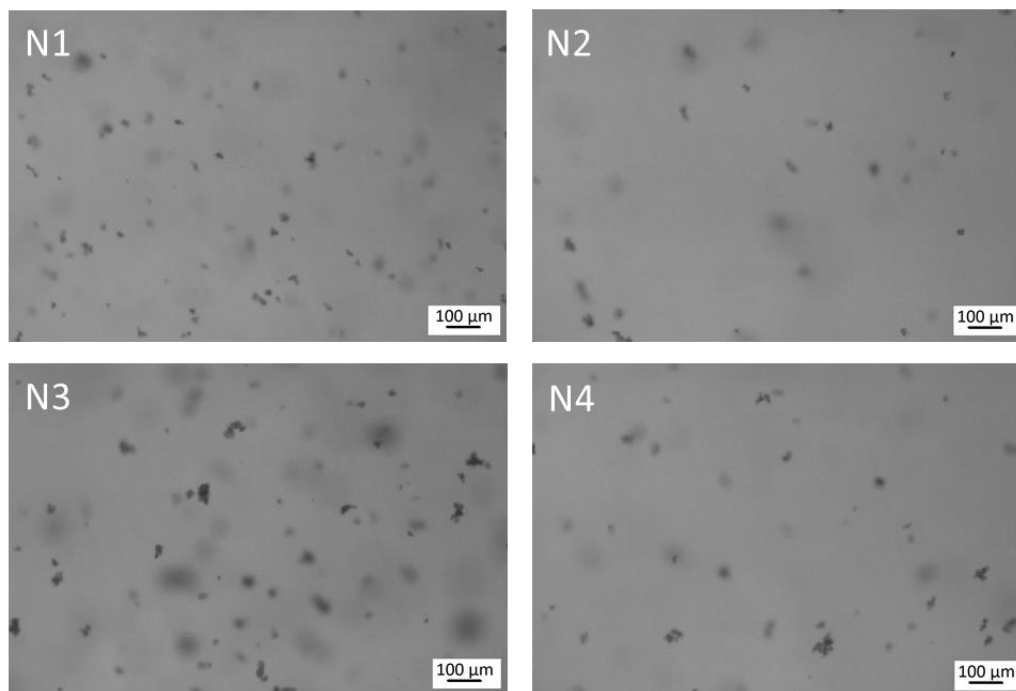


Figure 5.5 PVM images of seed crystals for experiment N1, N2, N3 and N4.

Moreover, the amount of seed crystals used in the experiments could be another factor affecting the dispersion homogeneity of the seed crystals in the slurry. As previously discussed, experiment N5 and N6 had a lower amount of seed crystals to get deeper insight into the influence that this factor may have on the final product attributes. The results of experiment N5 and N6 are presented in Figure 5.5.

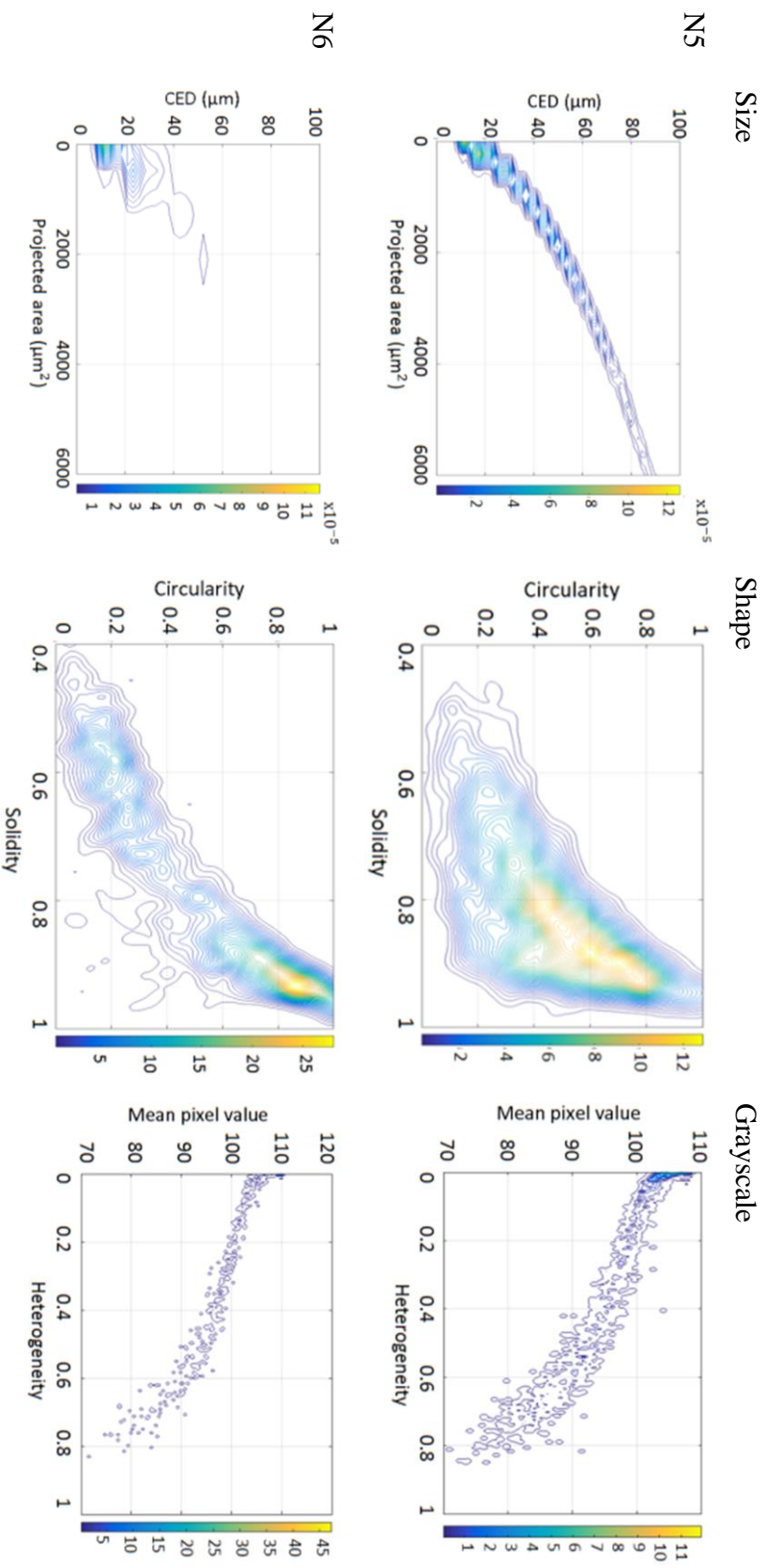


Figure 5.6 Population densities analysed during 5 minutes after addition of seeds in the vessel from left to right: size, shape and grey-scale for experiment N5 and N6.

For experiment N5, the area of the seed crystals is reaching values of greater than $4000 \mu\text{m}^2$ and the CED up to $80 \mu\text{m}$. A significant increase in the values of the equivalent diameter and the projected area of seed crystals can be noticed in all experiments performed. Experiment N6 shows similarities with experiments carried out at same stirring rate the area of the seed crystals is mostly below $1000 \mu\text{m}^2$ and the CED is below $40 \mu\text{m}$. However, the circularity-solidity spaces show differences in the distributions (Figure 5.6), with the population extended towards the lower left corner (medium solidity, low circularity) hence confirming the aggregation of seed crystals for the experiment. It can be seen that PVM images shows predominately agglomerated seed crystals (Figure 5.7).

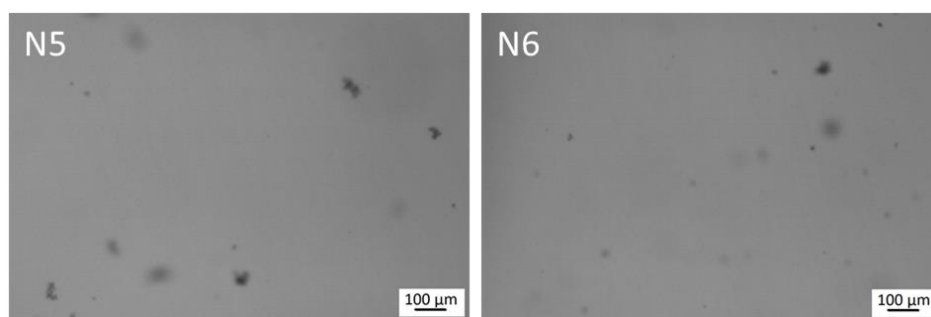


Figure 5.7 PVM images of seed crystals for experiment N5 and N6.

The results of these series of experiments highlight two important factors for influencing the experimental design. Firstly, with lower seed amount and improved sample dispersion, aggregation of seed crystals was not eliminated. Therefore, an investigation of the surface properties of milled and unmilled crystals with method such as zeta potential or surface energy analyser would be useful. Results from crystal surface measurements are advantageous in probing the agglomeration propensity of a compound, i.e. values of zeta potential near zero indicates that particles are prone to agglomeration or aggregation as they lack any electrostatic repulsive forces. Secondly, quantification of the degree of agglomeration for each experiment could be achieved by defining the limit or value of the descriptors for which a single crystal can be distinguished from an agglomerate. Borchert and co-workers¹⁷⁵ defined for the agglomerates specific limits of solidity (<0.85) and circularity (<0.5) hence splitting the population into two groups: single crystals and

agglomerates. However, these limits are shape dependent and these should be determined also for the particles under investigation in order to obtain a reliable result.

Influence of stirring rate. Trends of CED and particle number of the experiments are compared to investigate the effect of stirring rates on the degree of agglomeration of seed crystals in the crystalliser. Several literature works have discussed the interaction between the Kolmogorov turbulence microscale and agglomeration behaviour. David and co-workers¹⁸⁰ suggested that the probability of agglomeration is higher between smaller crystals than larger crystals and distinguish particles as being larger or smaller than the Kolmogorov microscale. Moreover, Rasmuson and co-workers¹⁸¹⁻¹⁸³ and Hollander and co-workers¹⁸⁴ demonstrated that for length scales greater than the particle size, the particles only experience laminar stresses.

Circle equivalent diameter and particle number plots during 10 minutes after seed addition in the crystalliser are reported in Figure 5.8. Very little difference is observed between the trends of N1, N2, N3 and N4 for which the increase of CED and decrease of particle number with time (from ca. 20 μm to ca. 35 μm) suggests that particles are growing through agglomeration. The first step in agglomeration formation is the collision of particles; the more particles present in solution the more frequent the collisions and the higher the likelihood of forming agglomerates. However, under intense agitation, it would be expected that for higher stirring rate, the agglomeration becomes less favoured compared to breakage resulting in smaller the particle size.¹⁸¹⁻¹⁸³ This was not observed since the selected higher stirring rate had very little or no effect on the increase in size and agglomeration of particles. Different trends of CED and particle number are observed for experiment N5 and N6. The trend of CED for N5 shows a maximum around 5 minutes which correspond to a minimum of the circularity followed by a subsequent decrease of CED. This implies that breakage or prevention of agglomeration process followed the initial dispersion of seeds.

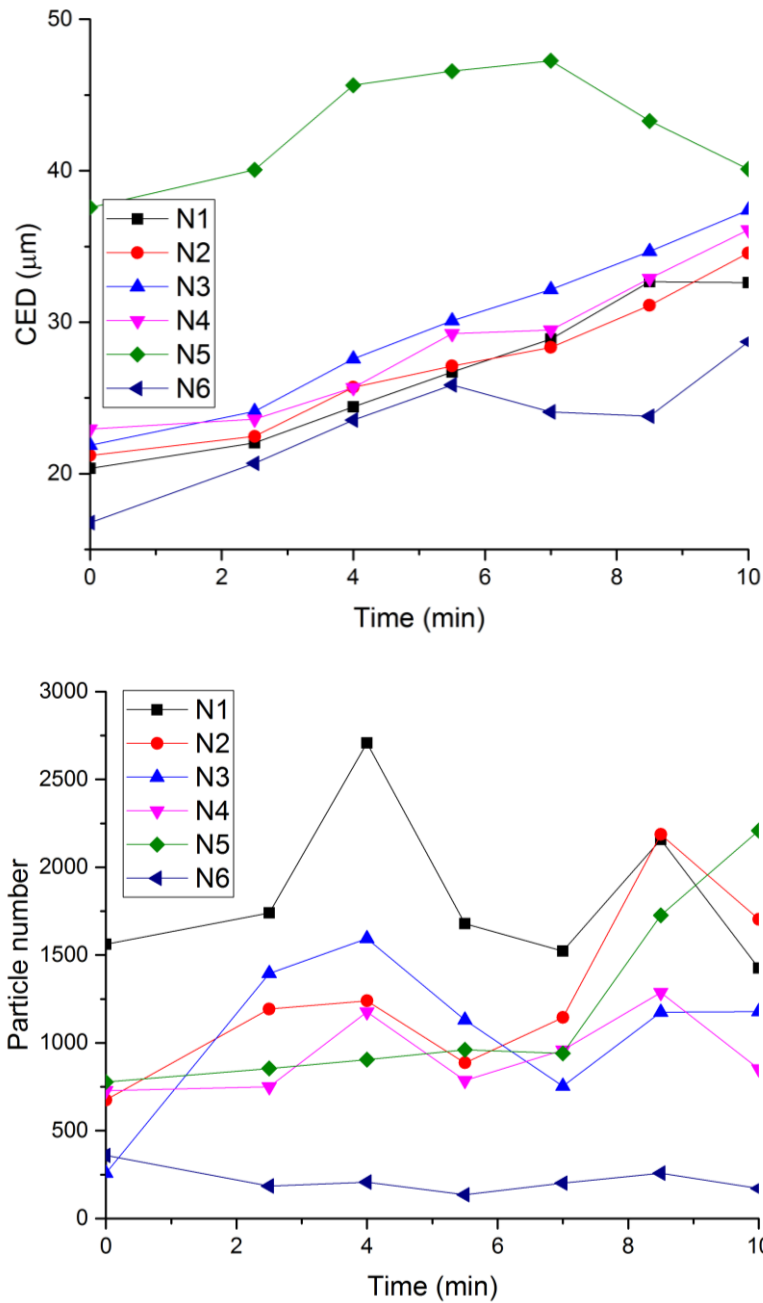


Figure 5.8 Mean of CED and particle number of experiments N1, N2, N3, N4, N5 and N6.

It is most probable that seed crystals are loosely aggregated in the feed suspension and under prolonged stirring are separated or de-agglomerated into smaller individual crystals. However, a better correlation between the mixing conditions and descriptors could be achieved if experiments would be performed for different operating conditions such as varying stirring rate, impeller dimension and volume.

Assuming the agglomeration kernel β to be the product of the collision efficiency β_c and the agglomeration efficiency Ψ , correlations are available for the latter which consider the influence of mixing parameters.^{80, 185} The use of simulation software like VisiMix would also potentially characterize mixing related parameters such as shear rate, maximum degree of axial non-uniformity and characteristic time between strong collisions. Such insights into the effect of local process parameters on agglomeration in the equipment used may allow selection of equipment and/or operating parameters that minimise these effects.

5.3.2 In situ monitoring of growth of GSK106

As previously mentioned, six experiments were performed to have a more fundamental understanding of agglomeration during the growth process of GSK106 under different operating conditions. An FBRM probe was used as in-situ PAT for real time monitoring of changes in particle size and shape resulting from growth or agglomeration processes by tracking changes in the particle chord length distribution over time. This tool coupled with PVM allows gathering detailed information about the growth process and any concurrent phenomena such as agglomeration, breakage and secondary nucleation which affect the resulting particle size distribution.

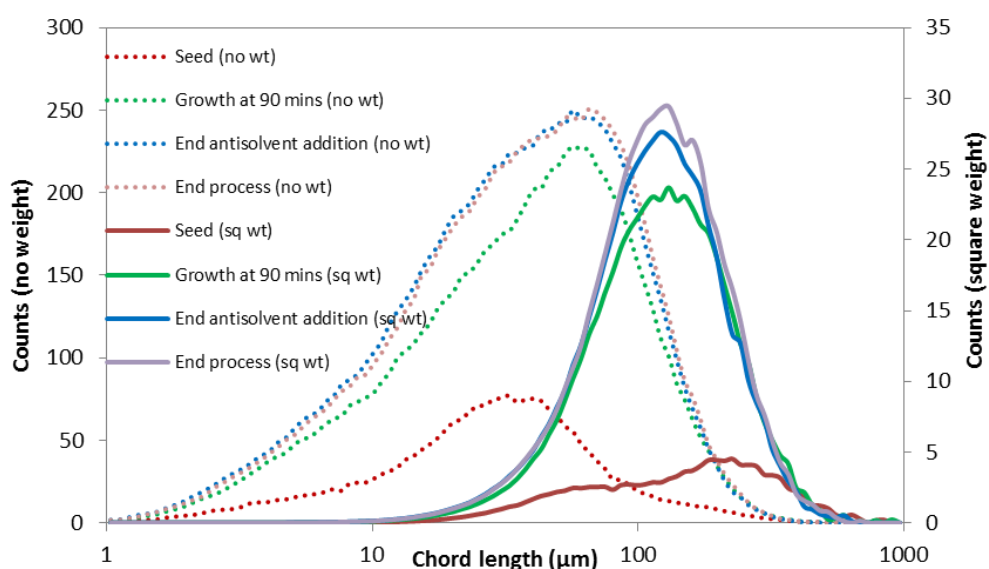


Figure 5.9 FBRM CLDs overlay collected at different stages during growth of agglomerated particles, from seeding to the end of the process for experiment N1.

An overlay of macro chord length distributions (CLDs) obtained from inline monitoring using FBRM for experiment N1 capturing the growth of seeds until the end of the process is shown in Figure 5.9.

It can be observed that the particles have grown from ca. 30 μm (aggregated/agglomerated seed crystals) to ca. 135 μm (end of process), increasing the number of coarse particles observed per second. As previously mentioned, seed crystals (d_{v50} in the range 3-4 μm) were agglomerated or aggregated before addition in the crystalliser. PVM images collected after 30 minutes were not used for image analysis of experiments N1 to N4 since it was not possible to distinguish particles due to the high suspension densities, a significant limitation of the technique.

Figure 5.10 shows the normalised macro FBRM chord length distributions along with the square-weighted mean chord length (SWMCL) of particles after the antisolvent addition period. Those distributions are unimodal and moved toward larger size classes. The rate of antisolvent addition influences the rate of generation of supersaturation hence the level of supersaturation and the extent of growth and nucleation. The different supersaturation versus time profile obtained at longer addition time (reduced antisolvent flow rate) should reduce the bulk supersaturation favouring condition for growth of large particles whilst rapid desupersaturation may lead to more secondary nucleation rather than the desired growth of the seeds. Generally, based on the SWMCL obtained, it is possible to state that substantial difference can be found between experiments and the addition rate of antisolvent or rate of supersaturation generation has no significant effect on the product mean size. Overall, the results suggest that the growth is the main mechanism involved in these processes, with the SWMCL changing according to $N6 > N4 > N2 > N3 > N5 > N1$.

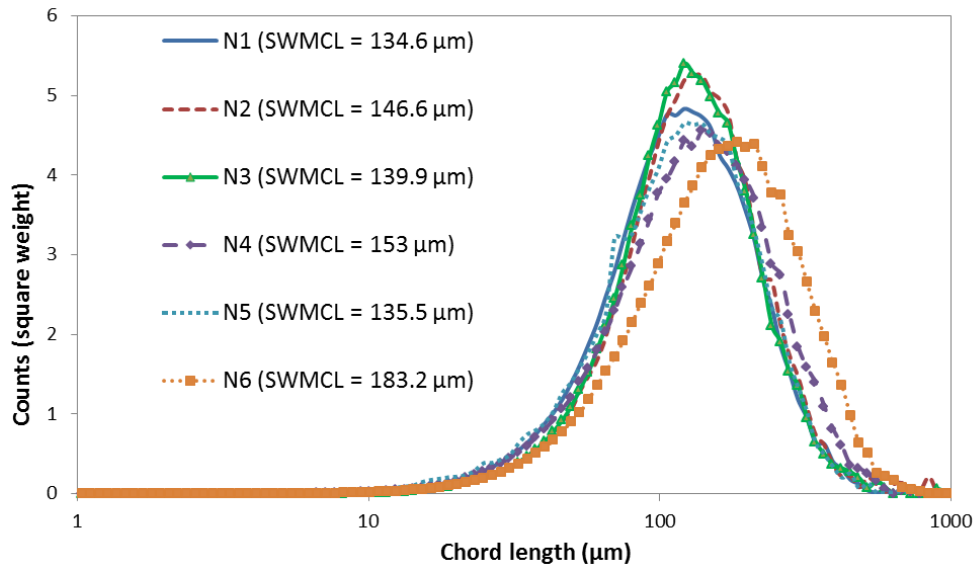


Figure 5.10 FBRM CLDs overlay along with mean square weight at end of the process (before temperature cycle is applied to experiment N5 and N6).

For experiments N5 and N6 when a lower seed loading (0.1% w/w) is used, the particles of experiments N6 reached a value for the SWMCL of 183.3 μm that is the higher mean observed, whilst the SWMCL of experiment N5 is ca.26 % lower than that value. Use of lower seed loading should lead to the increase of seed size because of higher crystallisable mass being available for less number of nuclei compared to the other experiments. An explanation for this difference in mean size may be found in the images reported in Figure 5.11. The agglomerates of experiments N5 seems formed of smaller particles and the further growth of constituent primary particles appeared to be hindered, whilst during experiment 6, the primary particles grown larger resulting in larger agglomerates. In addition, the pictures captured at 90 minutes after seeding for experiment N3, N5 and N6 and at 72 minutes for N4 show plates that have jagged edge which appear to be the result of fracture of plates indicating a breakage event. This is due to an increase of particle attrition at increased stirring rate for experiment N4 and N6.

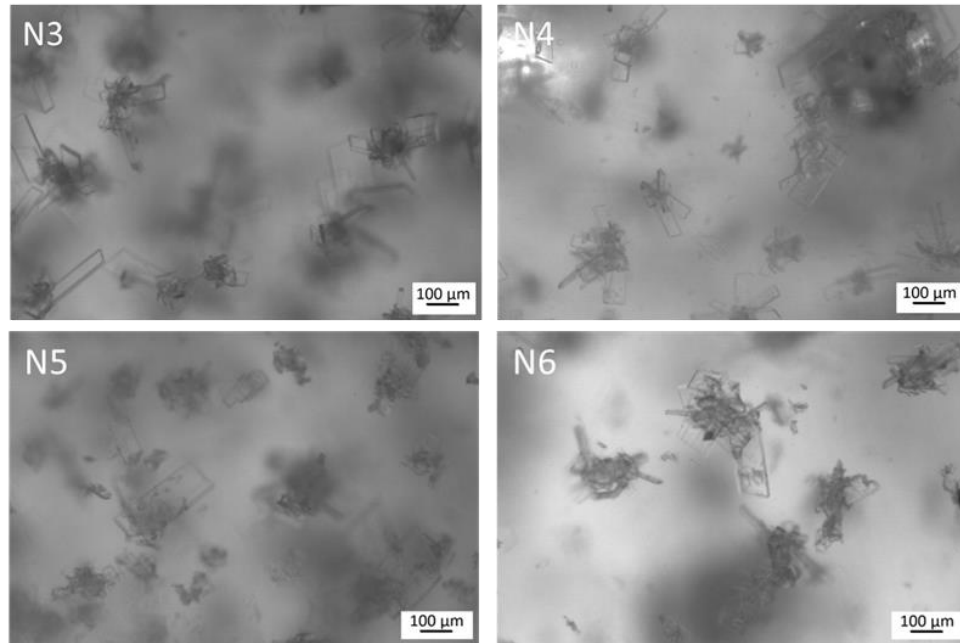


Figure 5.11 PVM images of agglomerates captured at 90 minutes after seeding for experiment N3, N5, N6 and at 72 minutes for experiment N4.

After the temperature cycle was applied, the SWMCL of particles in experiment N5 increased from 135.5 μm to 166.7 μm , whilst the mean sq.wt. of experiment N6 varied slightly from 183.3 μm to 183.7 μm . The use of temperature cycles during seeded crystallization process are often used in order to increase the mean size and the size uniformity of product and modify crystal morphology.¹⁸⁶⁻¹⁸⁸ This is achieved through heating–cooling cycle where the dissolution of smaller crystals is achieved during the heating period and the remaining crystals continuously grow during the cooling period.

5.3.3 Filtration and drying

The morphology of agglomerates obtained from N5 and N6 before and after temperature cycle from light microscopy (5X) is shown in Figure 5.12. A change of morphology is evident for particles obtained from experiment N6 whilst no significant change is observed for particles of experiment N5.

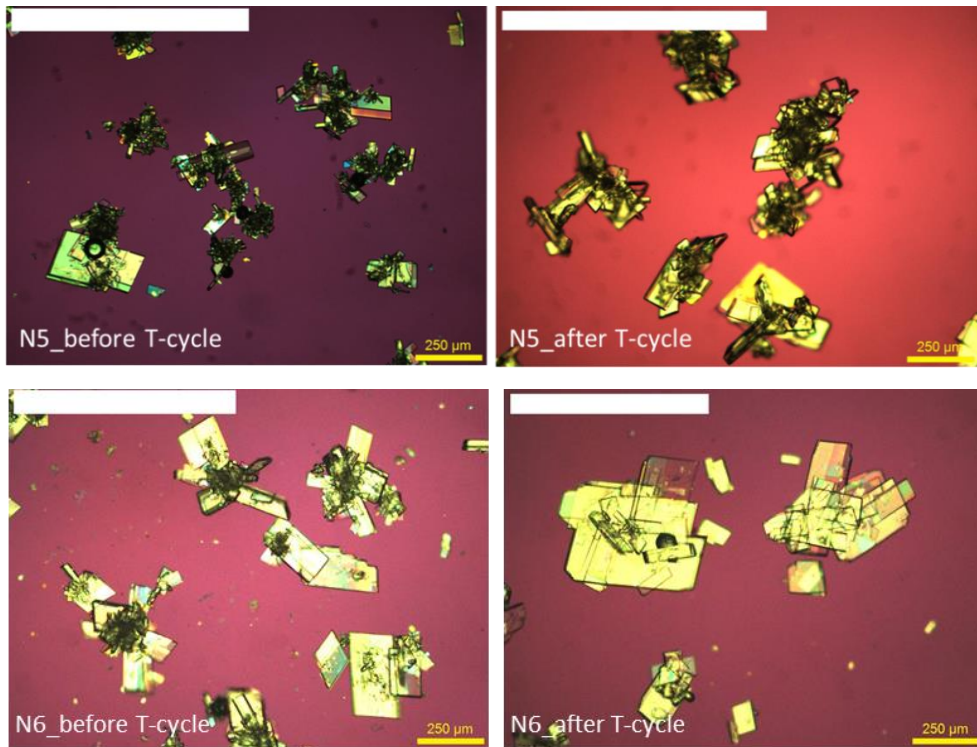


Figure 5.12 Microscopic images of agglomerates for experiment N5 and N6 at the end of the process.

The arrangements of single crystals in the agglomerates from off-line measurement can be observed in the scanning electron microscope (100X) of particles obtained from N1 and N6 in Figure 5.13.

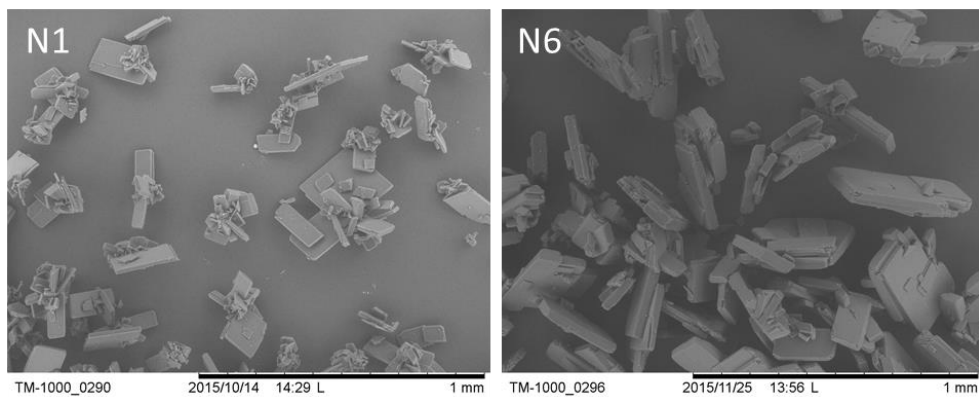


Figure 5.13 SEM and microscope image of experiment N1 and N6 after temperature-cycle.

For experiment N1 the agglomerate core is formed of smaller crystals, even their irregular shape, the characteristic dimensions of primary particles can be roughly

estimated as about 10-20 μm depth, 30-50 μm width and >200 μm long. After the temperature cycle, particles of experiment N6 lost their agglomerate core and increase their depth, the characteristic dimensions of primary particles was estimated as about 20-40 μm depth, 50-200 μm width and >250 μm long. After crystallization, the mass of crystals was filtered in a laboratory pressure filter-dryer and washed to remove DMSO from the cake until the residual content is less than 0.2% w/w to meet the specific requirement for formulation.

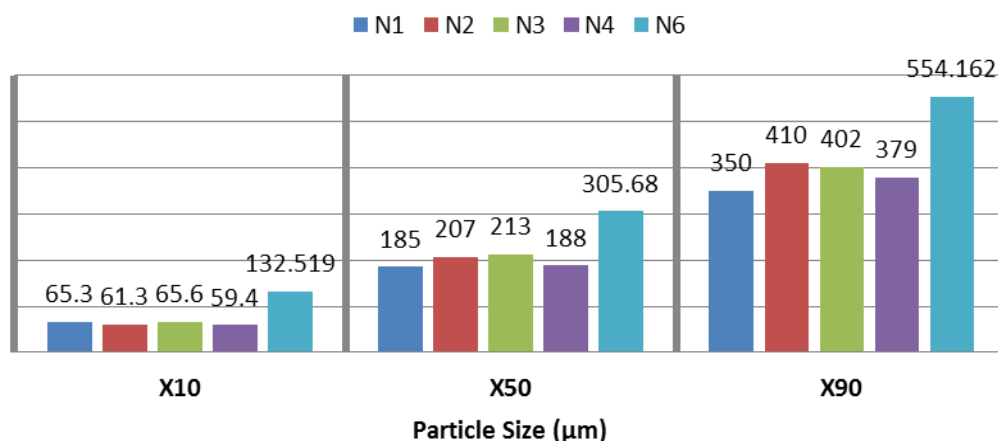


Figure 5.14 Result of the particle size analysis for GSK106 crystals obtained from the Malvern 2000 instrument.

Particle size dv_{10} , dv_{50} and dv_{90} for all experiments after filtration are reported in Figure 5.14. In general, the volume median diameter dv_{50} is ca. 200 μm , when the temperature cycle is applied the dv_{50} is ca. 300 μm , due to the partial dissolution of the smaller crystals and growth of the remaining crystals.

The microscope images in Figure 5.15 shows samples obtained from experiment N1 to N6 at the end of the filtration process, and during the attrition test, after 10 and 60 minutes at 90 rpm respectively (from left to right). It must be noticed that the crystals of experiments N5 and N6 were subjected to an additional temperature cycle post antisolvent addition. The breakage of particles was quantitatively assessed by measuring the particle size distribution using laser diffraction and the dv_{50} of sample taken after 10 and 60 minutes are reported in Figure 5.16.

In general, there are two key mechanisms to describe the breakage of particles: a) attrition, when smaller fragments are removed from edge of primary particles and b)

fracture, when primary particles break in two or more fragments plus an amount of smaller fragments. For all the experiments, the microscope images show fragments that appear to be the result of the fracture of large plates and the separation of the latter from the agglomerate core. Therefore, a fracture mechanism due to breakage of primary particles occurred during agitation. Moreover, the microscope images of the crystals after 10 minutes of agitation of crystals obtained from experiment N1 and N3 show that a relatively small amount of fragments is generated from fracture of primary particles, whilst a larger amount of fragments is generated for experiment N2 and N4. The operating conditions of this two experiments lead to the most fragile agglomerates compared to other conditions.

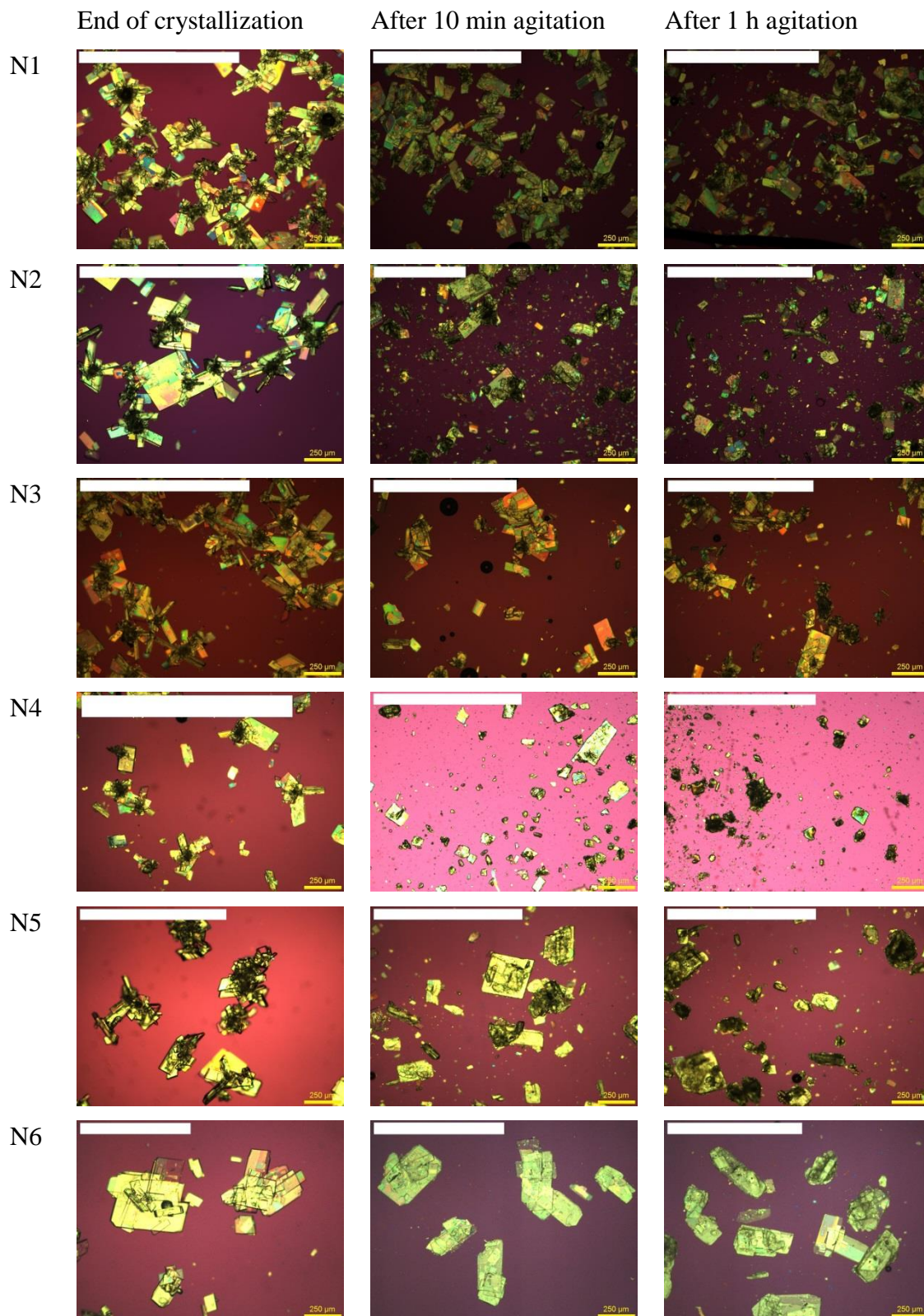


Figure 5.15 Microscope images of crystals end of process, after 10 and 1 hr after agitation at 90 rpm.

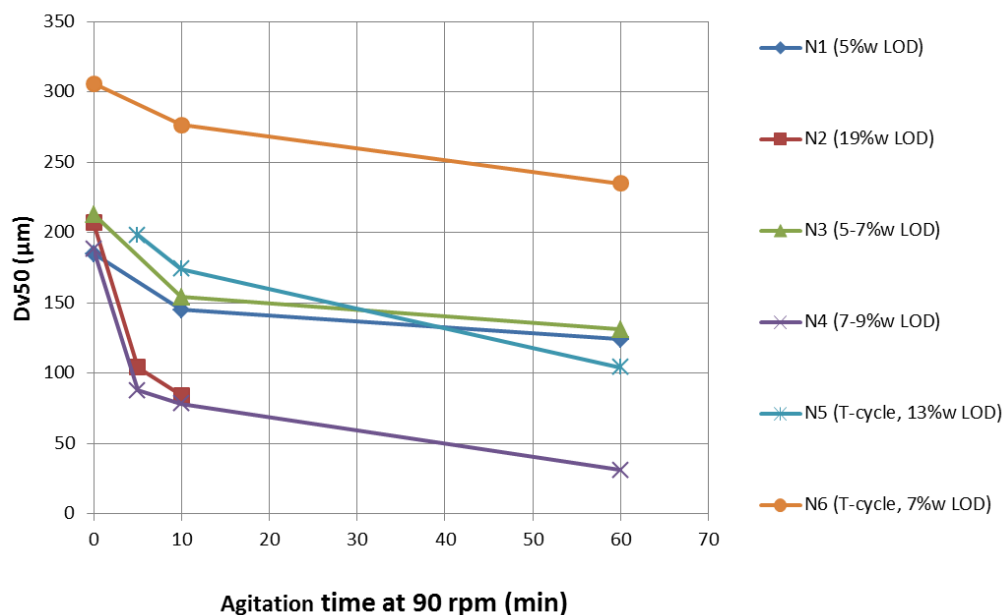


Figure 5.16 Decrease of dv50 during agitation at 90 rpm and loss on drying.

When compared to LOD values (Figure 5.16), attrition appears to have a higher impact on wet cakes rather than dry cakes, when LOD values were above 7%. This statement is different from previous work which involve the study of needle-shaped crystals, where less attrition was found for the agitated wet particles, suggesting that the collision between crystals are less favoured for higher moisture content due to the formation of a liquid film with lubricating effect which it is able to prevent attrition until the particles are dry.¹⁸⁹

By comparison, reduction of the median diameter (dv50) of crystals is substantially different for each experiment. The lowest reduction is observed for product obtained during experiment N6, N1 and N3 with 17%, 33% and 38% of the initial dv50, respectively; whilst significant breakage is observed for product of N4 with 83% reduction of the initial dv50. The temperature cycle during experiment N6 may positively contribute to increase the strength of the crystals. Moderate breakage is observed for N2 and N5, an average reduction of 59% and 47% of the initial dv50, respectively. Overall, the results suggest that the attrition is higher in the order N4>N2>N5>N3>N1>N6.

5.3.4 Comparison between probes and threshold

Comparison between PVM probes. Saving the sequence file and settings related to illumination of the vessel are important. Firstly, the software version at time of writing for the PVM probe (V19) is able to change several settings including brightness and contrast to allow better observation of crystals during inline monitoring. The software is able to save a sequence file that can be recalled for future analysis. When these images were converted to 8-bit intensity, no changes in grey-scale were observed compared to the settings used previously. This implies that only the setting for focus adjustment can be actively used to achieve a sharper definition of the crystals.

Secondly, the PVMA Toolbox relies on the use of sequential time stamped images for statistical analysis. When a series of images are converted to 8-bit images, the time stamping of the images was lost and replaced with the time at which the image was processed. To get round this issue, the images had to be separated and individually time stamped before processing and labelled as such. This couldn't be avoided because the new probe software allows saving a sequence file and not a set of images.

Variability of threshold values within same dataset. During the analysis of the images, a significant change in threshold values through the experiment was observed, which suggests that an assessment of the descriptor extracted with single or variable thresholds would be helpful to understand if the process is investigated correctly. Therefore, a set of 50 PVM images over a population of 1000 images collected from the beginning of each experiment was analysed. Sets of images with similar threshold values were grouped (the time and descriptors were generated separately). On completion of this processing, the trend of a descriptor is composed of multiple segments. This procedure was applied when a difference between 10 units between thresholds was detected.

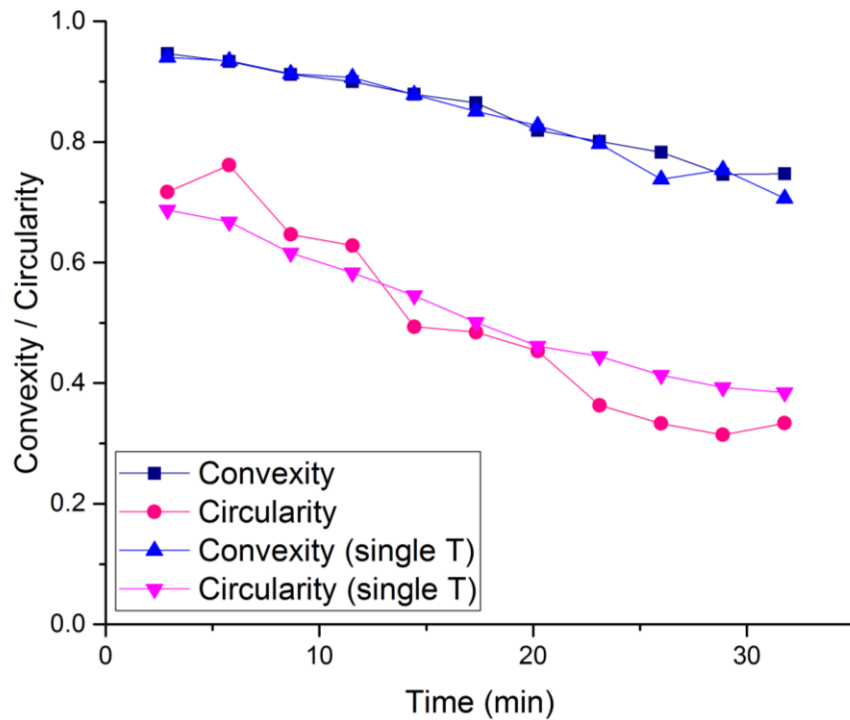


Figure 5.17 Comparison between descriptors obtained with a single threshold value or multi-segment thresholds for N1.

In

Figure 5.17, a comparison between the 2 descriptors generated with multi-segments or a single threshold (single T) value is reported. It can be noticed that the trend of convexity doesn't vary, therefore suggesting that a single threshold value can be used for the entire dataset. For circularity, 10% difference between measurements is observed, which suggest that the circularity obtained from a single threshold value is an approximate representation of the behaviour of the system.

This difference may be attributed to the non-uniform colours and the particle outlines of the measured particles along with the lighting condition that limits the effectiveness of a single threshold method to represent the trend of the descriptor.

However, when analysing thousands of images this procedure is extremely time-consuming and a compromise may be reached by choosing a threshold value that is more representative of the set of images.

5.4 Summary

The overall aim of this project was to study the influence of process conditions on the agglomeration behaviour of an industrial compound as determined by characterisation of particle attributes with both in-line and off-line techniques. FBRM and PVM probe were successfully integrated in a combined cooling antisolvent seeded crystallization process to improve understanding of agglomeration of GSK106. Implementation of a real-time imaging system such a PVM probe coupled with image analysis software further enhanced capabilities to obtain real-time information of the process and help distinguish processes occurring simultaneously such as growth and agglomeration/breakage. These PAT tools helped to identify that agglomeration/aggregation of seed crystals prior to addition to the crystalliser was likely occurring and suggesting an insufficient dispersion of the seeds in the slurry.

A novel image analysis tool aimed at characterizing the population of particles in terms of two classes, namely, agglomerates and single crystal was presented. This tool is based on the combination of MATLAB functions and recorded PVM images to derive descriptors; advantages of this are the higher number of particles analysed in each frame and the possibility to use this tool to implement a model free feedback control strategy for when FBRM performance are limited by complex morphologies.^{170, 175, 190}

During preliminary analysis of the trends from image analysis, CED, circularity and particle counts were capable of distinguishing differences between experiments. However circularity trend was not successful in describing whether seeds were agglomerated at the start of several experiments. This was believed to be an issue related to the quantification of the descriptor by its mean value but further investigation of this was outside the scope of this work.

To overcome this issue, a number of descriptors were evaluated accounting for size, shape and grey scale and displayed as population maps to describe the particle population attributes. For this work, solidity, circularity and heterogeneity were found to be the most effective in identifying the presence of agglomerates. Based on those descriptors, population of particles could be split into agglomerate and non-

agglomerates through the setting of appropriate threshold limits, however, the value of these limits requires additional experimentation to determine.¹⁷⁵

In all cases, unimodal chord length distributions and mean particle size (dv_{50}) in the range of 180-200 μm were obtained when the same seed loading was used. This suggests that the application of different process parameters and dispersion methods of seeds had limited effect on agglomerates size when same seed loading was used within the experimental parameters investigated. Breakage events were detected by the presence of jagged edge during several experiments, with more attrition resulting from faster stirring rates.

The behaviour of the agglomerates and their tendency to break were evaluated using a filtration-dryer unit. The highest degree of breakage was found for samples with moisture content above 7% and specifically for experiment N4 where shorter seed dispersion time, low ratio of solvent:antisolvent and higher stirring rate was applied. Lower degrees of breakage were found for sample obtained from experiment N6 and producing stronger agglomerates where the applied temperature cycle not only increased the mean particle size (dv_{50}) but also their strength.

Chapter 6. Spherical Agglomeration in Suspension of Lovastatin

6.1 Introduction

As discussed in Chapter 1, spherical agglomeration in suspension is a very promising particle design technique, in which seed crystals are agglomerated to form compacted spherical granules in order to improve bulk properties of powder such as bulk density, flowability and compressibility. The process offers an alternative to the wet granulation process which is more extensively used in industry. However, the presence of two liquids i.e. a binder which provides the inter-particle bond and the suspending medium, compared to one liquid in the granulation process, makes the agglomeration from suspension potentially more complex to control. Spherical agglomeration has been used in oil and gas industries to separate mineral particles from suspension of coal particles.¹⁹¹⁻¹⁹² It has also been demonstrated for a range of organic and pharmaceutical compounds as a means to overcome undesirable physical properties such as extreme morphologies or low bulk density.^{83, 85-86, 98, 193}

The material properties and process parameters that can influence the agglomeration process have been investigated and include API surface and bulk properties, solvent properties, solubility of the API in solvent system, relative solubility between bridging liquid and poor solvent, solid loading and particle size, amount of bridging liquid, agitation rate and time under prolonged agitation, use of baffles.^{2, 87, 194-195} For example, physicochemical properties that affect the mean agglomerate size during the wet agglomeration of lactose were identified to be interfacial tension between bridging liquid and dispersing medium, contact angle, relative volume of agglomerate and bridging liquid. These also impacted on the porosity of agglomerates.¹⁰⁹ Spherical agglomeration of lactose was carried out in a suspension of chloroform, using saturated lactose aqueous solution as bridging liquid to investigate different lactose seed size distributions ranging between 31-261 μm and the amount of bridging liquid at constant temperature. It was found that mean agglomerate size increased on decreasing particle size distribution of lactose seeds and increasing amount of bridging liquid; the porosity of agglomerates increased with increasing particle size distribution of lactose. Moreover, the size distribution of agglomerates was found to be independent from the amount of bridging liquid for particle size of 261 μm . In particular, for spherical agglomeration, many examples have been also reported on the improvement of flowability, compactibility and

compressibility by manipulation of solvent system, agitation rate, concentration of starting material, temperature, poor to good solvent ratio, feeding rate of API solution onto the poor solvent, amount and addition of bridging liquid.^{88, 93, 97, 196}

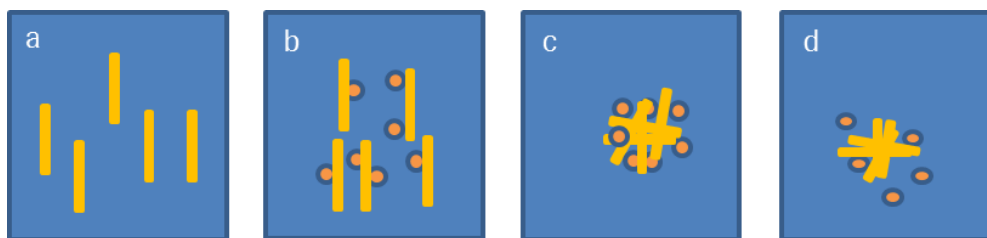


Figure 6.1 Proposed mechanism of agglomeration in suspension for two immiscible liquids: conditioning (a), wetting of seeds (b), coalescence (c) and consolidation (d). Adapted from reference 13.

In summary, the formation of spherical agglomerates can be described by the following process steps (Figure 6.1):¹⁹⁷

1. *Conditioning*: In the first step API–water slurry is agitated to achieve a good wetting of the surface of raw API particles.
2. *Wetting*: During the second step the bridging liquid which is immiscible with water, is mixed with the conditioned slurry to achieve wetting of the particle surface.
3. *Coalescence*: In the third step, API particles wetted with bridging liquid bind or coalesce together to form weak aggregates.
4. *Consolidation*: In the final step the aggregates are compacted to form spherical agglomerates through the formation of inter-particle bridges with the accompanying exclusion of binding liquid.

Implementing spherical agglomeration in a continuous operation can allow for scalable, production of different quantities with precise control over the particle attributes.⁸⁷ Also, this would reduce the number of discrete processing steps required during the production of pharmaceuticals by potentially eliminating downstream particle property altering unit operations such as milling, grinding, and granulation.

While a significant number of studies have been conducted on spherical agglomeration in suspension to investigate the mechanism several questions remain. Specifically, the relationship between the key process parameters and particle

attributes; how to specifically target improved mechanical properties via process design; reliable rules for rational solvent selection in addition to optimal approaches for process design, scale-up, and process control. As a result, there are very few general guidelines for the application of this technique to a given API and detailed reasoning behind the preparation of agglomerates in liquid phase under particular conditions is often not clarified. Therefore the application of the technique to other compounds can only be based on experience and/or trial and error. Such a lack of proper understanding limits the ability to control the process parameters to deliver agglomerates with reproducible and desirable properties, thereby limiting the potential uptake in industrial application.

The aim of the present work is:

- to provide a procedure for the screening of a suitable solvent to act as bridging liquid to deliver dense, compacted spherical agglomerates.
- classify agglomeration or non-agglomeration promoting solvents to draw rules for solvent selection based on physical properties of API and solvents.
- determine the range of bridging liquid amount for optimum operating condition and carry on preliminary experiments in batch crystallizer to potentially inform the design of continuous spherical agglomeration processes.

This systematic study was designed to investigate alternative morphologies than needle-like crystals since only few examples are available¹⁹⁸⁻¹⁹⁹ and compound with a relatively complex molecular structure such as lovastatin. To date, there have been no reports discussing the spherical agglomeration in suspension of this compound.

In-line PAT such as FBRM and PVM were successfully integrated in the system to identify process mechanisms such as coalescence and consolidation.

6.2 Experimental

6.2.1 Materials

6.2.1.1 Model compound: lovastatin

Lovastatin is a statin drug used for lowering cholesterol and reduce risk of cardiovascular disease. Cholesterol-lowering drugs like statins were world's top category in 2004 with more than 30 billion dollars in sale during the year. This compound was isolated in 1982 from the *Aspergillus terreus* after the discovery of a potent statin drug called mevastatin in 1976. However, despite the mevastatin was discovered first, lovastatin was the first statin drug to receive the approval by the US FDA (1987). Lovastatin is traded with more than 30 names around the world and most common are Mevacor® (Merck), Altoprev, Mevinolin and Monacolin K. It is a white crystalline powder with the molecular formula $C_{24}H_{36}O_5$ and it is shown in Figure 6.2.

It has a molecular weight of 404.54 g/mol, a density of 1.164 g/cm³, a melting point of 174.5°C and a boiling point of 206°C. Lovastatin is insoluble in water and soluble in ethanol, acetone and acetonitrile.

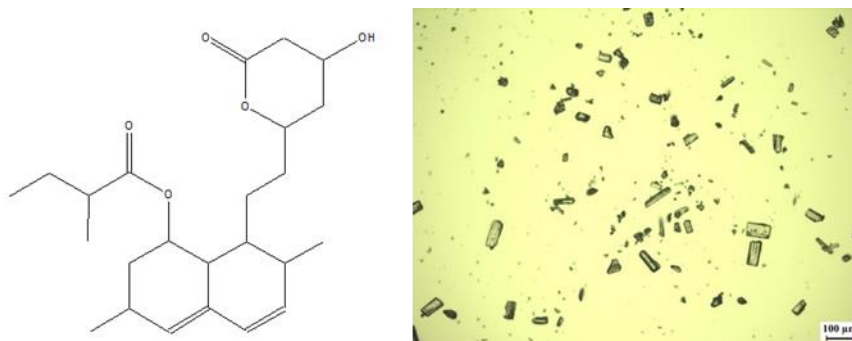


Figure 6.2 Molecular structure of lovastatin (left) and crystal habit (right).

Lovastatin has only one known polymorph and it can be characterised with space group $P2_12_12_1$ (orthorhombic system) with its packing arrangement shown in Figure 6.3. It has been reported that lovastatin may exhibit different morphologies depending on the solvent system used for crystallization.²⁰⁰

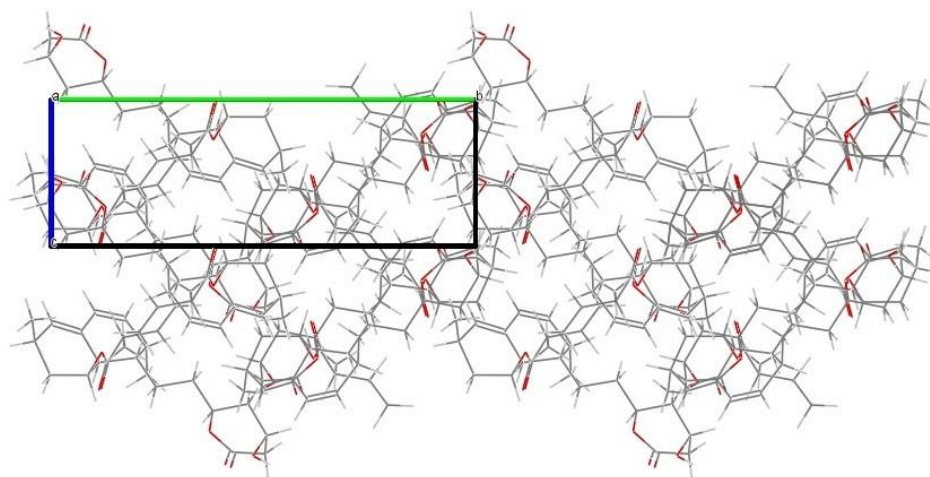


Figure 6.3 Lovastatin packing arrangement. CCDC reference CEKBEZ

Needle-shaped crystals were crystallised from strong polar and hydrogen bonding solvents like methanol and 2-propanol whilst more equant shape were obtained from non-polar/weak hydrogen bonding solvents like acetone and ethyl acetate.²⁰⁰ Lovastatin is a BCS class II drug and hence has a poor water solubility and high permeability. Several methods were reported in literature to enhance the solubility of lovastatin through physical modifications such as particle size reduction²⁰¹, drug dispersion in carriers²⁰² and chemical modifications such as amorphization.²⁰³ In particular, particle size reduction is one of the most common methods to increase dissolution rate of such drugs (when applicable), where the increased dissolution rate and bioavailability are alongside the potential disadvantage of additional handling and processing for size reduction. Milling may also impact efficient powder processing due to establishing unfavourable bulk properties such as compressibility, packability and flowability.⁵

Lovastatin was therefore selected as a model system to explore spherical agglomeration in suspension and assess the key operating parameters that may be manipulated to produce agglomerates which are easy to handle from the desired primary particle size as well as fulfil the dissolution and bioavailability target.²⁰⁴

6.2.1.2 Solvents

For spherical agglomeration from suspension, the dispersing medium or antisolvent used to suspend the solid was water and the bridging liquid which was varied in the

present work must be immiscible or partly miscible with the water. The solvents were selected based on the principle of spherical agglomeration from ICH class II and III of residual solvents and are presented in Table 6.1.

Table 6.1 Properties of solvents used as bridging liquid. From Murov²⁰⁵ and Van Oss²⁰⁶ Thati *et al.*²⁰⁷

Class	Solvents	Solubility in water at 20°C (g/100 g)	Interfacial tension/water at 20°C (dyn/cm)
Alcohols	1-butanol	7.7	24.6
	2-butanol	18.1	--
	1-pentanol	2.2	25.8
	1-octanol	0.096	27.5
	Isoamyl alcohol	2.7 (25°C)	23.8
	isobutanol	8.5 (25°C)	23
Alkenes	Cyclohexane	0.005	50.2
	Hexane	0.0014	51.1
	Heptane	0.0003	50.2
	Isooctane	insoluble	--
	Pentane	0.004	49
Acetates	Butyl acetate	0.7	14.5
	Ethyl acetate	8.7	24
	Isopropyl acetate	2.9 (25°C)	26
	Methyl acetate	24.4	24.7
	Propyl acetate	1.89	24.3
Aromatics	Toluene	0.052	28.5
	Anisole	0.1	35
Chlorinated	Carbon tetrachloride	0.1	26.3
	Chloroform	0.8	31.6
	Dichloromethane	1.3	28.3
Ethers	Diethyl ether	6.9 (25°C)	11
	tert-Butyl methyl ether	4.8	18.3
Ketones	Methyl ethyl ketone	29	24.6
	Methyl isobutyl ketone	1.9	23.6

6.2.2 Methods

6.2.2.1 Screening of bridging liquid using small scale experiments

The screening of bridging liquid was performed in the Crystalline experimental platform (Technobis). Experiments were set to identify whether agglomeration is promoted by the bridging liquid, the optimal range required for a bridging liquid to deliver strong spherical agglomerates and select a suitable bridging liquid to be used for larger scale experiments. The Crystalline system consists of eight independently controlled reactors fitted with 8 ml vials and equipped with turbidity detector, overhead stirring and cameras for imaging. A suspension of 5% w/w (0.2 grams of lovastatin in 4 grams of water) was prepared in each vial using an analytical balance Sartorius (SECURA124-1ORU). Water was selected as dispersing medium due the low solubility of lovastatin in water (0.0004 mg/ml at 25°C). The vials were stirred at 1000 rpm and the temperature was kept constant at 20°C within $\pm 0.1^\circ\text{C}$. Agitation was provided by an overhead stirrer with a three blade impeller. After an initial stirring period of 15 minutes used to suspend the solid particles, the bridging liquid was added in 20 μl increments with a Gilson pipette until a paste was formed. Solubility of lovastatin in the selected bridging liquid was investigated at 20°C using the gravimetric method described in Chapter 4.

For simplicity, the abbreviation BLR is used hereafter to indicate the ratio of the volume of bridging liquid expressed in millilitre to the solid mass expressed in grams.

Spherical agglomerates from several bridging liquids such as isopropyl acetate, toluene and methyl isobutyl ketone (MIBK), were grown using a volume of the bridging liquid per mass of lovastatin corresponding to the mid-point of the BLR range previously determined. For example, for the lovastatin-water-MIBK system, the critical range of BLR was found in the range 0.6-0.8, a BLR of 0.7 corresponding to the middle of the range was used to produce spherical agglomerates. These agglomerates were filtered and oven dried for 12 h. XRPD analysis was used to exclude any polymorphic transition during the agglomeration in suspension, since in previous studies²⁰⁸ using the same technique, polymorphic conversions were reported under prolonged stirring.

The solvents were then divided into two main categories such as agglomerating or non-agglomerating, depending on whether they promote spherical agglomeration of seed crystals or not. Finally, the two categories were analysed using the Principal Component Analysis tool PCA-X in Simca 14.1 by adding 250 descriptors describing each solvent from Molecular Operating Environment (MOE) alongside the experimental outcomes and a score scatter plot was generated.

6.2.2.2 Batch agglomeration in suspension experiments using single range and stepped shear approach

Lovastatin raw material 5% w/w was suspended in water (dispersing liquid) in a 250 mL Radleys reactor equipped with PTFE pitched blade turbine impeller (3.5 cm in diameter). The temperature was kept constant at 20°C within $\pm 0.1^\circ\text{C}$ by a chiller (Lauda Eco RE 420G). The vessel was equipped with FBRM (G400, Mettler Toledo®) and PVM (V819, Mettler Toledo®). These probes are used to monitor the process and investigate the different mechanisms involved like flocs formation, agglomeration and consolidation. . A platform configuration with a syringe pump for delivering the bridging liquid is illustrated in Figure 6.4.

MIBK was selected as bridging liquid from the screening experiments in Section 6.3.2 since the agglomerates could readily be produced at 1000 rpm in the Crystalline platform with a limited BL addition and by visual inspection appeared more compacted and spherical than those produced from other solvents in this group under the same stirring conditions.

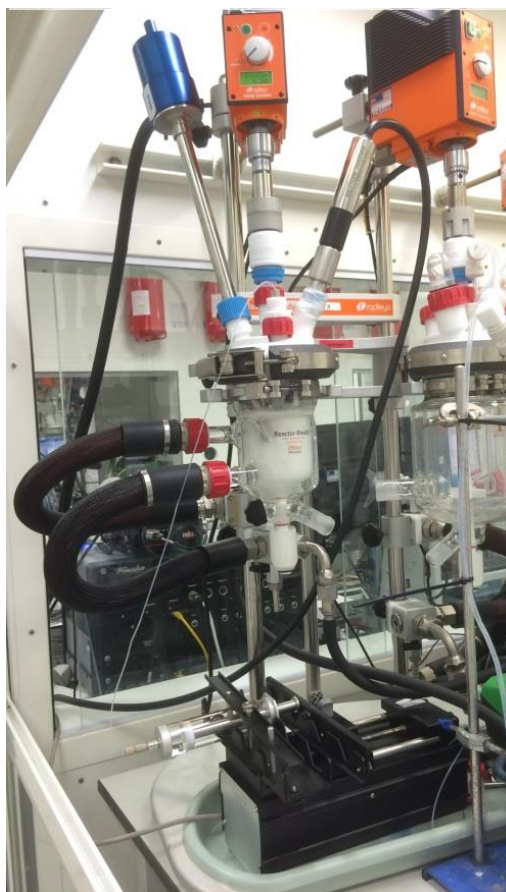


Figure 6.4 Setup for batch experiments comprising syringe pump and PAT.

The slurry was previously stirred for approximately 15 minutes to ensure complete suspension of seed crystals and then the bridging liquid, MIBK, was fed either by an advanced droplet system (Dolomite) or a syringe pump (Harvard PHD Ultra). These two platforms differ in the way of operation and the mode of delivering the bridging liquid in the vessel. The syringe pump delivers the bridging liquid in a continuous flow, whilst the advanced droplet system delivers as a continuous stream of small droplets. A syringe pump is a relatively easy device to operate, where the syringe barrel is placed in the syringe holder and the solvent is gradually dispensed by motion of a pusher block acting on the plunger of syringe. A flow rate of 0.55 ml/min was used for the addition of the bridging liquid with the syringe pump. The advanced droplet system consists of two microfluidic pumps that take the feeds from two separated chambers. The first chamber contains the bridging liquid whereas the second one contains the dispersing fluid. The two streams are pumped using capillary tubes to a microfluidic chip, where they are mixed together generating a stream of

monosized droplets. This stream of droplets will be delivered to the vessel by a capillary tube. The operating conditions of the advanced droplet system were obtained from an industrial confidential project²⁰⁹ carried out in the same department and used here to assess the application to this system, a microchip with a diameter of 190 μ m and a bridging liquid addition rate of 0.55 mL/min were used. A set of five batch experiments were performed to investigate the influence of operating parameters such as bridging liquid amount and agitation rate on attributes of the product obtained, i.e. Carr's Index (CI) and Hausner Ratio (HR). The Aero S dry dispersion unit connected to a Malvern Mastersizer 3000 with a general purpose tray and hopper was used for measurements of the particle size distribution. The operating conditions of the experiments can be found in Table 6.2. These experiments were carried out at agitation conditions in the range proved to be successful for batch operation in the literature, for example, it was found that agitation rate below 400 rpm were not successful for agglomeration or production of uniform spherical agglomerates, whilst a paste is formed when an agitation of 900 rpm was used.²¹⁰ Instead, the range of BLR was selected according to the information obtained from the screening experiments, e.g. the MIBK was found to produce spherical agglomerates in the range of 0.6-0.8 mL of MIBK per gram of lovastatin therefore three BLR values were attempted such as 0.6, 0.7 and 0.8.

Table 6.2 Experimental conditions of batch fixed shear approach experiments.

Exp.	Agitation rate (rpm)	BLR (ml BL/gr API)	BSR (ml BL/ml API)	Vol. of MIBK/Vol. of water
A1	550	0.6	0.71	0.03
A2	550	0.8	0.94	0.04
A3	700	0.7	0.82	0.035
A4	850	0.6	0.71	0.03
A5	850	0.8	0.94	0.04

These experiments were terminated when the desired amount of bridging liquid was added, with the purpose of investigating the properties of the product obtained from the experiments and eliminate the effect exerted from prolonged agitation.^{111, 120} One method, utilising a stepped shear approach²⁰⁹ was investigated using the same vessel configuration with a sequence of agitation rates previously tested in the batch experiments. This method, developed by colleagues at Strathclyde, showed that the stepped shear approach was more successful in terms of delivering better control over the stages involved in agglomerate formation and hence agglomerate attributes compared with fixed shear rate experiments i.e. more rounded, less porous, more compacted and narrower agglomerate size distribution.¹⁹⁷ The latter findings are in good agreement with the mechanism of agglomeration, where different agitation rates (or shear rates) can provide the required process conditions to enhance different stages of the process. For instance, the shear rate required for coalescence is generally higher than that required for consolidation as collision frequency for coalescence plays a positive role in bridging the wetted particles together. On the other hand, higher collision rate in the latter stage or consolidation stage would cause agglomerates attrition and reduce the agglomeration rate. In order to address the above problems, a different approach has been taken into consideration which involves the use of stepped shear approaches combined with bridging liquid addition strategies.

Three experiments were carried out to investigate the outcomes of the stepped shear approach whilst both addition rate (0.55 ml/min) and amount (0.7 ml of MIBK per gram of solid) of MIBK was fixed from the outcome of the screening experiments. In addition, the holding time at each stirring rate was always fixed at 20 minutes which implies that the total processing time for each experiment is the same. The procedures below were used:

1. Single stage addition: The total amount is added when the suspension is agitated at 550 rpm and then the slurry is stirred at 700 and 850 rpm.
2. Two stages addition: The amount is divided into two equal portions: one added to the suspension when agitation rate is 550 rpm and another when agitation rate is 700 rpm; then the suspension is stirred at 850 rpm.
3. Three stages addition: The amount is divided into three equal portions: each portion is added to the suspension when it is agitated at 550 rpm, at 700 rpm and at 850 rpm.

Table 6.3 Portion of bridging liquid (ml) delivered at each stage.

Exp.	Agitation rate (rpm)		
	550	700	850
B1	8.75 ml	0	0
B2	4.4 ml	4.35 ml	0
B3	2.92 ml	2.92 ml	2.91 ml

At the end of the experiment, the product were filtered and dried under vacuum at 25°C overnight. CI and HR were measured by using the cylinder method (10 mL) on particle sizes below 1 mm. The amount of bridging liquid is defined simply as bridging liquid volume to mass of solid suspended (BLR) and in the typical way found in literature with BSR² (volume of bridging liquid to volume of solid), where the volume of solid is determined as the weight of the lovastatin originally suspended divided by the density of the lovastatin. The bridging liquid to dispersing medium (BL/DM) is the ratio between volume of bridging liquid and the volume of the dispersing medium.

6.3 Result and discussion

6.3.1 Selection of bridging liquid using small scale experiments

The agitation rate for these experiments was fixed at 1000 rpm after a screening investigation of a set of agitation rates using a constant bridging liquid amount (BLR). As previously discussed, for spherical agglomeration the agitation rate along with the bridging liquid properties are important since they affect the performance of the agglomeration processes and the key particle properties include mean particle size and morphology. From visual observation of the vials, particles stirred at 400 rpm were not well suspended and accumulated at the bottom of the vial. The loose agglomerates produced under this agitation rate are therefore irregular and not completely agglomerated as can be seen clearly from Figure 6.5a, where a large number of primary particles are not agglomerated. When agitation was increased to 700 rpm, the agglomerates are more compacted but still show an irregular shape and a broad distribution of sizes from 10-500 μ m (Figure 6.5b)). On an increasing the agitation rate to 1000 rpm, the resultant agglomerates are observed to be larger, more densely compacted and achieve a more rounded, near spherical shape, as can be seen in Figure 6.5c. Based on this, the agitation rate was set to 1000 rpm to provide both adequate particle suspension and a spherical shape for the other solvents tested.

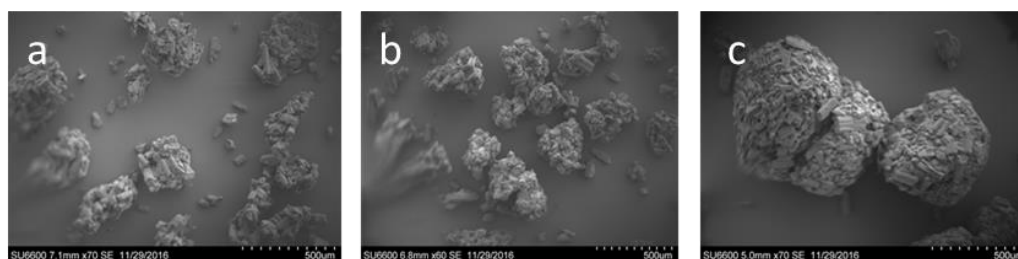


Figure 6.5 Stirring rate effect on screening experiments: a) 400 rpm, b) 700 rpm and c) 1000 rpm. MIBK used as bridging liquid.

Solvents were classified as agglomerating or non-agglomerating by investigation of the microscopic images from the Crystalline. Microscopic images illustrating the different stages of the spherical agglomeration of lovastatin are shown in Figure 6.6 and images of the vials related to these stages are shown in Figure 6.7.

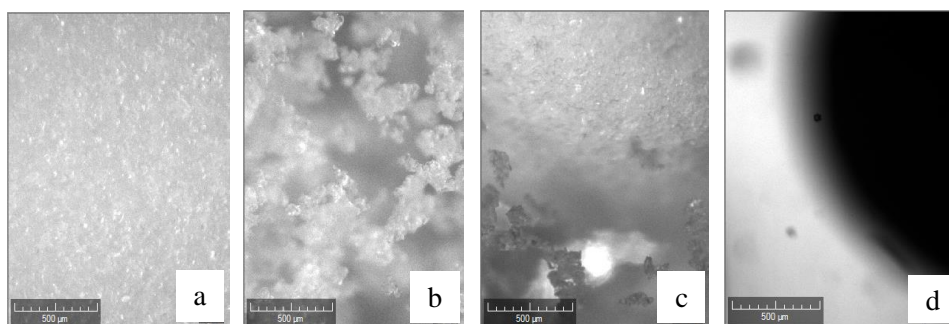


Figure 6.6 The evolution of lovastatin particles agglomeration during screening experiments in the Crystalline. Images were taken from the vial containing from 0 to 160 μl BL (MIBK), 4 mL DL and 0.2 g particles stirred at 20°C and 1000 rpm at (a) 0 mins showing suspended particles, (b) 120 μl of BL added, small flocs, (c) 140 μl of BL added, larger agglomerates becoming apparent and (d) 160 μl of BL added, where the curvature of a large agglomerate can be seen as the dark region nearly occluding the image.

In the first image (Figure 6.6a), the suspension is highly concentrated with solid particles and the initial period of 15 minutes of stirring is sufficient enough to produce a well-suspended slurry. After a portion of bridging liquid is added, the crystals gather into flocs of irregular shape and all sizes. These two steps are combined to give the first period of the agglomeration process, generally called the “wetting period”¹⁰⁴. At the end of the wetting period, the particle surface is fully covered by the bridging liquid and these loose flocs can slowly start to coalesce into agglomerates. After this period the embryonic agglomerates (flocs or aggregates) grow and consolidate by the mechanism of collision between particles and the equipment surface. Figure 6.6d shows spherical and compacted agglomerates obtained near the end of the agglomeration process. Therefore the range of BLR where spherical agglomerates could be produced corresponds to the situation in Figure 6.6 (b-d). The size of the final agglomerates reach a maximum diameter depending on the stirring speed and amount of bridging liquid added to the suspension. These observations are consistent with the expectation that agglomerates grow by coalescence due to interfacial tension and capillary forces between wetted crystals of lovastatin, that facilitate the formation of spherical agglomerates under agitation induced collisions.^{88, 111}

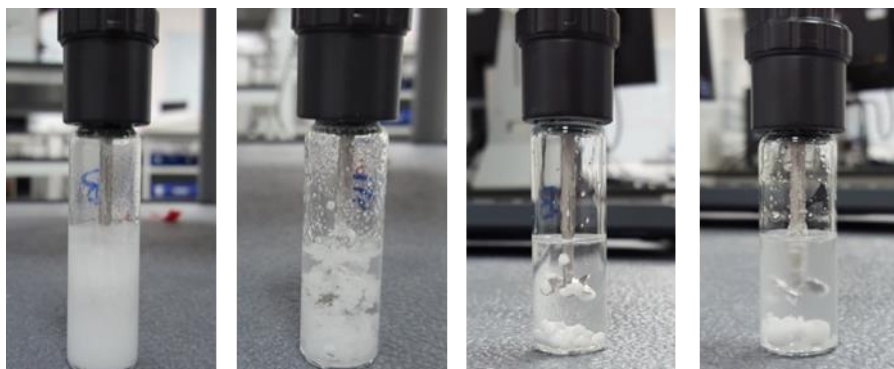


Figure 6.7 Pictures of crystalline vials from seed suspension to nearly paste behaviour.

For non-agglomerating solvents, the particles apparently gather into flocs and on further addition of bridging liquid, paste-like spheres appear until the excess is high enough to promote the dissolution of the solid, this is due to excessive solubility in the BL of the crystals. Non agglomerating solvents showed different behaviour such as formation of paste immediately, yielding the round sphere in Figure 6.8.

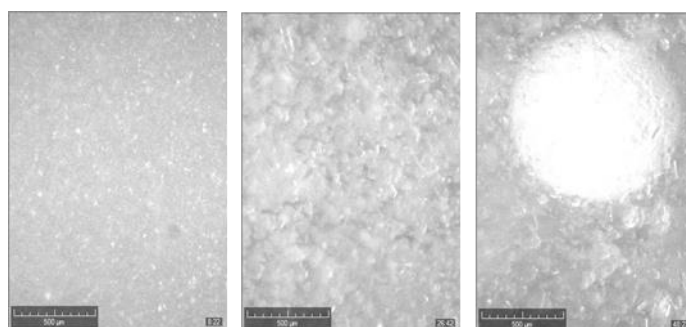


Figure 6.8 Non agglomerating behaviour from seed suspension to dissolution of seeds.

Encrustation was also observed during screening experiments. This appeared as a thin crust located mainly on the stirrer with an extent that depends on the slurry composition with a sticky paste formation leading to more encrustation. Figure 6.9 shows the effect of encrustation observed during the screening experiments with stainless steel stirrer provided with the Crystalline.



Figure 6.9 Encrustation on the stirrer (left) during screening of bridging liquid.

Formation of a paste, caused by the bridging liquid exceeding a maximum value causing particles, mostly surrounded by bridging liquid to behave as a paste rather than discrete wetted particles.²¹¹

6.3.2 Classification of agglomeration and non-agglomeration promoting solvents through molecular descriptors using PCA

A Principal Component Analysis (PCA) of 250 calculated solvent molecular descriptors derived from MOE was carried out using SIMCA-P. In PCA, the original dataset consisting of molecular descriptors for each solvent are transformed into another coordinate system where the new axes represent the principal components (PCs). The principal components are orthogonal, i.e. completely independent of each other and cover as much as the variation as possible in the dataset. In the present work, the entire experimental dataset was used to generate an 8 principal component model. The entire experimental dataset was then used to generate the score plot shown in Fig 6.10²¹²⁻²¹³.

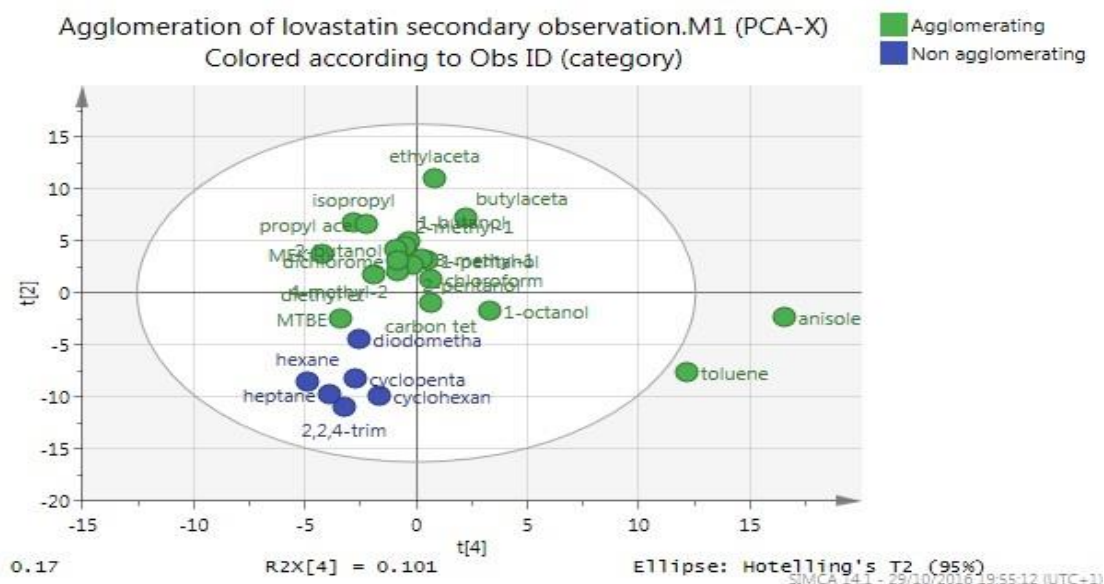


Figure 6.10 PCA Score Plot based on MOE descriptors for the solvents tested for classification of agglomerating and non-agglomerating behaviour.

The calculated MOE descriptors used were 2D descriptors and 3D descriptors (Appendix 2). 2D descriptors were used for properties that can be calculated from the molecular structures of each molecule and include formal charges and bonds with no dependence of the conformation of the molecule. 3D descriptors includes those that depend on the internal coordinates only and those that depend on absolute orientation of a molecule.²¹⁴ The resultant score plot in Figure 6.10 presents how each solvents and their associated 2D and 3D descriptors are described by the principal components (PCs) 2 and 4. Each opint on the plot represents one solvent and the colour represents the observed agglomeration behaviour. The scores shown clearly illustrate clustering of agglomeration probability based on the descriptors (or properties) of a solvent. It can be seen that agglomerating solvents are placed in the first and second quadrant whilst non-agglomerating solvents are largely located in the third quadrant. When compared with the loading plot the dominating characteristics of solvents were 2D descriptors including the sum of atomic polarizabilities, counts of atoms and bonds and 3D descriptors including solvent molecular volume and surface area, water accessible surface area. The non-agglomerating solvents were all alkenes that were chosen due to their low solubility in water. These results suggested that when a solvent is suitable for promoting spherical agglomeration, it is likely that solvents with similar molecular descriptors will also

be suitable. Further work is required to validate this, however the multivariate analysis represents a potential tool to inform BL selection.

However, properties involving solid-solvent interaction such as solubility, S/L interfacial tension, polarity, wettability and viscosity also contribute to the agglomeration performance. Thati *et al.* investigated few of these properties to guide the selection of bridging liquid.¹⁹⁴ Low solubility of active ingredient in the bridging liquid (<100mg/g of solvent) and good wettability ($\theta = 0^\circ$) were considered important prerequisites for the selection of BL but not sufficient on their own for the selection. Specifically, interfacial tension was important and in the systems tested, alkenes, toluene and chloroform, which have high interfacial tensions, were suitable whilst solvents with lower interfacial tensions (ethyl acetate and diethyl ether) not suitable.

However in this work, alkenes were not suitable to form spherical agglomerates. This behaviour was previously reported by Teychene *et al.*, who observed that for solvent systems with too high interfacial tension (of bridging liquid/water), the creation of large droplets and their coalescence are more probable phenomena than the creation of liquid bridges for spherical agglomerates.²¹⁵ With regard to solvent polarity, there is no clear correlation for its role in spherical agglomeration. Although for the agglomeration of paracetamol, polarity was chosen to represent the hydrogen bonding capabilities of solvents and potential for promoting spherical agglomeration.^{73, 171} This is only valid if hydrogen bonding functional groups are present on the molecule and on the crystal surface. The crystal surface will have a significant impact on solvent interactions and will be dependent on the unique crystallographic structure presented by each molecular crystal packing arrangement. In Figure 6.11, the volume of bridging liquid expressed in microliters is the volume used to produce spherical agglomerates of 0.2 grams of lovastatin suspended in 4 milliliters of water. The experimental results showed that the volumes of bridging liquid required to produce spherical agglomerates was variable depending on the solvent used, as might be expected. The solubility of the bridging liquid in the suspending medium (water) dictates the residual amount available for the creation of liquid bridge to bind the crystals, which impact on the volume of bridging liquid found for each solvent investigated.

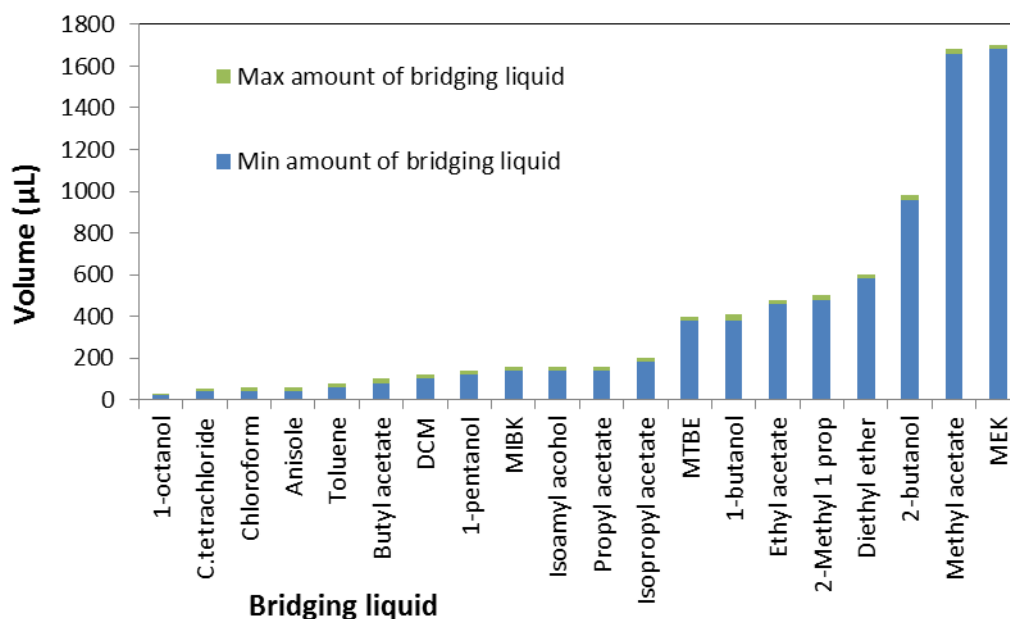


Figure 6.11 Volume of bridging liquid determined from screening experiments. For the sake of clarity, the green bar represents the bridging liquid range where spherical agglomerates could be produced, whereas incomplete agglomeration or irregular agglomerates with paste-like behaviour are observed for volumes below the minimum amount (blue bar) or above the maximum amount (sum of blue and green bar) respectively

1-octanol, carbon tetrachloride, chloroform, anisole, toluene and butyl acetate required a minimum volume in the range of 5-20 µl per ml of water to promote spherical agglomeration equivalent to a BSR_{min} between 0.11-0.47 and BSR_{max} between 0.18-0.58. For dichloromethane, 1-pentanol, MIBK, isoamyl alcohol, propyl acetate and isopropyl acetate, a minimum volume in the range of 25-45 µl per mL of water was required or BSR_{min} between 0.58-1.05 and a BSR_{max} between 0.7-1.16. The remaining solvents required a minimum volume in the range of 95-430 µl per ml of water or a BSR_{min} above 2.21. For the majority of the solvents, the range of operation for spherical agglomeration was found to be relatively narrow; 1-octanol and carbon tetrachloride required only 10 µl more than the minimum volume of bridging liquid to reach the maximum volume whilst the other solvents required 20 µl more. Above the maximum volume of bridging liquid (corresponding to BSR_{max}) the material formed either very large particles (more than 3 mm) or a paste whilst below the minimum volume (corresponding to BSR_{min}) the crystals are not agglomerated completely having very small size and irregular shape; those scenarios

correspond to the images in Figure 6.6c and Figure 6.6d for min and max amount of BSR respectively. Deducting the volume of bridging liquid required to exceed the water saturation at 20°C, all the solvents excluding tert butyl methyl ether (MTBE), diethyl ether, MEK and methyl acetate shown in Figure 6.11, required an excess of volume in the range of 0-71 µl to produce spherical agglomerates whilst for the remaining solvents the excess of volume required is above 120 µl.

6.3.3 Spherical agglomeration under fixed agitation rate

The XRPD data confirmed that agglomerates from MIBK were the same polymorphic form of the starting material and hence suitable for scale-up experiments (Figure 6.12).

MIBK shows low miscibility with water (1.8 g of MIBK/100 g of water at 20°C) and the lovastatin was found to have a low solubility in MIBK of 32.9 mg of lovastatin/g of MIBK at 20°C.

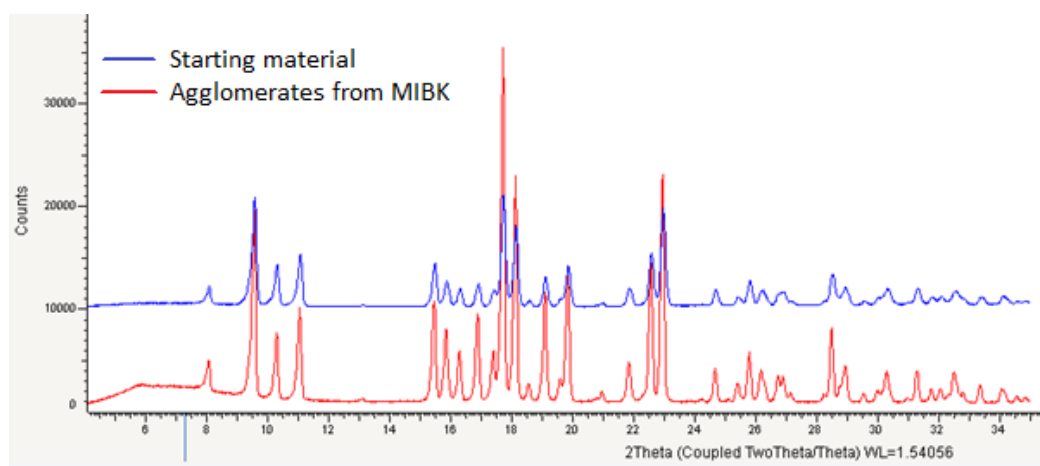


Figure 6.12 X-Ray powder diffraction pattern of lovastatin: starting material (blue) and agglomerates produced from MIBK (red).

A summary of the crystallization experiments performed are presented in Table 6.4, including the specific operating condition and outcomes of each agglomeration experiment. These experiments were selected to provide a benchmark of the lovastatin spherical agglomeration behaviour using the information of the screening experiments, as well as to assess whether the screening method was robust enough to

withstand the variations of vessel geometry and impeller type (hydrodynamics) during process scale-up.

For these experiments, an advanced droplet system (Section 6.2.2.2) was used to feed the bridging liquid into the batch crystalliser in a continuous flow, with the outlet located just above the impeller, to maximise particle wetting in the region where the mixing is most intense.

Table 6.4 shows the total FBRM counts/s collected during the experiments. These decreased from ca. 40000 to 700 counts/s (the smallest counts/s value detected among all the experiments), while the square weighted mean chord length (SWMCL) showed an increase from ca. 84 to 826 μm (larger mean chord length detected among the experiments).

Table 6.4 Counts/s and SWMCL after 15 mins of suspension of lovastatin in water and at the end of the experiments using MIBK as bridging liquid.

Exp.	Agitation rate (rpm)	BLR	FBRM counts (#/s)		SWMCL (μm)	
			Initial	Final	Initial	Final
A1	550	0.6	40934	15095	84.09	298.24
A2	550	0.8	39564	2739	84	641.16
A3	700	0.7	41639	13554	85.26	468.67
A4	850	0.6	41219	20759	83.40	380.90
A5	850	0.8	42425	710	82.34	826.12

Figure 6.13 shows that the in-situ FBRM data for the experiment carried out at 700 rpm and 0.7 BLR. The data shows the decrease in total counts/s of particles and the increase in the SWMCL after addition of BL. A line (black dotted line) has also been added to highlight when the saturation of the dispersing liquid with bridging liquid is exceeded, based on the reported solubility of MIBK in water of 1.8% at 20°C ²¹⁶, corresponding to the addition of 4.75 grams of MIBK to the suspension of 250 grams of water.

The size of agglomerates increased slightly before 10 minutes during the addition, where the bridging liquid contributed to the formation of aggregates/agglomerates

with a SWMCL of ca. 155 μm , and it is increased further from 155 to 468 μm when the other volume of bridging liquid is added, contributing to the formation of larger and compacted agglomerates (Figure 6.14). The tracking of chord length smaller than 10 μm was used as an indicator of attrition during the consolidation stage. For this experiment this approaches zero suggesting no evidence of attrition.

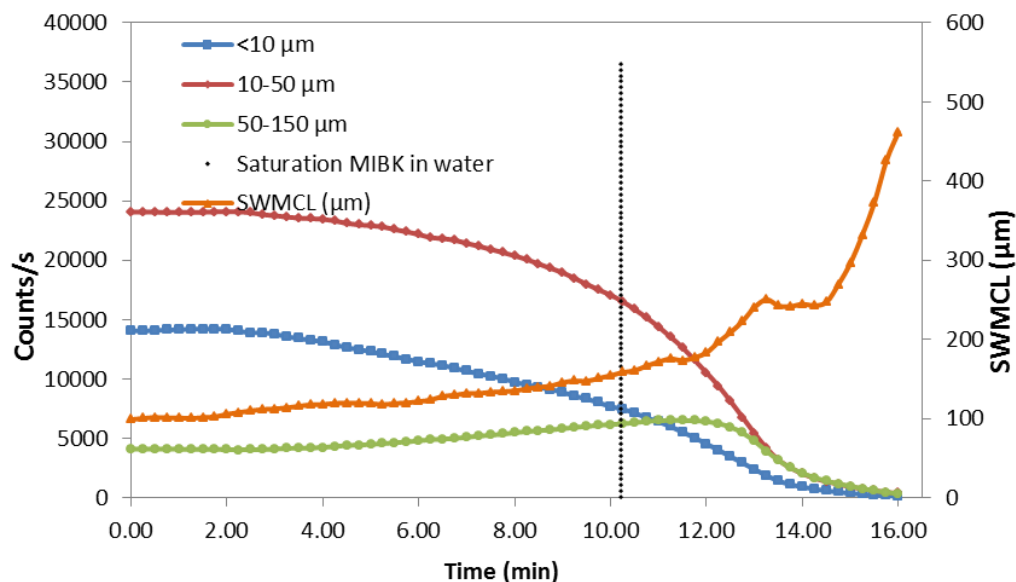


Figure 6.13 In situ FBRM counts/s and square weighted mean chord length for experiment carried at 700 rpm and 0.7 BLR.

A visual assessment of agglomerates produced in the different experiments is provided in Figure 6.14, which shows images of the retrieved product alongside microscope images of the agglomerates (5X magnification). Figure 6.14, shows the product obtained with 0.6 BLR at 550 rpm (A1) and 850 rpm (A4) had a distribution of crystals which are not completely agglomerated and the agglomerates are very small in size with an irregular shape.

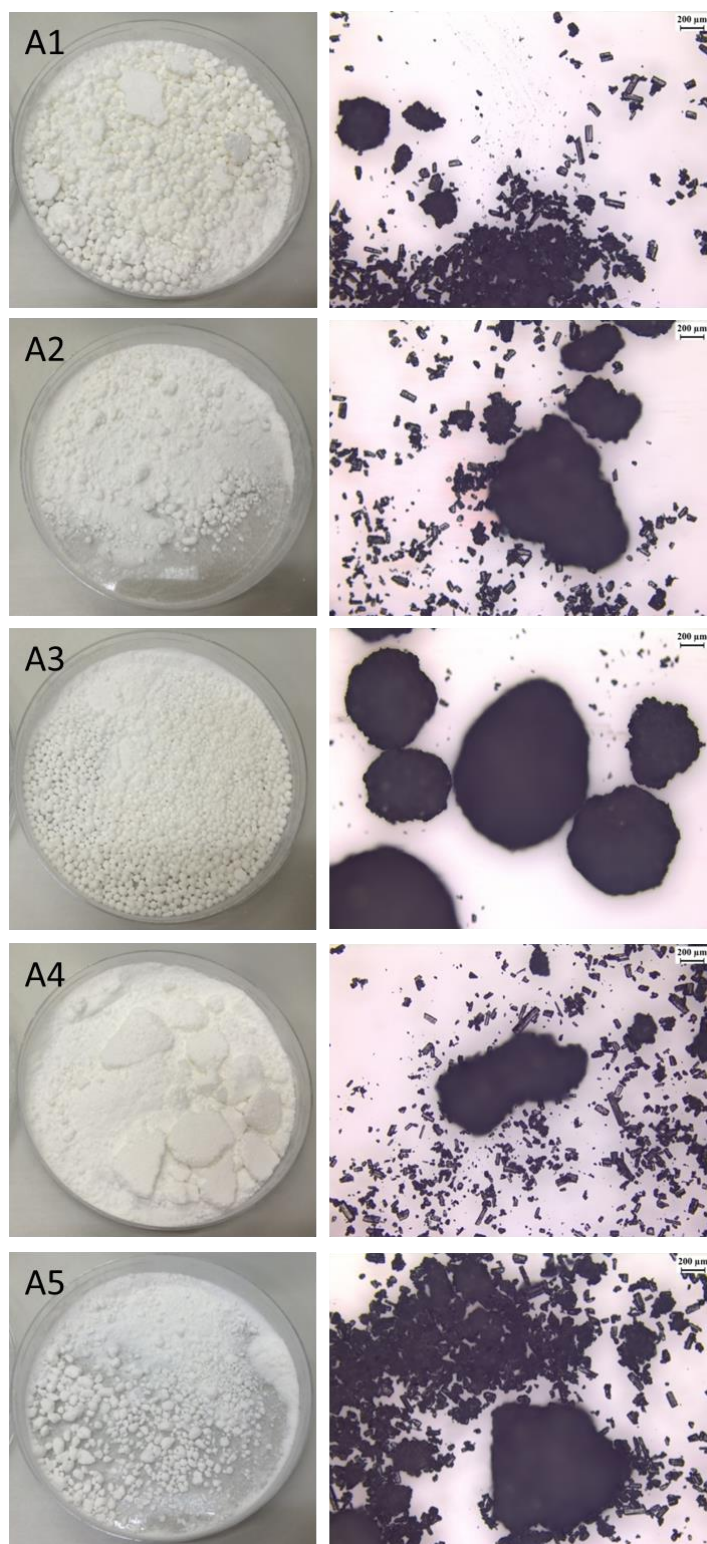


Figure 6.14 Product obtained from batch agglomeration in suspension experiments at 20°C using MIBK as bridging liquid. A1 and A2 from agitation of 550 rpm with low (BLR of 0.6) and high (BLR of 0.8) amount respectively; A3 from agitation of 700 rpm with BLR of 0.7; A4 and A5 from agitation of 850 rpm with low and high amount respectively.

The morphology of the particles from experiments with 0.7 BLR (middle of BLR range) shows a gradual improvement of the shape of the agglomerates that are nicely spherical and more uniform in size; this is the optimum volume of bridging liquid obtained from the screening that should be used to scale-up the process.

When the BLR was increased to a value of 0.8 the product mass extracted from the vessel was lower than the other experiments and the particles were not uniform in size and shape which can be observed from Figure 6.14 for the product of experiment A5. The excessive amount of bridging liquid caused the formation of softer irregularly shaped agglomerates. Consequently, a higher extent of encrustation was also observed on the FBRM probe and around the outlet of tubing used to deliver the bridging liquid compared to other experiments. Figure 6.15 shows the volume based particle size distributions by laser diffraction technique of product obtained from the batch experiments in comparison to the seeds of the raw material.

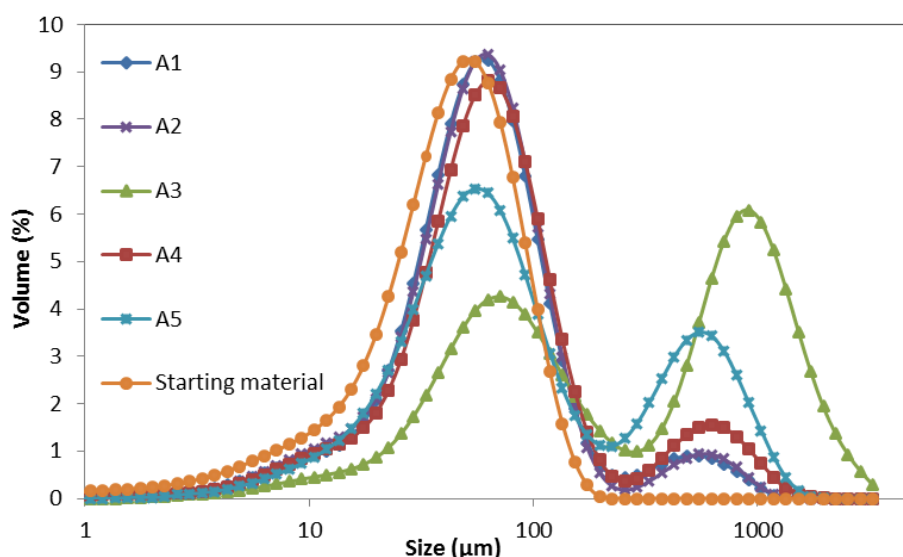


Figure 6.15 Particle size distributions by laser diffraction for lovastatin spherical agglomeration experiments A1-A5 and starting material.

These distributions are bimodal suggesting incomplete agglomeration, but with the particle size clearly moving towards larger size classes as agglomeration proceeds. The trends show the higher extent of agglomeration achieved with a BLR of 0.7 compared to other conditions. Further tests were performed to give an indication of the product performance in downstream unit operations, including measurement of

the powder bulk and tapped density and the derived flow properties indicators (CI and HI). Flow properties of the initial seed crystals and the agglomerated product are reported in Table 6.5. Improved flow and compression properties are expectations of spherical agglomeration where the improvement is generally attributed to the reduction of inter-particle friction due to the spherical shape^{120, 217}

Table 6.5 Properties of lovastatin samples in the range 0-1000 μm . BD = bulk density, TD = tapped density, CI = Carr's Index and HR = Hausner Ratio. Data are reported in the format mean \pm std dev based on 5 replicates.

Sample	BD (g/ml)	TD (g/ml)	CI (%)	HR
A1	0.449 \pm 0.011	0.542 \pm 0.020	16.9 \pm 2.8	1.21 \pm 0.04
A2	0.435 \pm 0.021	0.541 \pm 0.005	19.7 \pm 3.6	1.25 \pm 0.05
A3	0.417 \pm 0.011	0.476 \pm 0.013	12.5 \pm 0.0	1.14 \pm 0.00
A4	0.448 \pm 0.012	0.559 \pm 0.026	19.9 \pm 2.4	1.27 \pm 0.05
A5	0.437 \pm 0.025	0.525 \pm 0.013	16.8 \pm 4.4	1.20 \pm 0.06
Starting material	0.504 \pm 0.009	0.631 \pm 0.014	20.2 \pm 0.4	1.25 \pm 0.01

All the batches showed a lower bulk and tapped density compared to the raw material suggesting that the material whilst compacted has retained a significant porosity in the agglomerated form. However the results also highlight that A3 showed improved flowability with a significantly reduced CI compared with all other samples (values of HR less than 1.25 or CI less than 20 are indication of good flow)²¹⁸. It is worth noting that for product with higher quantity of non-agglomerated crystals, it is not expected an improved flowability since products should behave similarly to the starting material.

6.3.4 Spherical agglomeration under stepped shear approach

The stepped shear approach was a strategy adopted to manipulate the process conditions to control each stage of the transformation and manipulate particle size distribution and particle shape and obtain more spherical and compacted agglomerates. For those experiments, the syringe pump was used to deliver the bridging liquid into the crystalliser due to the unavailability of the advanced droplet

system. The Radleys reactor was equipped with the PVM probe for process monitoring and obtains more information on the degree of agglomeration of the compound and the transition between irregular and loosely flocs to spherical agglomerates otherwise not fully accessible with the FBRM probe. Therefore, the platform configuration differs in the operation and hydrodynamics condition, since the large PVM probe added to monitor the processes altered the local conditions plus the syringe pump delivers the solvent in a continuous flow, whilst the advanced droplet system delivers as a continuous stream of small droplets.

Unexpectedly, encrustation was observed on the PVM probe and over the tubing connected to the syringe pump for delivering the bridging liquid (Figure 6.16). Although encrustation was expected to be negligible for these experiments given the absence of significant supersaturation as a driving force for growth, a paste was formed in the tubing which bridged the gap between the probe and the crystalliser wall. The localised formation of paste reduced the bridging liquid to be available for the bulk of particles in the crystalliser, and if material would detach from the probe, the product quality may be adversely affected. Indeed, encrustation is generally unfavourable in all types of processing scenarios.



Figure 6.16 Paste on the tubing delivering bridging liquid and PVM probe (left) and paste on the FBRM probe (right).

Very few references are available about encrustation during spherical agglomeration; a gap in the literature exists on the influence of critical process parameters such as

mixing, equipment materials, addition and location of bridging liquid, accordingly there is a lack of information to overcome or mitigate it.¹¹¹

In this case, the addition location was moved to another port and was added at the surface equidistant from the wall and the impeller as previously reported for this process^{2, 87, 195} and the PVM probe was moved slightly up to allow better circulation of the slurry around the probe tip. Although this revised configuration did not prevent encrustation, negligible encrustation was observed on the FBRM probe which confirms that mitigation of the encrustation was achieved (Figure 6.16 (right)). In order to understand how the particles gradually change during the corresponding experiment and the related outcomes, each experiment will be discussed separately.

Single stage addition of bridging liquid.

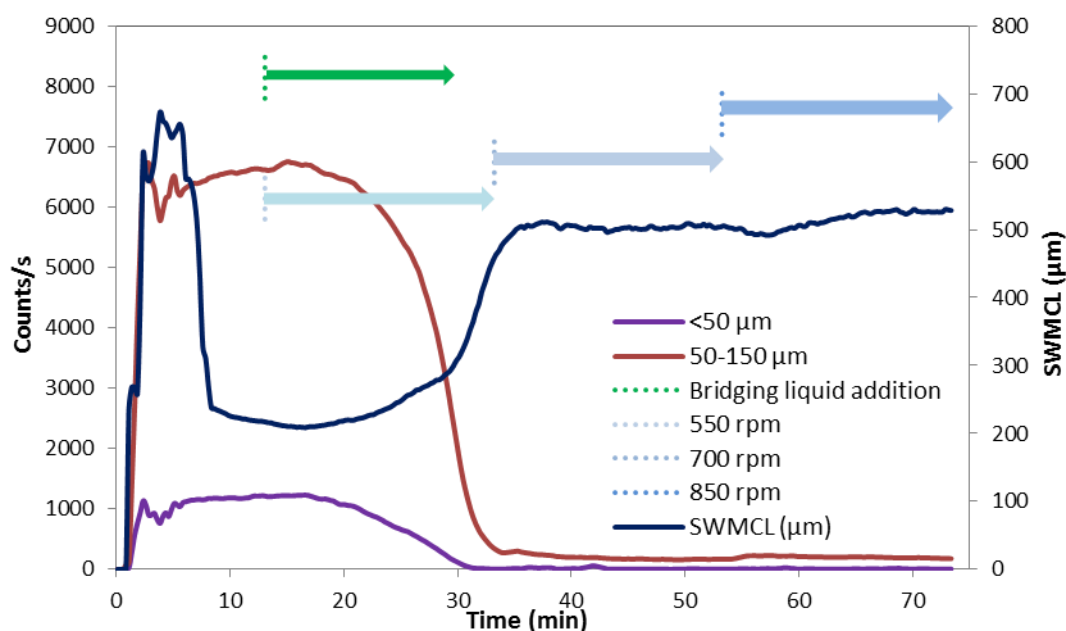


Figure 6.17 FBRM counts/s and SWMCL of the agglomeration experiment using one addition of bridging liquid at 550 rpm.

In Figure 6.17 the experiment with one addition of bridging liquid volume is shown. The addition was started after ca.10 mins to allow the slurry to be fully suspended, which is confirmed by the PVM images. Since a total time of 20 mins is chosen for each step stage, the addition of bridging liquid lasted 15mins 54 secs, thus an aging period of 4min 6 secs was added. FBRM data show both decrease in counts/s and

increase of the square weighted mean chord length (SWMCL) from 222 to 534 μm which indicates that agglomeration occurred in the system.

At the end of addition, the mean chord length increased to 480 μm before the system is switched to higher stirring rates to promote consolidation, when compacted larger agglomerates with a spherical shape appeared near to irregular and elongated agglomerates. The SWMCL showed a small increase from 480 to 506 μm during the subsequent agitation at 700 rpm which indicates that the increasing collision resulting from increased agitation rate in the vessel has only a minor influence on agglomerate size. This is consistent with the contribution of elevated agitation to the consolidation of the agglomerates which would result in the reduction of large internal voids, higher density and lower porosity.²¹⁹

Upon increasing agitation to 850 rpm, a further increase of the SWMCL from 506 to 534 μm is noticed which could be the result of further coalescence of remaining free particles or small agglomerates. No single crystals are detected at the end of the process by FBRM and PVM (Figure 6.18), for which particle count/s are nearly zero for chord lengths <50 μm . This range can be used to track agglomerate breakage or incomplete agglomeration. These results were used to confirm that the amount of bridging liquid added is correct.

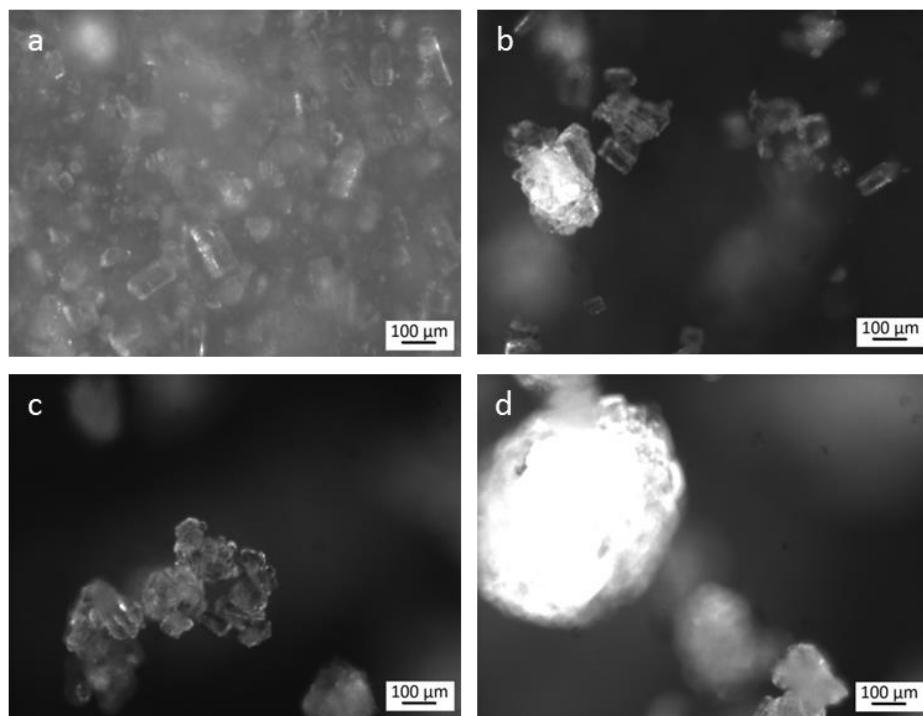


Figure 6.18 PVM images from experiment using one addition of bridging liquid. From top left to bottom right: a) slurry before addition; b) agglomerates at the end of addition at 550 rpm; c) agglomerates when agitated at 700 rpm; d) agglomerates at end of process at 850 rpm.

Figure 6.18 shows PVM images of agglomerates at different times after initiation of bridging liquid addition. As can be noted from the pictures, at the end of the injection of bridging liquid, the agglomeration process is not completed and the slurry is comprised of single crystals and agglomerates which are irregular in shape.¹¹¹ However, under prolonged agitation, irregular agglomerates became more compacted having a more spherical shape (Figure 6.18).¹⁰⁴



Figure 6.19 Image of lovastatin agglomerates (left) and microscope image of agglomerates (right) obtained from experiment using single stage addition of bridging liquid after drying.

Figure 6.19 shows pictures of agglomerates obtained from experiment using one addition of bridging liquid after drying. As can be noted from Figure 6.19 (left), the product comprises some extremely large agglomerates, oval in shape with irregular sizes. Figure 6.19 (right) shows a microscope image of agglomerates obtained with 5X magnification while the scale in the picture is 200 μm . A small fraction of fine crystals can also be observed in the microscope image and around the wall of the glass jar, which are likely to be generated post-processing through either fracture of primary particles or deagglomeration.

Two stages addition of bridging liquid.

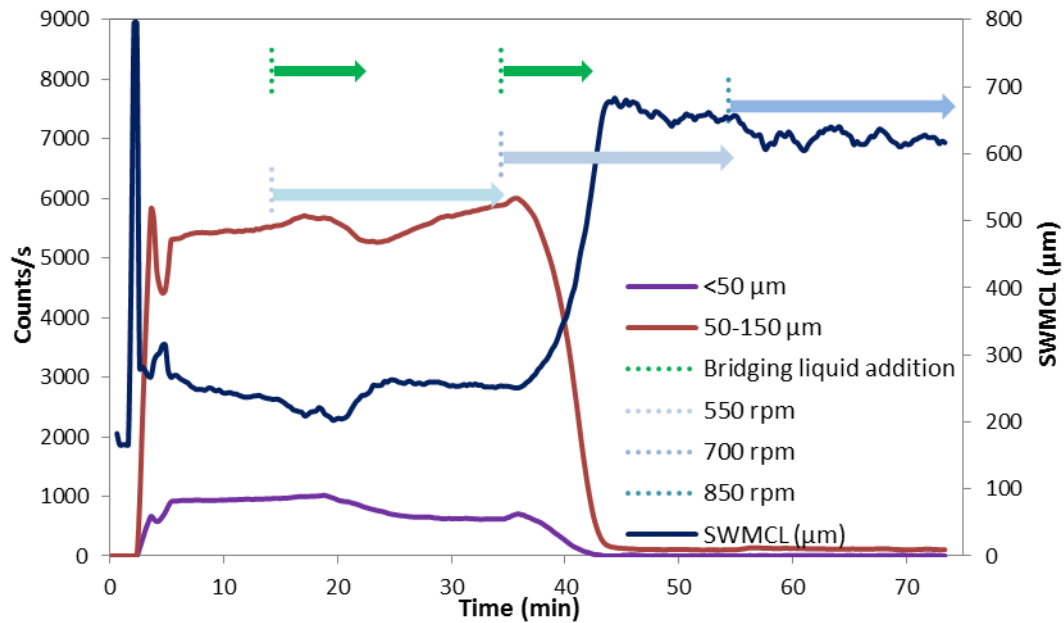


Figure 6.20 FBRM counts/s and SWMCL of the agglomeration experiment using two additions of bridging liquid at 550 rpm and 700 rpm.

Experiment with two equal addition of bridging liquid for 7mins 57 secs at 550 rpm and 700 rpm is shown in Figure 6.20. In this case, an aging period of 12 mins 3 secs at 500 rpm and 700 rpm respectively to achieve the total time of 20 mins at each step stage. The size of agglomerates increased slightly during the first addition, not enough bridging liquid was added to the system and negligible change of size (11%) from 235 to 261 μm , after which the SWMCL started to decrease suddenly forming dips. Dips may be attributed to the start of a consolidation stage, where bridging liquid starts to be diffused from the pores between aggregates to the outer surface forming a thin film.^{209, 220}

During the second addition, the SWMCL increased from 261 to 615 μm . This should be the result of the second addition of bridging liquid performed at a higher agitation rate (than the previous experiment) where increasing collision between wetted particles contributes to increase the SWMCL.

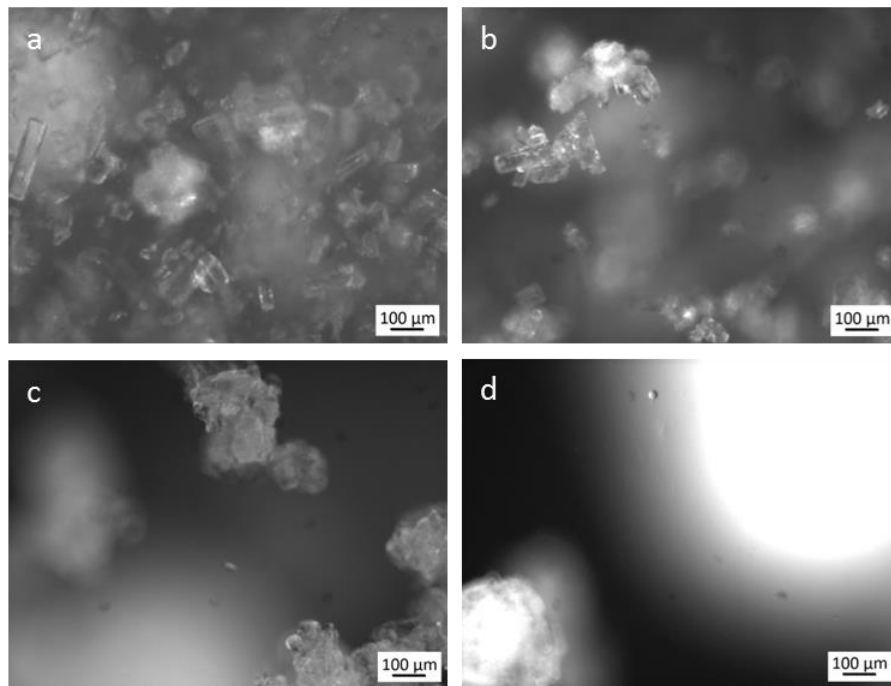


Figure 6.21 PVM images from experiment using two additions of bridging liquid. From top left to bottom right: a) slurry at the end of first addition at 550 rpm; b) agglomerates during the second addition; c) agglomerates at the end of second addition at 700 rpm; d) agglomerates at the end of process at 850 rpm.

Figure 6.21 shows PVM images of agglomerates at different times during the agglomeration experiment using two additions of bridging liquid. The scale in each picture is 100 μm . For this experiment, no difference is noticed about the shape of the agglomerates compared to the agglomerates of the previous experiment, and the PVM images doesn't show evidence of fines hence the agglomeration process is completed.

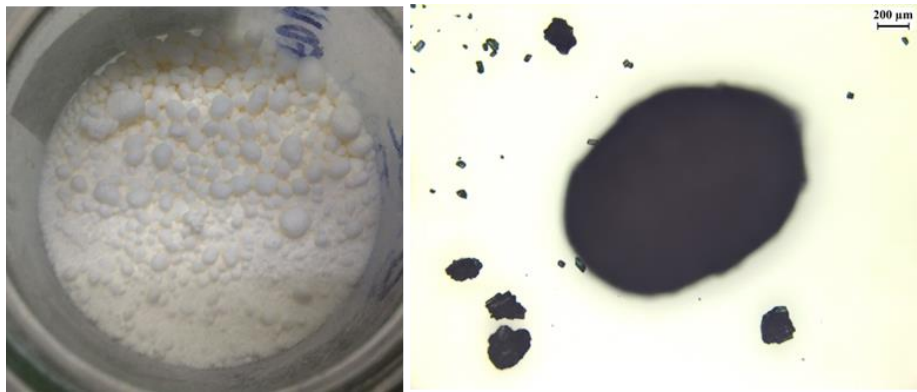


Figure 6.22 Image of lovastatin agglomerates (left) and microscope image of agglomerates (right) obtained from experiment using two stage addition of bridging liquid after drying.

Figure 6.22 shows pictures of agglomerates obtained from experiment using two additions of bridging liquid after drying. Agglomerates are smaller compared to the product obtained from the single stage addition experiment (Figure 6.19), oval in shape and not uniform in size. Figure 6.22 (right) shows a microscope image (5X magnification) of agglomerates while the scale in the picture is 200 μm.

Three stages addition of bridging liquid.

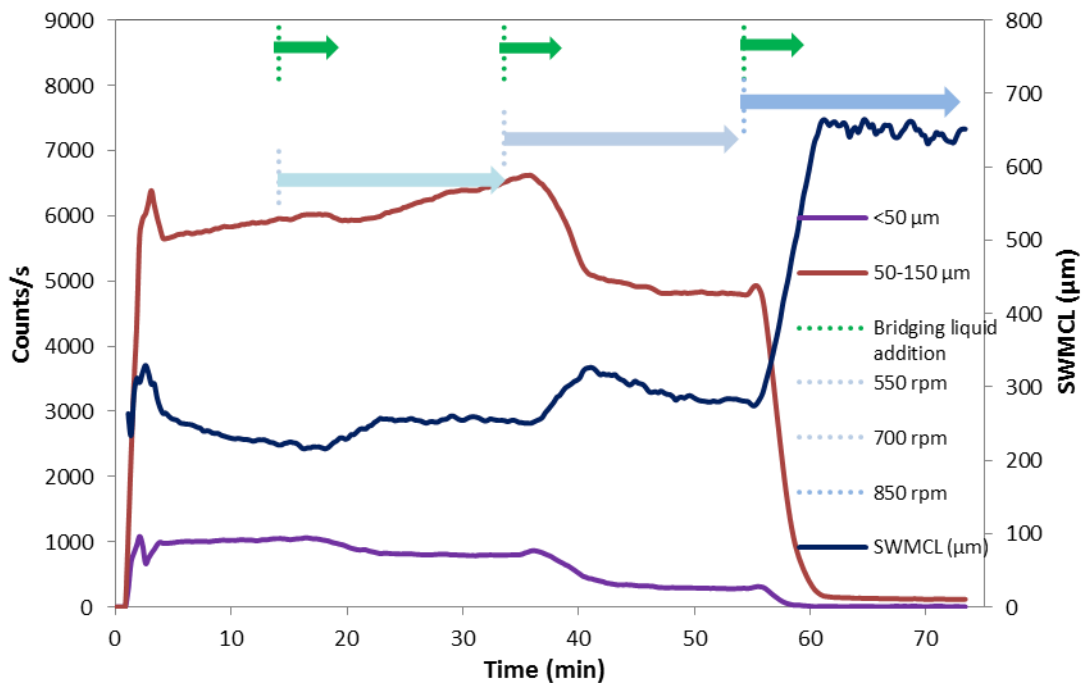


Figure 6.23 FBRM counts/s and SWMCL of the agglomeration experiment using three addition of bridging liquid at 550 rpm and 700 rpm.

Figure 6.23 shows the in situ FBRM data for the experiment with 3 equal addition of bridging liquid when the slurry was agitated at 550 rpm, 700 rpm and 850 rpm. In this case, an aging period of 14 mins 42 secs to achieve the total time of 20 mins at each step stage. This experiment produced agglomerates having the higher SWMCL of 654 μm , which is the result of the multiple addition of bridging liquid performed at each agitation rate where increasing collision between wetted particles show a positive contribution to increase the mean chord length through extended agglomeration.

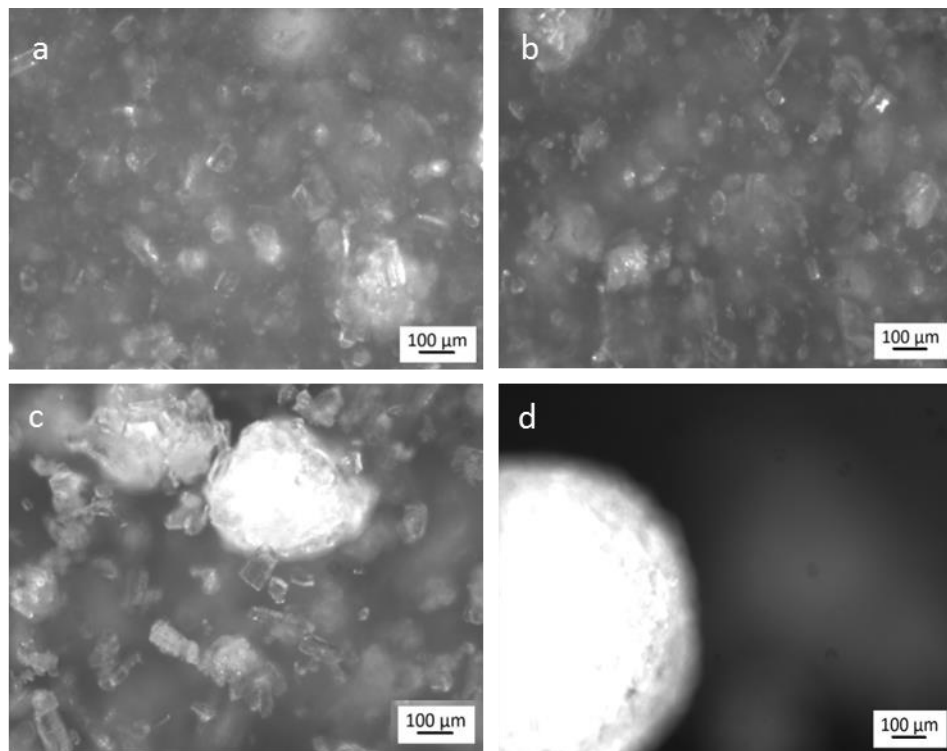


Figure 6.24 PVM images from experiment using three additions of bridging liquid. From top left to bottom right: a) slurry before addition; b) agglomerates at the end of first addition at 550 rpm; c) agglomerates at the end of second addition at 700 rpm; d) agglomerates at end of process at 850 rpm.

Figure 6.24 shows PVM images of agglomerates when the three equal portions of bridging liquid are added at each agitation rate. The scale in each picture is 100 μm . Also for this experiment, the agglomeration is completed since no single particles are left in solution at the end of the process.

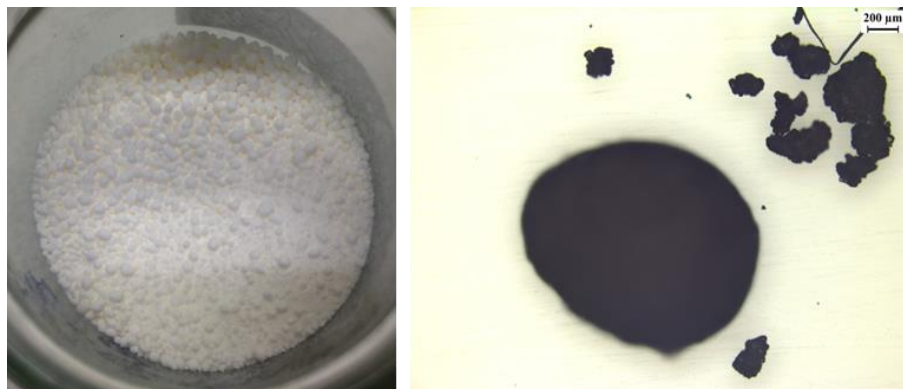


Figure 6.25 Image of lovastatin agglomerates (left) and microscope image of agglomerates (right) obtained from experiment using three addition of bridging liquid after drying.

A visual assessment of the improvement in agglomerate size and shape can be seen in Figure 6.25. These agglomerates are smaller compared to the previous experiments, also this process lead to an increase in mechanical strength of the particles, which it is confirmed by absence of fines in the microscope image (Figure 6.25 left), compared to the single and two stages addition experiments. Figure 6.26 shows the crystal size distribution for products obtained during the three batch agglomeration experiments with stepped shear approach.

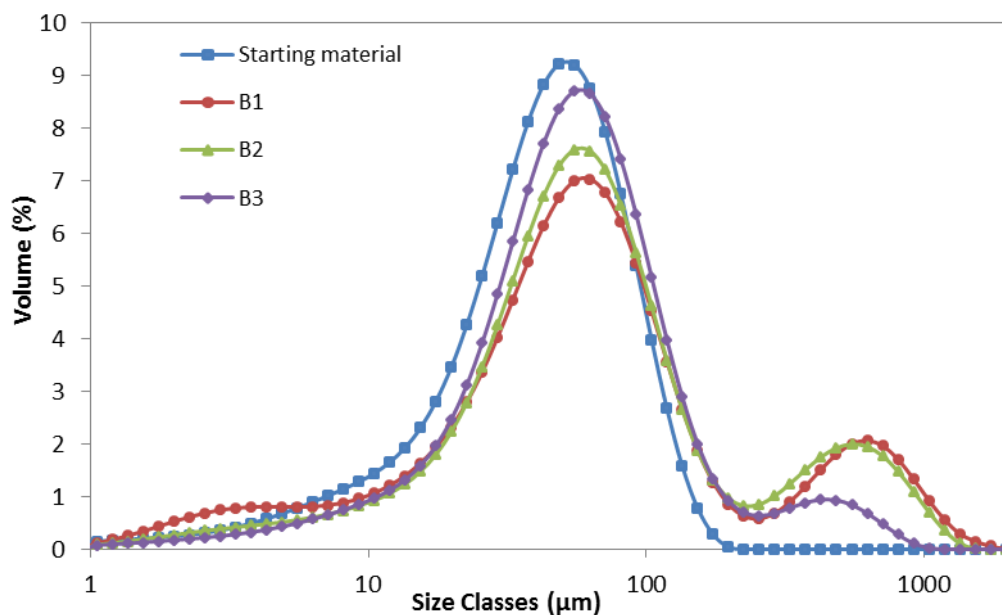


Figure 6.26 Particle size distributions by laser diffraction technique for lovastatin obtained during spherical agglomeration experiments B1-B3 and starting material.

For every sample collected at the end of the drying step, multimodal distributions are observed which are not consistent with the more uniform sizes evident from the in situ PVM images. In particular, for experiment with a single stage addition, three different distributions were observed: a distribution in the smaller size classes which is generated through breakage; a distribution similar to the distribution of the starting material and the distribution of the agglomerates of larger size. However, for the experiments with single and two stages addition no evidence of a distribution in the smaller size classes is observed.

This occurrence of fines may be the result of additional factors which affected the final product attributes such as breakage of primary particles or deagglomeration occurring post-processing and also during the size measurement. One method which could have been used to ascertain if breakage was occurring would have been to size the particles using both wet and dry dispersion and look for any differences in the PSD produced as previously suggested by McLeod *et al.*¹⁷⁷; this requires that a method for sizing using the wet dispersion unit should also be available.

Another way to look at these volume based distribution curves is to relate this breakage to the strength of the samples.¹⁷⁷ For all PSDs, the fraction of small and

large particles can then be found as the volume fraction of particles with $d < 11.9 \mu\text{m}$ (dv_{10}) and $d > 91.9 \mu\text{m}$ (dv_{90}) typical values for the starting materials. These fractions can be used to quantify the extent of agglomeration when the volume fraction percentage for the higher limit is found higher than the reference value, and for attrition and breakage, when the volume fraction percentage for the lower limit is found higher than the reference value.

The fraction of large particles was found to increase from 22.91% to 29.94%, for the sample obtained with three additions and with one addition; while it is increased further to 30.4% for the sample obtained by adding the bridging liquid two times. Conversely, the fraction of small particles, decreased from 10.89% to 7.32%, for the single stage addition and two stages addition respectively, while it is further decreased to 6.35% for the sample produced from the three stage addition process. Although the sample obtained from three additions has a lower number of agglomerates of larger particles, the smaller particles are sensibly reduced which indicates that the overall product is formed of particles that are stronger than the other samples and narrower agglomerates size distribution.

Table 6.6 Properties of lovastatin samples obtained from stepped shear approach experiments. Data are reported in the format mean \pm std dev based on 4 replicates.

Exp.	BD (g/ml)	TD (g/ml)	CI (%)	HR
B1	0.434 \pm 0.020	0.537 \pm 0.032	19.1 \pm 1.0	1.24 \pm 0.02
B2	0.405 \pm 0.006	0.497 \pm 0.010	18.4 \pm 0.4	1.23 \pm 0.01
B3	0.410 \pm 0.012	0.485 \pm 0.019	15.4 \pm 1.9	1.18 \pm 0.03

Table 6.6 shows the mean values of flow properties for the experiments carried out with fixed amount of bridging liquid and different number of portions (B1 corresponding to 1 portion of bridging liquid and so forth). The product obtained from the experiment with three additions of bridging liquid showed the best flowability with a CI of 15.45 and HR of 1.18 compared to the other products obtained with a single addition at 500 rpm and two addition of equal portion at 500 and 700 rpm respectively.

MIBK demonstrated to be a reliable solvent for the spherical agglomeration of lovastatin. Agglomerates with a SWMCL of 654 μm , having a more uniform size distribution and improved flowability (CI of 15.45) were produced when the MIBK was divided into three equal portions. However, it would be of interest to replicate these experiments using the advanced droplet system for the delivery of the bridging liquid where the dropwise addition was claimed to favour a narrower particle size distribution^{120, 221}

6.3.5 Conceptual design of continuous spherical agglomeration

As a general principle for moving from batch to continuous, some considerations must be taken into account:

- Set up the continuous agglomeration platform (vessels, heaters/chillers, and bridging liquid delivery platform);
- Ways of monitoring / controlling the product (control strategy);
- Residence time distribution;
- Moving from a direct control via FBRM in a batch system to a steady state control in a continuous system.

The continuous spherical agglomeration platform consists of two feeding vessels, where the suspension can be prepared and the bridging liquid is kept. Alternatively, a syringe pump can be used to transfer the bridging liquid when it is available. The number of vessels can be varied to extend the total residence time distribution, where a shorter residence time distribution would result in smaller agglomerate mean size. Two peristaltic pumps are used to pump the two feed streams, whilst the contents of the vessels are transferred in between the vessels using the positive pressure as long as the series of vessels are perfectly sealed (Figure 6.27).



Figure 6.27 Automated spherical agglomeration platform implemented with the Perceptive Engineering control interface.

The addition rates determine the mean residence time in each vessel according to the occupied volume of the vessels. In addition, the volume of the vessel can be varied by changing the level of the suspension inside the vessel due to inserting tubing at different relative level to the surface of the suspension. Therefore, the residence time can still be adjusted even though the total volume of tanks is fixed.

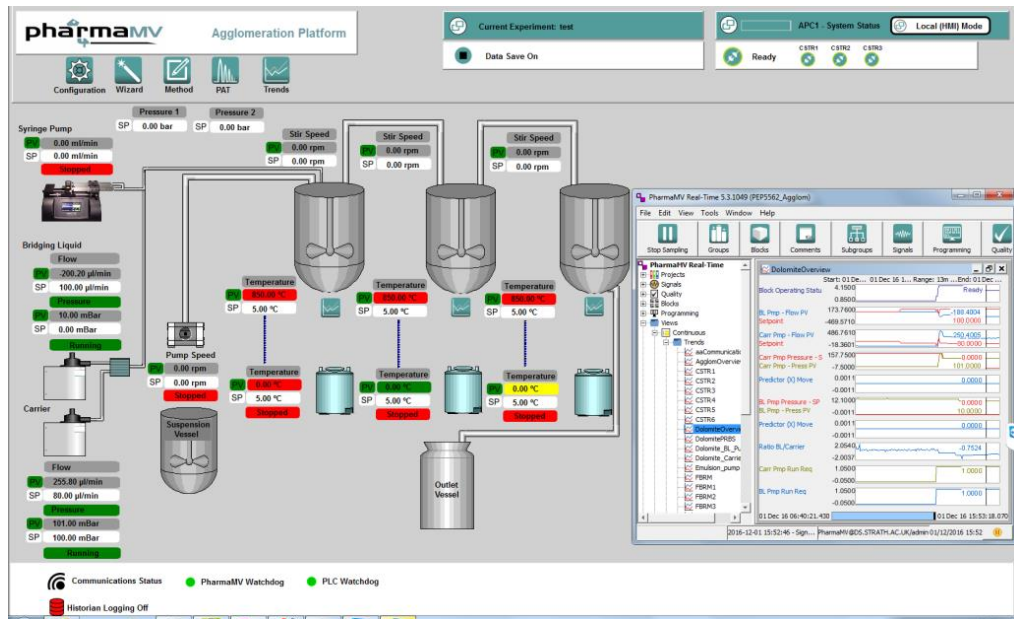


Figure 6.28 Perceptive Engineering control interface for the multi vessel spherical agglomeration platform.

The platform was automated by Perceptive Engineering providing a control interface for automated experimental operation of the spherical agglomeration platform (Figure 6.28); through PharmaMV software, the operating conditions or manipulated variables can be varied and the data can be collected from in-line probes including thermocouples, FBRM and IR to identify a suitable model. For example a series of steps was applied to the advanced droplet system to allow the identification of a linear model that could predict the flow of bridging liquid and carrier fluids, thus it could be used within model predictive control (MPC) architecture (Figure 6.29). Further details about MPC are given elsewhere.²²²

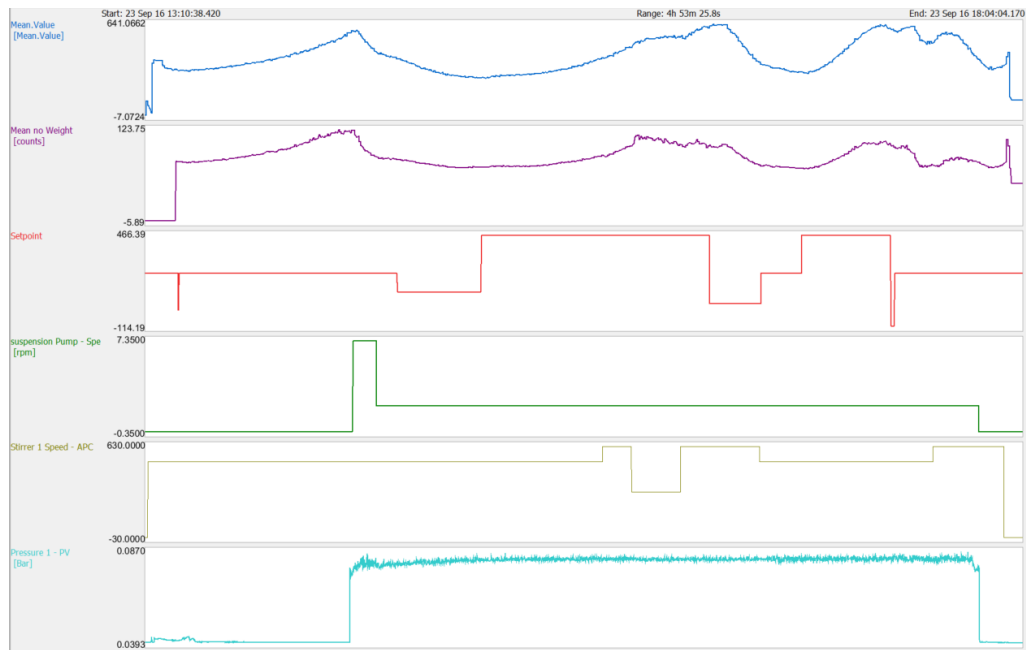


Figure 6.29 SWMCL, agitation rate and pressure profile used to identify the relation between process variables and product attributes.

Figure 6.30 shows pictures of agglomerates at different times after initiation of bridging liquid addition in the first vessel. As can be noted from the pictures when the excessive amount of bridging liquid is added, the product changed from powder (Figure 6.30a) to a paste-like product (Figure 6.30c). During the transition, agglomerates larger than 5 cm were produced (Figure 6.30b). However, this is not surprising since larger amount of bridging liquid was added during the run by varying the flow rate of the pump but the slurry from the first stage was added at a fixed rate for the entire operation, thus creating periods of imbalance between the amount of bridging liquid and the amount of crystals in suspension. This excessive amount of bridging liquid not only caused excessive agglomeration with production of very large agglomerates but lead to the formation of the paste, due to the lack of particles being available in suspension for the amount of bridging liquid being added. However a better operation would be to add the bridging liquid at the exact amount needed for the slurry coming inside the vessel and explore intermittent operation of the cascade. The intermittent operation was reported to be successful for the production of spherical agglomerates of benzoic acid through the continuous operation of a two-stage MSMPR system.⁸⁷



Figure 6.30 Product obtained from the continuous spherical agglomeration platform at 20°C using MIBK as bridging liquid.

This way of operation led to a more uniform size distribution with less fluctuation of the SWMCL and less oscillations when reached the controlled state of operation. Further work is required to establish new connection and experimental work in order to design a continuous spherical agglomeration process able to deliver a target PSD of lovastatin.

6.4 Summary

This work has demonstrated a systematic approach to spherical agglomeration process design, based on an experimental workflow. Initial small scale batch screening experiments with in-situ microscopic cameras were carried out to determine suitable solvents to be selected as bridging liquid for the spherical

agglomeration in suspension of lovastatin. XRPD analysis confirmed the stable form of lovastatin for the agglomerates. The results of the screening show that the amount of bridging liquid is critical for the formation of agglomerates and the spherical agglomerates can only be obtained in a narrow range of BSR for each solvent, which is variable between solvents depending on the solubility in water which dictates the amount of bridging liquid being available for bridging purpose. From the screening, MIBK was selected as a successful bridging liquid for spherical agglomeration of lovastatin, due to the formation of compacted spherical agglomerates based on eye observation.

Fouling was observed during the screening experiments when excess bridging liquid was added resulting from the formation of second phase behaving in a paste-like manner which adhered mostly on the impeller.

A novel application of the Principal Component Analysis (PCA) of 250 calculated molecular descriptors using MOE of solvents was presented and successfully used to determine properties of solvents related to agglomeration propensity. Using SIMCA-P, solvents were divided into groups in the score scatter plot and properties such as atomic polarizabilities, counts of atoms and bonds, solvent molecular volume and surface area and water accessible surface area were identified to be the most influential properties affecting the agglomeration of lovastatin.

Once established a PCA model, it could be used as a predictive tool for agglomeration propensity study when subsets or populations are identified. MIBK was selected for large scale experiments by visual inspection of the agglomerates obtained during the bridging liquid screening experiments. For the water-MIBK system at 20°C the BSR range is found to be 0.71 to 0.94. Agglomerates with improved flowability were obtained when using a BSR of 0.82 (or BLR of 0.7) with agitation rate of 700 rpm. PATs such as FBRM and PVM were integrated successfully for the first time to monitor the processes and gather information on the process dynamics. FBRM showed dips in the SWMCL which may be attributed to a consolidation stage after holding period. Throughout these experiments, significant encrustation was observed when highest amount of bridging liquid was used.

Application of a stepped shear approach by varying the agitation rate and bridging liquid injection showed that product with improved flowability and more uniform particle size distribution was achieved when the addition of bridging liquid is divided

in equal portions and these portions were added at different agitation rate. During the study, inline PVM probe was successfully integrated to capture the mechanisms present and assess completion of the agglomeration process. Mitigation of fouling was achieved by changing position of tubing of bridging liquid and distance between the tubing and probes. This also advanced the capabilities to move towards a QbD approach and the utilisation of a feedback control approach.

A platform for continuous spherical agglomeration was developed in the lab using a cascade of MSMPRs and automated in collaboration with Perceptive Engineering using a control interface through PharmaMV software. Different products were obtained through the manipulation of the flow rate of the bridging liquid in order to test the platform operation and the control interface.

Chapter 7. Conclusions and Future Work

7.1 Conclusions

Agglomerates in bulk powders can be desirable or undesirable depending on the intended downstream processing and application of the product. Agglomerates are generally unwanted in crystallization process as these can be more difficult to wash because mother liquor and impurities can become entrained inside the solid particles. Nevertheless in some cases the agglomeration is exploited in order to manipulate the product and achieve improved bulk powder properties. Spherical agglomeration/crystallization is of particular interest as it allows easier handling of powder, reduces dust, and improves flowability and compaction properties of the crystalline production.

In the work presented here (Chapter 4), the first application of spherical crystallization was focused on the improvement of the flow properties of the poorly flowable drug ibuprofen. Ethanol and water were investigated as solvent and antisolvent respectively, due to a previous study highlighting the formation of spherical agglomerates of ibuprofen for a specific ethanol:water composition in the presence of liquid-liquid phase separation¹⁴⁸. However, a liquid-liquid phase separation region has been identified for the first time. Four phase diagrams were determined experimentally at 4 temperatures and information on the location and shape of the phase boundaries were obtained allowing the testing of specific process conditions. This included a novel methodology using imaging analysis and small scale parallel crystallization platform to determine the phase diagrams. The phase diagrams comprised 5 different regions and the liquid-liquid phase region was found to increase in size with increasing temperature for specific solute concentration and temperatures, whilst disappearing at 20°C.

On the basis of the phase diagrams, crystallization with and without oiling out were investigated with the integration of FBRM, ATR-FTIR, and PVM. Using PATs, the nucleation process inside and outside the liquid-liquid phase region was distinguished. An experiment designed to suppress the occurrence of the liquid-liquid separation resulted in ibuprofen crystallised as plate-like crystals with low agglomeration degree, low flowability and low yield. When crystallization was carried out in the presence of liquid-liquid phase separation, ibuprofen crystallised as agglomerates with better flowability and higher yield. The recrystallized products

showed the same polymorphic form (stable form) and melting temperature of the raw material. The ternary phase diagram played a decisive role in designing the crystallization of ibuprofen from aqueous ethanol system and could allow control strategies to be defined to achieve consistent product.

Another technique which stems from spherical crystallization is spherical agglomeration of crystal in suspension. Agglomeration is carried out in a similar manner to spherical crystallization, except that the solid is dispersed in a suspending medium and not crystallised out, therefore reducing the number of stages to the agglomeration with the bridging liquid. Spherical agglomeration has also been demonstrated in a continuous mode for the production of spherical agglomerates of benzoic acid by using a two-stage MSMPRs, where one stage is used for the nucleation of crystals of benzoic acid and the second stage is used for the agglomeration of newly formed crystals by addition of the bridging liquid.⁸⁷

Spherical agglomerates of lovastatin were successfully prepared for the first time using the spherical agglomeration in suspension technique in a batch vessel with water as dispersing medium. Different solvents to act as bridging liquid were selected from ICH class 2 and 3 having low solubility in water as major criteria. A small scale parallel crystallization platform equipped with microscope camera was used to study the agglomeration propensity of lovastatin. The majority of solvents except alkenes led to spherical agglomerates; this may be due to the higher interfacial tension between the alkenes solution and water which generates large droplets with tendency to coalesce rather than create spherical agglomerates.

A PCA model was created based on molecular descriptors of solvents and these were classified as non-agglomerating solvents or agglomerating solvent. When compared with the loading plot, the main characteristics of solvent responsible for promoting the agglomeration were related to polarizability, solvent molecular volume and water accessible surface area.

Fouling was also observed during the screening experiments upon addition of excess of bridging liquid which caused phase separation. This phase was formed of paste-like irregular agglomerates which adhere mostly on the impeller. This highlights that even in conditions where nucleation and growth are not expected to occur, particle adhesion to vessel surfaces can lead to uncontrolled deposition and fouling.

On the basis of the bridging liquid screening experiments, MIBK was selected for larger scale (250mL) experiments. Agglomerates with improved flowability were obtained when MIBK with a ratio of 0.7 ml per gram of lovastatin and an agitation rate of 700 rpm was used. PAT tools such as FBRM and PVM were integrated successfully for the first time to monitor the processes and gather information on the process dynamics. FBRM showed dips in the SWMCL which suggest that a consolidation stage is taking place.

Further studies comprised the understanding of agglomeration process of an industrial relevant active ingredient by monitoring with PAT. In this research, the influence of different processing parameters on the degree of agglomeration and final agglomerates attributes was evaluated. Images of agglomerates and single crystals captured from the PVM probe were analysed using routines developed in MATLAB. This was the first time that such application was applied at industrial scale and it gives access to information otherwise unattainable from offline characterization methods. The monitoring of seed dispersion showed that aggregation or agglomeration of seed crystals was present before suspension into the crystalliser. This in turn influenced the dispersion in the crystalliser for the deaggregation/deagglomeration of seeds under intense agitation. The studies carried out have contributed to a better understanding of the relation between operating parameters and product obtained which is reflected on particle size and strength of agglomerates during agitation drying. It was concluded that the degree of breakage during agitation drying can be related to the moisture content and it was found to be lower for agglomerates produced under specific conditions and including a temperature cycle.

7.2 Future work

7.2.1 Ternary phase diagram of ibuprofen in ethanol-water solutions for understanding crystallization and agglomeration

The phase diagrams were successfully used to investigate the crystallization of ibuprofen in aqueous ethanol systems, where processes with or without oiling out allowed the production of different batches. With the determined phase diagrams, the ability to design and control processes was greatly improved since all the regions including the liquid-liquid phase separation regions were determined at four different temperatures. However, a useful extension of the work would be to investigate the product attributes from crystallization as a function of different trajectories of operation or exploiting different operation strategies such as combined cooling and antisolvent crystallization.

Further extension would be implementing model-based control and optimisation strategies in order to develop a robust process that delivers the desired particle attributes. However this would be possible when all the relevant mechanisms such as nucleation, growth, agglomeration/breakage and encrustation are identified and kinetic information extracted. Ibuprofen for example is a poorly flowable powder combined with a low dissolution rate. Utilising previously reported knowledge^{87, 223}, operating parameters could be adjusted to achieve the desired primary crystals and/or agglomerates properties in order to optimize both bioavailability and manufacturability of this compound. This could be achieved by decoupling nucleation from growth/agglomeration where using a single crystalliser or two separate crystallisers and adding a bridging liquid to aid the formation of agglomerates in a more spherical shape. In this way the spherical crystallization of ibuprofen could also be transferred from batch to continuous operation.

Alternatively, direct control methods which allow feedback from inline PAT could be used to achieve desired particle attributes more readily without information on kinetics. This may be feasible for crystallization processes when the immiscibility or appearance of a second liquid phase is limited otherwise it could be difficult or impossible either track concentration because of two phases of different composition are present and track particles counts since both droplets and crystals are counted.

Fouling was observed during crystallization of ibuprofen but was not investigated in this study. Presence of fouling or undesired nucleation on surface can lead to blockage, affect heat transfer and lead to product out of specification affecting particle size distribution and/or solid state. This may be studied by investigation of fouling induction time on different surfaces at different level of supersaturation and solvent compositions.

Due to moving of equipment from laboratories, equipment such as mercury porosimeter, tableting machine and mechanical strength machine selected for the off-line characterisation of product attributes were setup and calibrated at laboratory towards the end of the work so most of the off-line analysis were not carried out.

However, characterisation of the product would complete the work around the suitability for direct compression of the ibuprofen product.

7.2.2 Agglomeration study of an active pharmaceutical ingredient

All the experiments have shown agglomeration of the seed crystals in suspension prior to the addition in the crystalliser. This raises interesting questions about the surface properties of the crystals and their typical preparation methods within industry. Study of the surface properties of seed crystals produced by different seed preparation methods (e.g. wet or dry milling) could include zeta potential or surface energy analysis. Solvent parameters relating to hydrogen bonding ability have been highlighted in literature as important for relating a solvent to the potential to agglomerate. However, this is only valid if hydrogen bonding functional groups are present in the molecule and on the crystal surface.¹⁷¹ A repeat study utilizing different solvents would help understand the different solute/solvent interaction.

The influence of seed size was not investigated during this study, although it is claimed that agglomeration propensity is increased for smaller size of seed crystals, it would be of interest to evaluate the impact of this parameter on the agglomeration propensity of GSK106.

For this specific system, the agglomeration behaviour has been studied for varying operating conditions, and it was shown the potential of the new tool to detect agglomeration process for APIs. An investigation of process conditions and solvents for promoting growth of single crystals to determine descriptors values for single

crystals would complete the quantitative analysis of agglomeration by split the population of particles into single crystals and agglomerates.

7.2.3 Spherical agglomeration in suspension of lovastatin

Spherical agglomerates of lovastatin were successfully prepared by agglomeration in suspension technique in water-MIBK system. This was achieved by establishing an appropriate methodology for screening of a suitable bridging liquid and determines the critical optimal range using small scale experiments, and then using the information acquired during the screening to select a minimum number of experiments in order to identify the relationship between process parameters and quality attributes

This methodology for the screening of bridging liquid using the Crystalline platform provided a close similarity to the hydrodynamic conditions and material of construction to the common used large scale crystallisers compared to the previously reported methodology of contact angle measurements or bridging liquid suspension. An implementation of the Crystalline platform that allow the addition of bridging liquid in an automated manner, would move the manual and experimentally labour intensive operation to one with automated and controlled operation. This could be achieved with syringe pumps or advanced droplet formation system.

A PCA model was created using the solvent molecular properties as descriptors. It is reasonable and useful to create another model based on properties related to the solvent/surface interaction such as contact angle, interfacial tension, polarity or solvent parameters related to hydrogen bonding ability and viscosity and evaluate if it is possible to statistically isolate non-agglomerating to agglomerating solvents.

A novel continuous platform for spherical agglomeration was successfully designed, assembled and a control interface installed. The system is flexible enough to allow spherical agglomeration or agglomeration in suspension to be carried out, however more time is required for establishing other connection for PAT such as IR or UV and fix connection issues as well as update software. Additional work is required for calibration of syringe pump and connection of impeller of vessels and pressure transfer regulator valve between vessels. In addition, a more advanced training is

required to troubleshoot errors derived from connection issues when remote support is not available. Moving forward, a process control strategy must be implemented.

As previously discussed, PAT-based control method may be more implemented quicker when a model-based strategy may result in a very complicated model with too many parameters which may be the case of spherical agglomeration.

One option could be to use the SWMCL as trigger for moving to different agitation rate, although a value or expression for this variable must be defined.

References

1. Lipinski, C. A.; Lombardo, F.; Dominy, B. W.; Feeney, P. J., Experimental and computational approaches to estimate solubility and permeability in drug discovery and development settings. *Journal of Pharmaceutical Sciences* **1997**, *86* (1), 3-26. The article was originally published in *Advanced Drug Delivery Reviews* **23** (1997) 3-25. *Advanced Drug Delivery Reviews* **2001**, *46* (1), 3-26.
2. Katta, J.; Rasmuson, Å. C., Spherical crystallization of benzoic acid. *International Journal of Pharmaceutics* **2008**, *348* (1), 61-69.
3. Byn, S., Morris, K., Comella, S., Reducing time to market with a science-based management strategy. *Pharmaceutical Technology* **2005**, *2005* (5), 46-56.
4. Mehta, M. U.; Uppoor, R. S.; Conner, D. P.; Seo, P.; Vaidyanathan, J.; Volpe, D. A.; Stier, E.; Chilukuri, D.; Dorantes, A.; Ghosh, T.; Mandula, H.; Raines, K.; Dhanormchitphong, P.; Woodcock, J.; Yu, L. X., Impact of the US FDA "Biopharmaceutics Classification System" (BCS) Guidance on Global Drug Development. *Molecular Pharmaceutics* **2017**, *14* (12), 4334-4338.
5. Variankaval, N.; Cote, A. S.; Doherty, M. F., From form to function: Crystallization of active pharmaceutical ingredients. *AIChE Journal* **2008**, *54* (7), 1682-1688.
6. Aitipamula, S.; Banerjee, R.; Bansal, A. K.; Biradha, K.; Cheney, M. L.; Choudhury, A. R.; Desiraju, G. R.; Dikundwar, A. G.; Dubey, R.; Duggirala, N.; Ghogale, P. P.; Ghosh, S.; Goswami, P. K.; Goud, N. R.; Jetty, R. R. K. R.; Karpinski, P.; Kaushik, P.; Kumar, D.; Kumar, V.; Moulton, B.; Mukherjee, A.; Mukherjee, G.; Myerson, A. S.; Puri, V.; Ramanan, A.; Rajamannar, T.; Reddy, C. M.; Rodriguez-Hornedo, N.; Rogers, R. D.; Row, T. N. G.; Sanphui, P.; Shan, N.; Shete, G.; Singh, A.; Sun, C. Q. C.; Swift, J. A.; Thaimattam, R.; Thakur, T. S.; Thaper, R. K.; Thomas, S. P.; Tothadi, S.; Vangala, V. R.; Variankaval, N.; Vishweshwar, P.; Weyna, D. R.; Zaworotko, M. J., Polymorphs, Salts, and Cocrystals: What's in a Name? *Cryst Growth Des* **2012**, *12* (5), 2147-2152.
7. Bauer, J.; Spanton, S.; Henry, R.; Quick, J.; Dziki, W.; Porter, W.; Morris, J., Ritonavir: An Extraordinary Example of Conformational Polymorphism. *Pharmaceutical Research* **2001**, *18* (6), 859-866.
8. <https://www.fda.gov/Safety/Recalls/ucm233533.htm>.
9. McKeown, R. R.; Wertman, J. T.; Dell'Orco, P. C., Crystallization Design and Scale-Up. In *Chemical Engineering in the Pharmaceutical Industry*, John Wiley & Sons, Inc.: 2010; pp 213-247.
10. Falk, R. F.; Marziano, I.; Kougoulos, T.; Girard, K. P., Prediction of Agglomerate Type during Scale-Up of a Batch Crystallization Using Computational Fluid Dynamics Models. *Organic Process Research & Development* **2011**, *15* (6), 1297-1304.
11. Yu, L. X., Pharmaceutical Quality by Design: Product and Process Development, Understanding, and Control. *Pharmaceutical Research* **2008**, *25* (4), 781-791.
12. Allison, G.; Cain, Y. T.; Cooney, C.; Garcia, T.; Bizjak, T. G.; Holte, O.; Jagota, N.; Komar, B.; Korakianiti, E.; Kourti, D.; Madurawe, R.; Morefield, E.; Montgomery, F.; Nasr, M.; Randolph, W.; Robert, J.-L.; Rudd, D.; Zezza, D., Regulatory and Quality Considerations for Continuous Manufacturing. May 20-21, 2014 Continuous Manufacturing Symposium. *Journal of Pharmaceutical Sciences* **2015**, *104* (3), 803-812.

13. Leuenberger, H., New trends in the production of pharmaceutical granules: batch versus continuous processing. *European Journal of Pharmaceutics and Biopharmaceutics* **2001**, 52 (3), 289-296.
14. Plumb, K., Continuous processing in the pharmaceutical industry - Changing the mind set. *Chem Eng Res Des* **2005**, 83 (A6), 730-738.
15. Salvatore, M.; L., H. P.; Haitao, Z.; Richard, L.; Brahim, B.; I., B. P.; D., B. R.; L., C. C.; B., E. J. M.; F., J. T.; F., J. K.; S., M. A.; L., T. B., End-to-End Continuous Manufacturing of Pharmaceuticals: Integrated Synthesis, Purification, and Final Dosage Formation. *Angewandte Chemie International Edition* **2013**, 52 (47), 12359-12363.
16. Brown, C. J.; McGlone, T.; Yerdelen, S.; Srirambhatla, V.; Mabbott, F.; Gurung, R.; L. Briuglia, M.; Ahmed, B.; Polyzois, H.; McGinty, J.; Perciballi, F.; Fysikopoulos, D.; MacFhionnghaile, P.; Siddique, H.; Raval, V.; Harrington, T. S.; Vassileiou, A. D.; Robertson, M.; Prasad, E.; Johnston, A.; Johnston, B.; Nordon, A.; Srai, J. S.; Halbert, G.; ter Horst, J. H.; Price, C. J.; Rielly, C. D.; Sefcik, J.; Florence, A. J., Enabling precision manufacturing of active pharmaceutical ingredients: workflow for seeded cooling continuous crystallisations. *Molecular Systems Design & Engineering* **2018**.
17. <https://www.cmac.ac.uk/>.
18. Anderson, N. G., Practical Use of Continuous Processing in Developing and Scaling Up Laboratory Processes. *Organic Process Research & Development* **2001**, 5 (6), 613-621.
19. Konstantinov, K. Integrated Continuous Manufacturing of Therapeutic Protein Drug Substances. Provision U.S. Patent 61775060. 2013.
20. McGlone, T.; Briggs, N. E. B.; Clark, C. A.; Brown, C. J.; Sefcik, J.; Florence, A. J., Oscillatory Flow Reactors (OFRs) for Continuous Manufacturing and Crystallization. *Organic Process Research & Development* **2015**, 19 (9), 1186-1202.
21. Badman, C.; Trout, B. L., Achieving Continuous Manufacturing. May 20–21, 2014 Continuous Manufacturing Symposium. *Journal of Pharmaceutical Sciences* **2015**, 104 (3), 779-780.
22. Baxendale, I. R.; Braatz, R. D.; Hodnett, B. K.; Jensen, K. F.; Johnson, M. D.; Sharratt, P.; Sherlock, J.-P.; Florence, A. J., Achieving Continuous Manufacturing: Technologies and Approaches for Synthesis, Workup, and Isolation of Drug Substance May 20–21, 2014 Continuous Manufacturing Symposium. *Journal of Pharmaceutical Sciences* **2015**, 104 (3), 781-791.
23. Rogers, A.; Hashemi, A.; Ierapetritou, M., Modeling of Particulate Processes for the Continuous Manufacture of Solid-Based Pharmaceutical Dosage Forms. *Processes* **2013**, 1 (2), 67.
24. Knox, M.; Trifkovic, M.; Rohani, S., Combining anti-solvent and cooling crystallization: Effect of solvent composition on yield and meta stable zone width. *Chem Eng Sci* **2009**, 64 (16), 3555-3563.
25. Lindenberg, C.; Krattli, M.; Cornel, J.; Mazzotti, M.; Brozio, J., Design and Optimization of a Combined Cooling/Antisolvent Crystallization Process. *Cryst Growth Des* **2009**, 9 (2), 1124-1136.
26. Nagy, Z. K.; Fujiwara, M.; Braatz, R. D., Modelling and control of combined cooling and antisolvent crystallization processes. *Journal of Process Control* **2008**, 18 (9), 856-864.

27. Myerson, A. S., *Handbook of Industrial Crystallization*. 2002.
28. Mullin, J. W., *Crystallisation*. **2001**, 4th Edition, Oxford.
29. Nývlt, J.; Rychlý, R.; Gottfried, J.; Wurzelová, J., Metastable zone-width of some aqueous solutions. *Journal of Crystal Growth* **1970**, 6 (2), 151-162.
30. Miers, H. A.; Isaac, F., The Spontaneous Crystallisation of Binary Mixtures. Experiments on Salol and Betol. *Proceedings of the Royal Society of London. Series A* **1907**, 79 (531), 322-351.
31. Barrett, P.; Glennon, B., Characterizing the Metastable Zone Width and Solubility Curve Using Lasentec FBRM and PVM. *Chemical Engineering Research and Design* 80 (7), 799-805.
32. Nagy, Z. K.; Fujiwara, M.; Woo, X. Y.; Braatz, R. D., Determination of the Kinetic Parameters for the Crystallization of Paracetamol from Water Using Metastable Zone Width Experiments. *Ind Eng Chem Res* **2008**, 47 (4), 1245-1252.
33. Kubota, N., A new interpretation of metastable zone widths measured for unseeded solutions. *Journal of Crystal Growth* **2008**, 310 (3), 629-634.
34. Nývlt, J., Kinetics of nucleation in solutions. *Journal of Crystal Growth* **1968**, 3, 377-383.
35. Jiang, S.; ter Horst, J. H., Crystal Nucleation Rates from Probability Distributions of Induction Times. *Cryst Growth Des* **2011**, 11 (1), 256-261.
36. Mitchell, N. A.; Frawley, P. J., Nucleation kinetics of paracetamol-ethanol solutions from metastable zone widths. *Journal of Crystal Growth* **2010**, 312 (19), 2740-2746.
37. O'Grady, D.; Barrett, M.; Casey, E.; Glennon, B., The Effect of Mixing on the Metastable Zone Width and Nucleation Kinetics in the Anti-Solvent Crystallization of Benzoic Acid. *Chemical Engineering Research and Design* 85 (7), 945-952.
38. Ni, X.; Liao, A., Effects of Cooling Rate and Solution Concentration on Solution Crystallization of l-Glutamic Acid in an Oscillatory Baffled Crystallizer. *Cryst Growth Des* **2008**, 8 (8), 2875-2881.
39. Becker, R.; Döring, W., Kinetische Behandlung der Keimbildung in übersättigten Dämpfen. *Annalen der Physik* **1935**, 416 (8), 719-752.
40. Gibbs, J. W., On the equilibrium of heterogeneous substances. *First Part Trans. Connect. Acad. Sci.* **1876**, 3, 108-248.
41. Volmer, M., Kinetik der Phasenbildung. *Die Chemische Reaktion* **1939**, IV (Leipzig).
42. Garside, J. S., O., *Precipitation: Basic Principles and Industrial Applications*. Butterworth-Heinemann **1992**.
43. Mullin, J. W.; Nývlt, J., Programmed cooling of batch crystallizers. *Chem Eng Sci* **1971**, 26 (3), 369-377.
44. Helt, J. E.; Larson, M. A., Effects of temperature on the crystallization of potassium nitrate by direct measurement of supersaturation. *Aiche J* **1977**, 23 (6), 822-830.
45. Vekilov, P. G., Dense Liquid Precursor for the Nucleation of Ordered Solid Phases from Solution. *Cryst Growth Des* **2004**, 4 (4), 671-685.
46. Vekilov, P. G., The two-step mechanism of nucleation of crystals in solution. *Nanoscale* **2010**, 2 (11), 2346-2357.
47. Vekilov, P. G., Nucleation of protein crystals. *Progress in Crystal Growth and Characterization of Materials* **2016**, 62 (2), 136-154.

48. Galkin, O.; Vekilov, P. G., Control of protein crystal nucleation around the metastable liquid-liquid phase boundary. *P Natl Acad Sci USA* **2000**, *97* (12), 6277-6281.
49. Kashchiev, D.; Vekilov, P. G.; Kolomeisky, A. B., Kinetics of two-step nucleation of crystals. *The Journal of Chemical Physics* **2005**, *122* (24), 244706.
50. Wolde, P. R. t.; Frenkel, D., Enhancement of Protein Crystal Nucleation by Critical Density Fluctuations. *Science* **1997**, *277* (5334), 1975-1978.
51. Georgalis, Y.; Umbach, P.; Raptis, J.; Saenger, W., Lysozyme aggregation studied by light scattering .1. Influence of concentration and nature of electrolytes. *Acta Crystallogr D* **1997**, *53*, 691-702.
52. Igarashi, K.; Azuma, M.; Kato, J.; Ooshima, H., The initial stage of crystallization of lysozyme, a differential scanning calorimetric (DSC) study. *Journal of Crystal Growth* **1999**, *204* (1-2), 191-200.
53. Pontoni, D.; Narayanan, T.; Rennie, A. R., Nucleation and growth kinetics of colloidal silica. *Prog Coll Pol Sci S* **2004**, *123*, 227-230.
54. Chattopadhyay, S.; Erdemir, D.; Evans, J. M. B.; Ilavsky, J.; Amenitsch, H.; Segre, C. U.; Myerson, A. S., SAXS study of the nucleation of glycine crystals from a supersaturated solution. *Cryst Growth Des* **2005**, *5* (2), 523-527.
55. Ayazi Shamlou, P.; Jones, A. G.; Djamarani, K., Hydrodynamics of secondary nucleation in suspension crystallization. *Chem Eng Sci* **1990**, *45* (5), 1405-1416.
56. van der Heijden, A. E. D. M.; van der Eerden, J. P.; van Rosmalen, G. M., The secondary nucleation rate: a physical model. *Chem Eng Sci* **1994**, *49* (18), 3103-3113.
57. Garside, J.; Shah, M. B., Crystallization Kinetics from MSMPR Crystallizers. *Industrial & Engineering Chemistry Process Design and Development* **1980**, *19* (4), 509-514.
58. Girolami, M. W.; Rousseau, R. W., Initial breeding in seeded batch crystallizers. *Industrial & Engineering Chemistry Process Design and Development* **1986**, *25* (1), 66-70.
59. Ulrich, J.; Strege, C., Some aspects of the importance of metastable zone width and nucleation in industrial crystallizers. *Journal of Crystal Growth* **2002**, *237-239*, Part 3, 2130-2135.
60. Abu Bakar, M. R.; Nagy, Z. K.; Saleemi, A. N.; Rielly, C. D., The Impact of Direct Nucleation Control on Crystal Size Distribution in Pharmaceutical Crystallization Processes. *Cryst Growth Des* **2009**, *9* (3), 1378-1384.
61. Randolph, A. D.; Larson, M. A., Chapter 6 - CRYSTALLIZATION KINETICS. In *Theory of Particulate Processes*, Academic Press: 1971; pp 101-110.
62. Garside, J.; Jančić, S. J., Prediction and measurement of crystal size distributions for size-dependent growth. *Chem Eng Sci* **1978**, *33* (12), 1623-1630.
63. Burton, W. K.; Cabrera, N.; Frank, F. C., The Growth of Crystals and the Equilibrium Structure of their Surfaces. *Philosophical Transactions of the Royal Society of London. Series A, Mathematical and Physical Sciences* **1951**, *243* (866), 299-358.
64. Cubillas, P.; Anderson, M. W., Synthesis Mechanism: Crystal Growth and Nucleation. In *Zeolites and Catalysis*, Wiley-VCH Verlag GmbH & Co. KGaA: 2010; pp 1-55.

65. Fujiwara, M.; Chow, P. S.; Ma, D. L.; Braatz, R. D., Paracetamol Crystallization Using Laser Backscattering and ATR-FTIR Spectroscopy: Metastability, Agglomeration, and Control. *Cryst Growth Des* **2002**, *2* (5), 363-370.
66. Heng, J. Y. Y.; Thielmann, F.; Williams, D. R., The Effects of Milling on the Surface Properties of Form I Paracetamol Crystals. *Pharmaceutical Research* **2006**, *23* (8), 1918-1927.
67. Chikhaliya, V.; Forbes, R. T.; Storey, R. A.; Ticehurst, M., The effect of crystal morphology and mill type on milling induced crystal disorder. *European Journal of Pharmaceutical Sciences* **2006**, *27* (1), 19-26.
68. Descamps, M.; Willart, J. F.; Dudognon, E.; Caron, V., Transformation of Pharmaceutical Compounds upon Milling and Comilling: The Role of Tg. *Journal of Pharmaceutical Sciences* **2007**, *96* (5), 1398-1407.
69. Jones, A. G., Particle breakage, abnormal growth and agglomeration during industrial crystallization. *Analytical Proceedings* **1993**, *30* (11), 456-457.
70. Beckmann, W.; Beckmann, W., *Crystallization : basic concepts and industrial applications*. Wiley-VCH: Weinheim, Germany, 2013; p xiv, 346 pages.
71. Jones, A. G., 6 - Crystal agglomeration and disruption. In *Crystallization Process Systems*, Butterworth-Heinemann: Oxford, 2002; pp 155-189.
72. Cameron, B., Understanding agglomeration in crystallisation. **2015**.
73. Ålander, E. M.; Uusi-Penttilä, M. S.; Rasmuson, Å. C., Agglomeration of Paracetamol during Crystallization in Pure and Mixed Solvents. *Ind Eng Chem Res* **2004**, *43* (2), 629-637.
74. Brunsteiner, M.; Jones, A. G.; Pratola, F.; Price, S. L.; Simons, S. J. R., Toward a Molecular Understanding of Crystal Agglomeration. *Cryst Growth Des* **2005**, *5* (1), 3-16.
75. Nichols, G.; Byard, S.; Bloxham, M. J.; Botterill, J.; Dawson, N. J.; Dennis, A.; Diart, V.; North, N. C.; Sherwood, J. D., A Review of the Terms Agglomerate and Aggregate with a Recommendation for Nomenclature Used in Powder and Particle Characterization. *Journal of Pharmaceutical Sciences* *91* (10), 2103-2109.
76. Hounslow, M. J.; Mumtaz, H. S.; Collier, A. P.; Barrick, J. P.; Bramley, A. S., A micro-mechanical model for the rate of aggregation during precipitation from solution. *Chem Eng Sci* **2001**, *56* (7), 2543-2552.
77. Smoluchowski, M., Mathematical theory of the kinetics of the coagulation of colloidal solutions. *Z. Phys. Chem* **1917**, *92* (129).
78. Liew, T. L.; Barrick, J. P.; Hounslow, M. J., A Micro-Mechanical Model for the Rate of Aggregation during Precipitation from Solution. *Chem Eng Technol* **2003**, *26* (3), 282-285.
79. Mumtaz, H. S.; Hounslow, M. J.; Seaton, N. A.; Paterson, W. R., Orthokinetic Aggregation During Precipitation: A Computational Model for Calcium Oxalate Monohydrate. *Chemical Engineering Research and Design* **1997**, *75* (2), 152-159.
80. Ochsenbein, D. R.; Vetter, T.; Morari, M.; Mazzotti, M., Agglomeration of Needle-like Crystals in Suspension. II. Modeling. *Cryst Growth Des* **2015**, *15* (9), 4296-4310.
81. Hartel, R. W.; Randolph, A. D., Mechanisms and kinetic modeling of calcium oxalate crystal aggregation in a urinelike liquor. Part II: Kinetic modeling. *Aiche J* **1986**, *32* (7), 1186-1195.

82. Zauner, R.; Jones, A. G., Determination of nucleation, growth, agglomeration and disruption kinetics from experimental precipitation data: the calcium oxalate system. *Chem Eng Sci* **2000**, *55* (19), 4219-4232.
83. KAWASHIMA, Y.; OKUMURA, M.; TAKENAKA, H., Spherical Crystallization: Direct Spherical Agglomeration of Salicylic Acid Crystals During Crystallization. *Science* **1982**, *216* (4550), 1127-1128.
84. Martino, P. D.; Barthélémy, C.; Piva, F.; Joiris, E.; Palmieri, G. F.; Martelli, S., Improved Dissolution Behavior of Fenbufen by Spherical Crystallization. *Drug Development and Industrial Pharmacy* **1999**, *25* (10), 1073-1081.
85. Smith, H. M.; Puddington, I. E., Spherical Agglomeration of Barium Sulphate. *Can J Chem* **1960**, *38* (10), 1911-1916.
86. Farnand, J. R.; Smith, H. M.; Puddington, I. E., Spherical agglomeration of solids in liquid suspension. *The Canadian Journal of Chemical Engineering* **1961**, *39* (2), 94-97.
87. Peña, R.; Nagy, Z. K., Process Intensification through Continuous Spherical Crystallization Using a Two-Stage Mixed Suspension Mixed Product Removal (MSMPR) System. *Cryst Growth Des* **2015**, *15* (9), 4225-4236.
88. Kawashima, Y.; Imai, M.; Takeuchi, H.; Yamamoto, H.; Kamiya, K.; Hino, T., Improved flowability and compactibility of spherically agglomerated crystals of ascorbic acid for direct tableting designed by spherical crystallization process. *Powder Technol* **2003**, *130* (1-3), 283-289.
89. Kawashima, Y.; Capes, C. E., An experimental study of the kinetics of spherical agglomeration in a stirred vessel. *Powder Technol* **1974**, *10* (1), 85-92.
90. Kawashima, Y.; Capes, C. E., Further studies of the kinetics of spherical agglomeration in a stirred vessel. *Powder Technol* **1976**, *13* (2), 279-288.
91. Kawashima, Y.; Capes, C. E., Some Experiments on the Effect of Contact Angle in Agglomeration from Liquids. *Industrial & Engineering Chemistry Fundamentals* **1980**, *19* (3), 312-314.
92. Chow, A. H. L.; Leung, M. W. M., A study of the Mechanisms of Wet Spherical Agglomeration of Pharmaceutical Powders. *Drug Development and Industrial Pharmacy* **1996**, *22* (4), 357-371.
93. Kawashima, Y.; Cui, F.; Takeuchi, H.; Niwa, T.; Hino, T.; Kiuchi, K., Improvements in flowability and compressibility of pharmaceutical crystals for direct tableting by spherical crystallization with a two-solvent system. *Powder Technol* **1994**, *78* (2), 151-157.
94. Espitalier, F.; Biscans, B.; Authelin, J. R.; Laguerie, C., Modelling of the Mechanism of Formation of Spherical Grains Obtained by the Quasi-Emulsion Crystallization Process. *Chemical Engineering Research and Design* **1997**, *75* (2), 257-267.
95. Espitalier, F.; Biscans, B.; Authelin, J. R.; Laguerie, C., Modelling of the Mechanism of Formation of Spherical Grains Obtained by the Quasi-Emulsion Crystallization Process. *Chemical Engineering Research and Design* **75** (2), 257-267.
96. Kawashima, Y.; Imai, A.; Takeuchi, H.; Yamamoto, H.; Kamiya, K.; Hino, T., Improved flowability and compactibility of spherically agglomerated crystals of ascorbic acid for direct tableting designed by spherical crystallization process. *Powder Technol* **2003**, *130* (1-3), 283-289.

97. Kawashima, Y.; Okumura, M.; Takenaka, H., The effects of temperature on the spherical crystallization of salicylic acid. *Powder Technol* **1984**, *39* (1), 41-47.
98. Kawashima, Y.; Aoki, S.; Takenaka, H., SPHERICAL AGGLOMERATION OF AMINOPHYLLINE CRYSTALS DURING REACTION IN LIQUID BY THE SPHERICAL CRYSTALLIZATION TECHNIQUE. *CHEMICAL & PHARMACEUTICAL BULLETIN* **1982**, *30* (5), 1900-1902.
99. Kawashima, Y.; Naito, M.; Lin, S. Y.; Takenaka, H., An experimental study of the kinetics of the spherical crystallization of aylline sodium theophylline monohydrate. *Powder Technol* **1983**, *34* (2), 255-260.
100. Ueda, M.; Nakamura, Y.; Makita, H.; Imasato, Y.; Kawashima, Y., Particle Design of Enoxacin by Spherical Crystallization Technique. I. : Principle of Ammonia Diffusion System (ADS). *CHEMICAL & PHARMACEUTICAL BULLETIN* **1990**, *38* (9), 2537-2541.
101. Puechagut, H. G.; Bianchotti, J.; Chiale, C. A., Preparation of norfloxacin spherical agglomerates using the ammonia diffusion system. *Journal of Pharmaceutical Sciences* **1998**, *87* (4), 519-523.
102. GOHEL; #160; C., M.; PARIKH; #160; K., R.; SHAH; #160; H.; DUBEY; #160; R., R., *Improvement in flowability and compressibility of ampicillin trihydrate by spherical crystallization*. MedKnow Publications and Media: Mumbai, INDE, 2003; Vol. 65, p 4.
103. Sano, A.; Kuriki, T.; Kawashima, Y.; Takeuchi, H.; Hino, T.; Niwa, T., Particle Design of Tolbutamide by the Spherical Crystallization Technique. V. Improvement of Dissolution and Bioavailability of Direct Compressed Tablets Prepared Using Tolbutamide Agglomerated Crystals. *CHEMICAL & PHARMACEUTICAL BULLETIN* **1992**, *40* (11), 3030-3035.
104. Blandin, A.-F.; Rivoire, A.; Mangin, D.; Klein, J.-P.; Bossoutrot, J.-M., Using In Situ Image Analysis to Study the Kinetics of Agglomeration in Suspension. *Part Part Syst Char* **2000**, *17* (1), 16-20.
105. Thati, J.; Rasmuson, Å. C., Particle engineering of benzoic acid by spherical agglomeration. *European Journal of Pharmaceutical Sciences* **2012**, *45* (5), 657-667.
106. Kawashima, Y.; Cui, F.; Takeuchi, H.; Niwa, T.; Hino, T.; Kiuchi, K., Parameters determining the agglomeration behaviour and the micromeritic properties of spherically agglomerated crystals prepared by the spherical crystallization technique with miscible solvent systems. *International Journal of Pharmaceutics* **1995**, *119* (2), 139-147.
107. Kachrimanis, K.; Nikolakakis, I.; Malamataris, S., Spherical Crystal Agglomeration of Ibuprofen by the Solvent Change Technique in Presence of Methacrylic Polymers. *Journal of Pharmaceutical Sciences* *89* (2), 250-259.
108. Szabó-Révész, P.; Hasznos-Nezdei, M.; Farkas, B.; Göcző, H.; Pintye-Hódi, K.; Erős, I., Crystal growth of drug materials by spherical crystallization. *Journal of Crystal Growth* **2002**, 237-239, Part 3, 2240-2245.
109. Kawashima, Y.; Furukawa, K.; Takenaka, H., The physicochemical parameters determining the size of agglomerate prepared by the wet spherical agglomeration technique. *Powder Technol* **1981**, *30* (2), 211-216.
110. Blandin, A. F.; Mangin, D.; Rivoire, A.; Klein, J. P.; Bossoutrot, J. M., Agglomeration in suspension of salicylic acid fine particles: influence of some process parameters on kinetics and agglomerate final size. *Powder Technol* **2003**, *130* (1-3), 316-323.

111. Thati, J.; Rasmuson, Å. C., On the mechanisms of formation of spherical agglomerates. *European Journal of Pharmaceutical Sciences* **2011**, *42* (4), 365-379.
112. Kawashima, Y.; Kurachi, Y.; Takenaka, H., Preparation of spherical wax matrices of sulfamethoxazole by wet spherical agglomeration technique using a CMSMPR agglomerator. *Powder Technol* **1982**, *32* (2), 155-161.
113. Tahara, K.; O'Mahony, M.; Myerson, A. S., Continuous Spherical Crystallization of Albuterol Sulfate with Solvent Recycle System. *Cryst Growth Des* **2015**, *15* (10), 5149-5156.
114. McCurdy, V., Quality by Design. In *Process Understanding*, Wiley-VCH Verlag GmbH & Co. KGaA: 2011; pp 1-16.
115. Cronin, L.; Kitson, P. J.; Wilson, C. C., Process Understanding – Crystallization. In *Process Understanding*, Wiley-VCH Verlag GmbH & Co. KGaA: 2011; pp 199-227.
116. Briggs, N. E. B. Polymorph Control of Pharmaceuticals within a Continuous Oscillatory Baffled Crystalliser. University of Strathclyde, 2015.
117. Garekani, H. A.; Sadeghi, F.; Badiee, A.; Mostafa, S. A.; Rajabi-Siahboomi, A. R.; Rajabi-Siahboomi, A. R., Crystal Habit Modifications of Ibuprofen and Their Physicomechanical Characteristics. *Drug Development and Industrial Pharmacy* **2001**, *27* (8), 803-809.
118. Li, T.; Wen, H.; Park, K.; Morris, K. R., How Specific Interactions between Acetaminophen and Its Additive 4-Methylacetanilide Affect Growth Morphology: Elucidation Using Etching Patterns. *Cryst Growth Des* **2002**, *2* (3), 185-189.
119. Vetter, T.; Mazzotti, M.; Brozio, J., Slowing the Growth Rate of Ibuprofen Crystals Using the Polymeric Additive Pluronic F127. *Cryst Growth Des* **2011**, *11* (9), 3813-3821.
120. Sowa, M.; Klapwijk, A. R.; Ostendorf, M.; Beckmann, W., Particle Engineering of an Active Pharmaceutical Ingredient for Improved Micromeritic Properties. *Chem Eng Technol* **2017**, *40* (7), 1282-1292.
121. Smith, F., *Industrial Applications of X-Ray Diffraction*. Taylor & Francis: 1999.
122. Antonio, S. G.; Paiva-Santos, C. O.; Bezzon, V. D. N., Limits of Visual Detection for Finasteride Polymorphs in Prepared Binary Mixtures: Analysis by X-ray Powder Diffraction. *Journal of Pharmaceutical Sciences* **2014**, *103* (11), 3567-3575.
123. Watson, D. G., *Pharmaceutical analysis*. Churchill Livingstone Elsevier: 2012.
124. Chianese, A. K., H. J. M, *Industrial crystallization process monitoring and control*. Wiley-VCH: 2012.
125. Bakeev, K. A., *Process analytical technology*. John Wiley and Sons Ltd 2010.
126. Carr, R. L., Evaluating flow properties of solids. **1965**.
127. Hausner, H. *Friction conditions in a mass of metal powder*; Polytechnic Inst. of Brooklyn. Univ. of California, Los Angeles: 1967.
128. Li, X.; Yin, Q.; Zhang, M.; Hou, B.; Bao, Y.; Gong, J.; Hao, H.; Wang, Y.; Wang, J.; Wang, Z., Process Design for Antisolvent Crystallization of Erythromycin Ethylsuccinate in Oiling-out System. *Industrial & Engineering Chemistry Research* **2016**, *55* (27), 7484-7492.

129. Duffy, D.; Cremin, N.; Napier, M.; Robinson, S.; Barrett, M.; Hao, H. X.; Glennon, B., In situ monitoring, control and optimization of a liquid-liquid phase separation crystallization. *Chem Eng Sci* **2012**, *77*, 112-121.
130. Liu, Y. X.; Wang, X. J.; Ching, C. B., Toward Further Understanding of Lysozyme Crystallization: Phase Diagram, Protein-Protein Interaction, Nucleation Kinetics, and Growth Kinetics. *Cryst Growth Des* **2010**, *10* (2), 548-558.
131. Muschol, M.; Rosenberger, F., Liquid-liquid phase separation in supersaturated lysozyme solutions and associated precipitate formation/crystallization. *J Chem Phys* **1997**, *107* (6), 1953-1962.
132. Asherie, N.; Lomakin, A.; Benedek, G. B., Phase diagram of colloidal solutions. *Physical Review Letters* **1996**, *77* (23), 4832-4835.
133. Rosenbaum, D. F.; Zukoski, C. F., Protein interactions and crystallization. *Journal of Crystal Growth* **1996**, *169* (4), 752-758.
134. Berland, C. R.; Thurston, G. M.; Kondo, M.; Broide, M. L.; Pande, J.; Ogun, O.; Benedek, G. B., Solid Liquid-Phase Boundaries of Lens Protein Solutions. *P Natl Acad Sci USA* **1992**, *89* (4), 1214-1218.
135. Thomson, J. A.; Schurtenberger, P.; Thurston, G. M.; Benedek, G. B., Binary-Liquid Phase-Separation and Critical Phenomena in a Protein Water Solution. *P Natl Acad Sci USA* **1987**, *84* (20), 7079-7083.
136. Haas, C.; Drenth, J., Understanding protein crystallization on the basis of the phase diagram. *Journal of Crystal Growth* **1999**, *196* (2-4), 388-394.
137. Vivares, D.; Bonnete, F., Liquid-liquid phase separations in urate oxidase/PEG mixtures: Characterization and implications for protein crystallization. *Journal of Physical Chemistry B* **2004**, *108* (20), 6498-6507.
138. Niu, Y. H.; Yang, L.; Wang, H.; Wang, Z. G., Criteria of Process Optimization in Binary Polymer Blends with Both Phase Separation and Crystallization. *Macromolecules* **2009**, *42* (20), 7623-7626.
139. Akaba, M.; Nojima, S., Effects of phase separation on the crystallization behavior in a binary blend of poly(epsilon-caprolactone) homopolymer and poly(epsilon-caprolactone)-block-polybutadiene copolymer. *Polym J* **2005**, *37* (8), 584-591.
140. Veessler, S.; Lafferrere, L.; Garcia, E.; Hoff, C., Phase transitions in supersaturated drug solution. *Organic Process Research & Development* **2003**, *7* (6), 983-989.
141. Lafferrere, L.; Hoff, C.; Veessler, S., Polymorphism and Liquid-Liquid Demixing in Supersaturated Drug Solution. *Eng Life Sci* **2003**, *3* (3), 127-131.
142. Lafferrere, L.; Hoff, C.; Veessler, S., Study of liquid-liquid demixing from drug solution. *Journal of Crystal Growth* **2004**, *269* (2-4), 550-557.
143. Svard, M.; Gracin, S.; Rasmuson, A. C., Oiling out or molten hydrate-liquid-liquid phase separation in the system vanillin-water. *Journal of Pharmaceutical Sciences* **2007**, *96* (9), 2390-2398.
144. Bonnett, P. E.; Carpenter, K. J.; Dawson, S.; Davey, R. J., Solution crystallisation via a submerged liquid-liquid phase boundary: oiling out. *Chem Commun* **2003**, (6), 698-699.
145. Veessler, S.; Revalor, E.; Bottini, O.; Hoff, C., Crystallization in the presence of a liquid-liquid phase separation. *Organic Process Research & Development* **2006**, *10* (4), 841-845.

146. Rashid, A.; White, E. T.; Howes, T.; Litster, J. D.; Marziano, I., Effect of Solvent Composition and Temperature on the Solubility of Ibuprofen in Aqueous Ethanol. *J Chem Eng Data* **2014**, *59* (9), 2699-2703.
147. Manrique, J.; Martínez, F., Solubility of ibuprofen in some ethanol + water cosolvent mixtures at several temperatures. *Lat Am J Pharm* **2007**, *26*, 344-354.
148. Jbilou, M.; Ettabia, A.; Guyot-Hermann, A. M.; Guyot, J. C., Ibuprofen Agglomerates Preparation by Phase Separation. *Drug Development and Industrial Pharmacy* **1999**, *25* (3), 297-305.
149. Dudognon, E.; Danède, F.; Descamps, M.; Correia, N. T., Evidence for a New Crystalline Phase of Racemic Ibuprofen. *Pharmaceutical Research* **2008**, *25* (12), 2853-2858.
150. Rasenack, N.; W Müller, B., *Ibuprofen crystal with optimized properties*. 2002; Vol. 245, p 9-24.
151. Kachrimanis, K.; Ktistis, G.; Malamataris, S., Crystallisation conditions and physicochemical properties of ibuprofen–Eudragit® S100 spherical crystal agglomerates prepared by the solvent-change technique. *International Journal of Pharmaceutics* **1998**, *173* (1), 61-74.
152. Maghsoodi, M.; Barghi, L., Design of Agglomerated Crystals of Ibuprofen During Crystallization: Influence of Surfactant. *Iranian Journal of Basic Medical Sciences* **2011**, *14* (1), 57-66.
153. Umprayn, K.; Luengtummueng, A.; Kitiyadisai, C.; Pornpiputsakul, T., Modification of Crystal Habit of Ibuprofen Using the Phase Partition Technique: Effect of Aerosil and Tween 80 in Binding Solvent. *Drug Development and Industrial Pharmacy* **2001**, *27* (10), 1047-1056.
154. Kawashima, Y.; Niwa, T.; Handa, T.; Takeuchi, H.; Iwamoto, T.; Itoh, K., Preparation of Controlled-Release Microspheres of Ibuprofen With Acrylic Polymers by a Novel Quasi-Emulsion Solvent Diffusion Method. *Journal of Pharmaceutical Sciences* **78** (1), 68-72.
155. Rasenack, N.; W Müller, B., *Properties of Ibuprofen Crystallized Under Various Conditions: A Comparative Study*. 2002; Vol. 28, p 1077-89.
156. Rasenack, N.; Müller, B. W., Ibuprofen crystals with optimized properties. *International Journal of Pharmaceutics* **2002**, *245* (1), 9-24.
157. Mura, P.; Bettinetti, G. P.; Manderioli, A.; Faucci, M. T.; Bramanti, G.; Sorrenti, M., *Interactions of ketoprofen and ibuprofen with β -cyclodextrins in solution and in the solid state*. 1998; Vol. 166, p 189–203.
158. Yang, H.; Rasmuson, Å. C., Investigation of Batch Cooling Crystallization in a Liquid–Liquid Separating System by PAT. *Organic Process Research & Development* **2012**, *16* (6), 1212-1224.
159. Yang, H. Y.; Rasmuson, A. C., Investigation of Batch Cooling Crystallization in a Liquid-Liquid Separating System by PAT. *Organic Process Research & Development* **2012**, *16* (6), 1212-1224.
160. Cano, H.; Gabas, N.; Canselier, J. P., Experimental study on the ibuprofen crystal growth morphology in solution. *Journal of Crystal Growth* **2001**, *224* (3), 335-341.
161. Manrique, J.; Martinez, F., Solubility of ibuprofen in some ethanol plus water cosolvent mixtures at several temperatures. *Lat Am J Pharm* **2007**, *26* (3), 344-354.
162. Yang, H. Y.; Rasmuson, A. C., Ternary phase diagrams of ethyl paraben and propyl paraben in ethanol aqueous solvents. *Fluid Phase Equilib* **2014**, *376*, 69-75.

163. Kiesow, K.; Tumakaka, F.; Sadowski, G., Experimental investigation and prediction of oiling out during crystallization process. *Journal of Crystal Growth* **2008**, *310* (18), 4163-4168.
164. Gracin, S.; Rasmuson, Å., *Solubility of Phenylacetic Acid, p-Hydroxyphenylacetic Acid, p-Aminophenylacetic Acid, p-Hydroxybenzoic Acid, and Ibuprofen in Pure Solvents*. 2002; Vol. 47.
165. Duffy, D.; Cremin, N.; Napier, M.; Robinson, S.; Barrett, M.; Hao, H.; Glennon, B., In situ monitoring, control and optimization of a liquid-liquid phase separation crystallization. *Chem Eng Sci* **2012**, *77*, 112-121.
166. Deneau, E.; Steele, G., An In-Line Study of Oiling Out and Crystallization. *Organic Process Research & Development* **2005**, *9* (6), 943-950.
167. de Albuquerque, I.; Mazzotti, M., Crystallization Process Design Using Thermodynamics To Avoid Oiling Out in a Mixture of Vanillin and Water. *Cryst Growth Des* **2014**, *14* (11), 5617-5625.
168. Shekunov, B. Y.; York, P., Crystallization processes in pharmaceutical technology and drug delivery design. *Journal of Crystal Growth* **2000**, *211* (1-4), 122-136.
169. Luner, P. E.; Zhang, Y.; Abramov, Y. A.; Carvajal, M. T., Evaluation of Milling Method on the Surface Energetics of Molecular Crystals Using Inverse Gas Chromatography. *Cryst Growth Des* **2012**, *12* (11), 5271-5282.
170. Ochsenein, D.; Vetter, T.; Schorsch, S.; Morari, M.; Mazzotti, M., *Agglomeration of Needle-like Crystals in Suspension: I. Measurements*. 2015; Vol. 15, p 1923-1933.
171. Ålander, E. M.; Uusi-Penttilä, M. S.; Rasmuson, Å. C., Characterization of paracetamol agglomerates by image analysis and strength measurement. *Powder Technol* **2003**, *130* (1), 298-306.
172. Ålander, E. M.; Uusi-Penttilä, M. S.; Rasmuson, A. C., Characterization of paracetamol agglomerates by image analysis and strength measurement. *Powder Technol* **2003**, *130* (1-3), 298-306.
173. Faria, N.; Pons, M. N.; de Azevedo, S. F.; Rocha, F. A.; Vivier, H., Quantification of the morphology of sucrose crystals by image analysis. *Powder Technol* **2003**, *133* (1-3), 54-67.
174. Ros, F.; Guillaume, S.; Rabatel, G.; Sevilla, F., Recognition of Overlapping Particles in Granular Product Images Using Statistics and Neural Networks. *Food Control* **1995**, *6* (1), 37-43.
175. Borchert, C.; Sundmacher, K., Crystal Aggregation in a Flow Tube: Image-Based Observation. *Chem Eng Technol* **2011**, *34* (4), 545-556.
176. Hamilton, P.; Littlejohn, D.; Nordon, A.; Sefcik, J.; Slavin, P.; Andrews, J.; Dallin, P., Investigation of factors affecting isolation of needle-shaped particles in a vacuum-agitated filter drier through non-invasive measurements by Raman spectrometry. *Chem Eng Sci* **2013**, *101*, 878-885.
177. MacLeod, C. S.; Muller, F. L., On the Fracture of Pharmaceutical Needle-Shaped Crystals during Pressure Filtration: Case Studies and Mechanistic Understanding. *Organic Process Research & Development* **2012**, *16* (3), 425-434.
178. Hamilton, P.; Littlejohn, D.; Nordon, A.; Sefcik, J.; Slavin, P.; Dallin, P.; Andrews, J., Studies of particle drying using non-invasive Raman spectrometry and particle size analysis. *Analyst* **2011**, *136* (10), 2168-2174.

179. Ochsenbein, D. R.; Vetter, T.; Schorsch, S.; Morari, M.; Mazzotti, M., Agglomeration of Needle-like Crystals in Suspension: I. Measurements. *Cryst Growth Des* **2015**, *15* (4), 1923-1933.
180. David, R.; Marchal, P.; Klein, J. P.; Villermaux, J., Crystallization and Precipitation Engineering .3. A Discrete Formulation of the Agglomeration Rate of Crystals in a Crystallization Process. *Chem Eng Sci* **1991**, *46* (1), 205-213.
181. Alander, E. M.; Uusi-Penttila, M. S.; Rasmuson, A. C., Agglomeration of paracetamol during crystallization in pure and mixed solvents. *Ind Eng Chem Res* **2004**, *43* (2), 629-637.
182. Alander, E. M.; Rasmuson, A. C., Mechanisms of crystal agglomeration of paracetamol in acetone-water mixtures. *Ind Eng Chem Res* **2005**, *44* (15), 5788-5794.
183. Alander, E. M.; Rasmuson, A. C., Agglomeration and adhesion free energy of paracetamol crystals in organic solvents. *Aiche J* **2007**, *53* (10), 2590-2605.
184. Hollander, E. D.; Derksen, J. J.; Bruinsma, O. S. L.; van den Akker, H. E. A.; van Rosmalen, G. M., A numerical study on the coupling of hydrodynamics and orthokinetic agglomeration. *Chem Eng Sci* **2001**, *56* (7), 2531-2541.
185. Lindenberg, C.; Schöll, J.; Vicum, L.; Mazzotti, M.; Brozio, J., l-Glutamic Acid Precipitation: Agglomeration Effects. *Cryst Growth Des* **2008**, *8* (1), 224-237.
186. Bakar, M. R. A.; Nagy, Z. K.; Rielly, C. D., Seeded Batch Cooling Crystallization with Temperature Cycling for the Control of Size Uniformity and Polymorphic Purity of Sulfathiazole Crystals. *Organic Process Research & Development* **2009**, *13* (6), 1343-1356.
187. Abu Bakar, M. R.; Nagy, Z. K.; Rielly, C. D., Investigation of the Effect of Temperature Cycling on Surface Features of Sulfathiazole Crystals during Seeded Batch Cooling Crystallization. *Cryst Growth Des* **2010**, *10* (9), 3892-3900.
188. Simone, E.; Klapwijk, A. R.; Wilson, C. C.; Nagy, Z. K., Investigation of the Evolution of Crystal Size and Shape during Temperature Cycling and in the Presence of a Polymeric Additive Using Combined Process Analytical Technologies. *Cryst Growth Des* **2017**, *17* (4), 1695-1706.
189. Lekhal, A.; Girard, K. P.; Brown, M. A.; Kiang, S.; Khinast, J. G.; Glasser, B. J., The effect of agitated drying on the morphology of l-threonine (needle-like) crystals. *International Journal of Pharmaceutics* **2004**, *270* (1-2), 263-277.
190. Borsos, Á.; Szilágyi, B.; Agachi, P. Ş.; Nagy, Z. K., Real-Time Image Processing Based Online Feedback Control System for Cooling Batch Crystallization. *Organic Process Research & Development* **2017**, *21* (4), 511-519.
191. Petela, R., Prediction of the product size in the agglomeration of coal particles in a water-oil emulsion. *Fuel* **1991**, *70* (4), 509-517.
192. van Netten, K.; Moreno-Atanasio, R.; Galvin, K. P., A Kinetic Study of a Modified Fine Coal Agglomeration Process. *Procedia Engineering* **2015**, *102*, 508-516.
193. Sirianni, A. F.; Capes, C. E.; Puddington, J. E., Recent experience with the spherical agglomeration process. *The Canadian Journal of Chemical Engineering* **1969**, *47* (2), 166-170.
194. Thati, J.; Rasmuson, Å., *On the mechanisms of formation of spherical agglomerates*. 2011; Vol. 42, p 365-79.
195. Lin, P. Y.; Lee, H. L.; Chen, C. W.; Lee, T., Effects of baffle configuration and tank size on spherical agglomerates of dimethyl fumarate in a common stirred tank. *International Journal of Pharmaceutics* **2015**, *495* (2), 886-894.

196. Kawashima, Y.; Imai, M.; Takeuchi, H.; Yamamoto, H.; Kamiya, K., Development of Agglomerated Crystals of Ascorbic Acid by the Spherical Crystallization Technique for Direct Tableting, and Evaluation of Their Compactibilities [Translated][†]. *KONA Powder and Particle Journal* **2002**, *20*, 251-262.
197. Petela, R., Application of Flow Consecutor for coal upgrading. *Fuel Processing Technology* **1999**, *60* (1), 29-48.
198. Jitkar, S.; Thipparaboina, R.; Chavan, R. B.; Shastri, N. R., Spherical Agglomeration of Platy Crystals: Curious Case of Etodolac. *Cryst Growth Des* **2016**, *16* (7), 4034-4042.
199. Nokhodchi, A.; Maghsoodi, M., Preparation of Spherical Crystal Agglomerates of Naproxen Containing Disintegrant for Direct Tablet Making by Spherical Crystallization Technique. *AAPS PharmSciTech* **2008**, *9* (1), 54-59.
200. Lovette, M. A.; Doherty, M. F., Needle-Shaped Crystals: Causality and Solvent Selection Guidance Based on Periodic Bond Chains. *Cryst Growth Des* **2013**, *13* (8), 3341-3352.
201. Midler, M.; Paul, E. L.; Whittington, E. F.; Futran, M.; Liu, P. D.; Hsu, J.; Pan, S. H., Crystallization method to improve crystal structure and size. Google Patents: 1994.
202. Yadava, S. K.; Naik, J. B.; Patil, J. S.; Mokale, V. J.; Singh, R., Enhanced solubility and bioavailability of lovastatin using stabilized form of self-emulsifying drug delivery system. *Colloids and Surfaces A: Physicochemical and Engineering Aspects* **2015**, *481* (Supplement C), 63-71.
203. Khanfar, M.; Al-Nimry, S., Stabilization and Amorphization of Lovastatin Using Different Types of Silica. *AAPS PharmSciTech* **2017**, *18* (6), 2358-2367.
204. Peña, R.; Burcham, C.; Jarmer, D.; Ramkrishna, D.; K. Nagy, Z., *Modeling and optimization of spherical agglomeration in suspension through a coupled population balance model*. 2017; Vol. 167.
205. Murov, S. <http://murov.info/webercises.htm>.
206. Contact Angle and Surface Tension Determination and Preparation of Solid Surfaces. In *Interfacial Forces in Aqueous Media, Second Edition*, CRC Press: 2006; pp 131-155.
207. Thati, J. Particle engineering by spherical crystallization: Mechanisms and Influence of Process Conditions. KTH Royal Institute of Technology, 2011.
208. McKeown R., W. D. G. Spherical Agglomeration of API. *AICHE Conference* 2013. <http://www3.aiche.org/proceedings/content/Annual-2013/extended-abstracts/P302512.pdf>.
209. Nazer, R., Spherical agglomeration in suspension. Unpublished work. 2016.
210. Katta, J.; Rasmuson, Å. C., Spherical crystallization of benzoic acid. *International Journal of Pharmaceutics* **2008**, *348* (1-2), 61-69.
211. Amaro-González, D.; Biscans, B., Spherical agglomeration during crystallization of an active pharmaceutical ingredient. *Powder Technol* **2002**, *128* (2), 188-194.
212. Chemical Computing Group, I., Molecular Operating Environment (MOE), 2011.10. **2011**.
213. Wu, Z.; Li, D.; Meng, J.; Wang, H., Introduction to SIMCA-P and Its Application. In *Handbook of Partial Least Squares: Concepts, Methods and*

- Applications*, Esposito Vinzi, V.; Chin, W. W.; Henseler, J.; Wang, H., Eds. Springer Berlin Heidelberg: Berlin, Heidelberg, 2010; pp 757-774.
214. Johnston, A.; Bhardwaj-Miglani, R.; Gurung, R.; Vassileiou, A. D.; Florence, A. J.; Johnston, B. F., Combined Chemoinformatics Approach to Solvent Library Design Using clusterSim and Multidimensional Scaling. *Journal of Chemical Information and Modeling* **2017**, *57* (8), 1807-1815.
215. Teychené, S.; Sicre, N.; Biscans, B., Is spherical crystallization without additives possible? *Chemical Engineering Research and Design* **88** (12), 1631-1638.
216. https://www.dow.com/assets/attachments/business/pcm/solvents/methyl_isobutyl_ketone/tds/methyl_isobutyl_ketone.pdf
https://www.dow.com/assets/attachments/business/pcm/solvents/methyl_isobutyl_ketone/tds/methyl_isobutyl_ketone.pdf.
217. Maghsoodi, M., How spherical crystallization improves direct tableting properties: a review. *Advanced Pharmaceutical Bulletin* **2012**, *2* (2), 253-257.
218. Ph. Eur. 9.0, 231.
219. Morishima, K.; Kawashima, Y.; Kawashima, Y.; Takeuchi, H.; Niwa, T.; Hino, T., Micromeritic characteristics and agglomeration mechanisms in the spherical crystallization of buccillamine by the spherical agglomeration and the emulsion solvent diffusion methods. *Powder Technol* **1993**, *76* (1), 57-64.
220. Blandin, A. F.; Mangin, D.; Subero-Couroyer, C.; Rivoire, A.; Klein, J. P.; Bossoutrot, J. M., Modelling of agglomeration in suspension: Application to salicylic acid microparticles. *Powder Technol* **2005**, *156* (1), 19-33.
221. Thakur, A.; Thipparaboina, R.; Kumar, D.; Sai Gouthami, K.; Shastri, N. R., Crystal engineered albendazole with improved dissolution and material attributes. *CrystEngComm* **2016**, *18* (9), 1489-1494.
222. Rawlings, J. B., Tutorial overview of model predictive control. *IEEE Control Systems* **2000**, *20* (3), 38-52.
223. Peña, R.; Burcham, C. L.; Jarmer, D. J.; Ramkrishna, D.; Nagy, Z. K., Modeling and optimization of spherical agglomeration in suspension through a coupled population balance model. *Chem Eng Sci* **2017**, *167* (Supplement C), 66-77.

Appendices

Appendix 1 Supporting information related to chapter 5

Appendix 1 Table 1 Descriptors extracted from Reference Alander *et al.*¹⁷², Bortchert *et al.*¹⁷⁵ and Ochsenbein *et al.*¹⁷⁹

Number	Name, units	Formula	Description
1	Projected area, μm^2	A	Number of pixels in the particle.
2	Filled projected area, μm^2	A_f	Number of pixels in the particle with all internal holes filled.
3	Perimeter, μm	P	The distance around the continuous boundary of the particle.
4	Convex area, μm^2	A_{CH}	Number of pixels in the convex hull.
5	Convex perimeter, μm	P_{CH}	The distance around the boundary of the convex hull.
6	Major axis length, μm	L_{maj}	Length of the major axis of the ellipse that has the same normalized second central moments as the particle.
7	Minor axis length, μm	L_{min}	Length of the minor axis of the ellipse that has the same normalized second central moments as the particle.
8	Eccentricity	ε	Ratio of the distance between the foci of the ellipse and its major axis length.
9	Euler number	E_n	Number of objects in the particle minus the number of holes in the particle.
10	Equivalent diameter based on projected area, μm	$d_{proj} = \sqrt{\frac{4A}{\pi}}$	Diameter of circle with same projected area as the particle.

11	Equivalent diameter based on perimeter, μm	$d_{\text{per}} = \sqrt{\frac{P}{\pi}}$	Diameter of circle with same perimeter as the particle.
12	Solidity	$S_o = \frac{A}{A_{CH}}$	Ratio of area to convex area.
13	Convexity	$O = \frac{P_{CH}}{P}$	Ratio of convex perimeter to perimeter
14	Circularity	$C = \frac{4\pi A}{P^2}$	Ratio of area to area of circle with the same perimeter. Equivalent to shape factor.
15	Slenderness	$S_l = \frac{L_{\text{min}}}{L_{\text{maj}}}$	Ratio between minor and major axis lengths.
16	Shape factor	$F = \frac{d_{\text{proj}}^2}{d_{\text{per}}^2}$	Ratio between circle equivalent diameters based on projected area and perimeter.
17	Heterogeneity	H	Fraction of pixels that deviate more than 10% from the mean pixel value.
18	Mean pixel value	$\bar{p}\bar{x}$	Average value of the pixels constituting the particle.
19	Image number	n	Image in which the particle was identified.
20	Number of particles	N	Number of particles within the specified time step.

Appendix 2 Supporting information related to chapter 6

Appendix 2 Table 1 Descriptors extracted from References Johnston *et al.* ²¹⁴

Descriptors	Category	
2-D descriptors		
apol, bpol, Fcharge, mr, SMR, Weight, logP (o/w), SlogP, vdw_vol, density, vdw-area	Physical properties	Physical properties are calculated from the connection table of a molecule.
SlogP_VSA0-SlogP_VSA9, SMR_VSA0 - SMR_VSA7	Subdivided surface areas	The Subdivided Surface Areas are descriptors based on an approximate accessible van der Waals surface area calculation for each atom, vi along with some other atomic property, pi .
a_aro, a_count, a_heavy, a_ICM, a_IC, a_nH, a_nB, a_nC, a_nN, a_nO, a_nF, a_nP, a_nS, a_nCl, a_nBr, a_nI, b_1rotN, b_1rotR, b_ar, b_count, b_double, b_heavy, brotN, b_rotR, b_single, b_triple, VAdjMa, VAdjEq	Atom count and bond count	The atom count and bond count descriptors are functions of the counts of atoms and bonds.
chi0, chi0_C, chi1, chi1_C, chi0v, chi0v_C, chi1v, chi1v_C, Kier1 - Kier3, KierA1 - KierA3, KierFlex, zagreb	Kier&Hall Connectivity and Kappa Shape Indices	The Kier and Hall kappa molecular shape indices compare the molecular graph with minimal and maximal molecular graphs, and are intended to capture different aspects of molecular shape.
balabanJ, diameter, petitjean, radius, VDistEq, VDistMa, weinerPath, weinerPol	Adjacency and Distance Matrix Descriptors	The adjacency matrix, M, of a chemical structure is defined by the elements [Mij] where Mij is 1 if atoms i and j are bonded and zero otherwise. The distance matrix, D, of a chemical structure is defined by the elements [Dij] where Dij is the length of the shortest path from atoms i to j; zero is used if atoms i and j are not part of the same connected component.
a_acc, a_acid, a_base, a_don, a_hyd, vsa_acc, vsa_acid, vsa_base, vsa_don, vsa_hyd, vsa_other, vsa_pol	Pharmacophore Feature Descriptors	The Pharmacophore Atom Type descriptors consider only the heavy atoms of a molecule and assign a type to each atom.
Q_PC+ PEOE_PC+,	Partial Charge	Descriptors that depend on the

<p>Q_PCPEOE_PC-, Q_RPC+ PEOE_RPC+, Q_RPCPEOE_RPC-, Q_VSA_POS PEOE_VSA_POS, Q_VSA_NEG, PEOE_VSA_NEG, Q_VSA_PPOS, PEOE_VSA_PPOS, Q_VSA_PNEG PEOE_VSA_PNEG, Q_VSA_HYD PEOE_VSA_HYD, Q_VSA_POL PEOE_VSA_POL, Q_VSA_FPOS PEOE_VSA_FPOS, Q_VSA_FNEG PEOE_VSA_FNEG, Q_VSA_FPPOS PEOE_VSA_FPPOS, Q_VSA_FPNEG PEOE_VSA_FPNEG, Q_VSA_FHYD PEOE_VSA_FHYD, Q_VSA_FPOL PEOE_VSA_FPOL, PEOE_VSA+6 - PEOE_VSA+0, PEOE_VSA-0 - PEOE_VSA-6</p>	<p>Descriptors</p>	<p>partial charge of each atom of a chemical structure require calculation of those partial charges.</p>
<p>3-D descriptors</p>		
<p>E, E_ang, E_ele, E_nb, E_oop, E_sol, E_stb, E_str, E_strain, E_tor, E_vdw, E_rele, E_rsol, E_rvdw</p>	<p>Potential Energy Descriptors</p>	<p>The energy descriptors use the MOE potential energy model to calculate energetic quantities from stored 3D conformations.</p>
<p>ASA, dens, glob, pmi, pmiX, pmiY, pmiZ, rgyr, std_dim1 – std_dim3, vol, VSA</p>	<p>Surface Area, Volume and Shape Descriptors</p>	<p>Descriptors depend on the structure connectivity and conformation.</p>
<p>ASA+, ASA-, ASA_H, ASA_P, DASA, CASA+, CASA-, DCASA, dipole, diploeX, dipole, dipoleZ, FASA+, FASA- , FCASA+, FCASA- FCASA_H, FCASA_P</p>	<p>Conformation Dependent Charge Descriptors</p>	<p>Descriptors depend upon the stored partial charges of the molecules and their conformations.</p>

Publications

1) Enabling precision manufacturing of active pharmaceutical ingredients: Workflow for seeded cooling continuous crystallization

Cameron J. Brown, Thomas McGlone, Stephanie Yerdelen, Vijay Srirambhatla, Fraser Mabbott, Rajesh Gurung, Maria L. Briuglia, Bilal Ahmed, Hector Polyzois, John McGinty, Francesca Perciballi, Dimitris Fysikopoulos, Pól MacFhionnghaile, Humera Siddique, Vishal Raval, Tomás S. Harrington, Antony Vassileiou, Murray Robertson, Elke Prasad, Andrea Johnston, Blair Johnston, Alison Nordon, Jagjit S. Srai, Gavin Halbert, Joop H. ter Horst, Chris J. Price, Chris D. Rielly, Jan Sefcik, Alastair J. Florence, Molecular Systems Design & Engineering, 2018.
DOI: 10.1039/c7me00096k

2) Ternary phase diagrams of ibuprofen in ethanol/water solutions for understanding crystallization and agglomeration (drafting)

3) Spherical agglomeration from suspension of lovastatin: from solvent selection to scale up (drafting)

4) Temperature-dependent calibration of in-line process monitoring techniques toward the application of accurate solubility determination for crystallization (drafting)

Collaborative projects

1) REMEDIES (2016): Characterisation and modelling of hot melt extruder and extrusion processes.

2) CMAC (2016): Workflow for seeded cooling continuous crystallization of paracetamol.

3) CMAC-CPACT Strathclyde (2015): Temperature dependent calibration of in-line process monitoring techniques.

4) GSK 106 (2015): Investigation of the agglomeration of an API using PATs and image analysis scripts.

5) GSK 102 (2014-2016): Spherical agglomeration from suspension of an API.